RECEIVED
LAWRENCE
RADIATION LABORATORY

MAR 13 1969

LIBRARY AND
DOCUMENTS SECTION

UCRL-18651

Cy. 2

I. THE $|\Delta K| = 1$ ELECTRIC DIPOLE TRANSITIONS IN ODD-MASS DEFORMED NUCLEI

II. THE DECAY OF Ta^{176} TO LEVELS IN Hf^{176}

Frederick Michael Bernthal

(Ph. D. Thesis)

February 1969

TWO-WEEK LOAN COPY

This is a Library Circulating Copy which may be borrowed for two weeks. For a personal retention copy, call Tech. Info. Division, Ext. 5545

LAWRENCE RADIATION LABORATORY
UNIVERSITY of CALIFORNIA BERKELEY

UCRL-18651
Cy. 2

DISCLAIMER

This document was prepared as an account of work sponsored by the United States Government. While this document is believed to contain correct information, neither the United States Government nor any agency thereof, nor the Regents of the University of California, nor any of their employees, makes any warranty, express or implied, or assumes any legal responsibility for the accuracy, completeness, or usefulness of any information, apparatus, product, or process disclosed, or represents that its use would not infringe privately owned rights. Reference herein to any specific commercial product, process, or service by its trade name, trademark, manufacturer, or otherwise, does not necessarily constitute or imply its endorsement, recommendation, or favoring by the United States Government or any agency thereof, or the Regents of the University of California. The views and opinions of authors expressed herein do not necessarily state or reflect those of the United States Government or any agency thereof or the Regents of the University of California.

UCRL-18651

UNIVERSITY OF CALIFORNIA

Lawrence Radiation Laboratory
Berkeley, California 94720

AEC Contract No. W-7405-eng-48

I. THE $|\Delta K| = 1$ ELECTRIC DIPOLE TRANSITIONS IN ODD-MASS DEFORMED NUCLEI

II. THE DECAY OF Ta^{176} TO LEVELS IN Hf^{176}

Frederick Michael Bernthal

(Ph.D. Thesis)

February 1969

I. THE $|\Delta K| = 1$ ELECTRIC DIPOLE TRANSITIONS IN ODD-MASS DEFORMED NUCLEI

II. THE DECAY OF Ta^{176} TO LEVELS IN Hf^{176}

Contents

Abstract vi

I. Introduction 1

II. The $|\Delta K| = 1$ Electric Dipole Transitions in Odd-Mass Deformed Nuclei 4

A. Theoretical Background 4

1. E1 Transitions in the Extreme Single-Particle Model 4

2. The Collective Model 7

3. The Nuclear Coriolis Interaction 7

4. The Nilsson Model--The Single Particle in a Deformed Nucleus 11

5. E1 Transitions in the Nilsson Model 17

B. The Understanding of $|\Delta K| = 1$ E1 Transitions in Odd-A Deformed Nuclei--A Phenomenological Approach . . . 20

1. Method 20

2. The Coriolis Interaction--A Phenomenological Explanation for $|\Delta K| = 1$ E1 Branching Ratios 21

3. A 3-Parameter Phenomenological Interpretation of the Hf^{177} E1 Transitions Utilizing Properly Normalized Wave Functions 54

C. $\Delta K = -1$ E1 Transitions in Hf^{177} in the Unified Model . 61

1. Deficiencies of the Simple Nilsson Model 61

2. The Influence of Pairing and Octupole Vibrations on E1 Transitions 63

3. Method of Calculating Absolute $|\Delta K| = 1$ E1 Transition Strengths for Odd-A Deformed Nuclei 74

4. Results of Calculations 84

5. Discussion 87

6. Summary and Conclusions 107

III. The Decay of Ta^{176} to Levels in Hf^{176} 109

A. Introduction 109

B. Background 111

C. Experimental 113

1. Target and Source Preparation 113

2. Description of Experimental Apparatus 114

3. Experimental Results--Decay of Ta^{176} 135

D. Data Analysis and Construction of the Hf^{176} Level Scheme . 187

1. Sample Data Analyses 193

2. Spin and Parity Assignments 201

3. EC-β^+ Branching 211

E. Discussion of the Hf^{176} Level Scheme 212

1. K = 0+ Excited States 212

2. Comparison of the Known Hf^{176} Levels with Theory . . . 236

F. Proposed Further Study 240

G. Summary and Conclusions 247

Acknowledgments 249

Appendices 251

A. Precision Spectroscopy of Lu^{177m} Decay 251

B. Techniques of Precision Spectroscopy 263

C. The γ-γ Coincidence Data for Decay of Ta^{176} to Levels in Hf^{176} 280

D. The Decay of 3.7-hour Lu^{176m} to Levels in Hf^{176} 321

References 325

I. THE $|\Delta K| = 1$ ELECTRIC DIPOLE TRANSITIONS IN ODD-MASS DEFORMED NUCLEI

II. THE DECAY OF Ta^{176} TO LEVELS IN Hf^{176}

Frederick Michael Bernthal

Lawrence Radiation Laboratory
University of California
Berkeley, California 94720

February 1969

ABSTRACT

In Part I we combine elements of the collective and single-particle nuclear models to provide a unified model interpretation of the $|\Delta K| = 1$ electric dipole transitions in odd-A deformed nuclei. Attention is focused on the uniquely informative set of E1 transitions in Hf^{177} that results from decay of the singular Lu^{177m} nucleus. We show that the influences of Coriolis coupling, pairing, and octupole vibration-particle coupling may be used to successfully account for the anomalous E1 transition rates in Hf^{177}, and by implication, in other odd-A deformed nuclei. Precise experimental data have been gathered for comparison with the theory.

In Part II we describe a detailed experimental study of the decay of Ta^{176} to levels in Hf^{176}. Numerous semiconductor detection systems have been employed in conjunction with an on-line PDP-7 data acquisition system to gather γ-ray singles, conversion electron, and γ-γ coincidence data on this remarkably complex decay. Over 300 transitions have been observed to follow the Ta^{176} decay, and some 140 of these have been placed in the proposed Hf^{176} level scheme. We compare the experimental data on levels in Hf^{176} with contemporary theoretical expectations.

We also call attention to the exceptional quantity and quality of information on nuclear properties that can now be expected from the timely marriage of semiconductor-detector and on-line computer technology. The techniques and problems associated with precision γ-ray spectroscopic data acquisition and analysis are discussed.

I. INTRODUCTION

The rapid development of semiconductor nuclear radiation detection technology and the concomitant birth and development of on-line computers for rapid acquisition and analysis of nuclear data has in the past three years ushered in an era that must surely be the "golden age" of nuclear spectroscopy. The initial flood of data from the first small Ge(Li) and Si(Li) detectors quickly verified to a large extent many features of the Unified Model of low energy nuclear structure as it had developed during the decade of the 1950's.

By now however, the anticipation and excitement that accompanied the placement of any radioactive source before even the most modest Ge(Li) device, an excitement shared only a few short years ago by nearly every experimentalist with access to a source of neutrons or a particle accelerator, has largely passed. The riches of the mother lode are now not so easily won, though they are still abundant provided the prospective researcher has an accelerator nearby. Still, the reserve of easily obtainable information on nuclear structure is fast running out, and barring another order-of-magnitude breakthrough in detector resolution, even the in-beam spectroscopist will soon be left to contemplate a return to the plundered fields of nuclear study to painstakingly sift out the finer details that it is hoped will ultimately result in a truly unified description of the atomic nucleus.

In this paper, we shall describe two studies that we feel represent well this transition from the "Eureka!" days of nuclear research to the perhaps less exhilarating but in many ways more

rewarding and certainly more efficient age of programmed nuclear study. In Part I we discuss the abundance of information on nuclear structure that we have been able to obtain from a series of rather simple but precise measurements of the photon spectrum arising from decay of the singular Lu^{177m} nucleus. A theoretical study of the electric dipole transition strengths in Hf^{177} is described in detail as the definitive example of the $|\Delta K| = 1$ E1 transitions in odd-mass deformed nuclei, a class of transitions that long ago earned a reputation for anomalous behavior. The measurements that made possible this study are described in Appendix A.

In Part II, we turn full-circle from the rather involved theoretical interpretation of simple, "second-order" experimental data to describe an involved experimental study, the results of which are found to be so complex that only the most meager comparisons with contemporary theory are possible. The decay of Ta^{176} to levels in Hf^{176} is one of the most complicated natural decays known. Its study was undertaken partly because of some obvious relevance to the Hf^{177} nucleus discussed in such detail in Part I, and partly because, for the first time, the marriage of the computer and the semiconductor detector made practical the study of this most intricate decay. As is often the case in this type of work, the results were at once exciting and sobering--exciting because of the enormous complexity that nature has seen fit to reveal in this case; sobering because of the great amount of work that still remains to be done before a truly accurate and detailed picture of the Hf^{176} nuclear energy levels can be developed.

The sheer volume and complexity of the Ta^{176} decay data, and the abundance of meaningful information we have derived from that data have forced a break with the traditional custom of reporting the logic behind each assignment to the level scheme. We have instead chosen to display in what we trust is reasonably intelligible form all of the data, and to select for closer scrutiny only a few features of special interest.

Finally, a word about the philosophy with which we have approached this writing. From our few years experience as a graduate student, we have concluded with a good number of our comrades that the final practical function of a thesis, beyond fulfilling the academic and personal requirement, is that of passing on some information to the next generation of graduate students, most of whom will doubtless feel as we did (and still do at times) that hopeless sensation brought on by an apparently immense gulf of knowledge lying between themselves and the speaker at their first nuclear chemistry seminar. If we at times seem to have included an excessive number of superfluous paragraphs or references, it was with this purpose in mind. We trust that the frequent small "review" sections will not prove too distracting to the more sophisticated reader.

II. THE $|\Delta K| = 1$ ELECTRIC DIPOLE TRANSITIONS IN ODD-MASS DEFORMED NUCLEI

A. Theoretical Background

1. E1 transitions in the extreme single particle model

The conditions defining E1 transitions according to the theory of multipole radiation for a system going from initial state $|I_i\pi_i\rangle$ to final state $\langle I_f\pi_f|$ are

$$|I_i - I_f| \leqslant 1 \leqslant I_i + I_f$$

and

$$\pi_i\pi_f = -1$$

where I_i and I_f are the initial and final total angular momenta or spins of the system, and π represents correspondingly the parity. In principle, then, E1 radiation can be emitted (or absorbed) in transforming into each other any two nuclear states whose spins differ by 0 or 1 and are of opposite parity ($0^{\pm} \longrightarrow 0^{\mp}$ excepted).

In 1951, Weisskopf published a highly simplified model for estimating multipole radiative transition probabilities. His "single proton" formulae for calculating transition strengths were based on an extreme independent-particle model of the nucleus[1] and were set forth primarily "because of the rather unexpected agreement with experiment" encountered when calculations using his model of a proton changing quantum states within a uniform nuclear potential were compared with measured lifetimes of nuclear isomeric states. The

Weisskopf estimate for nuclear radiative transition probabilities is

$$T(E\lambda) = \frac{4.4\ (\lambda+1)}{\lambda[(2\lambda+1)!!]^2} \left(\frac{3}{\lambda+3}\right)^2 \left(\frac{\hbar}{197\ \mathrm{MeV}}\right)^{2\lambda+1} R^{2\lambda} \times 10^{21}\ \mathrm{sec}^{-1}$$

for electric multipole transitions, and

$$T(M\lambda) = \frac{1.9\ (\lambda+1)}{\lambda[(2\lambda+1)!!]^2} \left(\frac{3}{\lambda+3}\right)^2 \left(\frac{\hbar}{197\ \mathrm{MeV}}\right)^{2\lambda+1} R^{2\lambda-2} \times 10^{21}\ \mathrm{sec}^{-1}$$

for magnetic multipole transitions. The final proton state is always assumed to be an S-state ($\ell=0$) in these simple approximations. For E1 transitions, the former of these expressions reduces to

$$T_W(E1) = 1.5 \times 10^{14}\ A^{2/3}\ E_\gamma^3\ ,\quad E_\gamma \quad \text{in MeV}\ .$$

We have introduced here the Weisskopf estimate for two reasons: 1) Because the "hindrance factors", i.e. the ratios of theoretical-to-experimental multipole transition strengths are oftentimes expressed in Weisskopf units,

$$F_W = \frac{T_W(E1)}{T_{exp}(E1)}$$

and 2) to demonstrate the fact that whereas unexpectedly good agreement with experiment has often been obtained by applying the single-proton estimates to M1 and higher-order multipole transitions (except where "collective" effects are dominant), this has not in general been the case for E1 transitions. In fact, the recent compilation of

Perdrisat[2] lists some 150 E1 transitions, all of which are retarded compared to the Weisskopf estimates.

Of particular interest here are the E1 transitions in odd-mass deformed nuclei. As of 1966, Perdrisat found recorded in the literature lifetime measurements for 65 such E1's in the lanthanide and actinide regions of nuclear deformation. The Weisskopf hindrance factors for these E1 transitions are scattered over some six orders of magnitude, from $\approx 10^3$ up to 10^9, a large departure indeed from the simple single proton transition strengths!

Closer examination of the nuclear parameters influencing E1 transitions reveals, however, that it is unrealistic to expect good agreement between the Weisskopf estimates and experiment for these transitions. A cursory glance at the nuclear shell model as originally constructed by Mayer and Jensen[3] reveals no two single particle states of opposite parity and spin difference of 0 or 1 units existing in what is supposed to be a single "shell". This fact itself, in the light of the considerable success of the shell model, limits the usefulness of the original simple single-particle treatment of E1 transitions to no more than a convenient tool for comparison of experimental data. Moreover, the conclusion necessarily follows that the initial and final nuclear states involved in E1 transitions are not pure shell model states, but consist of mixtures of states which allow the radiative E1 transitions to proceed.

2. The collective model

The proposed important mechanisms for configuration mixing of nuclear states were summarized in the 1952 paper by A. Bohr,[4] wherein the coupling of intrinsic or single particle motion to collective motion of the nuclear surface was analyzed.

Observation of unusually large quadrupole moments, and rather distinct rotational band structure in the mass regions $A \approx 25$, $150 \leqslant A \leqslant 190$, and $A > 222$ gave experimental support to the arguments for the existence of rather strong permanent nuclear deformations in the regions between closed shells. Moreover, it soon became clear that the assumption of "strong coupling" of particle-to-collective motion in these regions provided the best agreement between theory and experiment.[5]

Although these historical notes may seem far removed from the specialized problem of interpreting E1 radiative transition rates, the foundation for an understanding of the several factors influencing the electric dipole radiative transition probabilities rests squarely upon the concept of the strong coupling of intrinsic and collective (both rotational and vibrational) nuclear motion.

3. The nuclear Coriolis interaction

Before proceeding with an examination of the influence of a deformed, i.e. non-spherical, nuclear potential on the single-particle shell model nuclear states, let us write explicitly the form of one of the mechanisms of configuration mixing--the rotation—particle coupling scheme, or nuclear Coriolis interaction.

Consider the vector coupling diagram in Fig. 1 applied to a deformed rotating spheroidal nucleus. If we accordingly consider only particle and rotational contributions to the nuclear spin, we may write the Schrödinger equation

$$H\Psi = (T_{rot} + \sum_p H_p)\Psi = E\Psi \tag{1}$$

where Ψ, the wave function, is of the general form

$$\Psi = \chi_{part} \cdot \phi_{vib} \cdot \mathcal{D}_{rot}$$

suggested by Bohr. The treatment of the nuclear wave equation as the product of separable rotational, vibrational, and particle modes allows the Hamiltonian (with omission for now of the higher energy vibrational components) to be written:

$$H = H_{rotation} + H_{intrinsic} + H_{coupling} \quad .$$

The third portion of the Hamiltonian includes the Coriolis interaction. For the sake of clarity the appropriate wave function Ψ, we refer to now as

$$|IMK\Omega\rangle = \sqrt{\frac{2I+1}{16\pi^2}}\ \phi[\chi_\Omega \mathcal{D}^I_{MK} + (-)^{I-j}\ \chi_{-\Omega}\mathcal{D}^I_{M-K}] \quad . \tag{2}$$

Using the wave functions (2) of Bohr, we may solve for the rotational energy T_{rot} of Eq. (1):

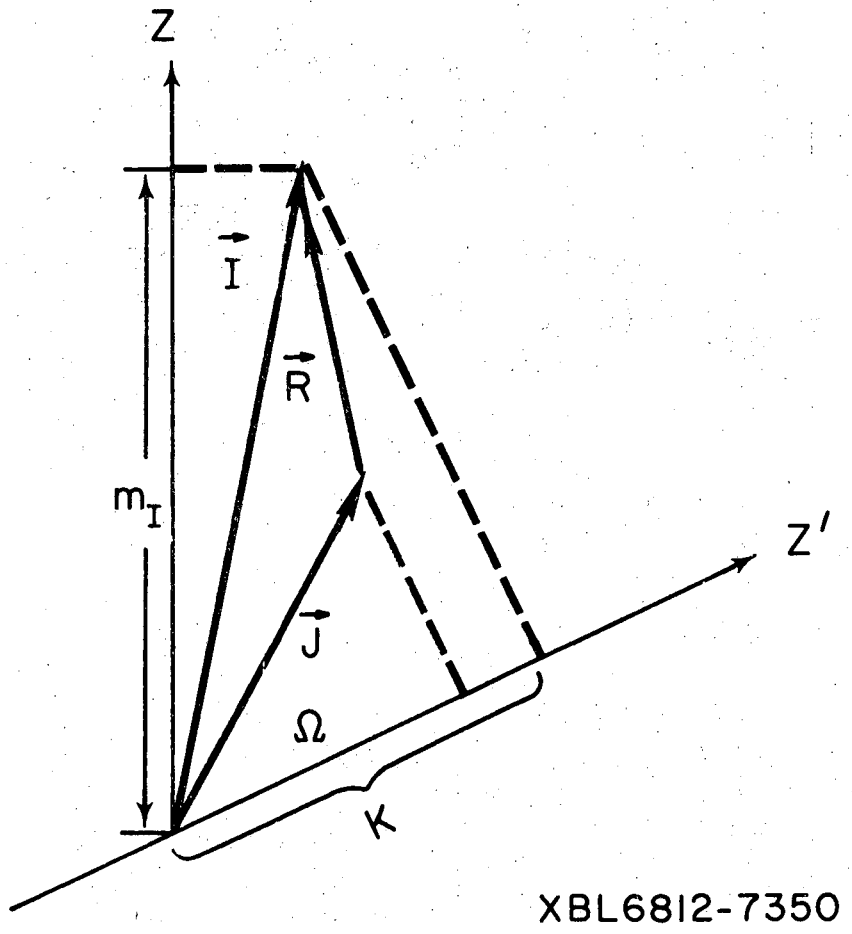

Fig. 1. Angular momentum vector diagram for a deformed rotating nucleus.

$$\langle T_{rot} \rangle = \sum_{i=1}^{3} \frac{\hbar^2 \langle \vec{R}_i^2 \rangle}{2\mathfrak{J}_i} = \sum_{i=1}^{3} \frac{\hbar^2 \langle (\vec{I}_i - \vec{j}_i)^2 \rangle}{2\mathfrak{J}_i}$$

where the i indices refer to the three body-centered axis, and $\vec{R}$, $\vec{I}$, and $\vec{j}$ are the momentum vectors indicated in Fig. 1, representing rotational, total, and particle components, respectively. For symmetry along the 3 axis, we then have

$$\langle T_{rot} \rangle = \frac{\hbar^2}{2\mathfrak{J}} [\langle (\vec{I} - \vec{j})^2 \rangle - (I_3 - j_3)^2] + \frac{\hbar}{2\mathfrak{J}_3} (I_3 - j_3)^2$$

where $\mathfrak{J} = \mathfrak{J}_1 = \mathfrak{J}_2$ and $\mathfrak{J}_3$ is small. Then

$$\langle T_{rot} \rangle = \frac{\hbar^2}{2\mathfrak{J}} [I(I+1) + \langle \vec{j}^2 \rangle - \langle 2\vec{J} - \vec{j} \rangle - (K-\Omega)^2]$$

$$+ \frac{\hbar^2}{2\mathfrak{J}_3} (K-\Omega)^2$$

and since $\vec{I} \cdot \vec{j} = I_3 j_3 + I_2 j_2 + I_1 j_1 = K\Omega + I_+ j_- + I_- j_+$

$$\langle T_{rot} \rangle = \frac{\hbar^2}{2\mathfrak{J}} [I(I+1) - K^2 - \Omega^2] + \frac{\hbar^2}{2\mathfrak{J}_3} (K-\Omega)^2$$

$$+ \frac{\hbar^2}{2\mathfrak{J}} \langle \vec{j}^2 \rangle - \frac{\hbar^2}{2\mathfrak{J}} (I_+ j_- + I_- j_+) \quad . \tag{3}$$

The diagonal contribution to the rotational energy is now contained in the first two terms of the above expression. Since $\vec{j}^2$ involves only particle motion, it may be considered with that portion of the Hamiltonian. Of particular interest here is the remaining term, i.e.

the rotation particle coupling (RPC) term

$$-\frac{\hbar^2}{2\mathfrak{J}}(I_+j_- + I_-j_+) \tag{4}$$

corresponding to Bohr's U_1 off-diagonal matrix elements coupling states differing by ± 1 in K quantum number. There is here a diagonal contribution to the energy only for $K = 1/2$. The effect of this RPC term has been considered in detail by Kerman.[6] The form is seen to be analogous to that describing the classical Coriolis interaction. Assuming a single particle coupled to the rotating nuclear mass, the general form of the RPC matrix elements is given by:

$$\langle I,K|I_\pm|I,\ K\mp 1\rangle = \sqrt{(I\pm K)(I\mp K+1)}$$

$$\langle j\Omega|j_\mp|j\Omega\pm 1\rangle = \sqrt{(j\mp\Omega)(j\pm\Omega+1)}\ .$$

The influence of the nuclear Coriolis interaction on E1 transitions will be examined in greater detail later. For now, suffice it to say that when the work described here was begun, it was already suspected that the RPC term (4) exercised a profound influence on $\Delta K = \pm 1$ E1 transitions.

4. The Nilsson model - the single particle in a deformed nucleus

The proper choice of the particle (χ_Ω) portion of the generalized wave function (2) is, of course, essential to the success of the unified model. In the regions of presumed permanent nuclear deformation, one must choose an appropriately "deformed" potential within which the single particle energy levels may be calculated. The now widely

accepted paper of Nilsson[7] described the results of such calculations, and correctly foretold the applicability of the results to "a wide range of different problems of nuclear physics".

Nilsson's treatment is a logical extension of the unified model to spheroidal nuclei. We review here only briefly the salient points. In Fig. 1, the projection Ω of the total particle angular momentum on the nuclear symmetry axis is made up of a sum, $\sum_i \Omega_i$; of the individual particle projections on the nuclear axis. Each particle state is doubly degenerate, corresponding to $\pm\Omega_i$ and the total χ_Ω is therefore the antisymmetrized product of individual wave functions χ_{Ω_i}. Ignoring as before the higher order vibrational modes of nuclear motion, the deformed nucleus can once again be considered within the framework of the Bohr strong coupling approximation, except that the problem now is that of a single particle moving in an average spheroidal nuclear potential. The key to the problem is Nilsson's choice of single particle Hamiltonian:

$$H = H_0 + C\,\vec{\ell}\cdot\vec{s} + D\,\vec{\ell}^{\,2} = \overset{\circ}{H}_0 + H_\delta + C\,\vec{\ell}\cdot\vec{s} + D\,\vec{\ell}^{\,2} \qquad (5)$$

where H_0 represents simply the three-dimensional harmonic oscillator potential, to which is added (as in the simple shell model) the spin-orbit coupling term, $\vec{\ell}\cdot\vec{s}$. The $\vec{\ell}^{\,2}$ term provides a crucial modification to the harmonic oscillator potential that effectively raises the nuclear potential near the center and lowers it near the edges. The practical consequence is a depression of high angular momentum states. The $\vec{\ell}^{\,2}$ term may also be considered to provide an interpolation between the harmonic oscillator and square well potentials appropriate to the spheroidal nuclear potential.

The Nilsson treatment proceeds by assuming axial symmetry (an assumption which seems in the light of recent experimental evidence to have been quite valid) and requiring that the Hamiltonian yield the empirical sequence of presumed single-particle levels considered in the shell model.

In this way the parameters C and D are fixed. A deformation parameter δ related to a second parameter η and the Bohr-Mottelson β by the following expressions

$$\delta \cong 0.95\beta \quad \text{and} \quad \eta = \frac{\delta}{x}\left[1 - \frac{4}{3}\delta^2 - \frac{16}{27}\delta^3\right]^{-1/6} ,$$

where

$$x = -\frac{1}{2}\frac{C_o}{\hbar\omega_0}$$

is introduced to describe the permanent nuclear deformation characterized by a "stretching" along the spheroidal symmetry axis.

Finally, the basis vectors $|N\ell\Lambda\Sigma\rangle$ are chosen corresponding to each particle quantum number Ω. (N represents the total oscillator quantum number.) The reader is at this point referred to Fig. 2 for definition of the various quantum numbers used in the Nilsson representation.

By considering the non-vanishing matrix elements of H between base vectors of the same N and Ω, Nilsson obtained his well-known and remarkably successful set of energy levels for the single particle states of the nucleus in a spheroidal potential. In the Nilsson

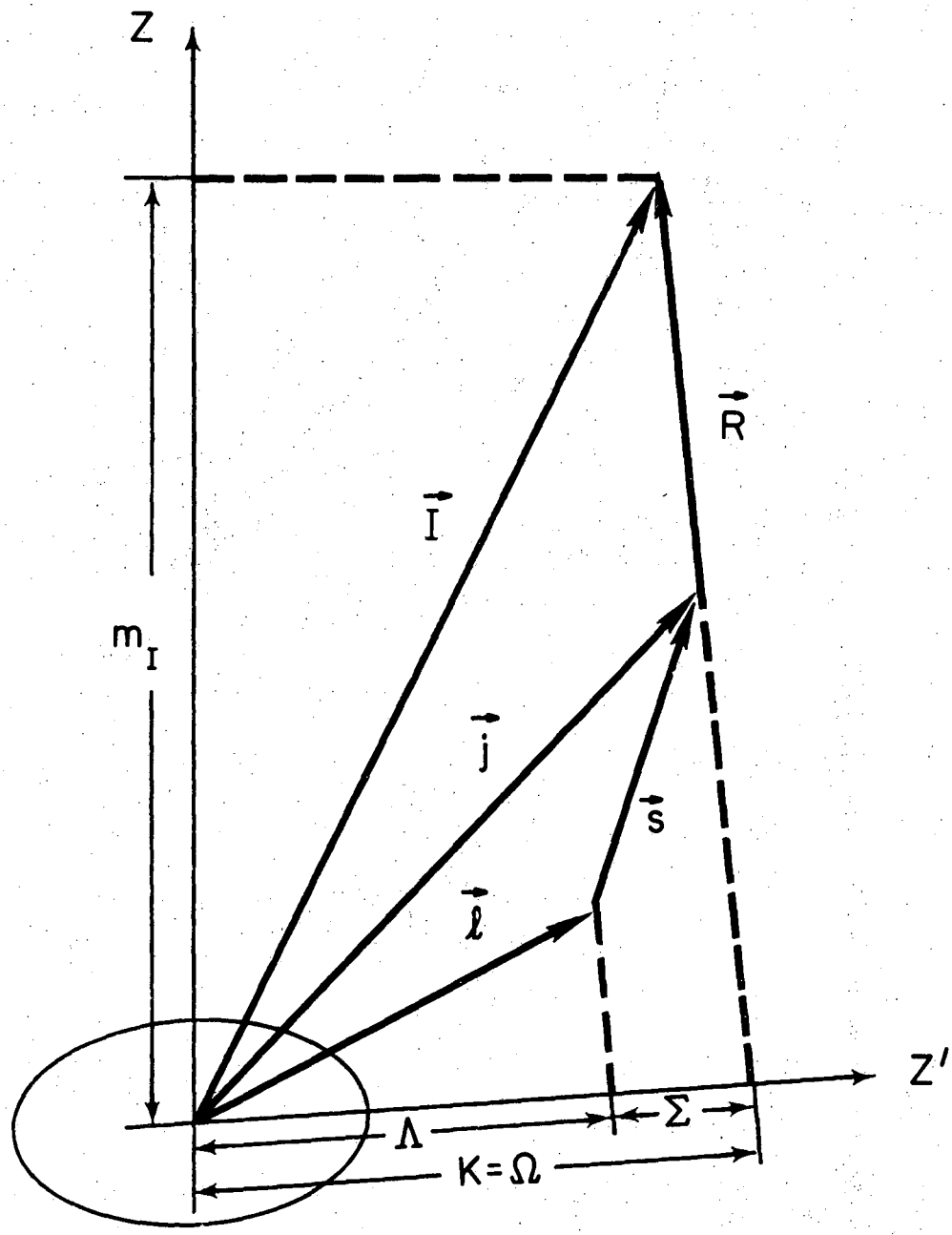

XBL6812-7351

Fig. 2. Angular momentum vector coupling diagram for the Nilsson representation of a deformed nucleus.

potential, the degeneracy of the shell model states is removed, resulting in $j + 1/2$ separate states differing in energy by ≈ 200 keV, well within the range of rotational energy excitations. As a result, it should not be surprising that appreciable interaction between particle and collective modes of nuclear motion can and does occur in the regions of permanent nuclear deformation.

Nilsson has tabulated as a function of deformation the eigenfunctions of the single particle states χ_Ω in terms of the basis states $|N\ell\Lambda\Sigma\rangle$ so that the appropriate single particle wave functions may be obtained as a sum of basis states:

$$\chi_\Omega = \sum a_{\ell\Lambda\Sigma} |N\ell\Omega\Sigma\rangle \quad .$$

By use of Nilsson's tabulations, a variety of nuclear problems in the regions of permanent nuclear deformation may be investigated. In particular, we will make frequent use of the Nilsson wave functions for calculating electromagnetic radiative transition probabilities and the effects of rotation-particle coupling on radiative transitions.

In his original calculations Nilsson uses the eigenvectors of a spheroidal <u>isotropic</u> harmonic oscillator potential as a basis set to calculate the single particle levels in a deformed nuclear potential. Nilsson splits the spheroidal H.O. potential H_0 (Eq. (5)) into two terms, one of which is spherically symmetric, and one of which represents the coupling of the particle to the nuclear symmetry axis as a function of deformation. The reader is again referred to Ref. 7 for details. The Nilsson basis set is chosen such that the spherically

symmetric term in the Hamiltonian is diagonal. The consequence of this treatment is that at large deformations, there occurs an approximate separation of particle motion into two components with oscillations (1) along the nuclear symmetry axis and (2) in a plane perpendicular to the symmetry axis. As Nilsson points out, it is possible to choose a representation that gives a more useful picture of the nucleonic motion at large deformations--one which may provide significant new selection rules for particle transitions in the limit of strong deformations.

Rassey[8] carried out such a calculation by using as a basis set the eigenvectors of a three-dimensional anisotropic H.O. The approximate "purity" of the single particle states in the limit of large deformation had already been used as a convenient basis for classifying states at large deformations in terms of their "almost good" asymptotic quantum numbers, $[Nn_z\Lambda]$. (n_z here represents the projection of N, the total oscillator quanta, on the nuclear symmetry axis.) At infinite deformations, the Nilsson states tend toward the pure single particle states characterized by "good" quantum numbers N, n_z and Λ. Gustafson, et al. have also recently carried out a set of calculations in the asymptotic representation with emphasis on the applicability to studies of nuclear fission.[9] With this understanding of the approximate "goodness" of the Nilsson asymptotic quantum numbers, we proceed to outline explicitly the relevant background necessary to our discussion of E1 radiative transition probabilities.

5. <u>E1 transitions in the Nilsson model</u>

The strength of a nuclear radiative transition of multipolarity λ between an initial state i and a final state f may be written in terms of the <u>reduced transition probability</u>[5]

$$B(\lambda, I_i \rightarrow I_f) = \sum_{\mu M_f} |\langle I_f M_f | \mathcal{M}'(\lambda, \mu) | I_i M_i \rangle|^2 \qquad (6)$$

where $\mathcal{M}'(\lambda, \mu)$ is the μ-component multipole transition operator of order λ. The probability for emission of a photon of frequency ω is

$$T(\lambda) = \frac{8\pi(\lambda+1)}{\lambda[(2\lambda+1)!!]^2} \frac{1}{\hbar} \left(\frac{\omega}{c}\right)^{2\lambda+1} (B\lambda) \text{ sec}^{-1} \quad . \qquad (7)$$

Confining our consideration to electric dipole transitions this expression becomes:

$$T(E1) = \frac{16\pi}{9\hbar} \left(\frac{E_\gamma}{\hbar c}\right)^3 B(E1) \qquad (8)$$

where E_γ represents the transition energy measured as the gamma-ray energy in MeV. Nilsson gives the appropriate expression for the (energy-independent) reduced transition probability (Cf. Ref. 5) as

$$B(E1) = e_{eff} \left(\frac{\hbar}{M\omega_0}\right) \frac{3}{4\pi} (I_i 1 K_i \Delta K | I_f K_f)^2 \times G^2(E1) \quad . \qquad (9)$$

The Nilsson G(E1) contains the dependence upon the radial matrix elements and the proper forms for use of the tabulated coefficients of the eigenvector for each single particle state. e_{eff} is the effective charge of

the nucleon, usually taken as $(1 - \frac{Z}{A})$ e, although Berlovich has pointed out the errors that may be introduced by use of this simple approximation in transition probability calculations.[10]

One consequence of the intensity rule (9) is immediately seen to be

$$|K_f - K_i| \leqslant 1$$

for E1 transitions. Although the "K selection rule" may be violated because of "impurities" in the total wave function, violation occurs only at unit cost of a factor of 10-100 increase in the lifetime of the initial state.

A number of more frequently violated selection rules are associated with the asymptotic quantum numbers discussed earlier.[11,12] The rules appropriate to E1 transitions are given in Table 1. All E1 transitions observed to date are at least twice-forbidden by these asymptotic selection rules.[13]

Table 1. E1 selection rules for the asymptotic Nilsson quantum numbers.[11,12]

Operator	$\Delta\Omega(\Delta)$	ΔN	Δn_z	$\Delta\Lambda$	$\Delta\Sigma$
$x \pm iy$	+1	±1	0	+1	0
	-1	±1	0	-1	0
z	0	+1	+1	0	0
	0	-1	-1	0	0

In summary, we note that the Nilsson model, by correctly predicting the splitting of the isotropic shell-model states at large permanent nuclear deformations, provides at least an initial explanation for the observation of E1 transitions in odd-mass deformed nuclei. The crossing of states with N quantum numbers differing by ± 1 at deformations $\delta = 0.2 - 0.3$ is not uncommon, and therefore the criterion for opposite parity states with spins differing $\leqslant 1$ unit is frequently satisfied. However, as we shall see, the Nilsson E1 hindrance factors are still often as much as 10^3, and display ambiguities that cannot be explained without invoking complex interactions between single particle and collective nuclear motion.

B. The Understanding of $|\Delta K| = 1$ E1 Transitions in Odd-A Deformed Nuclei--A Phenomenological Approach

1. Method

Initiation of the project described in the following pages was prompted by the efforts of Grin and Pavlichenkov[13] and Vergnes and Rasmussen[14] to account for the $\Delta K = 1$ E1 transitions in odd-A deformed nuclei, on a purely phenomenological basis. Because of the scarcity of precise experimental data with which to test the early theoretical investigations by these authors, a search was begun in the literature and experimental measurements were made for E1 transition intensities in several nuclei of interest. We will describe briefly the application to the data of the early simple theory of $\Delta K = 1$ E1's. The good qualitative agreement with experiment resulting from these applications seemed to justify a more detailed analysis of the problem, and we describe the results of a more precise phenomenological approach that yielded remarkably good agreement with the singularly interesting data gathered in our laboratory for the numerous E1 transitions in Hf^{177}. Because of the success encountered at this point, the final step of attempting a microscopic calculation of absolute E1 transition probabilities in the unified model seemed justified. We will describe in detail the nature and results of those calculations.

We have chosen to present the results of our work in this chronological fashion because we feel that it demonstrates rather convincingly the usefulness of the inductive approach to the solution of a problem in nuclear physics--an approach that has become more and

more common as researchers seek to explain the details of nuclear structure.

2. The Coriolis interaction--a phenomenological explanation for $\Delta K = \pm 1$ E1 branching ratios

The experimental E1 transition probabilities in odd-A deformed nuclei may be roughly separated into two classes on the basis of the quality of their agreement with the Nilsson model: 1) $\Delta K = 0$ transitions, for which agreement is generally good, and 2) $\Delta K = \pm 1$ transitions, for which the agreement of experiment with the Nilsson predictions tends to be poor. Vergnes proposed in 1962[15] that the discrepancies between theory and experiment for $|\Delta K| = 1$ E1's resulted from a perturbation of the single particle wave functions by the rotating nucleus. The papers of both Grin and Pavlichenkov[13] and Vergnes and Rasmussen in 1965[14] independently suggested a simple phenomenological first order perturbation treatment to explain the observed anomalous branching ratios of $\Delta K = \pm 1$ E1 transitions between members of the same pair of rotational bands. The method was to simply regard the principal and Coriolis-mixed E1 matrix elements as two adjustable parameters; consequently, in cases where experimental measurements of three or more E1's between the same two rotational bands were available, the validity of the assumption could be tested.

The reduced E1 strength for the $|\Delta K| = 1$ E1's may accordingly be written as

$$B(E1) \propto [M_0(I_i 1 K_i \Delta K | I_f K_f) + M_1 \sqrt{I_i(I_i+1) - K_i K_f}\ (I_i 1 K_{i(f)} 0 | I_f K_{i(f)})]^2 \tag{10}$$

where M_0 and M_1 are adjustable parameters representing the principal and Coriolis-mixed E1 matrix elements, respectively. The more general analysis of Grin[13] showed that, in a simple Nilsson calculation including the effects of the Coriolis-admixed components, Eq. (10) in fact describes all first-order contributions to the E1 moment. It should be emphasized that the validity of Eq. (10) is dependent upon the assumption that the magnitude of the Coriolis matrix elements is small relative to the energy separation between the states coupled by the Coriolis operator, i.e. one assumes that the use of simple first-order perturbation theory is valid. Then we can write the wave functions relevant to (10) as

$$\Psi = |I, K, \alpha_K\rangle + \sqrt{I(I+1) - K(K-1)} \times \sum_{\alpha_{K-1}} \hbar^2 \frac{\langle I,(K-1),\alpha_{K-1}|j_-|I,K,\alpha_K\rangle}{2\mathfrak{J}(E_{\alpha_{K-1}} - E_{\alpha_K})}$$

$$\times |I, K-1, \alpha_{K-1}\rangle + \sqrt{I(I+1) - K(K+1)} \sum_{\alpha_{K+1}} \hbar^2 \frac{\langle I,(K+1),\alpha_{K+1}|j_+|I,K,\alpha_K\rangle}{2\mathfrak{J}(E_{\alpha_{K+1}} - E_{\alpha_K})}$$

$$\times |I,(K+1),\alpha_{K+1}\rangle \qquad (11)$$

where the α_K refer to the appropriate single particle wave functions. The only spin-dependence in the wave functions is contained in the Coriolis matrix elements associated with the $I_\pm$ operator.

The validity of this model proposed in Refs. 13 and 14 and its remarkable success in predicting $|\Delta K| = 1$ E1 branching ratios for a number of experimental cases of interest will now be demonstrated.

a. Experimental data

Because of the rather stringent requirements which must be met in order that a given nuclide might display three or more $\Delta K = \pm 1$ E1 transitions between members of the same two rotational bands, the quantity of data available for testing the simple Coriolis mixing form (10) applied to E1 branching ratios is quite limited. There are six cases of interest known in the rare earth region of deformation: Yb^{173}, Lu^{175}, Hf^{177}, and the Tb series 155, 157, and 159. In each of these nuclei, three or more E1's are observed between the same intrinsic states. Hf^{177} is of unique importance, however, because of the numerous E1 transitions arising from the decay of the 161-day isomer Lu^{177m}.

In Table 2 we display the experimental data of interest pertaining to all but the Hf^{177} E1 photon intensities. The data for Lu^{175}, Tb^{155}, Tb^{157} and Tb^{159} were taken in this laboratory. The Yb^{173} data are from the literature.[16] Figures 3-5 compare the relative experimental reduced E1 branching ratios for these five isotopes with the simple Coriolis mixing theory of Refs. 13 and 14, and with the geometric branching rules of Alaga[17] which require, as is seen from Eq. (9) that the gamma-ray branching from members of a rotational band be proportional to the squared ratio of Clebsch-Gordan vector addition coefficients

$$\frac{B(E1)_{I_i \to I_f}}{B(E1)_{I_i \to I_f'}} = \left[\frac{(I_i 1 K_i \Delta K | I_f K_f)}{(I_i 1 K_i \Delta K | I_f' K_f)} \right]^2 ,$$

provided the K-quantum number is "good". It is noticed that there is a division of the "Theory including Coriolis mixing" bars in the odd-A

Table 2. Experimental relative intensities for $\Delta K = -1$ E1 transitions in some rare-earth odd-A deformed nuclei.

Isotope	Nilsson States	I_i	I_f	E_γ(keV)	I_γ^*	Ref.
Lu^{175}	$\frac{9}{2}-[514] \rightarrow \frac{7}{2}+[404]$	$\frac{9}{2}$	$\frac{7}{2}$	396	68	Our
			$\frac{9}{2}$	282	34	data
			$\frac{11}{2}$	145	3.8	
Yb^{173}	$\frac{7}{2}+[633] \rightarrow \frac{5}{2}-[512]$	$\frac{7}{2}$	$\frac{5}{2}$	351	53	(16)
			$\frac{7}{2}$	272	1960	
			$\frac{9}{2}$	172	406	
Tb^{155}	$\frac{5}{2}-[532] \rightarrow \frac{3}{2}+[411]$	$\frac{5}{2}$	$\frac{3}{2}$	227	100	Our
			$\frac{5}{2}$	161	7.5	data
			$\frac{7}{2}$	71	0.013	
Tb^{157}	"	$\frac{5}{2}$	$\frac{3}{2}$	326	100	Our
			$\frac{5}{2}$	265	0.18	data
			$\frac{7}{2}$	182	2.2	
Tb^{159}	"	$\frac{5}{2}$	$\frac{3}{2}$	363	100	Our
			$\frac{5}{2}$	305	0.50	data
			$\frac{7}{2}$	225	1.9	

* Since some of our data are unpublished, we note that errors on these data may be taken as 10%, except for the 71-keV Tb^{155} E1, where 20% is appropriate.

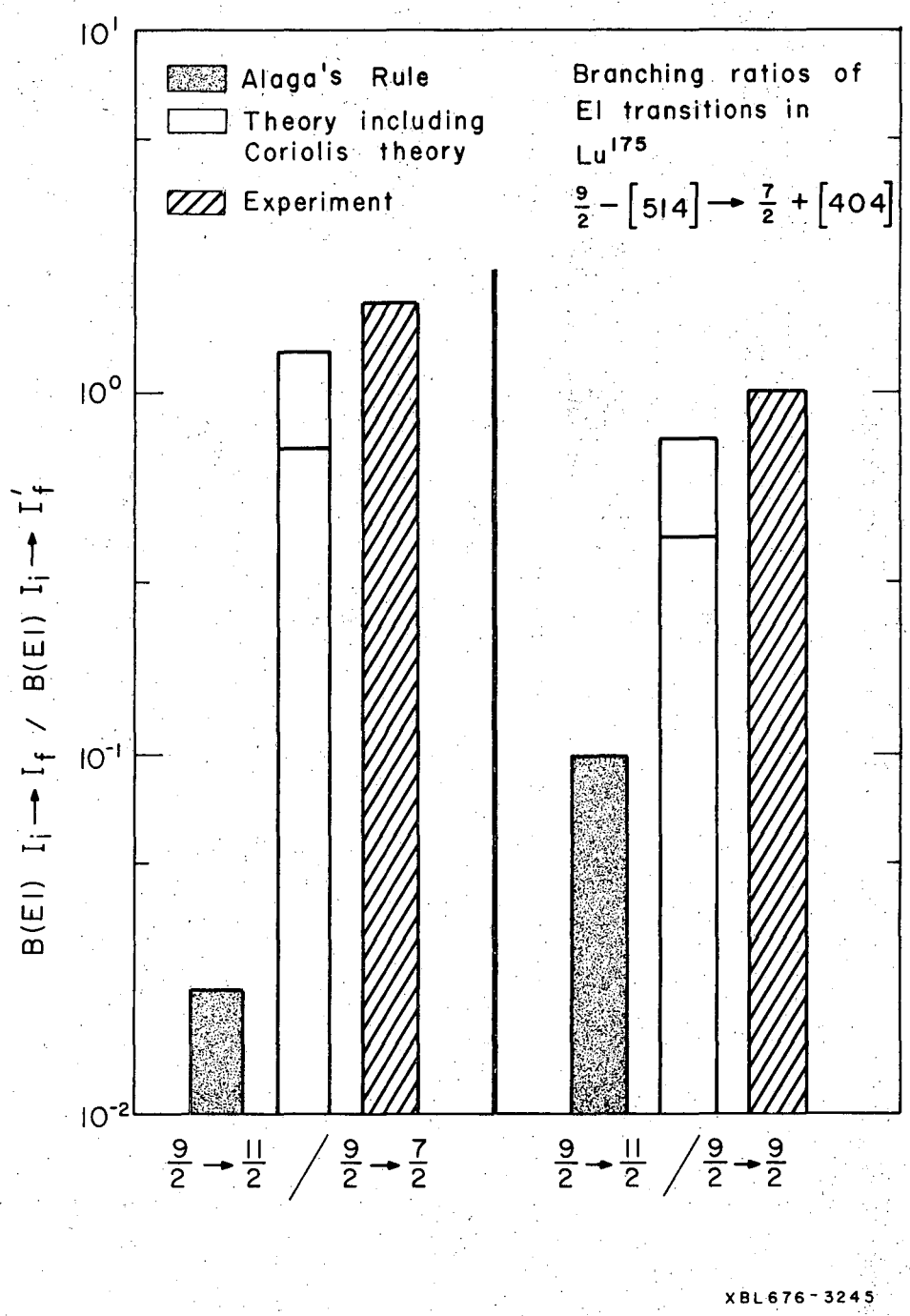

Fig. 3. The El branching ratios in Lu^{175}.

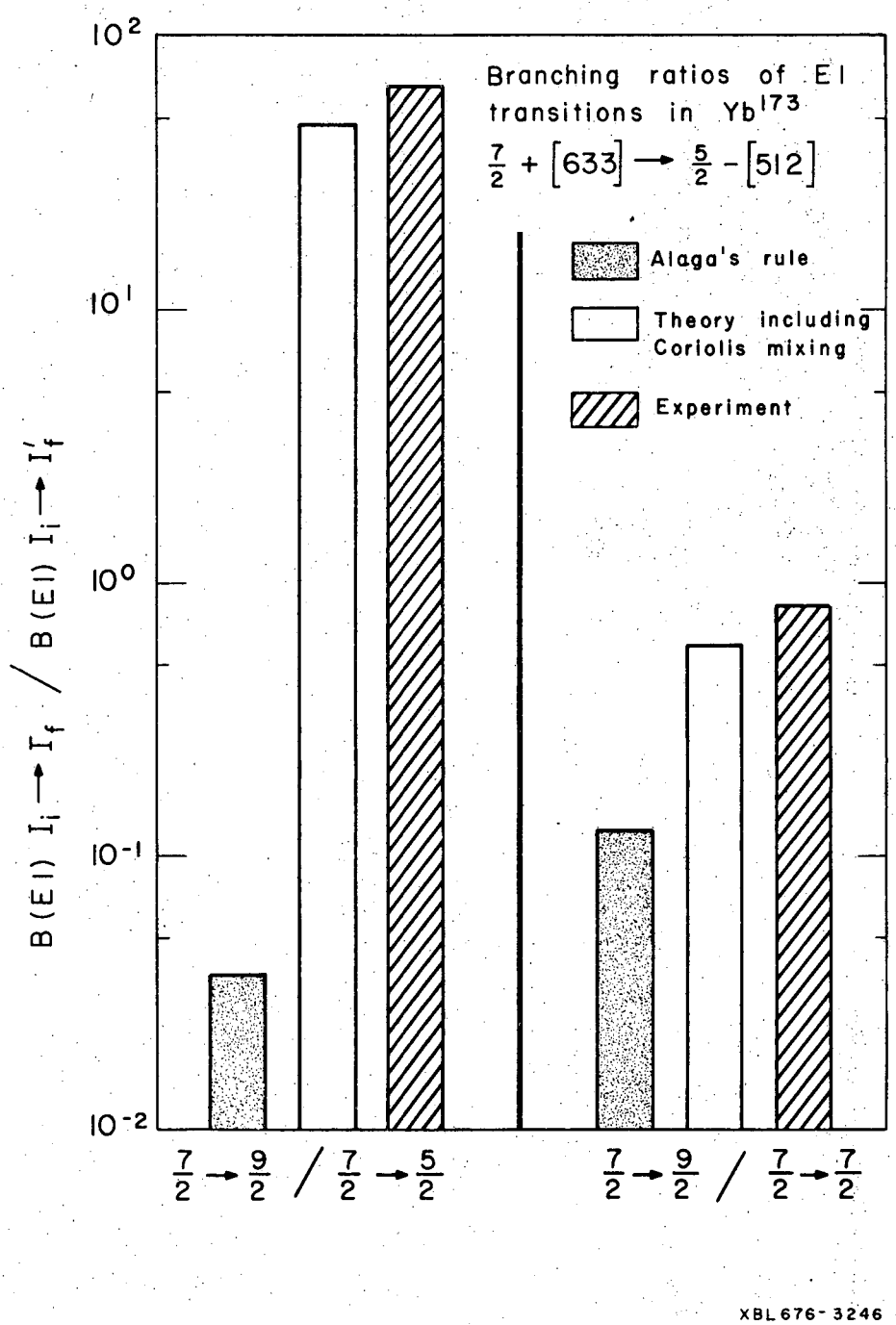

Fig. 4. The E1 branching ratios in Yb^{173}.

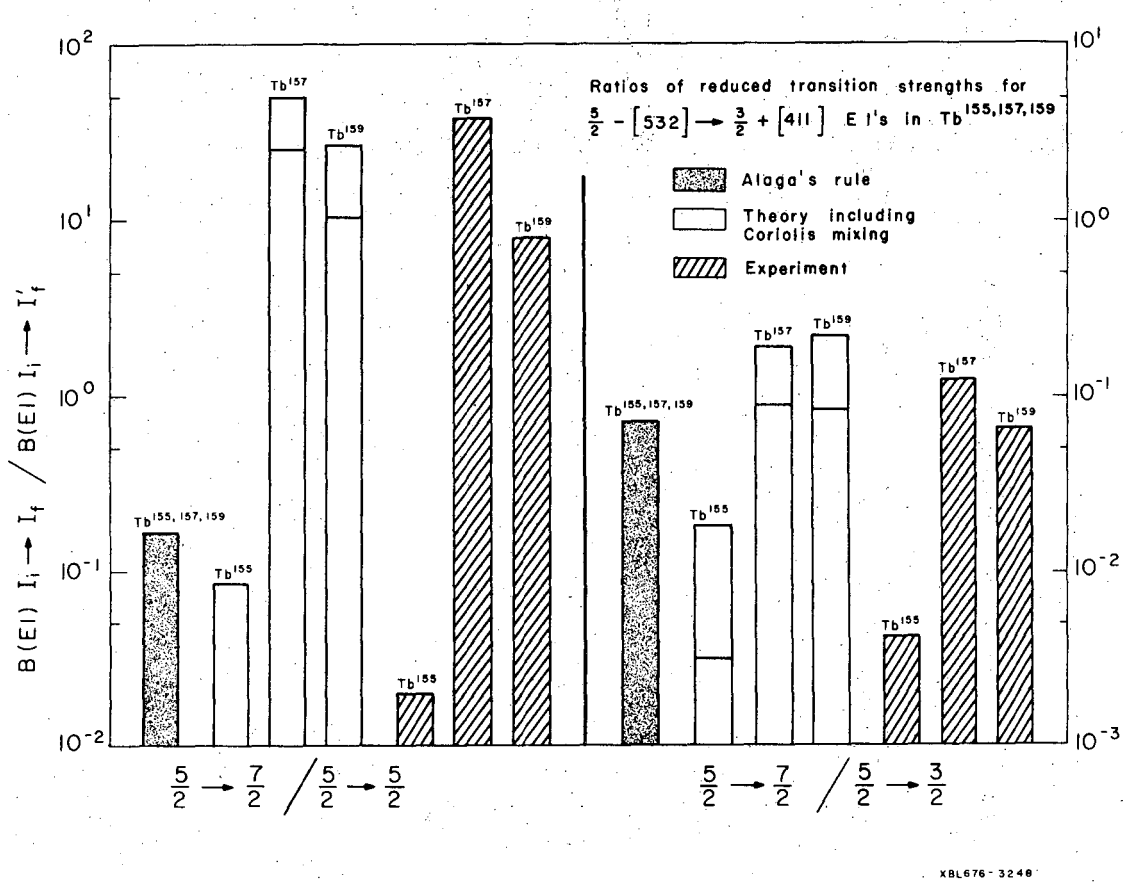

Fig. 5. The E1 branching ratios for the odd-A terbium isotopes.

Tb series (Fig. 5) and in the Lu^{175} display. The two different values designated arise from solution of the quadratic Eq. (10). Since we have no way of empirically determining the correct relative phases for the M_0 and M_1 parameters, we display both solutions. (The two solutions give similar results for Yb^{173}, therefore we have in this case indicated only a single theoretical value.)

Table 3 shows the much more extensive data we have obtained from the decay of Lu^{177m} to levels in Hf^{177}. Sixteen $\Delta K = -1$ E1 transitions leading from the $K = \frac{9}{2} + [624]$ to the $K + \frac{7}{2} - [514]$ rotational band presumably arise from this decay. Fourteen of these transitions have been observed, and their relative intensities have been precisely measured in our laboratory.[18] The relevant experiment details are discussed in Appendix A. In Fig. 6 we display for reference the now well established decay scheme of Lu^{177m}, as reported and modified earlier and in the present work.[18-22]

In Fig. 7 the results of the simple Coriolis treatment applied to the Hf^{177} E1 branching ratios are compared with experiment. The success of this early model in accounting for the extreme departures from Alaga's rules of the E1 branching from the spin $\frac{9}{2}+$ and $\frac{11}{2}+$ members of the $K = \frac{9}{2} + [624]$ band is particularly impressive.

It seems clear on the basis of the evidence presented in Figs. 3, 4, 5, and 7, that the presence of wave-function components presumably admixed via the Coriolis interaction is exerting a strong influence on the $\Delta K = -1$ E1 transitions strengths in the odd-A deformed nuclei. Moreover, the behavior of the E1 <u>branching</u> from a given single particle

Table 3. Experimental relative intensities and derived reduced transition strengths for Hf^{177} E1 transitions.

Initial spin	Final spin	E_γ (keV)	Intensity*	B(E1) $(MeV\text{-}fm^3)\times10^5$
9/2	7/2	321.3	8.8(5)	0.034(4)
9/2	9/2	208.3	512(21)	9.0(6)
9/2	11/2	71.7	7.2(4)	3.1(2)
11/2	9/2	313.7	10.0(5)	0.66(5)
11/2	11/2	177.0	27.8(1.2)	10.3(7)
11/2	13/2	(17.2)		
13/2	11/2	305.5	14.2(6)	2.32(13)
13/2	13/2	145.8	7.7(5)	11.6(9)
15/2	13/2	299.0	12.6(7)	4.3(3)
15/2	15/2	117.2	2.0(2)	11.5(1.3)
17/2	15/2	291.4	8.4(8)	7.0(7)
17/2	17/2	88.4	0.32(8)	9.4(2.4)
19/2	17/2	292.5	6.7(7)	8.9(9)
19/2	19/2	69.2	0.088(30)	8.6(2.9)
21/2	19/2	283.4	2.9(5)	11.0(2.0)
21/2	21/2	(41.0)		

*Normalized to 105.4-keV γ ray = 100. For most Ge(Li) detectors with thicker windows than ours, this is a poor choice for normalization, since 105 keV does not fall in the near-linear region of the efficiency curve. This may account for part of the discrepancy between our measured intensities for the strong lines and those quoted in Ref. 4. In general, we now measure I_γ about 10% greater than in Ref. 4 for those strong lines > 200 keV in energy.

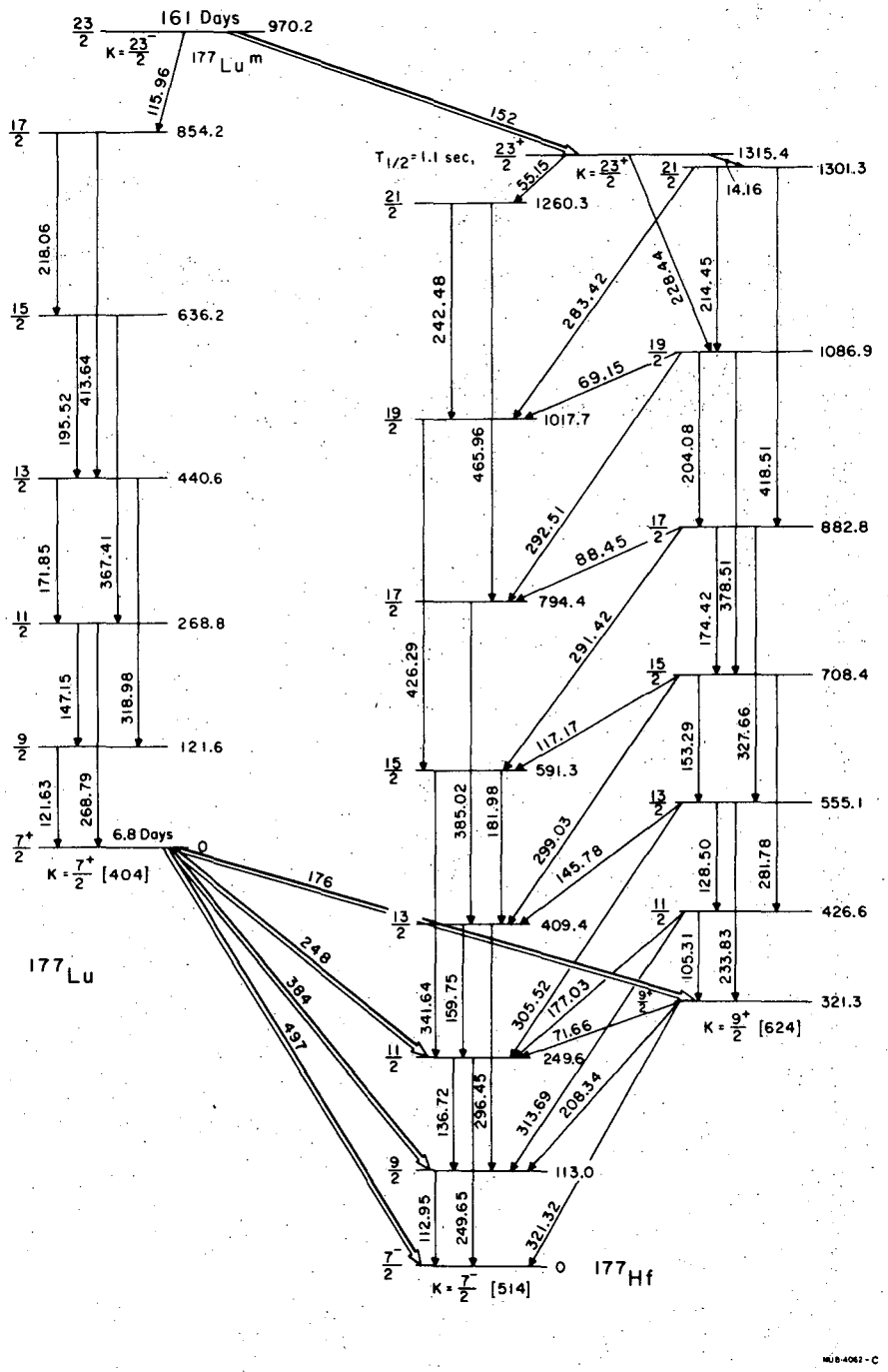

Fig. 6. The decay scheme of Lu^{177m} from Refs. 19-22 and the present work.

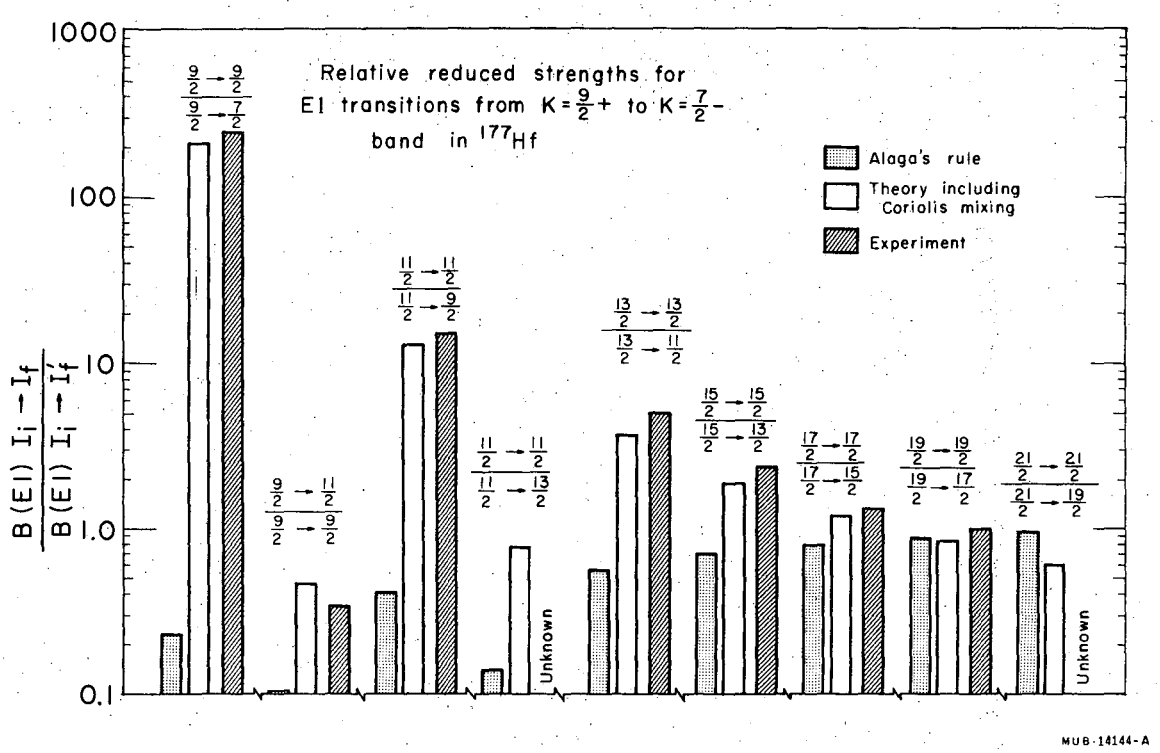

Fig. 7. Diagram of the E1 branching ratios in Hf^{177}.

state, or from a rotational band member of that state seems to be well-explained by the simple phenomenological approach of Refs. 13 and 14. However, the proper interpretation of the absolute E1 transition strengths requires a more rigorous analysis.

b. Deduction of experimental reduced transition strengths in Hf^{177}

The experimental values for B(E1) in Table 2 have been derived from two sources: 1) The lifetime of the 321-keV level in Hf^{177} has been measured by Berlovich et al.[23] to be $T_{1/2} = (6.9 \pm 0.3) \times 10^{-10}$ sec. Using this value and the M2/E1 mixing ratio 0.18 for the 321-keV E1 transition,[24] it is possible to calculate from relative intensity measurements the reduced strengths of the three E1 transitions leading from the $\frac{9}{2}$ + [624] band head.

2) The other values for the reduced E1 moments can in principle be indirectly derived using the rotational model of Bohr and Mottelson. The accuracy of this method is of course entirely dependent upon the degree to which the model properly describes the rotational band in question.

In contrast to the similar analysis first performed for Hf^{177} by Alexander et al.[19] which assumed the "goodness" of the $K = \frac{9}{2}$ + quantum number, we have in our treatment taken into account the contributions to the intraband transition strengths introduced by Coriolis-mixed components. In order to calculate these contributions, it is necessary to estimate the amplitudes of the various terms comprising the total single-particle wave function.

The wave equation for the $\frac{9}{2}$ + [624] band, including the proper wave amplitudes for the Coriolis-mixed components can in theory be obtained by diagonalizing the determinant describing the Coriolis secular perturbation:

$$
\begin{array}{c|ccccccc|}
K \backslash K' & \frac{1}{2} & \frac{3}{2} & \frac{5}{2} & \frac{7}{2} & \frac{9}{2} & \frac{11}{2} & \frac{13}{2} \\
\hline
\frac{1}{2} & E^{I}_{\Omega\alpha}-W & H_{\frac{1}{2},\frac{3}{2}} & 0 & 0 & 0 & 0 & 0 \\
\frac{3}{2} & H^{I}_{\frac{1}{2},\frac{3}{2}} & E^{I}_{\Omega\alpha}-W & H_{\frac{3}{2},\frac{5}{2}} & 0 & 0 & 0 & 0 \\
\frac{5}{2} & 0 & H_{\frac{5}{2},\frac{3}{2}} & E^{I}_{\Omega\alpha}-W & H_{\frac{7}{2},\frac{3}{2}} & 0 & 0 & 0 \\
\frac{7}{2} & 0 & 0 & H_{\frac{7}{2},\frac{5}{2}} & E^{I}_{\Omega\alpha}-W & H_{\frac{7}{2},\frac{3}{2}} & 0 & 0 \\
\frac{9}{2} & 0 & 0 & 0 & H_{\frac{9}{2},\frac{7}{2}} & E^{I}_{\Omega\alpha}-W & H_{\frac{9}{2},\frac{11}{2}} & 0 \\
\frac{11}{2} & 0 & 0 & 0 & 0 & H_{\frac{11}{2},\frac{9}{2}} & E^{I}_{\Omega\alpha}-W & H_{\frac{11}{2},\frac{13}{2}} \\
\frac{13}{2} & 0 & 0 & 0 & 0 & 0 & H_{\frac{13}{2},\frac{11}{2}} & E^{I}_{\Omega\alpha}-W
\end{array}
= 0
$$

(11a)

Here, the $H^I_{KK'}$ are the Coriolis matrix elements coupling two rotational states of spin I and $\Omega' = \Omega \pm 1$ based on the appropriate quasiparticle states. The unperturbed energy of the spin I rotational band member is denoted by $E^I_{\Omega\alpha}$, where $\Omega\alpha$ denotes the Nilsson quantum numbers $\Omega[Nn_z\Lambda]$ identifying the quasiparticle state upon which the the particular rotational band is constructed. For $\frac{9}{2} \leqslant I < \frac{13}{2}$, the determinant is of course reduced to rank $I + 1/2$.

The computer code BETABLE used to solve the Coriolis secular determinant was written by T. C. Clements at LRL.[25] It employs an iterative least-squares minimization routine that allows one to vary selected parameters and thereby obtain a best fit to the experimentally measured energies of rotational band members. The function minimized is in this case[25]

$$\mathcal{G}(H^I_{\Omega\Omega'}) = \sum_I [E^I_{\Omega\alpha}(H^I_{\Omega\Omega'}) - E^{\frac{9}{2}}_{\frac{9}{2}+[624]}(H^I_{\Omega\Omega'}) + W^I - W^{\frac{9}{2}}_{\frac{9}{2}+[624]} + \Delta(H^I_{\Omega\Omega'})]^2$$

where the quantity Δ is defined by

$$\sum_I [E^I_{\Omega\alpha} - E^{\frac{9}{2}}_{\frac{9}{2}+[624]} + W^I - W^{\frac{9}{2}}_{\frac{9}{2}+[624]} + \Delta] = 0$$

and the sum over I represents the spins of all levels the program is required to fit. The notation above is consistent with that used in

Eq. (11a). The function $g(H^{I}_{\Omega\Omega'})$ is seen to provide a rather sensitive estimate of the "goodness of fit", since it is simply the sum of the squares of the differences between the experimental and the fitted energies. We will in the following discussion indicate values for $g(H^{I}_{\Omega\Omega'})$ (in units keV^2) since they provide a convenient criterion for evaluating the overall quality of the fits.

In this case, we are interested in fitting the strongly perturbed $\frac{9}{2}$ + [624] band in Hf^{177} for the purpose of deriving the eigenvectors associated with the "best" solution of (11a). Figures 8 show plots of the quantity $[E(I) - E(I-1]/2I$ vs. $2I^2$ for the $K = \frac{9}{2}+$ and $K = \frac{7}{2}-$ bands in Hf^{177}. If the simple second order rotational form $E(I) = AI(I+1) + BI^2(I+1)^2$ were valid, both plots would define a straight line. It is seen that, while the $\frac{7}{2}$ - [514] band has its problems, the $\frac{9}{2}$ + [624] band deviates wildly from the predictions of the rotational model. Both the 17/2 and 19/2 members are depressed by some 7 keV, and the 21/2 member of this band is off by nearly 30 keV. It is to be hoped that these large deviations can be accounted for by considering the rotational-particle coupling elements, $H_{K,K\pm1}$ in Eq. (11a).

The first step in solving the problem is to determine which are the important admixtures in the rotational band. For an initial guess, one usually consults the Nilsson level diagram for the region in question. In Fig. 9 we display the latest such diagram for the region $82 < N < 126$.[9] One salient and fortuitous feature of the neutron level scheme in this region is the presence of only a single positive

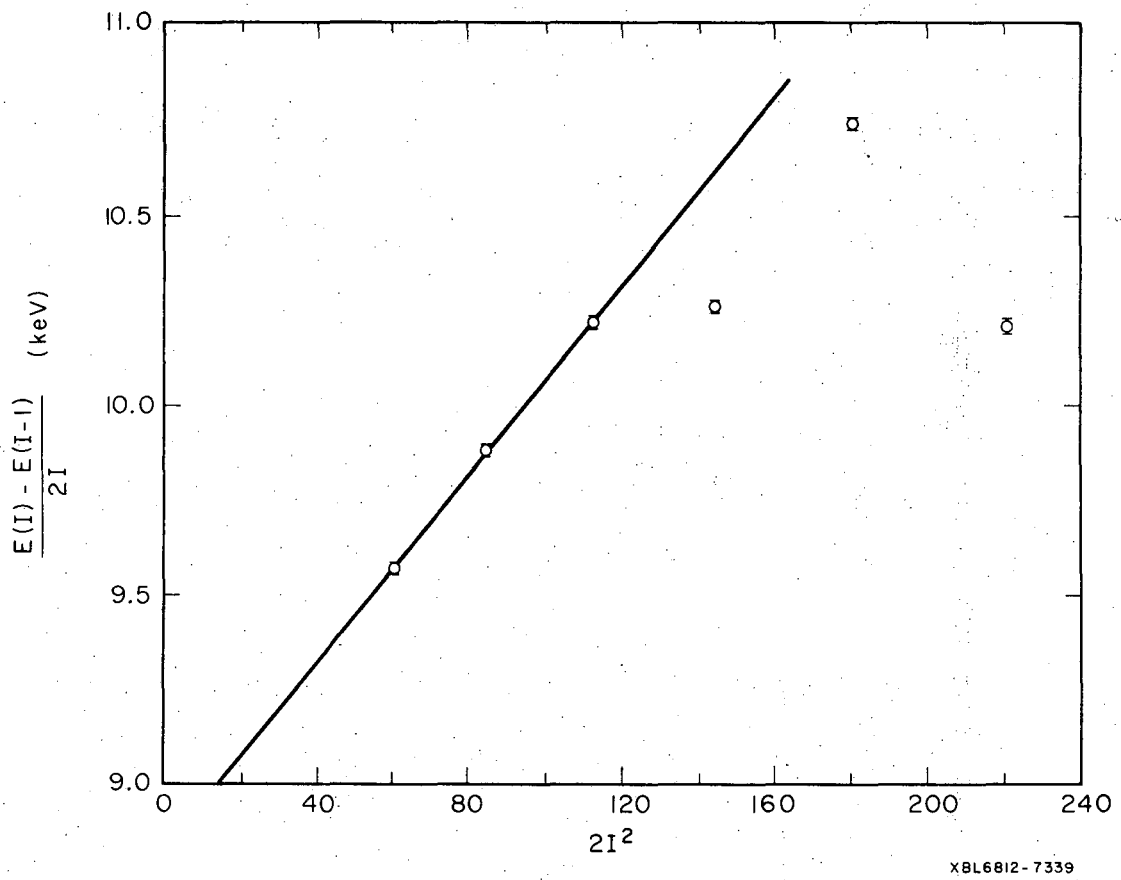

Fig. 8a. Rotational energy plot for the K = 9/2+ band in Hf^{177}.

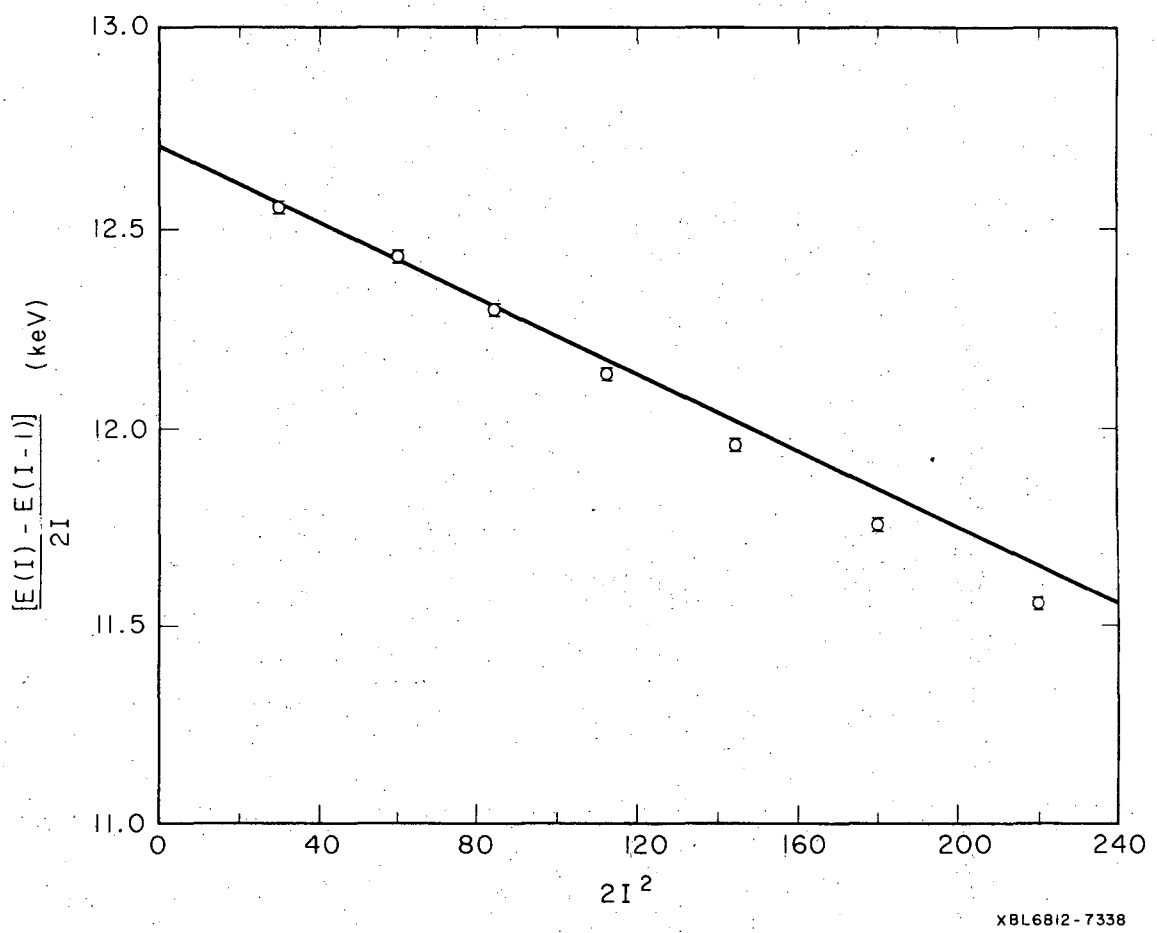

Fig. 8b. Rotational energy plot for the K = 7/2- band in Hf^{177}.

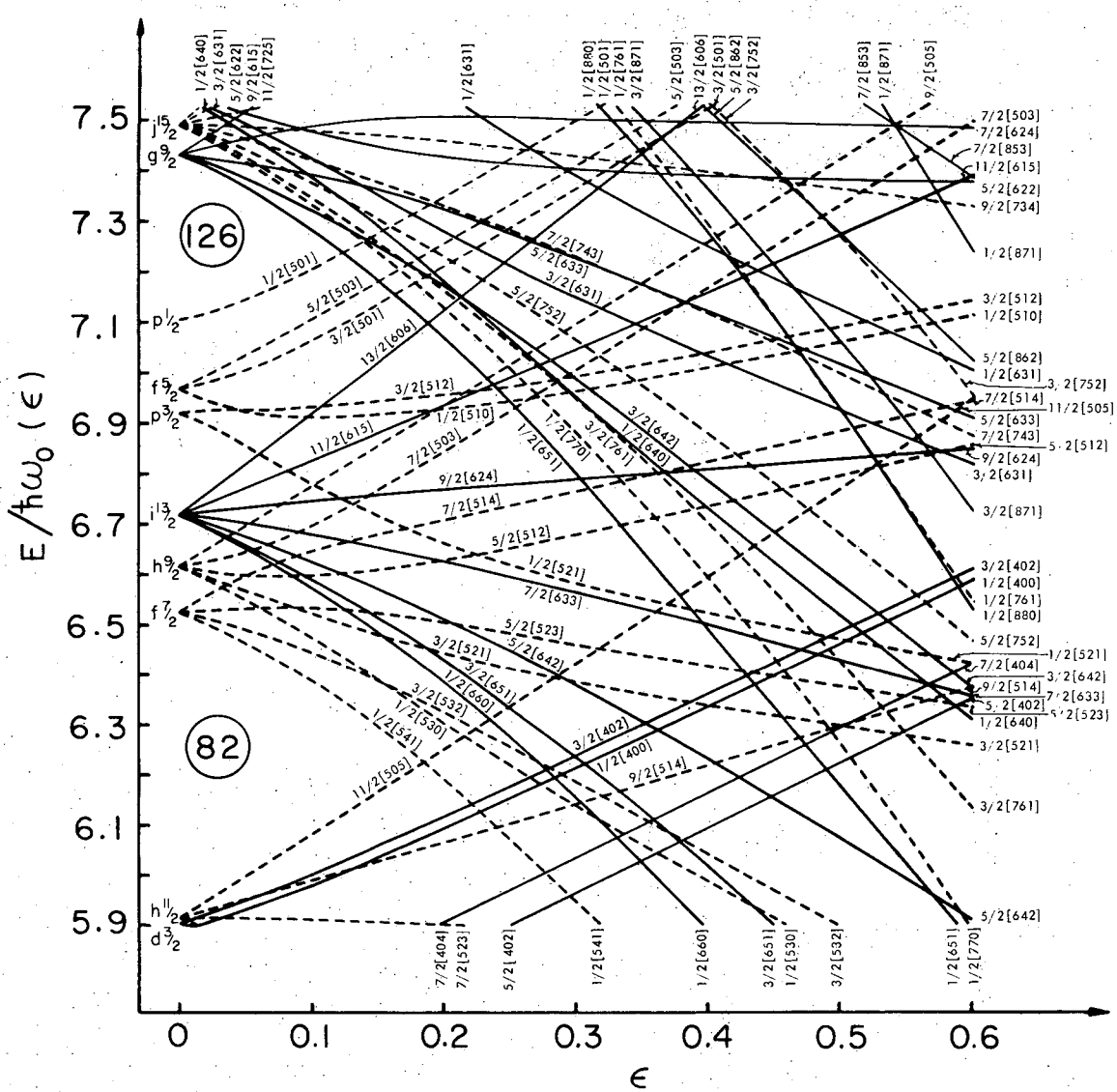

XBL 676-4060

Fig. 9. Nilsson energy diagram for 82 < N < 126.[84] (Note: In this diagram, the deformation parameter ϵ is exactly equal to δ as defined in the text.)

parity orbital, the $i_{\frac{13}{2}}$, between the closed shells 82 and 126. This greatly simplifies the problem, since we immediately expect the Coriolis perturbations affecting the $\frac{9}{2}+[624]$ band in Hf^{177} to arise principally from the other members of the $i_{\frac{13}{2}}$ orbital.

Solution of the Coriolis secular determinant (11a) for the $\frac{9}{2}+[624]$ band of Hf^{177} was first investigated by M. D. Holtz of our laboratory, making use of experimental data in Refs. 20, 24, and 26. In Fig. 10 we summarize the experimental information available on the positive parity states in Hf^{177}. Assuming a deformation $\eta = 4$ for the Hf^{177} nucleus, Holtz was able, with use of the Nilsson energy eigenvalues from Ref. 7, to fit all members of the $K = \frac{9}{2}+$ band and the first two members of the $K = \frac{7}{2}+$ band to within 0.2 keV of experimentally determined energies. Only four parameters were allowed to vary in this initial fit, the Coriolis elements $H^I_{\frac{5}{2},\frac{7}{2}}$, $H^I_{\frac{7}{2},\frac{9}{2}}$, and $H^I_{\frac{9}{2},\frac{11}{2}}$, and (within limits) the assumed quasiparticle energy

$$E^{\frac{9}{2}}_{\frac{9}{2}+[624]} = \sqrt{(\tilde{\varepsilon}_{\frac{9}{2}+[624]} - \lambda)^2 + \Delta^2}$$

for the $\frac{9}{2}+[624]$ Nilsson state. The fit for the preferred deformation $\eta = 5$[27,28] was found by Holtz to be less satisfactory, though still within 3 keV of experiment in all cases. As we will show, the eigenvectors are not particularly sensitive to this sizeable difference in the quality of the fit.

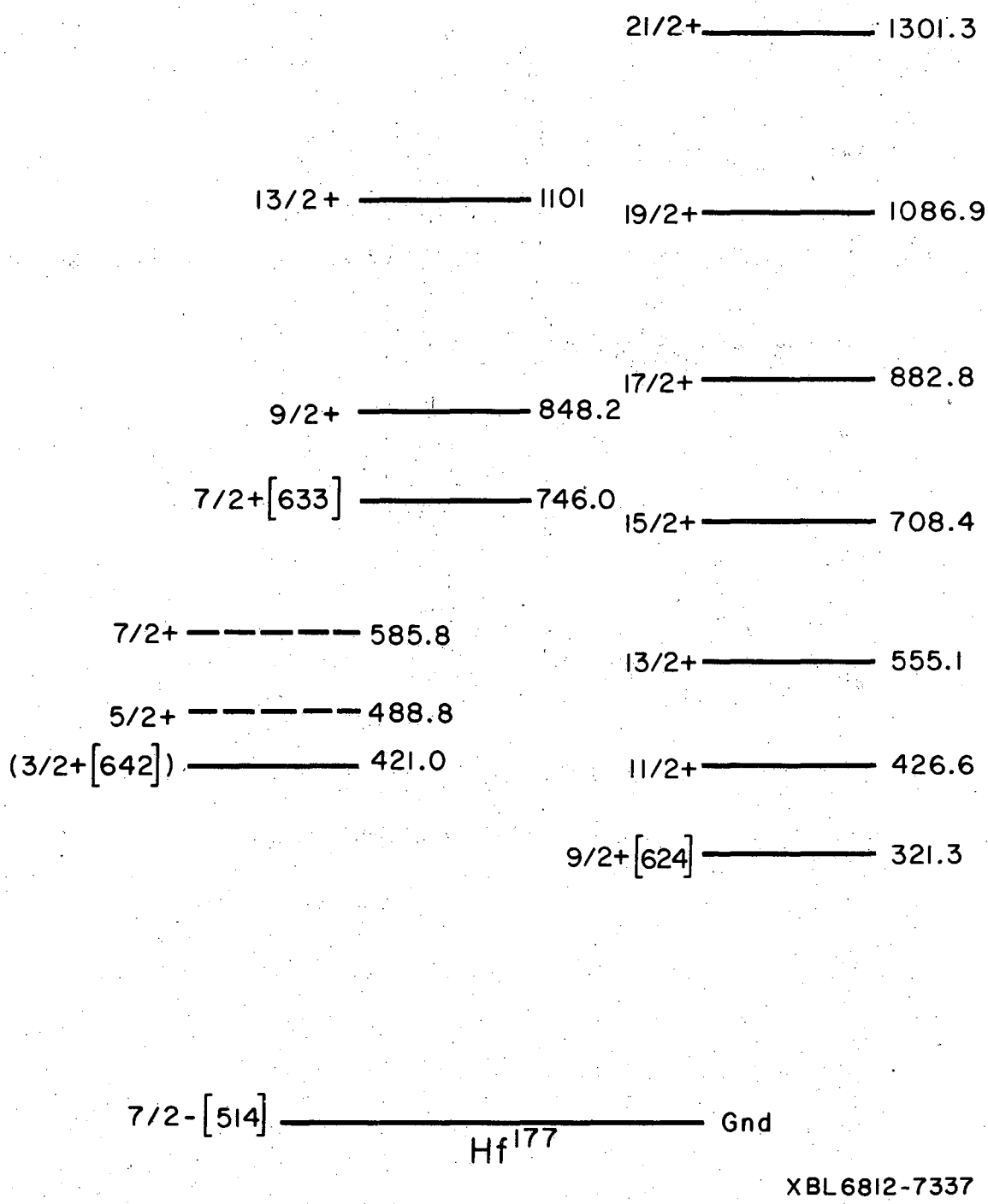

Fig. 10. Positive parity states in Hf^{177}, from Refs. 20, 24, and 26.

We have since repeated the calculations for the $K = \frac{9}{2}+$ band, this time using the new energies $\tilde{\varepsilon}_i$ taken from Ref. 9. Although the Nilsson wave functions used in the initial guess for the Coriolis elements $H^I_{KK'}$ were still taken from Ref. 7, this is not especially important since the program is allowed to vary those elements anyway.

In Table 4 we show the results of the three different fits performed for the Hf^{177} $\frac{9}{2}+$ [624] band. Calculation 1 is from the earlier unpublished data of M. D. Holtz, which data were used to obtain the results published in Ref. 18. It is seen that even with the revised quasiparticle energies (calculation 2) the fit for $\eta = 5$ is considerably poorer than for $\eta = 4$. But if all six off-diagonal elements are allowed to vary, the remarkably good fit denoted (3) is obtained. We must temper our enthusiasm for the quality of this fit somewhat, however, recognizing that one might argue that by varying a total of seven parameters to explain ten experimental bits of data, we could expect to fit nearly anything.

It is possible to counter this criticism somewhat, though not to dispose of it, by considering the credibility of the "best fit" values for the Coriolis matrix elements. Table 5 shows a comparison of the apparent values for those Coriolis matrix elements which were allowed to vary in each of the three cases under consideration. The striking feature of the data is the sizable attenuation of the RPC matrix elements near the Fermi surface. This effect can be partly explained by the pairing reduction factor $(U_1U_2 + V_1V_2)$ for the

Table 4. Experimental and fitted energies for Hf^{177} positive parity rotational bands.

$\Omega\alpha$	Spin	Energy of State (keV)			
		Theoretical Fit*			Experiment
		1	2	3	Refs. 20, 24 and 26
$\frac{7}{2}$ + [633]	$\frac{7}{2}$	746.0	748.6	746.0	746.0
	$\frac{9}{2}$	848.2	844.7	848.2	848.2
	$\frac{13}{2}$	--	1102.1	1101.0	1101.0
$\frac{9}{2}$ + [624]	$\frac{9}{2}$	321.2	321.0	321.3	321.3
	$\frac{11}{2}$	426.7	427.2	426.7	426.6
	$\frac{13}{2}$	555.3	555.9	555.2	555.1
	$\frac{15}{2}$	708.3	708.0	708.1	708.4
	$\frac{17}{2}$	882.8	882.8	883.0	882.8
	$\frac{19}{2}$	1086.6	1083.5	1086.9	1086.9
	$\frac{21}{2}$	1301.5	1304.0	1301.3	1301.3

*(1) $\eta = 4$, ε_i from Ref. 7, $H^I_{\frac{5}{2},\frac{7}{2}}$, $H^I_{\frac{7}{2},\frac{9}{2}}$, $H^I_{\frac{9}{2},\frac{11}{2}}$ and $E_{\frac{9}{2}+[624]}$ variable, $\frac{\hbar^2}{2\mathfrak{J}} = 15.4$ keV; $g(H^I_{\Omega\Omega'}) = 0.13$.

(2) $\eta = 5$, ε_i from Ref. 9, other conditions the same as for (1). $g(H^I_{\Omega\Omega'}) = 39$.

(3) $\eta = 5$, ε_i from Ref. 9, all off-diagonal elements variable, $E_{\frac{9}{2}+[624]}$ variable, $\frac{\hbar}{2\mathfrak{J}} = 15.4$ keV; $g(H^I_{\Omega\Omega'}) = 0.11$.

Table 5. Values of the Coriolis matrix elements $\langle f|j_{\pm}|i\rangle$ used in Hf^{177} $\frac{9}{2}$ + [624] band fits.

	Coriolis $\langle \Omega\pm1|j_{\pm}|\Omega\rangle$ Matrix Element											
	Initialized						Fitted					
Fit #	$\frac{1}{2}\leftrightarrow\frac{3}{2}$	$\frac{3}{2}\leftrightarrow\frac{5}{2}$	$\frac{5}{2}\leftrightarrow\frac{7}{2}$	$\frac{7}{2}\leftrightarrow\frac{9}{2}$	$\frac{9}{2}\leftrightarrow\frac{11}{2}$	$\frac{11}{2}\leftrightarrow\frac{13}{2}$	$\frac{1}{2}\leftrightarrow\frac{3}{2}$	$\frac{3}{2}\leftrightarrow\frac{5}{2}$	$\frac{5}{2}\leftrightarrow\frac{7}{2}$	$\frac{7}{2}\leftrightarrow\frac{9}{2}$	$\frac{9}{2}\leftrightarrow\frac{11}{2}$	$\frac{11}{2}\leftrightarrow\frac{13}{2}$
1	(6.60)	(6.46)	6.20	5.65	4.86	(3.60)			5.36	3.10	2.32	
2	(6.41)	(6.34)	6.09	5.61	4.84	(3.59)			6.01	2.92	2.72	
3	6.41	6.34	6.09	5.61	4.84	3.59	9.29	6.66	5.54	2.84	3.01	4.88

Parentheses indicate matrix element held constant.

Coriolis matrix elements. In cases where the two particle states are very near the Fermi surface or when both states are roughly equidistant above and below the Fermi surface, this factor can become substantially less than unity. For example, we find in the simple pair occupation calculations discussed later that the $\frac{9}{2}+[624] \leftrightarrow \frac{7}{2}+[633]$ factor $(U_1U_2 + V_1V_2)$ should be about 0.56. This number is quite consistent with the 50% "cut" observed for that matrix element in all three cases in Table 5. In general, however, the pair reduction factors for the Coriolis matrix elements are predicted to be near 1.0, and in few cases are they less than 0.9.

It is therefore difficult to account for the equally large cut in the $\frac{9}{2}+[624] \leftrightarrow \frac{11}{2}+[615]$ Coriolis matrix element on the basis of the simple model we have assumed. Arguments that can be advanced favoring the general validity of our approach include: 1) the consistency of the indicated $\frac{7}{2}+ \leftrightarrow \frac{9}{2}+$ matrix element with simple pairing theory and 2) the fact that the cutting of the $\frac{9}{2} \leftrightarrow \frac{11}{2}+$ matrix element is <u>less</u> in the 7-parameter $\eta = 5$ best fit than in either of the other two fits, and thus more consistent with first theoretical expectations. However, it ought also to be noted that we do not possess experimental information on the locations of the low-spin or high-spin members of the $i_{\frac{13}{2}}$ family of states. The Nilsson eigenvalues may not accurately describe the location of those quasiparticle states that are relatively far removed from the Fermi surface, in which case the mixing between various $i_{\frac{13}{2}}$ states may be appreciably different from that we have assumed.

For example, one possible explanation for the surprising increase we observe in Table 5 for the calculated $\frac{1}{2} \leftrightarrow \frac{3}{2}$ and $\frac{11}{2} \leftrightarrow \frac{13}{2}$ matrix elements might be advanced on the premise that deformation shifts occur when a particle is promoted to a strongly upsloping Nilsson orbital, (e.g. $\frac{11}{2}$ + [615], $\frac{13}{2}$ + [606]) or alternatively when a hole is created in a strongly downsloping orbital ($\frac{1}{2}$ + [660], $\frac{3}{2}$ + [651]). Smaller deformation for such configurations would imply a decrease in the amount of inertia and therefore an effective increase in the Coriolis matrix elements. Moreover, it is expected that at lower deformations the energy separation between the indicated states would decrease, thus increasing both the mixing between the states and the size of the Coriolis matrix elements.

A simple model whereby we can estimate the size of the postulated effect might be constructed as follows:

Neglecting pairing, one can assume a Hamiltonian for the even nuclear core that includes a "stiffness" term, H_{C_β}, opposing deformation. We have then

$$H_{C_\beta} = \frac{1}{2} C_\beta (\beta - \beta_{eq})^2$$

where β_{eq} defines the equilibrium quadrupole deformation. Adding this to the energy-dependence of an odd particle in the Ω_i Nilsson orbital above the Fermi level, the energy expression becomes

$$E = \varepsilon_{\Omega_i}(\beta) + \frac{1}{2} C_\beta (\beta - \beta_{eq})^2 \quad .$$

The Nilsson energy, ε, can be Taylor-expanded to include slope:

$$\varepsilon_{\Omega_i}(\beta) = \varepsilon_{\Omega_i}(\beta_{eq}) + S_{\Omega_i}(\beta-\beta_{eq}) + \ldots$$

where

$$S = \left(\frac{\partial\varepsilon}{\partial\beta}\right)_{\beta=\beta_{eq}}$$

and the dependence of the energy on deformation changes may be evaluated. Letting $\chi = (\beta-\beta_{eq})$, we have, for an energy minimum

$$\left(\frac{\partial E}{\partial\chi}\right) = 0 = S_{\Omega_i} + C_\beta\chi$$

and

$$\chi = -\frac{S_\Omega}{C_\beta} \quad .$$

Then to promote a particle from, e.g. the $\frac{9}{2}$ + [624] level of Hf^{177} to the $\frac{13}{2}$ + [606] level, a deformation shift

$$\Delta\chi = \frac{S_{\frac{9}{2}+} - S_{\frac{13}{2}+}}{C_\beta}$$

is expected. Here, $\Delta\chi$ is <u>negative</u> since $S_{\frac{13}{2}+} > S_{\frac{9}{2}+} \cong 0$, and the postulated effect is simply described. Similarly, to promote a particle from the $\frac{1}{2}$ + [660] level to the $\frac{9}{2}$ + [624] level, thereby creating a hole in the former state, we expect a change in deformation

$$\Delta\chi = \frac{S_{\frac{1}{2}+} - S_{\frac{9}{2}+}}{C_\beta} ,$$

again a negative quantity, implying a decrease in deformation.

Using the above expression, we can estimate the change in the Hf^{177} deformation expected for creating a hole in the $\frac{1}{2}+$ [660] state. From Fig. 9 we have

$$S_{\frac{1}{2}+} \cong - \frac{1.2\hbar\omega_0}{0.5} \cong 17 \text{ MeV} .$$

We now require an estimate of the stiffness parameter, C_β. Ideally, one would like to obtain C_β from experimental B(E2) values for exciting the β-vibrational state in neighboring even-even nuclei, since $B(E2) \propto \frac{\hbar}{\sqrt{BC_\beta}}$. Unfortunately, no such information is available for the Hf nuclei, so we must rely upon theoretical estimates of C_β to complete our calculation.

Recent calculations by Tsang, Nilsson, and Swiatecki[29] using a modified Nilsson deformed harmonic oscillator potential indicate C_β for Hf^{176} is 664 MeV. This value is a factor of 10 greater than that predicted by a pure liquid drop model, and perhaps roughly a factor of two larger than the value predicted from the semi-empirical mass formula of Myers and Swiatecki.[30] If we assume the value 664 MeV to be approximately correct, we obtain for the shift in deformation

$$\Delta\chi = \frac{S_{\frac{1}{2}+} - S_{\frac{9}{2}+}}{C_\beta} = -\frac{17}{664} \cong 0.026 \quad ,$$

or only about 10%. However, it appears that the limited experimental data available for C_β in the rare-earth nuclei can deviate substantially from theoretical predictions in many cases.[31] It would therefore not be too surprising if the above estimate were off by a factor of two. But granted even a 20% deformation shift, assuming an approximately linear dependence of moment of inertia $\mathfrak{J}$ on β, it appears at this point that the postulated effect is not sufficient to explain the apparent 50% increase in the $\frac{1}{2} - \frac{3}{2}$ Coriolis matrix element in question. We conclude that, although it is difficult to infer the genesis of the "abnormal" Coriolis matrix elements in Table 5, it is clear that some modifications in the commonly-applied simple theory are necessary to properly explain the observed effects.

We must also refer once more to Fig. 9 and mention that the members of the $g_{\frac{9}{2}}$ orbital were found by Holtz not to significantly affect the results of the fit, so we have omitted those states from our calculations as well. It is expected that they are unimportant, since the Coriolis matrix elements between members of the $g_{\frac{9}{2}}$ and $i_{\frac{13}{2}}$ orbitals are less by at least a factor of six than the analogous intra-orbital matrix elements between members of the $i_{\frac{13}{2}}$ family of states. Naturally, the possibilities that the Nilsson wave functions do not accurately describe the situation, or that pairing theory is deficient in some respect

should not be overlooked. What we have shown is perhaps not as clear as Tables 4 and 5 might indicate. We can only say that it is possible, within the framework of present theory, to obtain rather precise fits to the experimental data with parameters whose values are not unreasonable.

Finally then, in Table 6 we display the quantities of special interest, namely the computed eigenvectors for each of the members of the $K = \frac{9}{2}+$ band in Hf^{177}. As we remarked earlier, the eigenvectors are not particularly sensitive to the details of the energy fit, and we illustrate the point by reproducing for comparison the three sets of eigenvectors obtained for each of the three different calculations described earlier. Although $\mathcal{g}(H^{I}_{\Omega\Omega'})$ varies from 0.11 for (3) to 39 for (2), there is very little difference in the computed wave function coefficients. We have therefore not repeated the calculations we describe in the subsequent pages, but reproduce results obtained earlier[18] using the eigenvectors (1).

The immediate use for the wave function coefficients in Table 6 is in determining the intraband reduced transition strengths B(E2), for the $\frac{9}{2}+$ [624] band in Hf^{177}. The E1 transition moments in Table 2 (with the exception of those leading from the $\frac{9}{2}+$ [624] band head) can be deduced from experimental relative intensities by use of the following forms:[5]

$$B_K(E2)_{I+2\to I} = \frac{15}{32\pi} e^2 Q_0^2 \frac{(I+1-K)(I+1+K)(I+2-K)(I+2+K)}{(I+1)\ (2I+3)\ (I+2)\ (2I+5)} \qquad (12a)$$

for levels depopulated by "crossover" transitions, or

Table 6. Computed wave function coefficients associated with the eigenvectors describing the fitted energies for the Hf^{177} $\frac{9}{2}$ + [624] band.

I	Fit*	Ω, $i_{13/2}$ orbital $\frac{1}{2}$	$\frac{3}{2}$	$\frac{5}{2}$	$\frac{7}{2}$	$\frac{9}{2}$	$\frac{11}{2}$	$\frac{13}{2}$
$\frac{9}{2}$	1	0.004	0.014	0.062	0.255	0.965		
	2	0.002	0.011	0.059	0.244	0.968		
	3	0.003	0.011	0.053	0.234	0.971		
$\frac{11}{2}$	1	0.006	0.029	0.110	0.354	0.916	0.148	
	2	0.004	0.024	0.106	0.343	0.921	0.147	
	3	0.005	0.023	0.094	0.325	0.926	0.165	
$\frac{13}{2}$	1	0.020	0.052	0.159	0.427	0.867	0.194	0.021
	2	0.011	0.041	0.154	0.416	0.874	0.194	0.016
	3	0.017	0.042	0.136	0.340	0.882	0.221	0.025
$\frac{15}{2}$	1	0.017	0.073	0.206	0.477	0.822	0.219	0.033
	2	0.012	0.059	0.202	0.473	0.827	0.219	0.026
	3	0.017	0.059	0.178	0.439	0.839	0.256	0.041
$\frac{17}{2}$	1	0.056	0.113	0.260	0.519	0.770	0.228	0.042
	2	0.031	0.086	0.250	0.518	0.779	0.231	0.033
	3	0.051	0.097	0.227	0.481	0.792	0.274	0.053
$\frac{19}{2}$	1	0.033	0.127	0.298	0.598	0.732	0.235	0.050
	2	0.023	0.104	0.292	0.552	0.736	0.237	0.039
	3	0.035	0.109	0.262	0.510	0.756	0.288	0.065
$\frac{21}{2}$	1	0.119	0.195	0.359	0.570	0.665	0.222	0.051
	2	0.063	0.142	0.339	0.579	0.685	0.232	0.042
	3	0.120	0.183	0.326	0.539	0.688	0.278	0.069

*The results from calculations as follows:
(1) $\eta = 4$, ε_i from Ref. 7, 4 variables, $\mathcal{g} = 0.13$ keV^2. (2) $\eta = 5$, ε_i from Ref. 9, 4 variables, $\mathcal{g} = 39$ keV^2. (3) $\eta = 5$, ε_i from Ref. 9, 9 variables, $\mathcal{g} = 0.11$ keV^2.

$$B_K(E2)_{I+1\to I} = \frac{15}{16\pi} e^2 Q_0^2 \frac{K^2(I+1-K)(I+1+K)}{I(I+1)(2I+3)(I+2)} \tag{12b}$$

for levels giving rise to "cascade" M1-E2 transitions. These expressions, however, assume the purity of the K quantum number. We know from the Coriolis band-fit for the $\frac{9}{2}$ + [624] band that each spin state is in fact characterized by a wave equation containing appreciable mixtures of components for which $K \neq \frac{9}{2}$, which we represent by

$$\Psi = \sum_{K=\frac{1}{2}}^{13/2} a_K \psi_K \ , \ \sum_K a_K^2 = 1 \ .$$

The expressions (12a) and (12b) are now

$$B(E2)_{I+2\to I} = \frac{15}{32\pi} e^2 Q_0^2 \left[\sum_K a_K B_K^{\frac{1}{2}}(E2) \right]^2 \tag{12a'}$$

$$B(E2)_{I+1\to I} = \frac{15}{16\pi} e^2 Q_0^2 \left[\sum_K a_K B_K^{\frac{1}{2}}(E2) \right]^2 \ . \tag{12b'}$$

In deducing the E1 strengths, it is of course preferable to use (12a) and the presumably pure E2 crossover gamma-ray intensity as a reference, and this we have done, except of course for the E1 transitions leading from the $\frac{11}{2}$ + member of the band. Here, the M1-E2 mixing ratio is also required. This quantity can normally be deduced from the crossover-to-cascade gamma-ray intensities and is given by

$$\frac{1}{\delta^2} = \frac{T'(M1)}{T'(E2)} = \frac{\left[\sum_K \sqrt{T_K(E2)}\, a_K c_K\right]^2}{\lambda\left[\sum_K \sqrt{T'_K(E2)}\, a_K b_K\right]^2} - 1$$

where

$$\lambda = \frac{T(E2)}{T'(E2) + T'(M1)} = \frac{\left[\sum_K \sqrt{T_K(E2)}\, a_K c_K\right]^2}{\left\{\left[\sum_K \sqrt{T'_K(E2)}\, a_K b_K\right]^2 + \left[\sum_K \sqrt{T'(M1)}\, a_K b_K\right]^2\right\}}$$

The primed and unprimed quantities refer to cascade and crossover transition probabilities, respectively, and the coefficients a_K, b_K, and c_K are the wave function amplitudes from Table 6 for the I, I-1, and I-2 spin members of the band. All of the transition probabilities are of course for photon emission only.

The experimental crossover-to-cascade ratios λ from decay of Lu^{177m} have thus been used to obtain the plot in Fig. 11, showing the M1-E2 mixing ratios for calculations carried out both with and without considering the effects of Coriolis mixing. Extrapolation to spin $\frac{11}{2}$ yields the desired quantity $1/\delta^2 (= 8.8)$ for that spin state, and allows us to compute the remaining E1 transition strengths. In all the calculations we have assumed the intrinsic quadrupole moment $Q_0 = 6.85$ barns.[32] The experimental errors in Table 2 do not reflect the error in Q_0.

Within the limitations of the rotational model, we have in this way derived "experimental" values for the absolute E1 transition

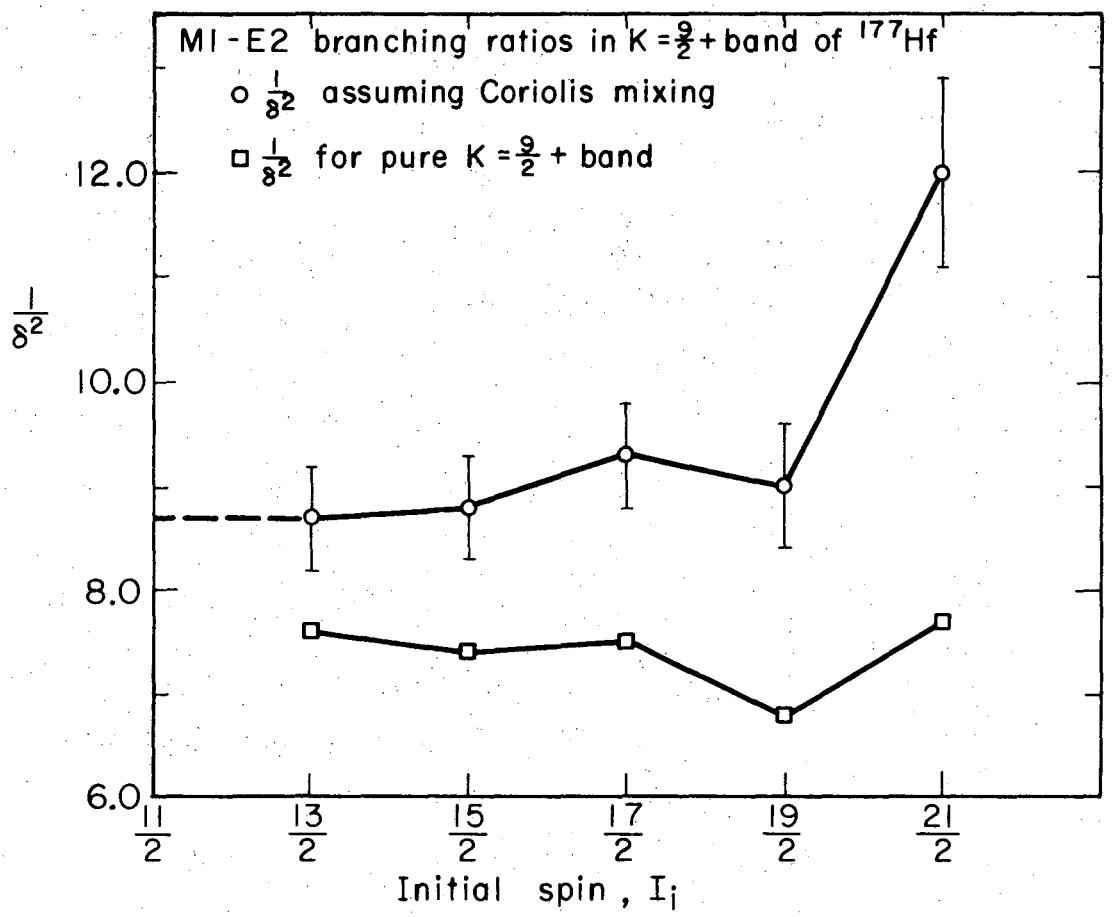

XBL675-3026

Fig. 11. The M1-E2 mixing ratio for cascade transitions in the K = 9/2 + band of Hf^{177}. Derived from crossover-to-cascade ratios of γ-ray intensities from decay of Lu^{177m}.

probabilities of all the $\Delta K = -1$ E1's in Hf^{177} for which we have measured relative γ-ray intensities. Moreover, the magnitude of the various components of differing K mixed with the "$K = \frac{9}{2} + [624]$" rotational band is seen to be large, and it is no longer unexpected that the admixed components might exercise profound influence on the E1 transition moments.

3. <u>A 3-parameter phenomenological interpretation of the Hf^{177} E1 transitions utilizing properly normalized wave functions</u>

We have seen from diagonalization of the full rotational energy matrix including the perturbing Coriolis off-diagonal elements that the simple first-order wave functions of Eq. (11) will not be properly normalized, and if used in a calculation, they therefore cannot be expected to yield correct absolute E1 transition probabilities. A more sophisticated phenomenological treatment of the problem would simply make use of the Nilsson wave amplitudes obtained from the Coriolis matrix diagonalization described in the previous section. The terms which should then be considered up to first order in analysis of the Hf^{177} E1 transitions are the following: (1) the principal $\frac{9}{2} + [624] \rightarrow \frac{7}{2} - [514]$ component, (2) the Coriolis-admixed $(K = \frac{7}{2} +) \rightarrow \frac{7}{2} - [514]$ components and (3) the $\frac{9}{2} + [624] \rightarrow (K = \frac{9}{2} -)$ Coriolis-admixed components. Using the wave amplitudes for the strongly coupled $\frac{7}{2} + [633]\ i_{\frac{13}{2}}$ component listed in Table 6, and estimating by first order perturbation theory the much smaller mixing of $K = \frac{9}{2} -$ components into the $K = \frac{7}{2} - [514]$ ground band, we can modify Eq. (10) to read

$$B(E1) = [M_0(I_i 1\tfrac{9}{2} - 1|I_f\ \tfrac{7}{2})\ a_{\frac{9}{2}}\ b_{\frac{7}{2}} + M_1'(I_i 1\tfrac{7}{2}\ 0\ |I_f\ \tfrac{7}{2})\ a_{\frac{7}{2}}\ b_{\frac{7}{2}}$$
$$+ M_2'(I_i 1\tfrac{9}{2}\ 0|I_f\ \tfrac{9}{2})\ a_{\frac{9}{2}}\ b_{\frac{9}{2}}]^2 \tag{15}$$

where it is assumed

$$\Psi_i \doteq a_{\frac{9}{2}}\ \psi_{\frac{9}{2}+} + a_{\frac{7}{2}}\ \psi_{\frac{7}{2}+} + \ldots,\ \sum_K a_K^2 = 1$$
$$\Psi_f = b_{\frac{7}{2}}\ \psi_{\frac{7}{2}-} + b_{\frac{9}{2}}\ \psi_{\frac{9}{2}-} + \ldots,\ \sum_K b_K^2 = 1\ . \tag{16}$$

The addition to Eq. (10) of a third term is now no longer redundant because it is not valid to assume that $a_{\frac{9}{2}} \cong 1$. If $a_{\frac{9}{2}} \cong 1 \cong b_{\frac{7}{2}}$, then (15) becomes

$$B(E1) \cong \Big[M_0(I_i 1\tfrac{9}{2} - 1|I_f\ \tfrac{7}{2}) + M_1(I_i 1\tfrac{7}{2}\ 0|I_f\ \tfrac{7}{2})$$
$$\times\sqrt{I(I+1) - K_iK_f} + M_2(I_i 1\tfrac{9}{2}\ 0|I_f\ \tfrac{9}{2})\sqrt{I(I+1) - K_fK_i}\Big]^2\ .$$

Using the algebraic forms for Clebsch-Gordan coefficients, this may be reduced to

$$\frac{B(E1)^{\frac{1}{2}}}{(I_i 1\tfrac{9}{2} - 1|I_f\ \tfrac{7}{2})} = (M_0 + \sqrt{2}\,M_2) - \sqrt{2}\,(I_f - \tfrac{5}{2})[M_1 + M_2]$$

for the cases where $\Delta I = -1$, to

$$\frac{B(E1)^{\frac{1}{2}}}{(I_i 1\tfrac{9}{2} - 1|I_f\ \tfrac{7}{2})} = (M_0 + \sqrt{2}\,M_2) + \frac{7\sqrt{2}}{2}\ [M_1 + M_2]$$

for the cases where $\Delta I = 0$, and to

$$\frac{B(E1)^{\frac{1}{2}}}{(I_i 1 \frac{9}{2} - 1 | I_f \frac{7}{2})} = (M_0 + \sqrt{2}\, M_2) + \sqrt{2}\,(I_f + \tfrac{7}{2})\,[M_1 + M_2]$$

for $\Delta I = +1$. We see (cf. Ref. 33) that indeed the reduced E1 moments can be described in terms of two new variables $A_1 = [M_0 + \sqrt{2}\, M_2]$ and $A_2 = [M_1 + M_2]$. Therefore (15) reduces to (10) if the principal $K = \frac{9}{2} + [624]$ and $K = \frac{7}{2} - [514]$ components are assumed to dominate the wave function for all spin states of their respective rotational bands.

The validity of this approximation, and the accuracy of the treatments first applied to the $\Delta K = -1$ E1's in Refs. 13 and 14 can be evaluated by considering the plots in Fig. 12 which compare with experiment the absolute E1 transition strengths predicted by simple theory for the $\Delta I = -1$ and $\Delta I = 0$ E1's in Hf^{177}. (The single $\Delta I = +1$ transition $[I_i = \frac{9}{2} \rightarrow I_f = \frac{11}{2}]$ observed agrees well with the theory, as we have seen from the branching ratios displayed in Fig. 7.) To obtain the parameters M_0 and M_1, the experimental values of B(E1) for the highly-hindered 321-keV $\frac{9}{2}+ \rightarrow \frac{7}{2}-$ transition and for the essentially unhindered 208-keV $\frac{9}{2}+ \rightarrow \frac{9}{2}-$ transition were used in Eq. (10) and the quadratic equations were solved simultaneously to yield the two straight line solutions indicated.

It is seen in Fig. 12 that for spins greater than $\frac{13}{2}$, the calculated absolute transition probabilities exhibit increasing positive disagreement with experiment because of the predominance of the spin-dependent factor in the Coriolis matrix elements $\langle f | I_{\pm} j_{\mp} | i \rangle$.

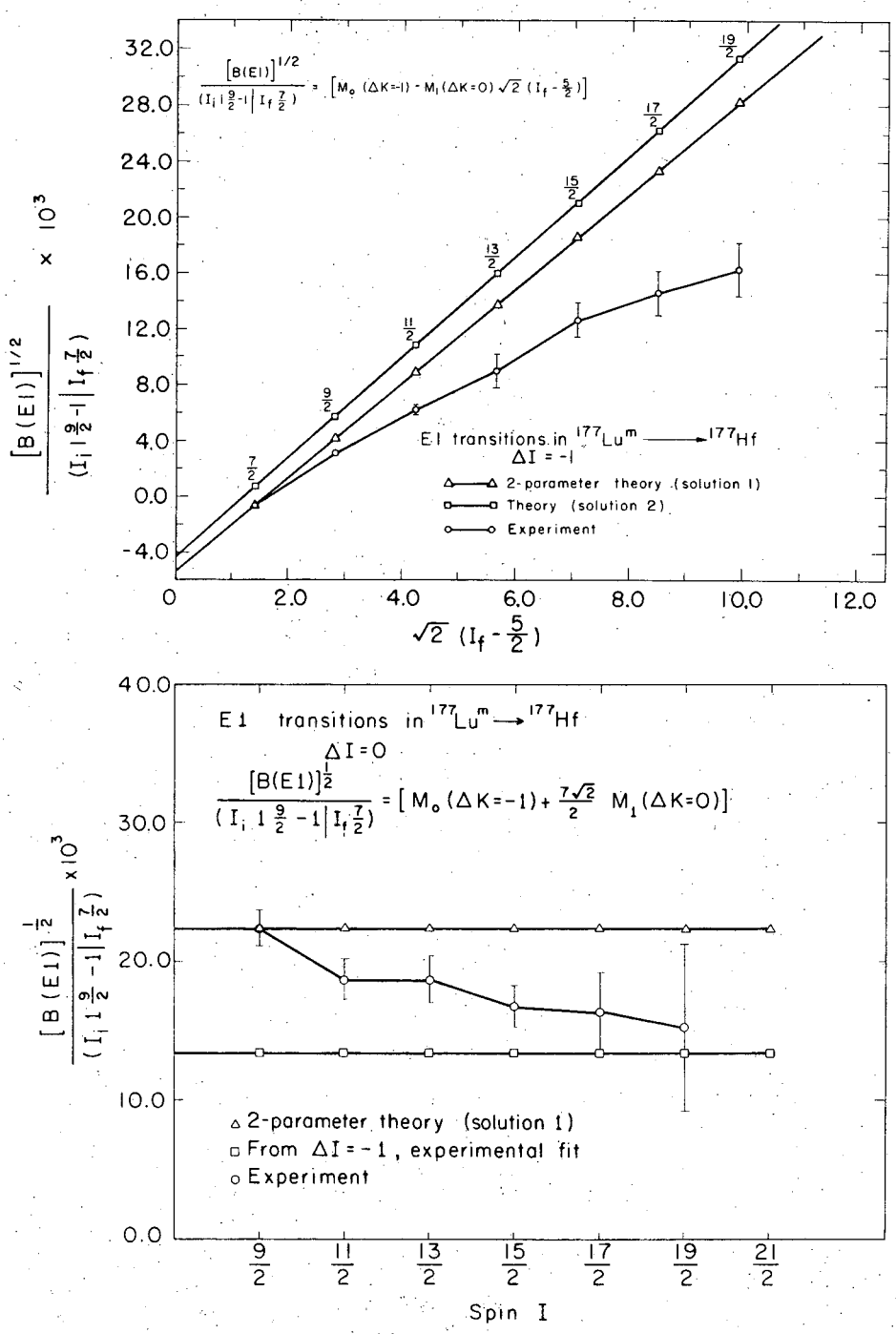

XBL 691-94

Fig. 12. Comparison between experiment and the theory of Refs. 13 and 14 for the absolute E1 transition strengths in Hf^{177}.

The inadequacy of the first-order perturbation treatment is here clearly evident. In fact, interference from $\Delta K = 0$ components is so large in this case as to be comparable in magnitude to the "principal" $\Delta K = -1$ component.

When normalized Coriolis-mixed wave functions (16) from a full matrix diagonalization are used, however, the two parameter theory no longer gives a linear plot and much closer agreement with experiment can be obtained. Moreover, the third term in Eq. (15) can give still better fits to experimental values of the E1 strengths. Figures 13 and 14 show the normalized three parameter fit in comparison with the simple two-parameter fit and with experiment. In this case a system of three equations in three unknowns was obtained from the E1 triad leading from the $\frac{9}{2}+$ band head to the $\frac{7}{2}-$, $\frac{9}{2}-$, and $\frac{11}{2}-$ members of the ground rotational band, and solution of the equations yielded appropriate values for the parameters M_0, M_1, and M_2 in Eq. (15).

The remarkable quality of the fit thus obtained prompted an attempt to account for the observed absolute E1 strengths within the framework of the unified model. In the next section we discuss the results of that study.

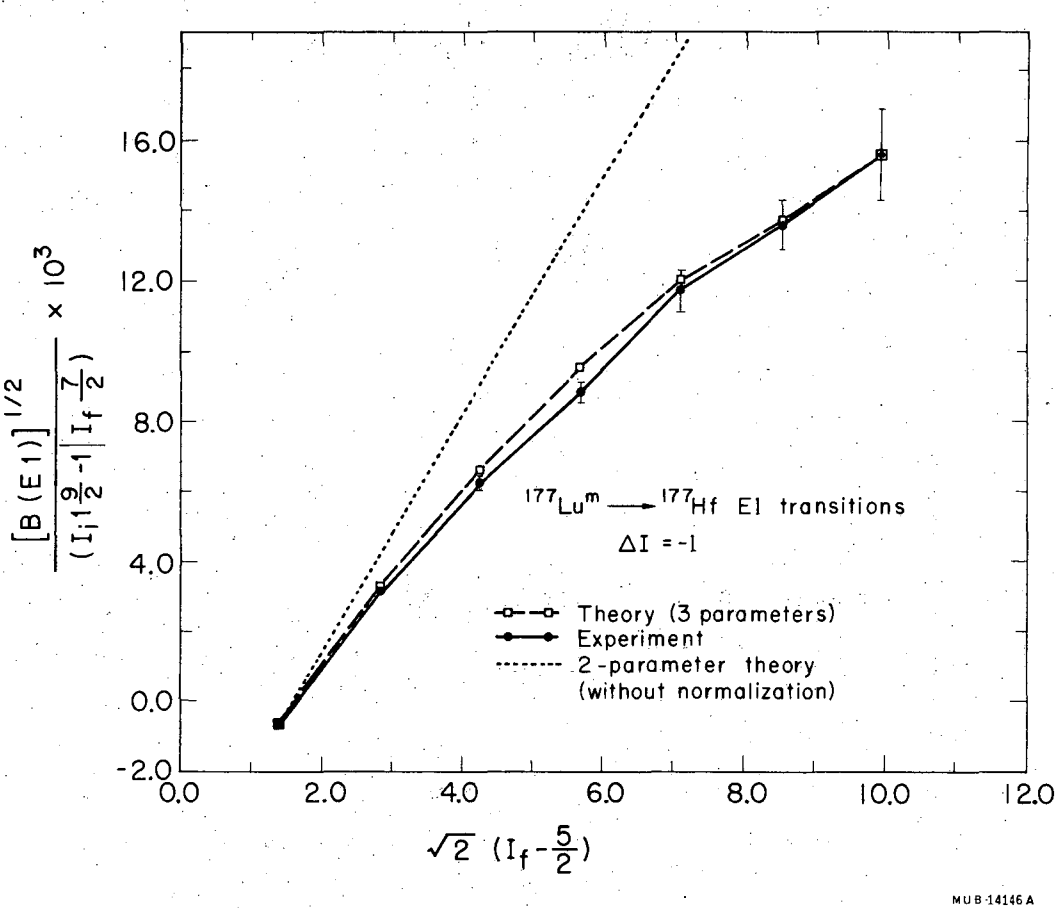

Fig. 13. The normalized three-parameter fit of absolute reduced E1 strengths in Hf^{177} for the $\Delta I = -1$ class of transitions. Theory for $M_0 = 5.5 \times 10^{-3}$, $M_1 = 3.4 \times 10^{-3}$, and $M_2 = -4.5 \times 10^{-4}$.

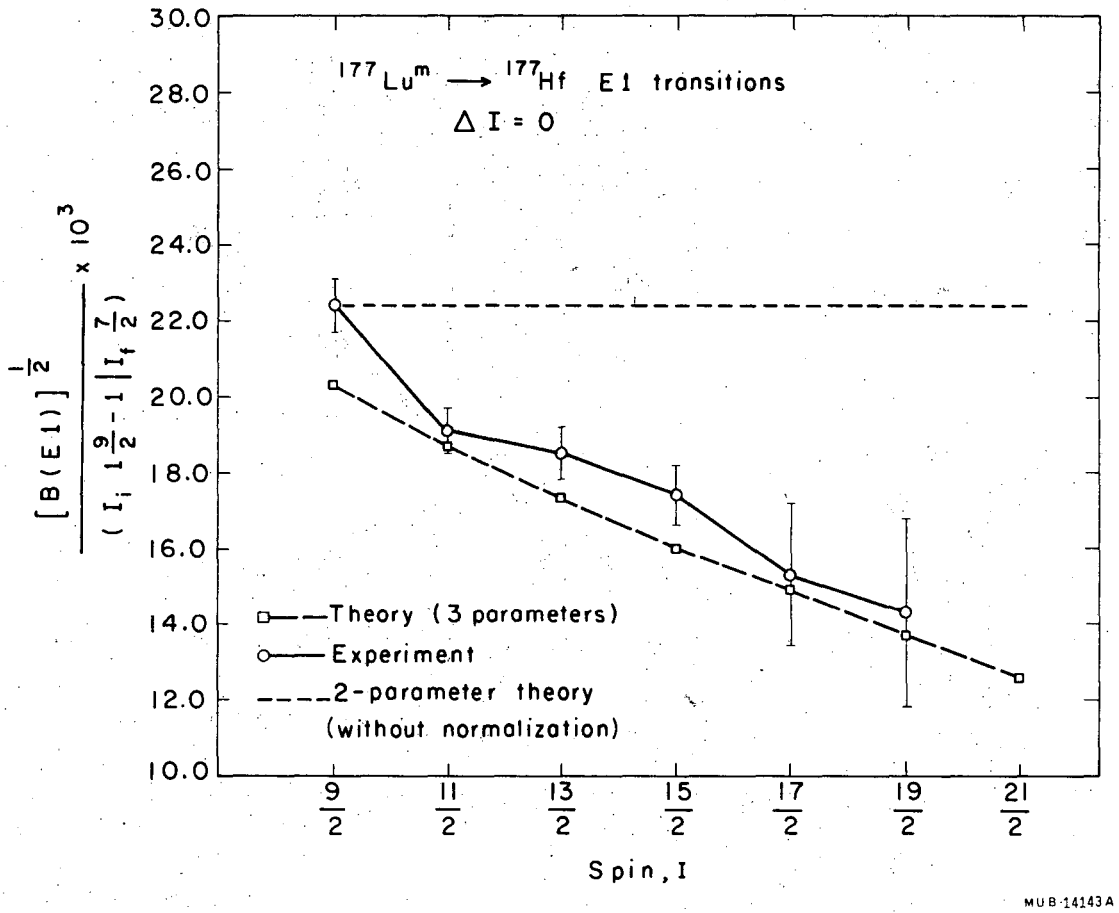

Fig. 14. Normalized three-parameter fit of the reduced E1 strengths in Hf^{177} for the $\Delta I = 0$ class of transitions.

C. $\Delta K = -1$ E1 Transitions in Hf^{177} in the Unified Model

1. Deficiencies of the simple Nilsson model

The 16 E1's in Hf^{177} provide an exceptionally rigorous experimental test for theoretical study of $|\Delta K| = 1$ E1 transitions. As is typical for this class of transition, the Nilsson hindrance factors for the Hf^{177} E1's vary radically from near unity in several cases to $\sim 10^3$ in the case of the 321-keV transition between the $\frac{9}{2}+$ [624] and $\frac{7}{2}-$ [514] band heads. Such wide variation in E1 rates between the same intrinsic states is, as we have seen, not explained by simple transition rate theory.

Moreover, not even a calculation that considers the effects of Coriolis coupling within the framework of the Nilsson model can successfully account for the observed absolute transition rates. The results of such a calculation are displayed in Table 7. The wave functions assumed were of the form (16), where the coefficients for the large wave amplitudes associated with the members of the $i_{\frac{13}{2}}$ single particle state were taken from the matrix diagonalization described earlier. In addition, all other significant components were considered, including those belonging to states (such as $\frac{7}{2}+$ [624]) having very small wave amplitudes, but large unhindered E1 transition moments according to the Nilsson asymptotic selection rules. Cancellation of the two large Coriolis-mixed components $\frac{7}{2}+$ [633] $\rightarrow \frac{7}{2}-$ [514] and $\frac{7}{2}+$ [624] $\rightarrow$ $\frac{7}{2}-$ [514] reduces the calculated magnitude of any Coriolis-mixed E1 components to the order $\sim 10^{-4}$, much too small to account for the large interfering components evidenced by experiment.

Table 7. Calculated partial E1 moments for Hf^{177} E1 transitions. Obtained using the Nilsson model estimates only.

	G(E1)	Estimated E1 transition amplitude
9/2 + [624] → 7/2 - [514]*	2.6×10^{-2}	5.7×10^{-3}
7/2 + [633] → 7/2 - [514]	-1.3×10^{-2}	1.4×10^{-3}
7/2 + [624] → 7/2 - [514]	1.0	-1.4×10^{-3}
7/2 + [613] → 7/2 - [514]	0.137	2.5×10^{-4}
7/2 + [604] → 7/2 - [514]	-0.190	very small
9/2 + [624] → 9/2 - [514]	0.960	-3.8×10^{-4}
9/2 + [624] → 9/2 - [505]	-6.2×10^{-3}	1.2×10^{-4}

*Principal component.

The possible influence of pairing on the $\Delta K = 0$ and $|\Delta K| = 1$ E1 transitions in odd-A nuclei was discussed in Ref. 14. It was found by Vergnes and Rasmussen that inclusion of pair-reduction factors tended to destroy the already relatively good agreement with the Nilsson model of the $\Delta K = 0$ E1's, while aiding the agreement between experiment and theory for the $|\Delta K| = 1$ E1 transitions. But it is clear from Table 7 that in the case of Hf^{177} even the effects of pairing could not repair the situation--there simply is not available a calculated admixed term of sufficient amplitude to account for the effects seen in Figs. 13 and 14.

Vergnes and Rasmussen also proposed, however, that the coupling of single particle states with collective excitations of the even nuclear core ought to be considered in attempting to explain the enhanced E3 transition rates observed in rare earth nuclei. Moreover, the possible influence of such "odd-particle with octupole-phonon" components on $\Delta K = 0$ E1 transitions was first suggested by these authors.

2. <u>The influence of pairing and octupole vibrations on E1 transitions</u>

The strong influence of Coriolis coupling on the Hf^{177} E1's has already been discussed and demonstrated. Recent developments[34-36] in the theoretical interpretation of the collective octupole vibrational mode in deformed nuclei and its apparent application to the interpretation of the $\Delta K = 0$ class of E1 transitions strengths[37,38] suggest a similar important influence on the $\Delta K = 1$ E1 transitions, all of which evidently have relatively large $\Delta K = 0$ Coriolis-mixed components. In the following pages we will show that a detailed calculation carried out within the

framework of the "unified model", and considering the effects of 1) Coriolis coupling; 2) pairing; and 3) octupole vibration-particle coupling on the $\Delta K = -1$ E1 transitions in Hf^{177} is capable of explaining rather well the anomalies of the absolute E1 transition rates in this particular case.[19] We first consider briefly those elements of pairing theory and of the collective model necessary to an understanding of the ensuing discussion.

a. The influence of pairing on the transition rates

The influence of pairing on the multipole transition matrix elements and on the Coriolis coupling matrix elements must be carefully assessed in order to carry out the proposed calculations.

The successful development of the theory of superconductivity[39,40] suggested that, even as electrons in the superconducting state apparently have a tendency to pair into quasi-bound states of equal and opposite momenta, so nucleons near the nuclear Fermi surface may display pair correlation properties of a type similar to those found in superconductors. More specifically, the appearance of a sizeable energy gap between the ground and first excited states of even-even nuclei was considered to be analogous to the energy gap in superconductors arising from the coherent interaction of electrons.[41]

In a semi-quantitative way, we may picture the origin of pairing effects on nuclear electromagnetic transition probabilities as follows: If the nuclear Fermi surface is represented by λ, and the single-particle average field level by ε_i, the Boyolyubov-Valatin transformation

of the Hamiltonian describing a system of interacting particles leads to the new quasi-particle nuclear states, a superposition of the old nuclear "hole" and particle states.[41] The previously completely occupied "Fermi sea" becomes a "vacuum", a modification analogous to that occurring to the Fermi gas of electrons in a crystal lattice when the superconducting state is achieved. The occupation parameters U_i^2 and V_i^2 are then used to denote the probabilities of finding the quasi-particle nuclear state unoccupied or occupied by a pair of nucleons. Transformation from particle and hole states to the new quasi-particle states depends on the particular choice, $U_i = 1$ $(V_i = 0)$ for states above the Fermi surface $(\varepsilon_i > \lambda)$ and $U_i = 0$ $(V_i = 1)$ for states below the Fermi surface. U_i and V_i may be determined from

$$U_i^2 = \frac{1}{2}\left[1 + \frac{\tilde{\varepsilon}_i - \lambda}{E_i}\right]$$

$$V_i^2 = \frac{1}{2}\left[1 - \frac{\tilde{\varepsilon}_i - \lambda}{E_i}\right]$$

which also expresses the normalization condition $U_i^2 + V_i^2 = 1$. E_i is the energy of the quasi-particle state, which is (for ε_i, as usual, relative to the Fermi level λ)

$$E_i = \sqrt{(\tilde{\varepsilon}_i - \lambda) + \Delta^2}$$

where Δ, the nuclear gap is approximately one-half the observed energy gap in even-even nuclei, and is defined by

$$\Delta = G \sum_i U_i V_i$$

G being the pairing force constant. The $\tilde{\varepsilon}_i$ are defined by

$$\tilde{\varepsilon}_i = \varepsilon_i - GV_i^2$$

where ε_i is the average self-consistent field energy of the single particle state i. The pairing force parameters G are usually chosen to be approximately[27]

$$G_P \cong \frac{18}{A} \text{ MeV} \quad \text{for protons and}$$

$$G_N \cong \frac{25}{A} \text{ MeV} \quad \text{for neutrons.}$$

In even-even nuclei the pairing gap manifests itself as an energy difference between the ground and first excited state. Formally, the ground state is considered to be the vacuum state of the quasi-particles, defined by

$$\alpha_i \Psi_0 = 0 \quad .$$

Creation of two quasi-particles produces a new state $\Psi_{1,2} = \alpha_{i_1}^\dagger \alpha_{i_2}^\dagger \Psi_0$ with energy approximately equal to the sum of the two individual quasi-particle state energies:

$$E = E_1 + E_2 = \sqrt{(\tilde{\varepsilon}_1 - \lambda)^2 + \Delta^2} + \sqrt{(\tilde{\varepsilon}_2 - \lambda)^2 + \Delta^2}$$

so that for $\tilde{\varepsilon}_i \cong \tilde{\varepsilon}_2 \cong \lambda$ the minimum excitation energy is 2Δ. For odd nuclei, the situation is different since the vacuum state no longer defines the ground state of the nucleus. Instead, the ground state $\Psi_0 = \alpha^\dagger_{i_1} \Psi_0$ has the energy of the lowest one-quasiparticle state, (i.e. the state with energy closest to λ) and $E_0 \cong \Delta$. The excited states are given by the quasi-particle excitations, and there is no observed energy gap. The energy of the single quasi-particle state is therefore just $E_i = \sqrt{(\tilde{\varepsilon}_i - \lambda)^2 + \Delta^2}$.

The effect of pairing interactions on spherical nuclei was considered in detail by Kisslinger and Sorenson,[42] and of special interest to us is their expression for the influence of pairing on electromagnetic transition probabilities. Here, the one quasi-particle matrix elements of the electromagnetic multipole operators are related to the single-particle matrix elements by

$$\langle \Psi_0^0 \, \alpha_{j_f m_f} | M(\sigma\ell) | \alpha^\dagger_{j_i m_i} \Psi_0^0 \rangle = (U_f U_i - (-1)^T V_f V_i) \langle j_f m_f | M | j_i m_i \rangle \tag{17}$$

where $\sigma = M$ or E corresponding to the magnetic or electric 2^ℓ-pole operator, $\alpha^\dagger_{jm}(\alpha_{jm})$ is the quasi-particle creation (annihilation) operator, and T is 0 or 1, depending upon whether the operator does not or does change sign upon time reversal. The reduced transition strength then becomes

$$B(\sigma\ell) = B_{SP}(\sigma\ell) \, R^2, \quad R = (U_i U_f \pm V_i V_f) \quad .$$

The effect on electromagnetic transition probabilities of the so-called pairing reduction factor R was also considered by Grin,[43] Urin[44] and, more extensively, by Soloviev[45] for the case of deformed nuclei. Vergnes and Rasmussen discussed in some detail the effects of pairing on E1 transitions in odd-A nuclei, and, as we have mentioned, demonstrated the inadequacy of pairing effects alone in attempting to explain anomalies in the E1 rates. The conclusions of Vergnes and Rasmussen were supported in similar studies by Berlovich,[10,46] and Gadetskii and Pyatov.[47] The latter authors, it should be noted, have made detailed calculations employing conventional and projected BCS wave functions, both with and without consideration of the effects of "blocking" (excluding for pair occupation the single-particle orbital) in each case. Nevertheless, they conclude "our calculations have not led to satisfactory agreement between the theoretical and experimental B(E1) values."

Finally, mention should be made of the Ikegami-Udagawa[48] (IU) method of approximating the pair reduction factors for electric gamma-ray transition probabilities with use of experimental data on the odd-even mass difference. Their method, applied originally only to spherical nuclei, is of some interest to the E1 transitions we consider, although the level density in deformed nuclei may cast some doubt on the validity of the assumptions in these cases.

Briefly, the IU method assumes the energy of the lowest quasi-particle state, $E_f = \sqrt{(\varepsilon_f - \lambda)^2 + \Delta^2}$ to be given by $E_f \cong \Delta$, i.e. it is assumed that $\varepsilon_f \cong \lambda$ and that the lowest single particle state

is close to the Fermi surface. The quantity Δ is evaluated from odd-even mass differences[49] where it is assumed $\Delta \cong \frac{1}{2} P_{p(n)}(Z, N)$. Then the hindrance factor R for electric transitions is reduced from the form[48]

$$R = (U_i U_f - V_i V_f)^2 = \frac{1}{2}\left[1 + \frac{(\varepsilon_i - \lambda)(\varepsilon_f + \lambda) - \Delta^2}{E_i E_f}\right] \tag{18}$$

to

$$R = \frac{(E_i - E_f)^2}{4 E_i E_f}\left[\left(\frac{E_i + E_f}{\varepsilon_i - \varepsilon_f}\right)^2 - 1\right] . \tag{19}$$

For transitions to the ground state, where $(\varepsilon_f - \lambda) \cong 0$, this becomes

$$R \cong \frac{1}{2}\frac{E_\gamma}{E_\gamma + \Delta} \tag{20}$$

the form used by Berlovich[46] in applying the method to a study of anomalous E1 transitions. In the calculations we will describe, we have generally used the form (18) to determine the pair reduction factors, though results from (20) are also provided for comparison.

b. <u>The influence of collective motion on E1 transition rates</u>

The theory of collective vibrations in nuclei, first dealt with in quantitative detail by Bohr and Mottelson,[4,5] suggested the interpretation of certain nuclear states as arising from core vibrations of the nuclear matter. In the region of strong permanent nuclear deformation, the quadrupole vibrational modes can be either of two types: 1) those which preserve cylindrical symmetry (β-vibrations) and 2) those which

lead to small excursions from cylindrical symmetry, (γ-vibrations). The theory of quadrupole vibrations has been extended by others to give, in general, a fairly good picture of low-lying states of even parity in heavy nuclei.[50-54]

In addition to these quadrupole vibrational modes the existence of higher-order vibrations was early suggested by Christy and Alder, et al.[55] to explain the systematic occurrence of negative-parity states of excitation less than 1 MeV in the actinide region of deformation.[56,57] The observation of octupole vibrational states in deformed nuclei in both the lanthanide and actinide regions has since become a rather common occurrence, but a quantitative theoretical explanation of the experimental data introduces considerable mathematical difficulty. Lipas and Davidson[58] have treated quantitatively the octupole collective vibrations, simplifying the problem by assuming the occurrence of only the Y_{30} and $Y_{3\pm2}$ harmonic modes, together with the β- and γ-vibrational modes in describing the nuclear shape. Further consideration of the topic has come from Leper,[59] Lipas, et al.,[60] and Vogel.[36]

Recently, Soloviev and co-workers at Dubna have carried out extensive calculations entirely within the framework of their "superfluid" nuclear model, using the method of approximate second quantization.[61-63] The Dubna group has attempted with considerable success to explain the quadrupole and octupole collective vibrational modes at the most fundamental level, i.e. in terms of residual interactions between the individual nucleons. Such interactions give rise not only to pairing correlations, but also to the collective surface vibrations usually

interpreted according to the liquid drop model. Using such a truly microscopic, many-body approach to the nuclear problem, Soloviev has predicted a variety of properties of the nuclei in the lanthanide and actinide regions of deformation.

It is possible, however, by using a phenomenological approach, to treat the problem of non-rotational collective states in a more simple but, for our purposes, quite meaningful way. Donner and Greiner have recently extended further the earlier work of Lipas and Davidson[60] describing the nuclear octupole harmonic oscillations and, using the "dynamic collective theory",[64] have made detailed calculations and predictions concerning the properties of the nuclear octupole states in deformed nuclei.[34] Proceeding entirely within the framework of the collective model, the authors consider the electric dipole transitions in these nuclei to arise from admixtures of the giant dipole resonances into the octupole excitations, and make quantitative estimates of these admixtures and their consequent electric transition rates. We present here the points necessary to our later discussion.

The octupole states are treated using a strong-coupling model which couples the octupole phonons to a spheroidal nucleus. The form of the total Hamiltonian describing the system is:[29]

$$H = H_2 + H_3 + H_{23} + H_{rot} + H_{vib,rot} + H_{cor}$$

where H_2 represents the quadrupole vibrations, H_3 the octupole vibrations, H_{23} the interaction between these two vibrations, H_{rot} the rotational motion of the nucleus, $H_{vib,rot}$ the rotational-vibrational

interaction, and H_{cor} the Coriolis portion of that interaction. The total Hamiltonian is rather complex, but for solution of the unperturbed problem, the octupole energy levels are formed using

$$H_0 = H_2 + H_3 + H_{rot} + \frac{(I_3 - J_3)^2 - \hbar^2}{16\, B_2\, a_{22}^2} \quad .$$

The last term represents the major (diagonal) energy contribution from the rotation-vibration interaction, and removes the degeneracy of the several octupole states characterized by K and J_3, the axial projections of the total and octupole angular momenta, respectively. Four sets of octupole states are predicted, three of them based on a one-phonon octupole vibration superimposed on the 1) ground, 2) β-vibrational, and 3) γ-vibrational states, and the fourth being composed of the two phonon positive parity octupole states. The predicted octupole vibrational bands are further split by the interaction H_{23} which is treated as a perturbation. The reader is referred to Ref. 34 for details of the wave functions and Hamiltonian used.

Of particular interest to our problem are the calculations carried out in Ref. 34 estimating the magnitude of the Coulomb interaction between the giant dipole resonances and the octupole vibrations, since it is this interaction that is presumed to give rise to the collective E1 transitions in the even-even deformed nuclei. Detailed wave functions for the giant dipole resonances have been given by Arenhövel, et al.[65] Since the energy of the giant dipole resonances is ≈ 15 MeV, and the interaction energy is estimated to be ~ 0.74 MeV[34] a first order perturbation treatment is sufficient, and the perturbed

octupole wave functions are

$$\left| \Phi^{IMK}_{n_3 n_{20} n_{22} |K-J_3|} \right\rangle = \left| \Psi^{IMKJ_3}_{n_{30} n_{20} n_{22} |K-J_3|} \right\rangle + \sum \frac{\langle X|W|\Psi \rangle}{E_{n_{20}\sigma} - E_3} \left| X^{IMK}_{n_{20} n_{22} \sigma} \right\rangle \tag{21}$$

where the Ψ are the unperturbed octupole states, X represents the wave function of the giant dipole resonance, W is the Coulomb interaction, the n represent the number of phonons in coordinate space $a_{\ell m}(\ell=1,2,3)$, and σ is the projection of the giant dipole resonance on the symmetry axis. We are concerned with the simplest octupole state, for which $K = 0$, $J_3 = 0$, $n_3 = 1$, $n_{20} = 1$, $n_{22} = 0$ and $\sigma = 0$. Then (21) becomes

$$\left| \Phi^{IM0}_{1100} \right\rangle = \left| \Psi^{IM00}_{1000} \right\rangle + C_0 \left| X^{IM0}_{100} \right\rangle \tag{22}$$

with the giant dipole admixture coefficient given by

$$C_0 = - \frac{\mathcal{K}'(1200|30)}{E_{10} - E_3} \frac{\hbar}{\sqrt{2 B_3 E_3}} \beta_0 \tag{23}$$

for $E_3 = \hbar \sqrt{\frac{C_{30}}{B_3}}$, β_0 the permanent quadrupole deformation parameter, and the coupling constant $\mathcal{K}'$.[34]

Using the dipole operator given by Refs. 64 and 65, the reduced transition strengths for the collective E1 transitions arising from the octupole vibrational states can be calculated with the proper wave

functions of equation (22). In single particle units, the pertinent relation for the $(K_i = 0^- \rightarrow K_f = 0^+)$, $|K_i - J_3| = 0$ class of E1 transitions is:[34]

$$\frac{B(E1)}{B_{SP}(E1)} = 5.74 \times 10^{-2}\ A\ C_0^2\ (I_i 100 | I_f\ 0) \tag{24}$$

where C_0 is given by (23).

Equation (24) provides a useful estimate of the collective E1 transition strengths in even-even deformed nuclei for the most commonly encountered case. If the coupling constant $\mathcal{K}'$ is known,[64,66] the only free parameter is the octupole transition amplitude $\langle a_3 \rangle = \frac{\hbar}{\sqrt{2B_3E_3}}$. It is this parameter that is crucial to the calculations for $\Delta K = 1$ E1 transitions in odd-A nuclei. $\langle a_3 \rangle$ can be determined from

$$B(E3) = [\frac{3}{4\pi}\ Z\ R_0^3 \langle a_3 \rangle\ (3300|00)]^2$$

if B(E3) is experimentally measured by Coulomb excitation, for example, but little data of this type is available, and we have no information on the value of $\langle a_3 \rangle$ for Hf^{176} or Hf^{178}. Consequently, in the calculations we describe, $\langle a_3 \rangle$ is allowed to be a free parameter.

3. <u>Method of calculating absolute $\Delta K = 1$ E1 transition strengths in odd-A deformed nuclei</u>

Before proceeding with the calculation of the Hf^{177} E1 transition strengths, let us review briefly the material we have just presented, and its relevance to the problem.

In section (1) we examined the difficulties encountered when one attempts to calculate the E1 transition moments within the Nilsson model, even when the effects of Coriolis coupling and pairing are considered. The difficulties were not unexpected, however. When viewed from the perspective of the Nilsson model in the light of later developments in the "superconducting" theory of nuclear matter, it was seen in 2a that electric dipole transitions provide a most sensitive test of the adequacy of present nuclear models. Finally, the early suggestion of Vergnes and Rasmussen[14] concerning the possible importance of the octupole vibrations in explaining the anomalies of E1 transitions has recently been followed by calculations which apparently demonstrate the significant influence of octupole vibrational modes on $\Delta K = 0$ E1 transitions in odd-A deformed nuclei.[37,38] These results, coupled with the conclusions we have noted in (I.B.5) have suggested a similar important influence on $|\Delta K| = 1$ E1 transitions, all of which apparently have relatively large $\Delta K = 0$ components.

In our calculations we have adapted the approach of Faessler et al.,[38] while making use of the recent contribution by Donner and Greiner[34] toward the understanding of the E1 transitions originating from octupole vibrational states in deformed even-even nuclei. We use as a starting point the Nilsson model, but include the clearly important Coriolis coupling effects. However, the nucleus is now treated as an assemblage of quasi-particles, and, although we stop short of the microscopic treatment of Soloviev,[62] nevertheless particular attention is given to the quasi-particle states in the vicinity of the Fermi surface.

Finally, the interaction between quasi-particles and nuclear surface vibrations is considered and found to be of critical importance to the success of the calculations.

We begin by writing the Hamiltonian for the odd-quasiparticle system of stable quadrupole deformation and harmonic octupole vibrations. This is

$$H = H_{SP} + H_{coll} + H_{VPC} + H_{RPC}$$

which is a composite in four terms of: 1) the Nilsson Hamiltonian[7]

$$H_{SP} = \frac{1}{2}\hbar\omega_0 \left(-\Delta + r^2\right) - \hbar\omega_0\beta_0 r^2 Y_{20} + C\vec{\ell}\cdot S + D\vec{\ell}^{\,2} \;;$$

and 2) the Hamiltonian describing the collective motions

$$H_{coll} = H_{rot} + H_{vib}$$

which is a sum associated with the single particle coupled to a rotating symmetric top

$$H_{rot} = \frac{\hbar^2}{2\mathcal{J}_0}\left[\left(\vec{I}^{\,2} - I_3^2 - j_3^2\right) + \vec{j}^{\,2}\right]$$

and with the harmonic octupole oscillator

$$H_{vib} = -\frac{\hbar^2}{2B_3}\frac{\partial^2}{\partial a_{30}^2} + \frac{C_{30}}{2}a_{30}^2$$

where B_3 is the nuclear mass parameter and C_{30} is the oscillator

"spring constant"; finally, we have the 3) rotation-particle and 4) vibration-particle coupling interaction Hamiltonians:

$$H_{RPC} = -\frac{\hbar^2}{2\mathcal{J}_0}\left[I_+ j_- + I_- j_+\right]$$

$$H_{VPC} = -\hbar\omega_0\, a_{30}\, r^2\, Y_{30} \quad . \tag{25}$$

In the above, the moment of inertia is given for the spheroid by

$$\mathcal{J}_0 = 3B_2\beta_0^2$$

where B_2 is the mass parameter associated with the permanent quadrupole deformation and β_0 is the deformation parameter mentioned earlier.

The unperturbed wave functions will be of the product form $\Psi = \chi_{part}\phi_{vib}\mathcal{D}_{rot}$ or more explicitly

$$\Psi_0 = \sqrt{\frac{2I+1}{16\pi^2}}\left(\mathcal{D}^I_{MK}\,\chi_{\Omega\alpha} + (-)^{I-\frac{1}{2}}\pi\,\mathcal{D}^K_{M-K}\,\chi_{\Omega\alpha}\right)\Big|\, n_{30}\Big\rangle$$

and will be denoted by

$$\Psi_0 = |I;\Omega\alpha;\, n_{30}\rangle$$

where the $\Omega\alpha$ are the appropriate Nilsson single particle states and n_{30} is the number of octupole phonons with $J_3 = 0$. The octupole oscillator wave functions are conveniently described to first order in second quantization notation as[38]

$$|n_{30}\rangle = \frac{1}{\sqrt{n_{30}!}} \left(\hat{\beta}^{\dagger}_{30}\right)^{n_{30}} |0\rangle + \ldots \tag{27}$$

where $\beta^{\dagger}_{30}$ is the well-known phonon creation operator related to the a_{30} coordinate by

$$a_{30} = \frac{\hbar}{\sqrt{2B_3E_3}} \left(\hat{\beta}_{30} - \hat{\beta}^{\dagger}_{30}\right) .$$

The ground state wave function (27), $|n_3 = 0\rangle$, it will be recalled is just

$$|0\rangle = N_0 \, e^{\frac{-B_3\omega_0}{2\hbar} a^2_{30}} .$$

The wave function (27) gives no contribution in first order to the E1 transition probability, since it describes in no way the nuclear charge polarization required to generate electric dipole transitions.[66-68] The E1 transitions themselves can be interpreted as arising from small admixtures of the giant dipole resonance, as we have seen in (II.C.2.b). For now, we wish only to make use of (27) to find the perturbed wave functions appropriate to calculating the $\Delta K = -1$ E1 transition strengths in the odd-A nucleus Hf^{177}.

To that end, we require the matrix elements coupling the ground quasi-particle state with the excited quasiparticle-phonon state. These elements are[38]

$$\langle I;\ \Omega\alpha_f;\ 1|H_{VPC}|I;\ \Omega\alpha_i;\ 0\rangle = -\hbar\omega\frac{\hbar}{\sqrt{2B_3E_3}}\sum_{\ell_i\ell_f n_i n_f} a_{\ell_i\Lambda_i}a_{\ell_f\Lambda_f}\delta_{\Lambda_i\Lambda_f}$$

$$\times\sqrt{7(2\ell_i+1)/4\pi(2\ell_f+1)}\times(\ell_i 3\Lambda_i 0|\ell_f\Lambda_f)(\ell_i 300|\ell_f 0)$$

$$\times\langle N_f\ell_f|r^2|N_i\ell_i\rangle \quad .$$

Finally, we also need the well-known Coriolis matrix elements coupling states differing in K quantum number by one unit:

$$\langle I;\ \Omega_f\alpha_f;\ 0|H_{RPC}|I;\ \Omega_i\alpha_i;\ 0\rangle = -\frac{\hbar^2}{2\mathcal{J}_0}\ \{[I(I+1) - K_i(K_i+1)]^{\frac{1}{2}}$$

$$\times\delta_{K_f K_i+1}\langle\Omega_f|j_+|\Omega_i\rangle + [I(I+1) - K_i(K_i-1)]^{\frac{1}{2}}$$

$$\times\langle\Omega_f|j_-|\Omega_i\rangle\ \} \quad .$$

We now write the wave functions describing the odd-quasiparticle subjected to both rotational and vibrational perturbations as a sum:

$$\Psi = \Psi_0 + \Psi_{RPC} + \Psi_{VPC}$$

where the subscripts denote the origin of the terms.

In general, the vibration-particle coupling Hamiltonian H_{VPC} will have significant matrix elements between those states having the same K quantum number (and of course opposite parity). This coupling, in effect,

mixes the octupole band of the one state with the other state and vice versa. Although there can also be mixing between particle states for which $\Delta K = \pm 1$, in general these matrix elements will not be more than a few percent of the elements for the $\Delta K = 0$ case. This is because the $K = 1-$ octupole band is higher in energy and the E1 strength from this band is expected to be considerably weaker.[34,38] Therefore we can write the general form of the wave functions (28) giving rise to significant $\Delta K = \pm 1$ E1 components:

$$\Psi = |I;\ \Omega\alpha;\ n=0\rangle + \sum_{(\Omega\pm1),\alpha_i} \mu_{\alpha_i} |I;\ (\Omega\pm1)\alpha_i;\ 0\rangle + \sum_{(\Omega\pm1)\alpha_i} \eta_{\alpha_i} |I;\ (\Omega\pm1)\alpha_i;\ 1\rangle \tag{29}$$

where n is the number of octupole phonons, $\Omega\alpha$ are the appropriate Nilsson single-particle wave functions, $(\Omega \pm 1)\alpha_i$ are the significant Coriolis-mixed wave function components of amplitude μ_{α_i}, and η_i are the amplitudes of the particle-octupole phonon states. The coefficients μ_{α_i} are obtained by a first order perturbation treatment, or by diagonalization of the full Coriolis mixing matrix when necessary. Second order perturbation theory is used to obtain the coefficients η_{α_i} since the H_{VPC} matrix elements are always small compared to the energy of the one-phonon octupole states.

In the notation of (28) and (29) we can, for example, write explicitly the wave function components necessary to calculate the $\Delta K = -1$ Hf^{177} E1 transition probabilities.

The zeroth order wave functions Ψ_0 are

$$\Psi_{0_i} = |I_i;\ \tfrac{9}{2} + [624];\ n_{30} = 0\rangle$$

$$\Psi_{0_f} = |I_f;\ \tfrac{7}{2} - [514];\ n_{30} = 0\rangle \quad .$$

We can write the coefficients μ_i (when they are obtained by first order perturbation) for mixing of $(\Omega = \frac{7}{2}+)$ components into the $\frac{9}{2} + [624]$ band as:

$$\mu_{\alpha_i} = -\frac{\hbar^2}{2\mathcal{J}} R' \frac{\langle I_i;\ (\Omega_i = \frac{7}{2}+)\alpha_i;\ 0|I_+ j_-|I_i;\ \frac{9}{2} + [624];\ 0\rangle}{\left(E_{\frac{9}{2}+[624]} - E_{\frac{7}{2}+\alpha}\right)} \quad . \tag{30}$$

The coefficients η_{α_i} in the case of second-order mixing of the octupole band of the $\frac{7}{2} - [514]$ (ground) state into the initial $\frac{9}{2} + [624]$ band are given by:

$$\eta_{\alpha_i} = -\frac{\hbar^2}{2\mathcal{J}} R' \frac{\langle I_i;\ (\Omega_i = \frac{7}{2}+)\alpha_i;\ 0|I_+ j_-|I_i;\ \frac{9}{2} + [624];\ 0\rangle}{\left(E_{\frac{9}{2}+[624]} - E_{\frac{7}{2}+\alpha_i}\right)}$$

$$\times R \frac{\langle I_i;\ \frac{7}{2} - [514];\ n_{30} = 1|H_{VPC}|I_i;\ (\frac{7}{2}+)\ \alpha_i;\ n_{30} = 0\rangle}{E_{\frac{9}{2}+[624]} - [E_{\frac{7}{2}-[514]} + E_3]} \tag{31}$$

where the pair reduction factors $R' = (U_1U_2 + V_1V_2)$ and $R = (U_1U_2 - V_1V_2)$ refer to the Coriolis and vibration-particle matrix elements, respectively.

The expression giving the total E1 transition strength for the Hf^{177} transitions can now be written. We introduce for clarity the following expressions for the initial and final nuclear states:

$$|i\rangle = A_0|I;\ \tfrac{9}{2} + [624];\ 0\rangle + \sum_{\Omega_i}\sum_{\alpha_i} \mu_{\Omega_i\alpha_i}|I;\ (\Omega_i+)\alpha_i;\ 0\rangle + \sum_{\Omega_i}\sum_{\alpha_i} \eta_{\Omega_i\alpha_i}|I;\ (\Omega_i-)\alpha_i;\ 1\rangle \tag{32a}$$

$$\langle f| = B_0\langle I;\ \tfrac{7}{2} - [514];\ 0| + \sum_{\Omega_f}\sum_{\alpha_f} \langle I;\ (\Omega_f-)\alpha_f;\ 0| + \sum_{\Omega_f}\sum_{\alpha_f} \eta_{\Omega_f\alpha_f}\langle I;\ (\Omega_f+)\alpha_f;\ 1| \ . \tag{32b}$$

The total reduced transition strength will be a sum of quasi-particle and collective components. The quasi-particle portion is obtained from Eq. (9) and with constants appropriate to Hf^{177} reduces to

$$B_{qp}(E1) = 0.320[A_0B_0G_0(E1)R_0(I_i 1\tfrac{9}{2} - 1|I_f\ \tfrac{7}{2}) + \sum_{\Omega_i\alpha_i}\sum_{\Omega_f\alpha_f} \mu_{\Omega_i\alpha_i}\mu_{\Omega_f\alpha_f}G_{if}(E1)R_{\alpha_i\alpha_f}(I_i 1K_i\Delta K|I_fK_f)]^2 \tag{33}$$

while the collective part is given by[34,38]

$$B_{coll}(E1) = 0.906 \left[\sum_{\Omega_i \alpha_i} \sum_{\Omega_f \alpha_f} \left(\eta_{\Omega_i \alpha_i} + \eta_{\Omega_f \alpha_f} \right) \mu_{\Omega_i \alpha_i} \mu_{\Omega_f \alpha_f} \, C_0 \right.$$

$$\left. \times \, (I_i 1 K_i 0 | I_f K_f) \right]^2 . \tag{34}$$

In order that we may add the E1 amplitudes, we normalize the collective portion and the total reduced strength becomes:

$$B_{total}(E1) = 0.320[B_{qp}(E1) \pm 8.0 \, B_{coll}(E1)]^2 . \tag{35}$$

The uncertainty in sign results from our lack of knowledge about the phase relation between the quasi-particles and octupole phonon. Though we have no reason to prefer one phase over the other, we find that the positive sign in (35) gives results in good agreement with experiment, while the negative sign does not.

Using the wave functions (32) and the general form (35), we have calculated the reduced transition probabilities for all the E1 transitions in Hf^{177}. The constants in (33) and (34) assume the nuclear charge radius $R = 1.2A^{\frac{1}{3}}$ Fermi, and the permanent quadrupole deformation $\eta = 5$. As before, the rotational constant $\frac{\hbar^2}{2\mathcal{J}_0}$ is taken to be 15.4 keV throughout. For each set of calculations, a single value of $\langle a_3 \rangle$, the octupole transition amplitude, was chosen to optimize the results, where $\frac{\hbar}{\sqrt{2B_3E_3}}$ is related to C_0 and to the octupole-particle coupling constant χ' by Eq. (23). We have taken $E_3 = 1.2$ MeV. The semi-empirical

pairing reduction factors $R_{\alpha_i \alpha_f}$ have been calculated using the form (18), invoking appropriate constraints on the location of the Fermi level λ as indicated by experimental data for Hf^{177}. The average single particle field energies ε_i from Ref. 9 have been used to approximate $\tilde{\varepsilon}_i$, and the gap parameter Δ has been taken to be 0.60 MeV. The pertinent wave function coefficients were obtained by a quadratic interpolation between $\eta = 2$, 4 and 6 using the Nilsson coefficients in Ref. 7.

4. Results of calculations

Table 8 shows the results of our calculations for the absolute E1 transition rates in the nucleus Hf^{177}. Also shown for comparison are the values of B(E1) obtained using the three-parameter phenomonological treatment described earlier. Absolute values of B(E1) calculated with an appropriate choice of $\langle a_3 \rangle$ in several cases of interest are displayed. Column 1 (NC) of the "microscopic theory" shows the results obtained when reasonable assumptions with regard to Coriolis mixing and pairing are taken into account and the calculations are performed within the Nilsson model, but no octupole mixing is assumed. There is clearly little relation between these results and experiment. Columns 2 and 3 (NCO and NCO') show the results for a calculation similar to that represented in Column 1, but with inclusion of the octupole-particle coupling influence. The results labeled NCO are obtained when the Ikegami-Udagawa approximation for R is assumed valid, and $\lambda \cong \tilde{\varepsilon}_{\frac{7}{2}-[514]}$. In order to give agreement with experiment for the

Table 8. Theoretical reduced E1 transition strengths for Hf^{177}.

initial spin K=9/2+	final spin K=7/2-	reduced strength B(E1) (MeV-fm^3) × 10^5					
		3-parameter fit	microscopic theory				experiment
			NC[a]	NCO[b]	NCO'[c]	NCOBCS[d]	
9/2	7/2	0.034	3.4	0.031	0.038	0.034	0.034(4)
9/2	9/2	7.5	0.74	10.0	6.3	2.4	9.0 (6)
9/2	11/2	3.5	0.05	6.5	3.9	1.6	3.1(2)
11/2	9/2	0.69	2.1	0.69	0.42	0.70	0.66(5)
11/2	11/2	9.7	0.87	12.4	7.8	2.9	10.3(7)
11/2	13/2	7.6	0.06	11.5	6.9	3.1	
13/2	11/2	2.6	1.3	3.5	2.3	2.3	2.32(13)
13/2	13/2	10.1	0.77	11.9	7.4	2.8	11.6(9)
15/2	13/2	5.0	0.74	7.0	4.6	4.4	4.3(3)
15/2	15/2	9.7	0.59	10.4	6.4	2.3	11.5(1.3)
17/2	15/2	7.3	0.34	10.7	7.2	6.8	7.0(7)
17/2	17/2	8.9	0.40	8.6	5.2	1.9	9.4(2.4)
19/2	17/2	8.2	0.14	13.6	9.2	9.1	8.9(9)
19/2	19/2	7.9	0.24	6.8	4.0	1.4	8.6(2.9)
21/2	19/2	11.0	0.01	16.3	11.2	11.8	11.0(2.0)
21/2	21/2	6.9	0.10	5.1	2.9	0.93	

[a]Assumes $\lambda = \tilde{\varepsilon}_{7/2-[514]}$, $\langle a_3 \rangle = 0$, and $R_0 = (U_{9/2+[624]}U_{7/2-[514]} - V_{9/2+[624]}V_{7/2-[514]}) = 0.42$.

[b]$\lambda = \tilde{\varepsilon}_{7/2-[514]}$, $\langle a_3 \rangle = 0.180$, $R_0 = 0.42$.

[c]$\lambda = \tilde{\varepsilon}_{7/2-[514]} + 60$ keV, $\langle a_3 \rangle = 0.142$, $R_0 = 0.34$.

[d]$\lambda = \tilde{\varepsilon}_{7/2-[514]} + 70$ keV, BCS solution, $\langle a_3 \rangle = 0.142$, $R_0 = 0.16$.

highly hindered 321-keV E1, $\langle a_3 \rangle$ must be adjusted to 0.170. However, the apparent value R_0 indicated by the three-parameter fit of data (Figs. 13 and 14) is ≈ 0.34. In the column labeled NCO' therefore we show the results for $\lambda \cong (\tilde{\varepsilon}_{\frac{7}{2} - [514]} + 60)$ keV, $R_0 = 0.34$, and $\langle a_3 \rangle = 0.142$. Finally, in column NCOBCS we include a tabulation of results obtained using pair reduction factors calculated by Vergnes and Rasmussen[14] from a solution of the BCS wave functions for $N = 105$.

The values B(E1) labeled NCO and NCO' obtained using semi-empirical pair reduction factors are within a factor of two of experimentally derived values for all fourteen of the observed Hf^{177} E1 transitions. Moreover, the strengths predicted for the unobserved 17.2- and 41.0-keV transitions indicate that indeed their gamma-ray intensities should be below the detection limit of presently available systems. The agreement with experiment using the BCS pair reduction factors, though still within an order of magnitude for all cases, is somewhat poorer because the orbital energies $\tilde{\varepsilon}_{\Omega\alpha}$ differ from the best values for this particular nucleus, and this BCS solution predicts $R_0 = 0.16$.

In summary, although more accurate knowledge of the pairing reduction factors and of the collective strengths B(E1) and B(E3) in odd-mass nuclei is essential to confirm the validity of our treatment, the results of our calculations indicate that the theoretical basis for the quatitative interpretation of E1 transitions in odd-mass, deformed nuclei is established.

5. Discussion

Because of the uniquely abundant information on $\Delta K = 1$ E1 transitions (and therefore on nuclear structure) provided by the nucleus Hf^{177}, we shall devote essentially all of the ensuing discussion to a careful consideration of the significance and reliability of the results we have obtained in our calculations for that nucleus, and to a detailed assessment of the presumed nuclear parameters that have produced those results. The independent thesis work of Piepenbring[69] has recently proposed the general validity of an octupole vibration-particle coupling model in interpreting $\Delta K = 1$ E1 transitions as well as K-forbidden E1 transitions in odd-A deformed nuclei; therefore we will not belabor the point by extending our calculations to other cases for which extensive experimental data are not available, though we shall discuss some very important differences between our assumptions and those of Piepenbring.

To extract maximum information from the single experimental case for which excellent data are available, it is of course necessary to consider carefully the various parameters involved in the calculations, and the results they yield within the model we have chosen. It is, first of all, interesting in this regard to consider the various components contributing to the total E1 transition strengths. Counting both collective and single-particle components a total of some 35 terms has been considered, of which perhaps 10-15 (depending on the spin) are found to be of major significance.

It is evident that the total E1 transition moments are rather complicated mixtures of several components. Some of the components we

considered are of course small, and particularly at low spins, do not contribute significantly to the E1 transition strength. In general, the experimental E1 transition strengths may be considered to arise from three sources:

(i) single-particle components having large wave amplitudes but small G(E1) values in the Nilsson model, either because the wave functions do not overlap appreciably, or more frequently because they have $\Omega_i\alpha_i \rightarrow \Omega_f\alpha_f$ transition amplitudes of opposite phase, e.g., the principal single particle component $\frac{9}{2}+[624] \rightarrow \frac{7}{2}-[514]$ and the large Coriolis mixed component $\frac{7}{2}+[633] \rightarrow \frac{7}{2}-[514]$;

(ii) single-particle components having small wave amplitudes, but large allowed E1 matrix elements; e.g., $\frac{9}{2}+[624] \rightarrow \frac{9}{2}-[514]$, $\frac{7}{2}+[624] \rightarrow \frac{7}{2}-[514]$;

(iii) collective octupole components arising from the vibration-particle coupling, H_{VPC}. The results of our calculations show that these terms, introduced via the $\Delta K = 0$ Coriolis-mixed particle components, dominate the $\Delta K = 0$ contributions to the total E1 strength.

The complexity of the situation is perhaps best illustrated by comparing the values for the three parameters M_0, M_1, and M_2 used in the experimental fit with the various contributing terms calculated from the theoretical model. The results of such a comparison are shown in Table 9 for the calculations assuming $\lambda = (\tilde{\varepsilon}_{\frac{7}{2}-[514]} + 60)$ keV and $R_0 = 0.34$. Since the parameters M_0, M_1, and M_2 were adjusted using the experimental strengths of the three E1 transitions leading from the $\frac{9}{2}+[624]$ band head, the calculated values are shown as they

Table 9. Calculated contributions to the experimentally derived parameters M_0, M_1 and M_2 (for $\frac{9}{2}+ \rightarrow \frac{9}{2}-$ transition) for Hf^{177} E1 transitions.

initial band	final band	octupole phonons n_i	n_f	mixing coeff. product[a]	$(U_iU_f-V_iV_f)$	E1 matrix element[b]	product
9/2+[624]	7/2-[514]	0	0	0.96	0.34	1.7×10^{-2}	5.5×10^{-3}
						Experimental	$M_0=5.5\times10^{-3}$
7/2+[633]	7/2-[514]	0	0	0.25	-0.57	-8.3×10^{-3}	1.2×10^{-3}
"	"	1	0	-5.1×10^{-2}		-7.3×10^{-2}	3.7×10^{-3}
"	"	0	1	-8.9×10^{-2}		-7.3×10^{-2}	6.5×10^{-3}
7/2+[624]	"	0	0	-4.4×10^{-3}	0.64	0.56	-1.6×10^{-3}
"	"	1	0	1.7×10^{-3}		-7.3×10^{-2}	-1.2×10^{-4}
"	"	0	1	3.0×10^{-3}		-7.3×10^{-2}	-2.2×10^{-4}
7/2+[613]	"	0	0	6.4×10^{-3}	0.64	6.2×10^{-2}	2.5×10^{-4}
"	"	1	0	8.8×10^{-4}		-7.3×10^{-2}	-6.4×10^{-5}
"	"	0	1	1.5×10^{-3}		-7.3×10^{-2}	-1.0×10^{-4}
							Sum=0.96×10^{-2}
				Experimental	$\sqrt{I_i(I_i-1)-K_i(K_i-1)}$	$M_1=3$	$M_1=1.0\times10^{-2}$
9/2+[624]	9/2-[505]	0	0	6.3×10^{-2}	0.87	-3.4×10^{-3}	-1.9×10^{-4}
"	"	1	0	7.5×10^{-3}		-7.3×10^{-2}	-5.5×10^{-4}
"	"	0	1	1.3×10^{-2}		-7.3×10^{-2}	-9.5×10^{-4}
"	9/2-[514]	0	0	-3.5×10^{-3}	-0.31	0.54	5.9×10^{-4}
"	"	1	0	-7.9×10^{-4}		-7.3×10^{-2}	5.8×10^{-5}
"	"	0	1	-1.4×10^{-3}		-7.3×10^{-2}	1.0×10^{-4}
							Sum=-0.94×10^{-3}
				Experimental	$\sqrt{I_f(I_f+1)-K_f(K_f+1)}$	$M_2=3$	$M_2=-1.3\times10^{-3}$

[a]Represents the wave function coefficient product for the indicated initial and final particle or particle-phonon states.

[b]For particle components, $\sqrt{3/4\pi}\, e_{eff}(\hbar/M\omega_0)^{1/2}G(E1)$; for collective components, derived from Eq. (1). We have assumed $e_{eff}=-(Ze/A)$.

apply to one particular transition, the $\frac{9}{2}+ \rightarrow \frac{9}{2}-$ 208-keV E1, for which all first-order Coriolis-mixed components can contribute to the total E1 strength. Despite the fairly large number of terms of first or second order magnitude which apparently are important already at such low spin, the results are seemingly unambiguous. Particularly significant is the fact that the relative phases of the parameters M_0, M_1, M_2 are correctly predicted. Moreover, the results are not merely the consequence of chance cancellation among a series of large terms of varying phase. Rather, the collective octupole E1 components between the $|\frac{7}{2}+ [633]; n = 0, 1\rangle$ and $\langle\frac{7}{2}- [514]; n = 1, 0|$ particle-phonon states are seen to dominate the Coriolis-mixed M_1 term. Although the zero-phonon single particle components, as we have shown (cf. Table 7), nearly cancel one another, the collective strength provides a clear explanation of the large Coriolis-mixed E1 matrix elements indicated in the earlier phenomenological treatments of Refs. 13 and 14. Finally, the proper prediction of both the phase and the magnitude of the smaller M_2 parameter provides convincing evidence for the validity of the approach we have chosen for our calculations.

However, the relative simplicity of the situation for transitions from the lowest spin member of the $\frac{9}{2}+$ [624] band deteriorates with increasing rotational energy. As Table 9 shows, the discrepancy between experiment and theory grows with increasing spin, until at high spins a factor of two disagreement can be seen in some instances. Table 10 shows a comparison of the important terms contributing to the total reduced E1 moment for the $\frac{9}{2}+ \rightarrow \frac{9}{2}-$ E1 transition and for the

Table 10. Theoretical partial reduced E1 moments for Hf^{177}; $I_i = I_f = \frac{9}{2}$ and $I_i = I_f = \frac{21}{2}$.*

Nilsson States $\Omega\alpha_i$	$\Omega\alpha_f$	Octupole phonons n_i	n_f	Partial E1 Amplitudes, $B^{\frac{1}{2}}(E1)(\times 10^3)$ $I = \frac{9}{2}$	$I = \frac{21}{2}$
"Principal" Component					
$\frac{9}{2}$ + [624]	$\frac{7}{2}$ - [514]	0	0	2.34	2.27
Second order S.P. Components					
$\frac{11}{2}$ + [615]	$\frac{9}{2}$ - [514]	0	0	0.	-0.14
	$\frac{9}{2}$ - [505]	0	0	0.	0.27
$\frac{11}{2}$ + [606]	$\frac{9}{2}$ - [505]	0	0	0.	0.09
$\frac{7}{2}$ + [633]	$\frac{9}{2}$ - [514]	0	0	0.05	0.49
	$\frac{5}{2}$ - [532]	0	0	-0.07	-0.50
	$\frac{5}{2}$ - [523]	0	0	-0.47	-3.03
	$\frac{5}{2}$ - [512]	0	0	0.18	1.14
$\frac{7}{2}$ + [624]	$\frac{9}{2}$ - [505]	0	0	-0.01	-0.11
	$\frac{5}{2}$ - [523]	0	0	0.03	0.25
$\frac{7}{2}$ + [613]	$\frac{5}{2}$ - [512]	0	0	-0.06	-0.60
$\frac{5}{2}$ + [642]	$\frac{7}{2}$ - [514]	0	0	0.05	0.32
$\frac{5}{2}$ + [633]	$\frac{7}{2}$ - [514]	0	0	-0.03	-0.09

(continued)

Table 10. Continued

Nilsson States $\Omega\alpha_i$	$\Omega\alpha_f$	Octupole phonons n_i	n_f	Partial E1 Amplitudes, $B^{\frac{1}{2}}(E1)(\times 10^3)$ $I = \frac{9}{2}$	$I = \frac{21}{2}$
S.P. Components with Collective Enhancement					
$\frac{9}{2}$ + [624]	$\frac{9}{2}$ - [514]	0	0	0.52	0.55
		1	0	0.05	0.05
		0	1	0.10	0.10
	$\frac{9}{2}$ - [505]	0	0	-0.17	-0.16
		1	0	-0.50	-0.48
		0	1	-0.86	-0.83
$\frac{7}{2}$ + [633]	$\frac{7}{2}$ - [514]	0	0	0.84	0.78
		1	0	2.66	2.45
		0	1	4.60	4.25
$\frac{7}{2}$ + [624]	$\frac{7}{2}$ - [514]	0	0	-1.11	-1.57
		1	0	-0.09	-0.13
		0	1	-0.15	-0.22
$\frac{7}{2}$ + [613]	$\frac{7}{2}$ - [514]	0	0	0.17	0.23
		1	0	-0.05	-0.07
		0	1	-0.08	-0.11
$\frac{5}{2}$ + [642]	$\frac{5}{2}$ - [523]	0	0	0.07	0.43
		1	0	0.17	1.09
		0	1	0.30	1.90

(continued)

Table 10. Continued

Nilsson States		Octupole phonons		Partial E1 Amplitudes, $B^{\frac{1}{2}}(E1)(\times 10^3)$	
$\Omega\alpha_i$	$\Omega\alpha_f$	n_i	n_f	$I = \frac{9}{2}$	$I = \frac{21}{2}$
$\frac{5}{2}$ + [642]	$\frac{5}{2}$ - [512]	0	0	-0.02	-0.12
		1	0	-0.19	-1.19
		0	1	-0.33	-2.06
			Sum =	7.94×10^{-3}	5.25×10^{-3}
			B(E1) =	6.3×10^{-5}	2.8×10^{-5}

*Calculation NCO' in Table 8.

$\frac{21}{2}+ \rightarrow \frac{21}{2}-$ transition. Of particular interest are the higher order $\frac{5}{2}+$ [642] $\rightarrow \frac{5}{2}-$ [523] and $\frac{5}{2}+$ [642] $\rightarrow \frac{5}{2}-$ [512] components which exhibit rather large collective contributions to the total E1 strength for those transitions between the higher spin members of the two rotational bands. However, because these contributions are nearly equal and opposite in phase, they essentially cancel. We conclude from this result that the quality of the three-parameter fit may have been somewhat fortuitous, resulting microscopically from a near-cancellation of several terms important for large values of the spin-dependent RPC matrix elements. On the other hand, the theoretical model we have chosen that indicates the presence of large third-order $\frac{5}{2}+$ [642] $\rightarrow \frac{5}{2}-$ [523] and $\frac{5}{2}+$ [642] $\rightarrow \frac{5}{2}-$ [512] collective E1 components may be a deficient or partially incorrect model, which brings us to the next part of our discussion: a consideration of the uncertainties and weaknesses of the model.

Although the point is not crucial to the description of collective E1 transitions,[60,69] Faessler et al.[38] pointed out the convenience of representing phenomenologically the nuclear charge polarization giving rise to collective E1 transitions as resulting from small admixtures of the giant dipole resonance. The timely contribution of Donner and Greiner[34] provided an explicit interpretation of this effect, and the authors presented expressions whereby the collective E1 moments in deformed nuclei could be related directly to the giant dipole admixtures. We have chosen therefore to relate our expression (34) describing the collective E1 moments in odd-A deformed nuclei to the parameter C_0,

representing the magnitude of the giant dipole admixture to the octupole vibrational mode. A significant test of the consistency of our results with the general model of Ref. 34 is then provided by examining the parameter $\langle a_{30} \rangle = \frac{\hbar}{\sqrt{2B_3E_3}}$.

Because of the near-cancellation of two E1 components nearly equal and opposite in phase, the calculated strength for the highly hindered 321-keV E1 transition in Hf^{177} is extremely sensitive to the choice of $\langle a_{30} \rangle$. (In general the remaining transitions are much less sensitive, though the calculated branching ratios are rather easily upset.) Although there exist unique values $\langle a_{30} \rangle$ which yield the best fit to experimental data, we should not attach too much significance to the last decimal places. Nevertheless, it is clear that the values indicated for $\langle a_{30} \rangle$ in the E1 "best fits" are in the range 0.1-0.2, consistent with the octupole amplitude expected in this region, and hence consistent with the "giant dipole model" and with such experimental data as are available.[34] The parameter $\langle a_{30} \rangle$ can best be determined from experimental values of B(E1) and B(E3) for collective transitions between the ground and octupole vibrational states in even-even nuclei. Unfortunately, no such data are available to date for the even-even nuclei Hf^{176} and Hf^{178}. Experimental B(E1) and B(E3) information for at least one of these two nuclei is necessary for a more critical evaluation of our choices for $\langle a_{30} \rangle$

The uncertainties associated with the collective model description of octupole vibrations also deserve consideration. If we concede that the simple octupole harmonic oscillator Eq. (27) provides an

approximately correct description of the excited nuclear surface, then we also assume that the nucleus possesses a static quadrupole deformation, and we further assume a constant moment of inertia. Both of these assumptions ought to be good to first order for the strongly deformed Hf^{177} nucleus although, to be sure, at spin $\frac{21}{2}$ and energy ≈ 1 MeV the situation may become more complex under the influence, for example, of Coriolis anti-pairing effects.[70-72] For the sake of simplicity, however, we have assumed the parameters η, Q_0, and $\mathcal{J}$ associated with the equilibrium quadrupole deformation to be constants. Having disposed of these problems, we finally note that the octupole vibration-particle interaction Hamiltonian (25) is taken to be proportional to $r^2 \cdot Y_{30}$ rather than the $r^3\, Y_{30}$ of Ref. 69. Vogel[36] has pointed out that the octupole potential of the type $\propto r^2\, Y_{30}$ describes more accurately the equipotential surface of the nuclear mass possessing quadrupole and octupole deformation.

There are also, of course, uncertainties associated with the Nilsson single-particle energies and wave functions upon which we have so heavily relied. For example, the term

$$H_\delta = -\frac{4}{3}\,\delta\sqrt{\frac{\pi}{5}}\,\hbar\omega_0\, r^2\, Y_{20}$$

of the Nilsson Hamiltonian (5) has non-vanishing matrix elements between states for which $\Delta N = 0, \pm 2$, but the terms for which $\Delta N = \pm 2$ are neglected since they are usually small compared to the average energy separation between such states. However, the sensitivity of E1 transition strengths to small wave function admixtures having large

"unhindered" E1 matrix elements has been clearly shown (cf. Table 6), and we consequently should not dismiss out of hand the possible effect of $\Delta N = \pm 2$ mixtures in the $K = \frac{9}{2} + [624]$ and $K = \frac{7}{2} - [514]$ bands in Hf^{177}.

The Nilsson diagram for odd neutrons, $82 < N < 126$, (Fig. 9) shows that the situation in the case of Hf^{177} is relatively uncomplicated. No candidates for direct mixing in either the $\frac{9}{2} + [624]$ or $\frac{7}{2} - [514]$ bands are to be found within at least 6 MeV of either state at deformation $\epsilon = 0.25$. The matrix elements $\langle N'\ell' | H_\delta | N\ell \rangle$ being of the order ≈ 100 keV, we expect to find wave function admixtures generally < 2%. These could be significant for <u>unhindered</u> E1 matrix elements (cf. Table 5), but in the case of the most eligible $\frac{9}{2} + [404] \rightarrow \frac{7}{2} - [514]$ transition moment, the asymptotic quantum number selection rules indicate that the hindrance will be similar to that for the $\frac{9}{2} + [624] \rightarrow \frac{7}{2} - [514]$ principal E1 component. We therefore conclude that the changes in our results introduced by excluding $\Delta N = \pm 2$ mixing from the calculations will be small. It is well to remember, however, that in some cases the $\Delta N = \pm 2$ mixing can be quite large and can exercise a significant influence on both energy level[73] and transition probability[69] calculations.

Finally we note with regard to the single particle wave functions used in our calculations that new wave functions in the asymptotic representation have recently become available.[74] At large deformations these may be more desirable than those employed in the present work. Another more significant departure from the original Nilsson wave functions can be achieved by replacing the single-particle harmonic oscillator

potential with one of the Woods-Saxon type.[69] There are indications that this form of the nuclear potential, applied to deformed nuclei, may give better agreement with experiment than the harmonic oscillator potential employed by Nilsson and others.

We must also consider the limitations of the rotational model, upon which we place heavy reliance in deducing the experimental E1 strengths in Hf^{177}, and in obtaining the proper wave function mixtures for use in the theoretical calculations. Although the band-fitting procedure described earlier allows one to arrive at what seems to be a "unique" eigenfunction describing the rotational band in question, there is often some difficulty interpreting the parameters required to achieve the fit. For example, it is not clear whether the "cutting" of Coriolis matrix elements, particularly between states on opposite sides of the Fermi surface, is the result of deficiencies in the rotational model and the presumed RPC interaction itself, of inadequacies in pairing theory for interactions near the Fermi surface, or simply of more subtle phenomena not yet detailed in present theory. Nevertheless, the effect is noted here, as it has been elsewhere in calculations of this type.[75] Moreover, the "uniqueness" of the solution achieved is also open to some question, for although there is usually a single best solution, there are often other good solutions obtainable with somewhat (though not greatly) different eigenfunctions. In short, the method appears to be valid, but the interpretation of the results in terms of present theory is sometimes difficult.

We also note our omission of any explicit accounting for the rotation-vibration interaction. Though the coefficient "B" of the

$I^2(I+1)^2$ term commonly used as a "vibration correction" in rotational band calculations is known to be of second order and, judging from Fig. 8 certainly is so in Hf^{177}, still we have doubtless in our calculations included small terms no more deserving of consideration than the neglected "RVC" terms. In lieu of further experimental evidence, this fact should again make us cautious about too literal an interpretation of the results here obtained.

Finally, the extreme sensitivity to the pairing reduction factor R_0 for the fit to the highly hindered 321-keV E1 transition has been remarked upon earlier. In view of this sensitivity, it seems appropriate to examine the issue further. The Fermi surface in Hf^{177} is assumed to lie nearly midway between the two Nilsson single-particle states $\frac{9}{2}+$ [624] and $\frac{7}{2}-$ [514] (cf. Fig. 9). It is evident from the form of the reduction factor, $R = (U_1U_2 - V_1V_2)$ for electric transitions, that this circumstance can result in near total cancellation of the single-particle transition amplitude. But the quantitative theoretical interpretation of the effect is difficult, as evidenced by the rather discouraging display of data in Table 11. It appears that we may select a value to our liking anywhere in the range 0.07 - 0.93! Consequently, in our calculations we have adopted a fairly simple semi-empirical approach in determining the single particle orbital occupation parameters U and V. The eminently simple form (20) requires only a knowledge of the energy gap Δ, a parameter that can be estimated from odd-even mass differences. We have chosen the value $\Delta = 0.60$ MeV in our calculations as a good compromise on the basis of the calculations of Ref. 27. The odd-even

Table 11. Theoretical pair reduction factors for Hf^{177} transitions.

$R_0 = (U_{\frac{9}{2}+[624]} U_{\frac{7}{2}-[514]} - V_{\frac{9}{2}+[624]} V_{\frac{7}{2}-[514]})$	Method	Ref.
0.17	B.C.S. "Model A"	(14)
0.07	B.C.S. "Model B"	
0.14	B.C.S., without blocking	(47)
0.58	B.C.S. Projected wave functions	
0.74	B.C.S. with blocking	
0.93	B.C.S. with blocking and projected wave functions	
0.60	I.U. method, different	(46)
0.79	values for average	
0.76	field energies ε_i .	

neutron mass difference P_n^{exp} is calculated by Nilsson and Prior[27] to be 0.66 MeV. One set of results in Table 8 (NCO) has been shown for the value $R_0 = 0.42$ calculated from Eq. (20) for the critically important pair reduction for the $\frac{9}{2}+[624] \rightarrow \frac{7}{2}-[514]$ strength. This value (0.42) is quite close to the value 0.34 indicated by the experimental parameter M_0 used in the very successful three-parameter fit of E1 data. It might thus appear we have been able to approximately determine the occupancy numbers for the $\frac{9}{2}+[624]$ and $\frac{7}{2}-[514]$ orbitals in Hf^{177} from experimental E1 transition probabilities (if we assume the Nilsson wave functions are reliable for calculating such very small ($\sim 10^{-2}$) G(E1) values).

We are fortunate in now having the recent Hf^{178} (d,t) Hf^{177} and Hf^{178} (d,p) Hf^{177} reaction data of Rickey and Sheline[26] and their derived single-particle orbital occupation probabilities, U^2. The data of interest to our discussion are shown in Table 12. Using the DWBA predictions of Satchler for the (d,p) and (d,t) cross-sections for a particular state, the authors are able to obtain the ratio U^2/V^2, and thus determine U and V, since $U^2 + V^2 = 1$. We also show their results for the experimentally derived Nilsson $C^2_{j\ell}$ wave function coefficients for each state.

The experimental pair reduction factor $(U_{\frac{9}{2}+[624]} U_{\frac{7}{2}-[514]} - V_{\frac{9}{2}+[624]} V_{\frac{7}{2}-[514]})$ calculated from these data is 0.18, about a factor of two smaller than that indicated from the experimental E1 data. The two data are certainly not, however, mutually exclusive, in view of the approximations inherent to the DWBA calculations, and of the undertainties in the Nilsson E1 moment calculations for such highly hindered transitions.

Table 12. Occupation numbers U^2 and wave function coefficients $C^2_{j\ell}$ for Hf^{177}, (Ref. 26).

Level energy (keV)	$\Omega[Nn_z\Lambda]$ assigned	Derived $U^2_{\Omega\alpha}$	$C^2_{\frac{5}{2}3}$	$C^2_{\frac{7}{2}3}$	$C^2_{\frac{9}{2}5}$	$C^2_{\frac{11}{2}5}$	$C^2_{\frac{9}{2}4}$	$C^2_{\frac{11}{2}6}$
Gnd	$\frac{7}{2}$ - [514]	0.427		0.048	0.700	0.065		
324	$\frac{9}{2}$ + [624]	0.724					0.092	0.148
504	$\frac{5}{2}$ - [512]	~0.3	~0.04	~0.7				
1058	$\frac{7}{2}$ - [503]	0.94		0.542				
851	$\frac{7}{2}$ + [633]	0.01					0.40	

It is also of some interest to compare the values $C^2_{j\ell}$ in Table 12 with the values for those parameters assumed in our calculations. Though the authors caution against attaching too much significance to the absolute values $C^2_{j\ell}$, the relative values are thought to be fairly reliable. For the $\frac{7}{2}$ - [514] (ground) state in Hf^{177} we see, as expected, that the $\ell = 5$ component associated with the $h_{\frac{9}{2}}$ orbital dominates. Mixing from the $h_{\frac{11}{2}}$ and the $f_{\frac{7}{2}}$ orbitals is seen to be quite small, as expected. It is more difficult to understand the fairly large component from $i_{\frac{11}{2}}$ indicated for the $\frac{9}{2}$ + [624] band, but the strongly perturbed nature of this band may provide at least partial explanation for the magnitude of that term. It is, however, comforting to see the relatively weak contribution from $g_{\frac{9}{2}}$, indicating the $\Delta N = 2$ mixing, $\frac{9}{2}$ + [624] $\leftrightarrow$ $\frac{9}{2}$ + [404] is indeed quite small, as we assumed in our calculations.

To conclude this discussion, we make reference to the recent work of Soloviev and co-workers[62,63] wherein the interaction of phonons and quasi-particles in odd-A deformed nuclei is examined in considerable detail for several cases in the rare-earth region of deformation. With use of their "superfluid" model of the nucleus, the authors show that such interactions can lead to substantial mixing of phonon and quasi-particle states, and to the appearance of non-rotational collective states and states having complex phonon-quasiparticle structure. It is particularly interesting to note that their calculations for the Hf^{177} nucleus (disregarding rotation-particle coupling) show the $\frac{9}{2}$ + [624] state to be essentially free (99.5%) of quadrupole or octupole phonon perturbation, lending further support to our assumption in both the

Coriolis matrix diagonalization and throughout the calculation of the E1 strengths that the strong perturbations observed in the $\frac{9}{2}$ + [524] band of Hf^{177} are essentially "RPC" in nature. Moreover, these results are consistent with our assumptions with regard to the magnitude of the octupole phonon interaction. For example if we apply the vibration-particle coupling matrix element $\langle f|H_{VPC}|i\rangle$ in a simple perturbation calculation to obtain the first order mixing of the phonon-particle state $|\frac{7}{2} + [633];\ n_3 = 1\rangle$ into the ground band $\frac{7}{2}$ - [514] of Hf^{177}, we have a mixing coefficient

$$\left| C_{n_3=1} \right| = \frac{R\langle \frac{7}{2};\ \frac{7}{2} + [633];\ 1|H_{VPC}|\frac{7}{2} - [514];\ 0\rangle}{E_{\frac{7}{2} - [514]} - [E_{\frac{7}{2} + [633]} - E_3]} \cong 0.15$$

where the notation is consistent with that used earlier, and $\langle a_3 \rangle = 0.14$, $E_3 = \sqrt{\frac{C_3}{B_3}} = 1.2$ MeV. If, for the sake of argument, we assume the above component to be the only "impurity" in the $\frac{7}{2}$ - [514] band, the normalization condition indicates about two percent $\left|\frac{7}{2} + [633];\ n_3 = 1\right\rangle$ "character" in the ground band of Hf^{177}. Soloviev finds the Hf^{177} ground band to be 96% $\frac{7}{2}$ - [514], but his calculations for the parameter E_3 yield 1.9 and 2.2 MeV for Hf^{176} and Hf^{178}, respectively, somewhat high when compared with the value for E_3 indicated by the experimental levels $I^{\pi}K=1-0$ at 1643 and 1722 keV in Hf^{176} (cf. data reported for Hf^{176} in part II). Since the above case is the most important in Hf^{177}, we may conclude that the model we have employed in our calculations is not inconsistent with the more sophisticated calculations of the Dubna school of theoreticians.

In order to confirm the validity of our treatment, the following experimental data would be of special interest:

1) Careful measurement of the conversion electron spectrum of Lu^{177m} ought to be performed using a high-resolution magnetic spectrometer comparable to the iron-free instrument at Berkeley. These data would presumably provide an independent check of the assumptions we have made regarding the highly perturbed $\frac{9}{2}$ + [624] band in Hf^{177}. It would be particularly desirable to be able to verify the M1-E2 mixing ratios we have predicted in Fig. 11. We have made some investigation into this experimental problem, especially with regard to the difficulty of obtaining a "mass-free", intense source of Lu^{177m}. The details are discussed in Appendix A.

2) Additional direct lifetime measurements for members of the $\frac{9}{2}$ + [624] rotational band would be desirable, although present techniques and electronic limitations make such measurements ($\approx 10^{-10}$ sec) extremely difficult if not impossible.

3) The reduced strengths, B(E1) and B(E3), to the collective octupole states in Hf^{176} and/or Hf^{178} must be measured to provide an experimental check on the value of $\langle a_{30} \rangle$, the collective model octupole transition amplitude in this region. Though the recent data of the Risø group on even-even gadolinium,[76] dysprosium,[77] and erbium[78] nuclei provide some encouraging insight for this problem, the results for Hf nuclei are to our knowledge not yet available.

4) Other information of interest might be provided by measurement of the g-factor of the 1.1-sec. three-quasiparticle state in Hf^{177}.

5) Finally, the obvious need is for more systematic, precise data on $\Delta K = \pm 1$ and K-forbidden E1 transition strengths in other odd-A deformed nuclei. As we have seen earlier, although there are a few other cases of more than minor interest, to date there has been no candidate of the caliber of Hf^{177} that has presented itself for review in either the lanthanide or actinide region of deformation.

The interpretation of anomalous $|\Delta K| = 1$ and K-forbidden E1 transitions in terms of pairing, Coriolis coupling, and octupole collective contributions was suggested in principle by Ref. 14 and treated later in Refs. 18 and 69; we have, it is hoped, tentatively confirmed the explicit validity of the model, at least as it applies to Hf^{177}. There is, however, some disagreement on interpreting the origin of collective E1 components in odd-A nuclei. Piepenbring,[69] on the one hand, approached the problem by performing a microscopic Soloviev-type calculation assuming a somewhat different mean field and (neglecting the effects of blocking and the refinement of projected wave functions) obtained values for E_3 apparently in somewhat better agreement with experiment than did Soloviev for Hf^{176}. However, the microscopic model chosen in Ref. 69 to describe the octupole force results in a transition strength ratio $T_{collective}(E1)/T_{particle}(E1)$ that is a rather sharply decreasing function of spin. For example, increasing the spin from $\frac{3}{2}$ to $\frac{9}{2}$ decreases the ratio by a factor of 80. Consequently, it is significant that the calculated octupolar contribution in Hf^{177} is relatively small, and the calculated absolute E1 strengths (results are shown in Ref. 69 only for the $\frac{9}{2}+ \rightarrow \frac{9}{2}-$ and $\frac{9}{2}+ \rightarrow \frac{11}{2}-$ transitions) are not in good agreement with experiment.

On the other hand, we have adopted a simpler model which interprets the collective E1 components as arising from small admixtures of the giant dipole resonance, an assumption based on a purely phenomenological picture of the charge polarization associated with the octupole vibrational mode. That we have been able to obtain good agreement with experiment using reasonable values of the single adjustable parameter (analogous to the free parameter in Ref. 69) describing the octupole strength seems to indicate that the restrictions placed upon the octupole vibrations in Ref. 69 are too severe, and that coupling of the dipole oscillations of the nuclear core with the giant dipole resonances is at least important, if not dominant in the case of Hf^{177}. More experimental information of the type mentioned earlier is certainly necessary to resolve the issue.

6. Summary and conclusions

The 16 E1 transitions arising from the decay of 161 d. Lu^{177m} provided the opportunity for an exceptionally rigorous and detailed experimental test of the theory of $\Delta K = 1$ E1 transitions in odd-A deformed nuclei. We were able to show that the "anomalous" electromagnetic transition strengths of this type can be explained within the framework of the unified model, and we examined in detail the significant information on nuclear structure and nuclear models provided by the nucleus Hf^{177}. Although the general applicability of the interpretation of $\Delta K = 1$ E1 transitions in terms of Coriolis coupling, pairing, and octupole vibration-particle coupling remains to be shown, the results of our calculations for the nucleus Hf^{177} indicate that the theoretical basis for the quantitative interpretation of E1 transitions in odd-mass deformed nuclei is established.

We have also demonstrated the wealth of information on nuclear structure that can be derived by a careful analysis of second- and third-order nuclear decay information now obtainable using optimized Ge(Li) detector systems. The problem we have discussed and the method used in its solution illustrates one more case where experiment has led the way to a better understanding of the essential unity and consistency of contemporary nuclear theory.

III. THE DECAY OF Ta^{176} TO LEVELS IN Hf^{176}

A. Introduction

In part I of this work we have described in detail the rather extensive information on nuclear theory that we have in one case been able to extract from a careful study of second order nuclear decay properties. Needless to say, such work would have been impossible before the advent of the Ge(Li) and Si(Li) lithium-drifted semiconductor "family" of detectors. The initial impact of these devices upon the field of nuclear physics and chemistry has been described by several authors (cf. e.g. Ref. 79 and references cited therein, or for a more general discussion the review article by Hollander[80]). Still, it ought to be realized that the measurements reported in Appendix A became feasible only some two years ago, after numerous second-order breakthroughs in the fabrication of the Ge(Li) and Si(Li) devices themselves and, more importantly, after major improvements in the design and quality of the component parts available for low-noise electronics. It is therefore no longer uncommon to find large volume (7-40 cm^3) Ge(Li) detectors yielding system resolution of 2.0 - 3.0 keV (FWHM) for Co^{60}, depending on the size of the device, and small diodes $\leqslant 1$ cm^3 in volume capable of giving resolution considerably less than 1 keV at energies below 150 keV. The result of these developments in detector technology has been an avalanche of data on nuclear properties, data which have in a few short years placed the theoretician in the unenviable position of being asked to explain a myriad of complex nuclear properties <u>after</u> they have been observed.

However, at the same time that the semiconductor revolution in radiation detection was in its boisterous youth, a quieter revolution in data acquisition and reduction techniques was occurring. And in the past two years, the age of the on-line computer for data acquisition and analysis has become a reality.

In the following pages we shall describe a practical consequence of the combined impact the above revolutions have had on the field of nuclear spectroscopy. We have chosen for consideration the highly complex decay of 8-hour Ta^{176} to levels in Hf^{176}, partly because of its relevance to the theoretical calculations described in part I for Hf^{177}, and partly because we felt at the beginning of this study that we finally had available equipment equal to the task of unravelling one of the most complicated natural decays known. The degree to which this feeling was correct can be judged from the work we now report.

B. Background

Very little was known of the decay of Ta^{176} at the time this study was begun. The complexity of the decay was perhaps first witnessed by Harmatz, et al.[81] in their early permanent-magnet conversion electron study. No attempt was made at that time to construct a decay scheme, and subsequent attempts to do so using NaI(Tl) scintillation detectors were largely unsuccessful.[82,83] The recently published Table of Isotopes[84] consequently shows only the levels of Hf^{176} reproduced in Fig. 15. The proposed spin (1-) of the parent Ta^{176} nucleus presumably results from coupling of a $\frac{5}{2}$ - [512] neutron with a $\frac{7}{2}$ + [404] proton. If this assignment is correct, then the β-decay is first-forbidden hindered ($\Delta\Lambda = -2$), and it is not expected that the positive parity ground band of Hf^{176} will be heavily populated by the β^+-EC decay of Ta^{176}. Moreover, we do not expect that states of spin greater than 3 will be appreciably populated.

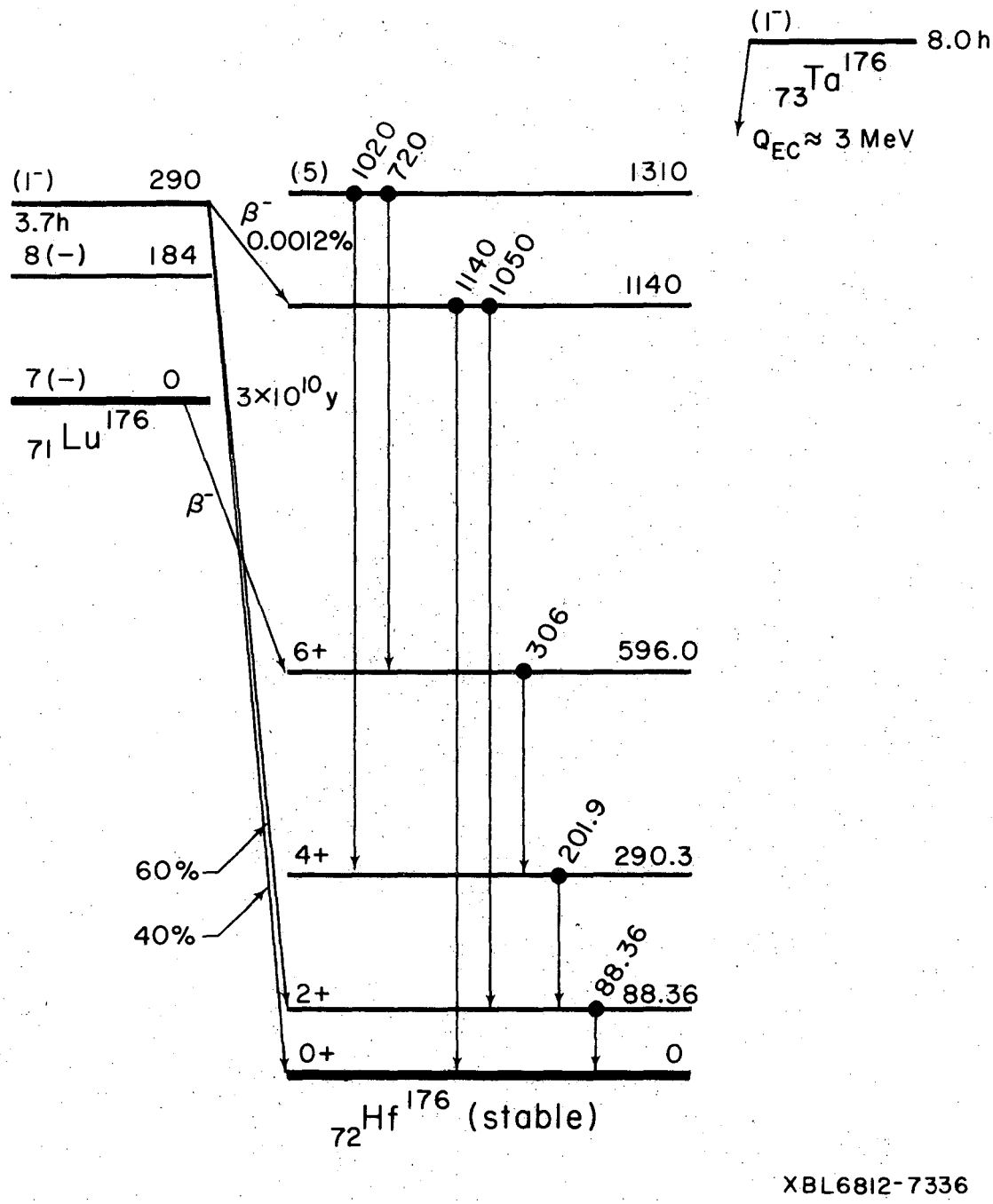

Fig. 15. The level scheme of Hf^{176} from previous work.[84]

C. Experimental

1. Target and source preparation

The Ta^{176} activity was prepared by the $Lu^{175}(\alpha,3n)Ta^{176}$ reaction. Samples of approximately 35 mg. of isotope separated 99.94% enriched $Lu_2^{175}O_3$ were irradiated at the LRL 88-inch cyclotron with 43 MeV alpha particles. The powder target was distributed in an aluminum backing plate so that the maximum depth of target material was $\leqslant$ 0.15 mm. A 0.13 mm aluminum foil covered the $Lu_2^{175}O_3$ powder so that the α-particle energy incident on the powder was about 40 MeV. Irradiation periods of two hours at 18μA beam current were found to produce ample activity (≈ 3-4 R/hour gamma field at surface).

The Ta activity was separated from other reaction products by extraction from 6N HCl solution using 2,4-dimethyl-3-pentanone (diisopropyl ketone), a procedure described in Ref. 85. Sources for counting could generally be readied within three hours after the end of irradiation. Small amounts of Ta^{178}, Ta^{177} and Ta^{175} contamination were noted in the γ-ray spectra.

The sources for γ-ray counting were prepared by evaporating to dryness small quantities of the carrier-free extracted Ta in water solution deposited on aluminum counting plates, or in the case of the samples for the Compton-suppressed singles work, on Teflon discs. To prepare electron sources, the activity was liquid deposited onto 0.25-mil gold-anodized mylar sandwiched with aluminum lacquer between 5-mil aluminum annular discs to provide electrical contact and structural stability.

2. Description of experimental apparatus

A variety of detection systems has been used to make measurements of: a) the singles γ-ray spectrum; b) the conversion electron spectrum; c) the γ-ray "pair" spectrum; d) the entire γ-γ coincidence spectrum of Ta^{176}. We shall describe briefly the pertinent apparatus in each case, the method of calibration where appropriate, and any problems encountered with each system.

a. Singles γ-ray spectra of Ta^{176} decay were taken using 1) a 10 cm^3 planar Ge(Li) detector with resolution 2.5 keV at 1.33 MeV (Fig. 16); 2) a 1 cm^3 "thin window" Ge(Li) detector with resolution of 0.8 keV at 122 keV; 3) a 7 cm^3 planar Ge(Li) detector used in conjunction with the Compton suppression system at LRL Livermore, and displaying resolution 2.3 keV at 1.33 MeV.

The energies and intensities of the γ-rays from decay of Ta^{176} were first determined using detector (1) described above. The crystal was calibrated for photopeak efficiency using a set of eight absolutely calibrated standard γ-ray sources obtained from the IAEA laboratories.* Hf^{180m} was used to obtain additional relative efficiency points in the rather poorly defined region from 130 - 500 keV, and Na^{24} was used as

*These 10 μCi standard sources (Am^{241}, Co^{57}, Hg^{203}, Na^{22}, Cs^{137}, Mn^{54}, Co^{60}, Y^{88}) are all now calibrated to $\leqslant$ 1% by the IAEA and may be obtained from the IAEA Division of Research and Laboratories, Vienna. Distribution is annual, and orders must generally be placed at least eight months in advance of the January 1 distribution date.

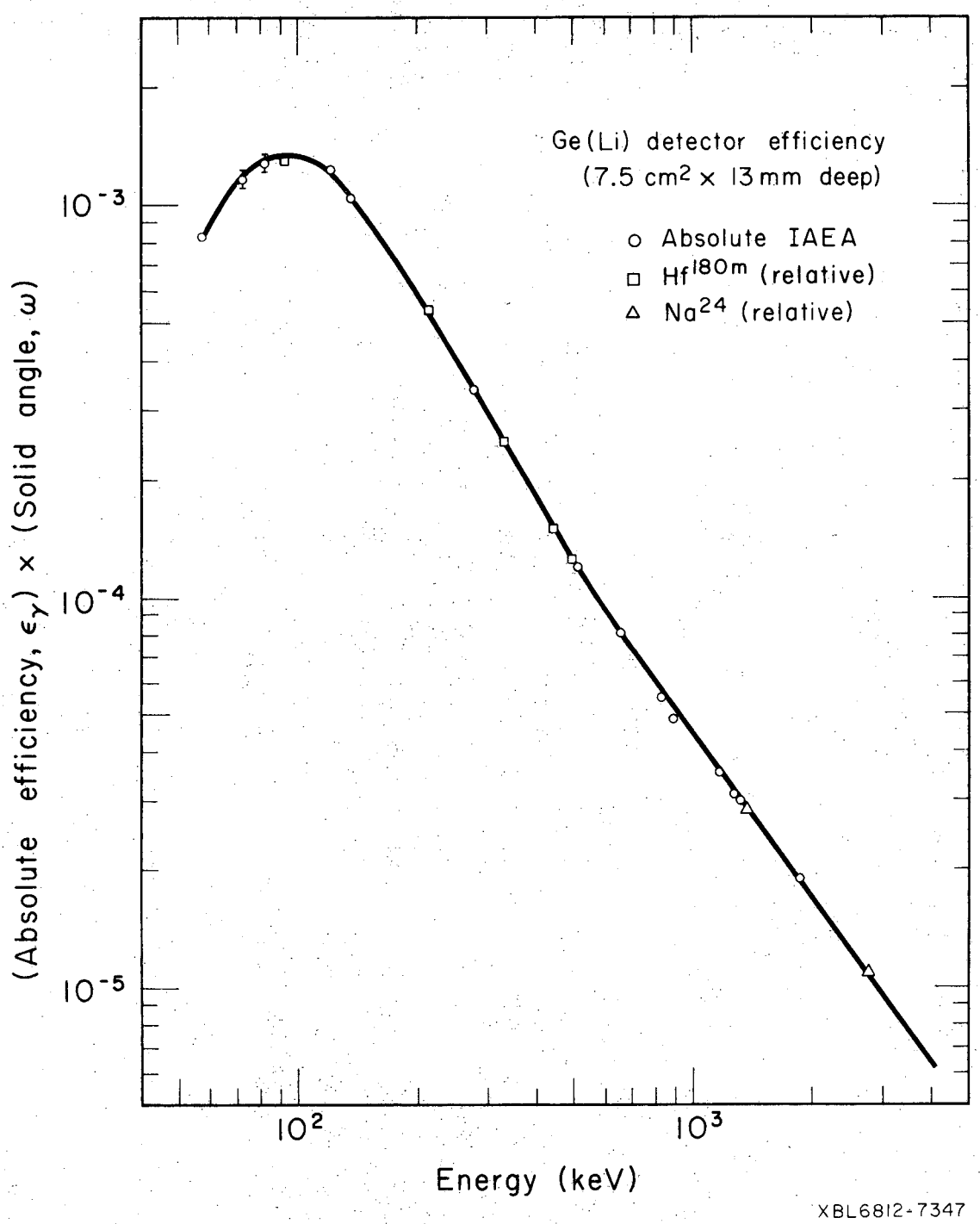

Fig. 16. Absolute photopeak efficiency vs. energy for the 10 cm^3 planar Ge(Li) detector.

a relative intensity standard to extend the curve as shown in Fig. 15 to 2.75 MeV. A linear extrapolation of the curve was assumed valid for measurements > 2.75 MeV. The Hf^{180m} relative intensities were taken from the compilation of Haverfield.[79]

Low energy singles data were also taken using the similarly calibrated "thin window" detector described in Appendix A in connection with the Lu^{177m} work.

Finally, we have been fortunate to have been able to retake the Ta^{176} singles data using the Ge(Li) Compton-suppression system at LRL, Livermore. This apparatus has been described in detail in the recent review article by Camp.[86] The combination of a 7 cm^3 Ge(Li) diode and a 9" diameter by 9" long cylinder of NaI(Tl) shielding surrounding the diode allows excellent resolution to be combined with a 70:1 Co^{60} peak-to-Compton ratio. Although relatively "hot" sources are required because of the 10" source-to-detector distance, the 8-hr. half-life of Ta^{176} was sufficiently long to allow us to gather excellent data in only two experimental "runs".

In all of our work we have used the high-rate amplifier system designed by Goulding, et al.[87] and built at LRL. The pole-zero compensation and base-line restoration features of this system in conjunction with a pulse pile-up and slow rise-time rejection unit enable one to achieve counting rates up to 7500/sec with no appreciable loss in energy resolution or peak-to-background ratio. The operating characteristics of the system at count rates up to 50 kHz are described in Ref. 87. In Fig. 17-a we show the essential features of the high-rate amplifier

system currently in use at this laboratory. Figure 17-b shows a block diagram of the linear gate and pile-up rejection units intended for use with the amplifier system, 17-a.

With the exception of the Compton-suppressed data, which were taken with a Nuclear Data Model 161-F 4096-channel analyzer, nearly all of our singles data have been taken using a PDP-7 computer "on-line" as a sophisticated pulse-height analyzer capable of performing numerous functions simultaneously. Pulses from the amplifier system (Figs. 17 and 18) are received by a computer-interfaced 4096-channel ADC of the "successive binary approximation" (SBA) type described by Robinson et al.[88] and built at LRL. The remaining data-acquisition hardware peripheral to the PDP-7 and the computer software have been developed by Robinson and Meng and are described briefly in Ref. 89.

Two of the most important functions that can be simply performed by the computer are gain and base-line stabilization. Since the computer is required to generate a very stable DC level for control of the CRT "Y axis", a convenient and simple feedback control to insure detection system gain and baseline stability suggests itself. Robinson and Goulding have designed and built a device to perform this function and it is currently in use at both the LRL HILAC and in our laboratory. A computer subroutine continuously monitors digital information on the centroid locations of the two peaks falling in the windows chosen for gain and base-line stabilization. The incrementally adjusted "Y axis" CRT signal is fed several times a second into high quality (drift less than 1 mV/sec) voltage stretchers of the same variety used in the multiplexer described

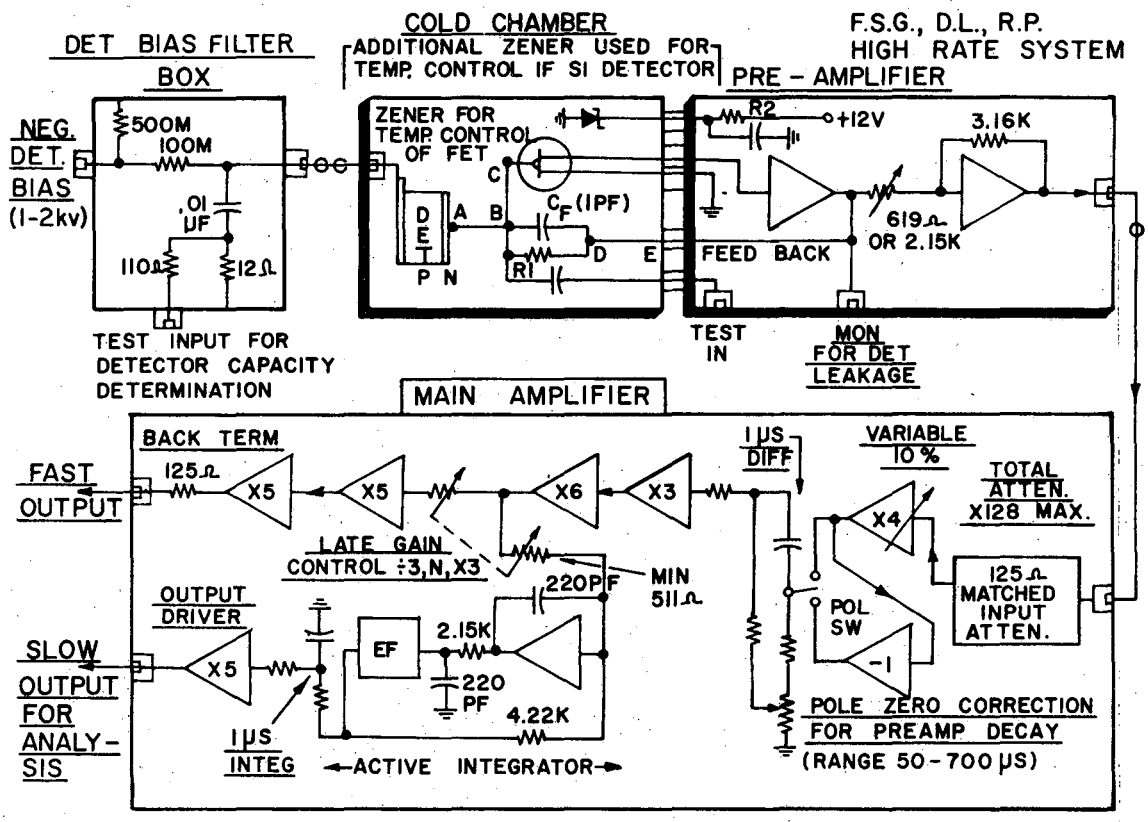

Fig. 17-a. Schematic diagram of the high-rate amplifier system currently in use at this laboratory. (Ref. 87).

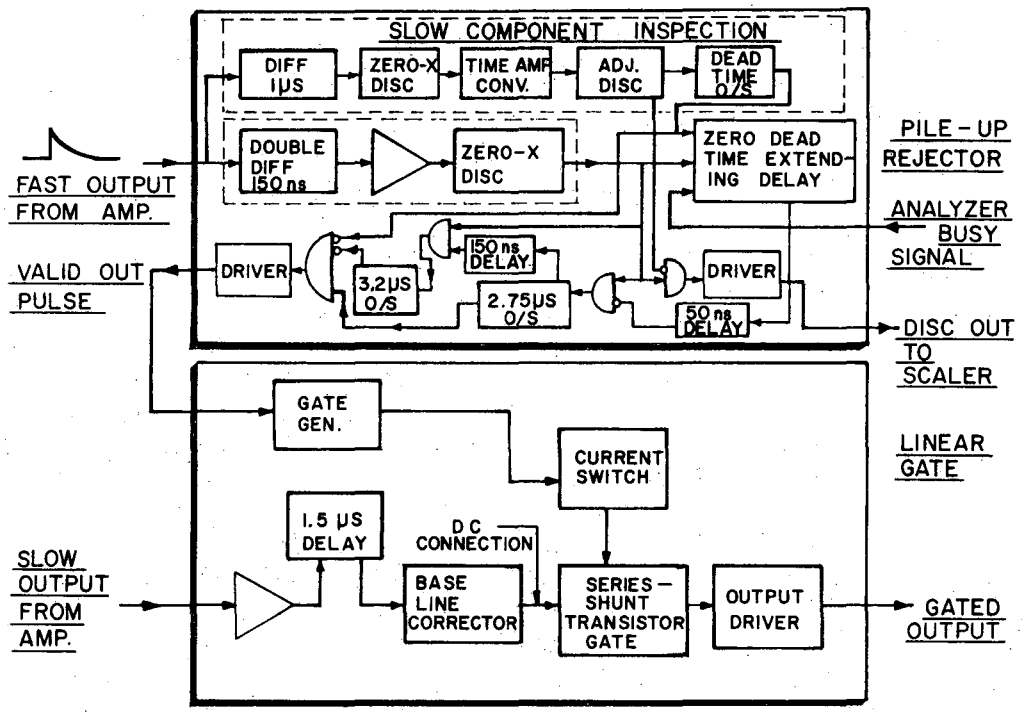

XBL 675-1474

Fig. 17-b. Block diagram of the pile-up rejector and gate for use with the high-rate amplifier system (Ref. 87).

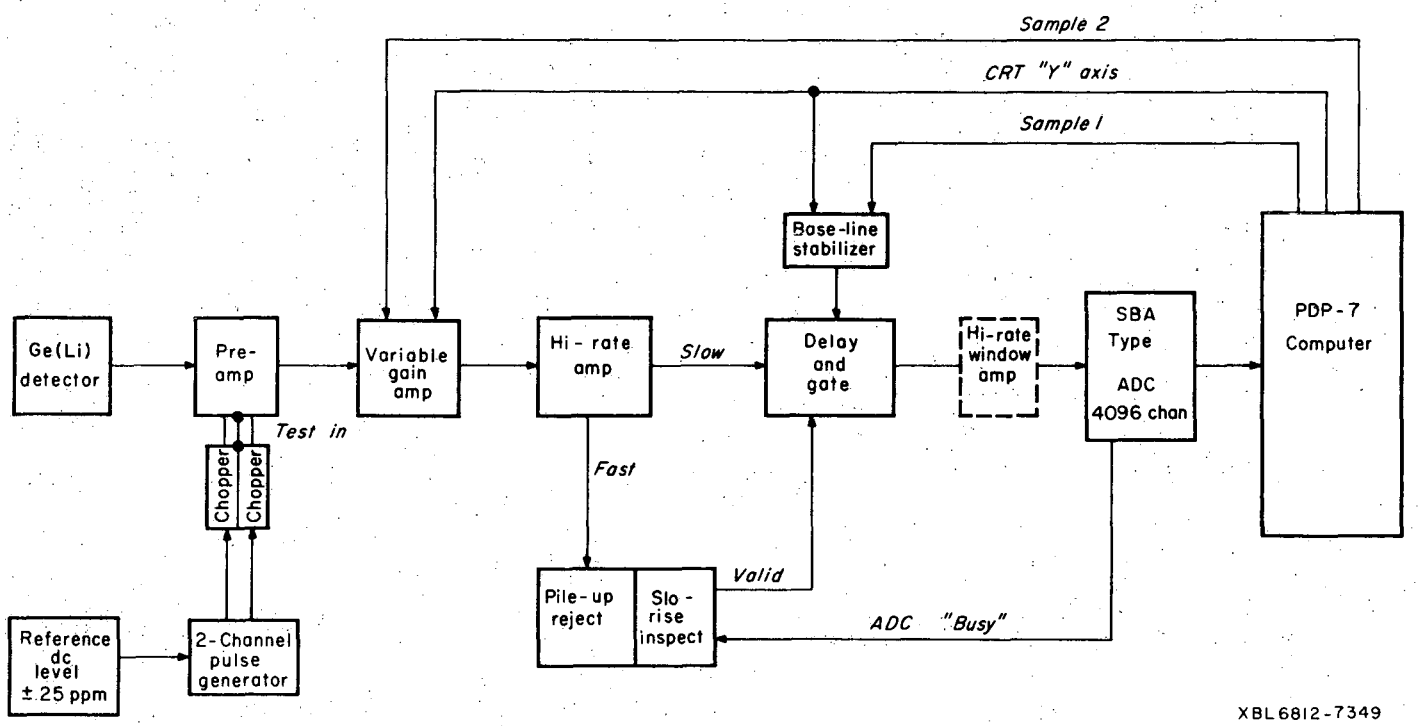

Fig. 18. Block diagram of a typical "singles" data-taking system.

in (III.B.2d). In the case of the baseline control unit the stretcher output is used directly to modify the output DC "pedestal" level of the high rate linear gate (Fig. 17-b), while in the case of the gain stabilizer, it supplies the gate voltage to a single FET in a variable gain inverting amplifier normally inserted between the detector preamplifier and main amplifier. The inverting amplifier can in this way effectively modify the gain of the preamplifier output up to 2% and thereby insure system stability.[90] Performance of the above stabilization system has been remarkably good. We are unable to notice significant degradation in system resolution at count rates as high as 15000/sec.

The gain and base-line stabilization functions have been carried out by using reference peaks internal to the spectrum where practicable, or when necessary by using an external tail-pulse generator input to the detector preamplifier. The DC reference level of the pulser is taken directly from a precision voltage source of commercial manufacture with long-term drift stability specified as less than 0.0025%.* This device also provides a switch-selectable DC voltage output precise to 0.0025%, a feature we have used to check system linearity (Appendix B).

Figure 18 shows a block diagram of a typical setup for acquiring precision "singles" spectroscopic data.

---

*"Dial-A-Source" Model No. DAS-46L, General Resistance Inc., New York 55, N.Y.

b. We have also gathered conversion electron data using a 3 mm deep × 1 cm^2 Si(Li) diode fabricated by R. P. Lothrop and coworkers at this laboratory. With 650 volts bias and an operating temperature ≈ 110°K, we were able to obtain resolution of 2.5 keV FWHM for the 1.06 MeV Bi^{207} K conversion line, comparable to the Ge(Li) photon resolution at similar energy. Using an experimental arrangement similar to that described by Easterday, et al.[91] it is possible from the relation

$$\alpha = \frac{A_{e^-}}{(\omega\varepsilon)_{e^-}} \times \frac{(\omega\varepsilon)_\gamma}{A_\gamma}$$

to calibrate absolutely the Si(Li) electron detection efficiency $(\omega\varepsilon)_{e^-}$ and thereafter to obtain directly and simultaneously conversion coefficients by finding the appropriate peak areas, A_{e^-} and A_γ, provided the Ge(Li) gamma-ray photopeak efficiency $(\omega\varepsilon)_\gamma$ is previously known. The technique has been discussed in detail by Haverfield.[79] In Fig. 19 we reproduce the Si(Li) detector efficiency curve obtained using a number of standard sources.

c. Of the three possible interactions between a photon and matter only scattering is ordinarily of no use to the spectroscopist. If sufficient energy ($> 2m_0c^2$) is available, the phenomenon of pair production can be utilized advantageously to yield significant additional information on the photon emission spectrum of a nucleus. The advantages of the so-called "pair" spectrum are two: 1) improved resolution because of the statistical advantage of using only $(E_\gamma - 2m_0c^2)$ of energy in the Ge(Li) diode to define an event of energy E_γ; 2) remarkably good peak-to-background ratios at energies greater than about 1.5 MeV. A distinct

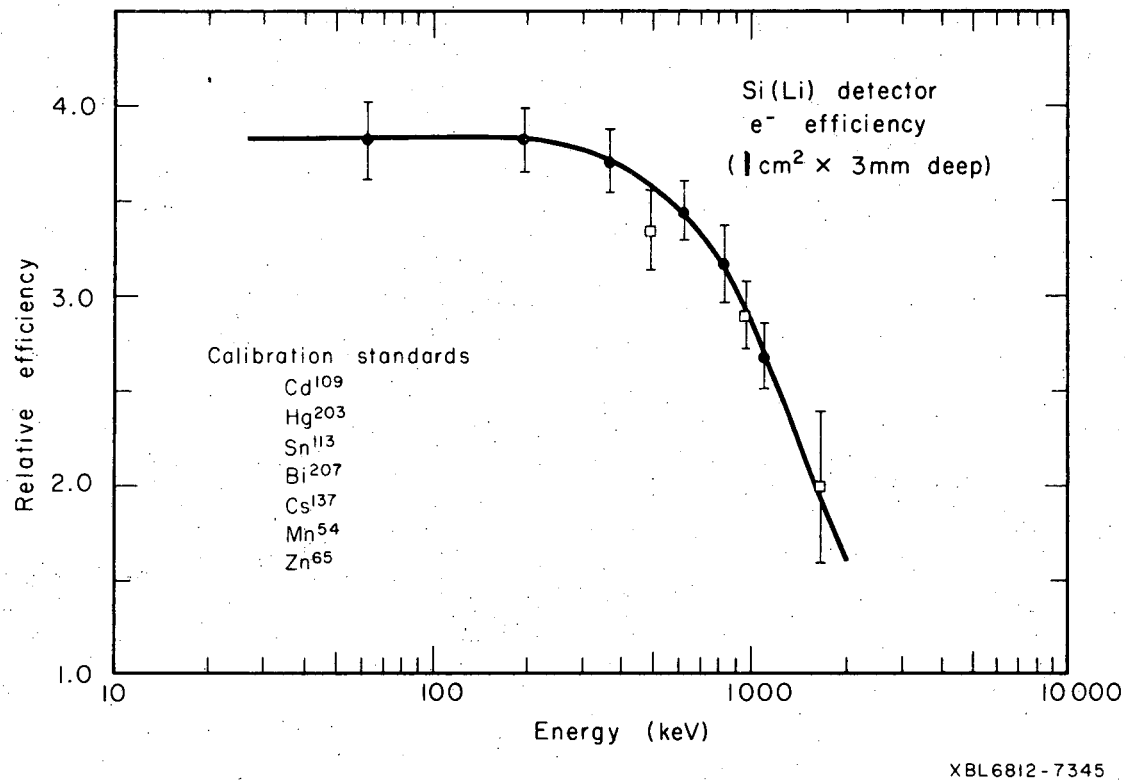

Fig. 19. Si(Li) electron full-energy peak efficiency vs. energy. Error bars represent the combined uncertainties of the Ge(Li) efficiency and the standard conversion coefficients.

disadvantage of the "pair" spectroscopy method is, of course, its low efficiency, resulting from the triple coincidence requirement between the Ge(Li) diode and the two detectors needed to identify the 511 - 511 keV events at 180° geometry.

We have used the 5-crystal pair spectrometer designed by Yamazaki and Hollander[92] to obtain the pair spectrum of Ta^{176}. The apparatus consists of a NaI(Tl) annulus split into four optically isolated sections encircling a Ge(Li) planar detector 10 cm^3 in volume with resolution 2.2 keV FWHM at 1333 keV. Figures 30 show the pair spectrometer and a block diagram of the associated electronics. Although this device could in principle also be used to obtain Compton-suppression in normal γ-ray singles operation, the size of the NaI(Tl) annulus and the relatively unfavorable geometry afford only about a factor of three reduction in the Co^{60} Compton continuum.

d. Finally, we describe the system used for the on-line acquisition of Ge(Li)-Ge(Li) γ-γ coincidence data. The hardware for this system was designed, built, and interfaced to the PDP-7 at LRL by Robinson, Gin, and Goulding.[93] In Figs. 21 we show the PDP-7 data acquisition system and a close-up photograph of the peripheral hardware required for multiparameter data taking. The block diagram of the system can be interpreted from the paneling shown in Fig. 21-b.

Two programs have been written by Robinson and Meng[94] for computer control and handling of multiparameter data. The first of these programs, MULTIDR, controls the initial analysis, display, and digitizing of the data for incremental storage on IBM standard magnetic tape. The details

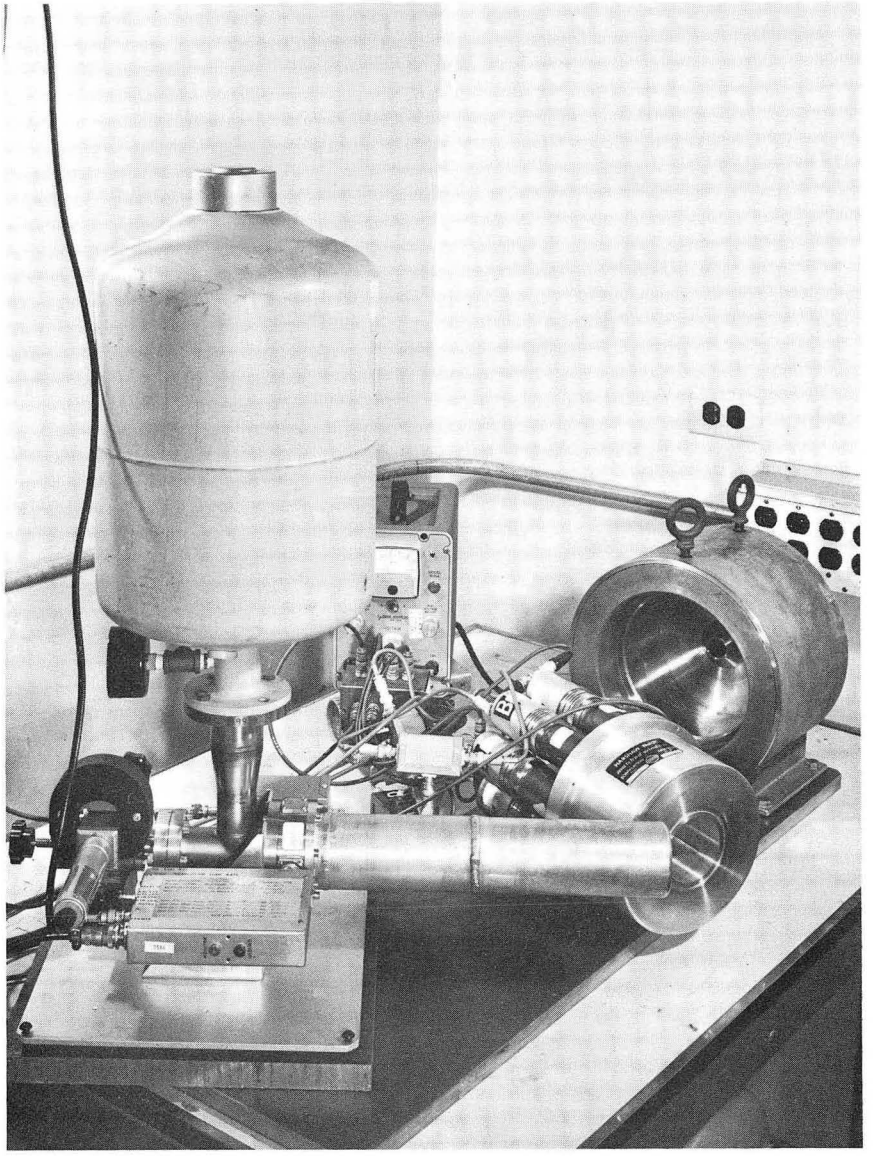

XBB 6811-7296

Fig. 20-a. The five-crystal Ge(Li) pair spectrometer shown disassembled.

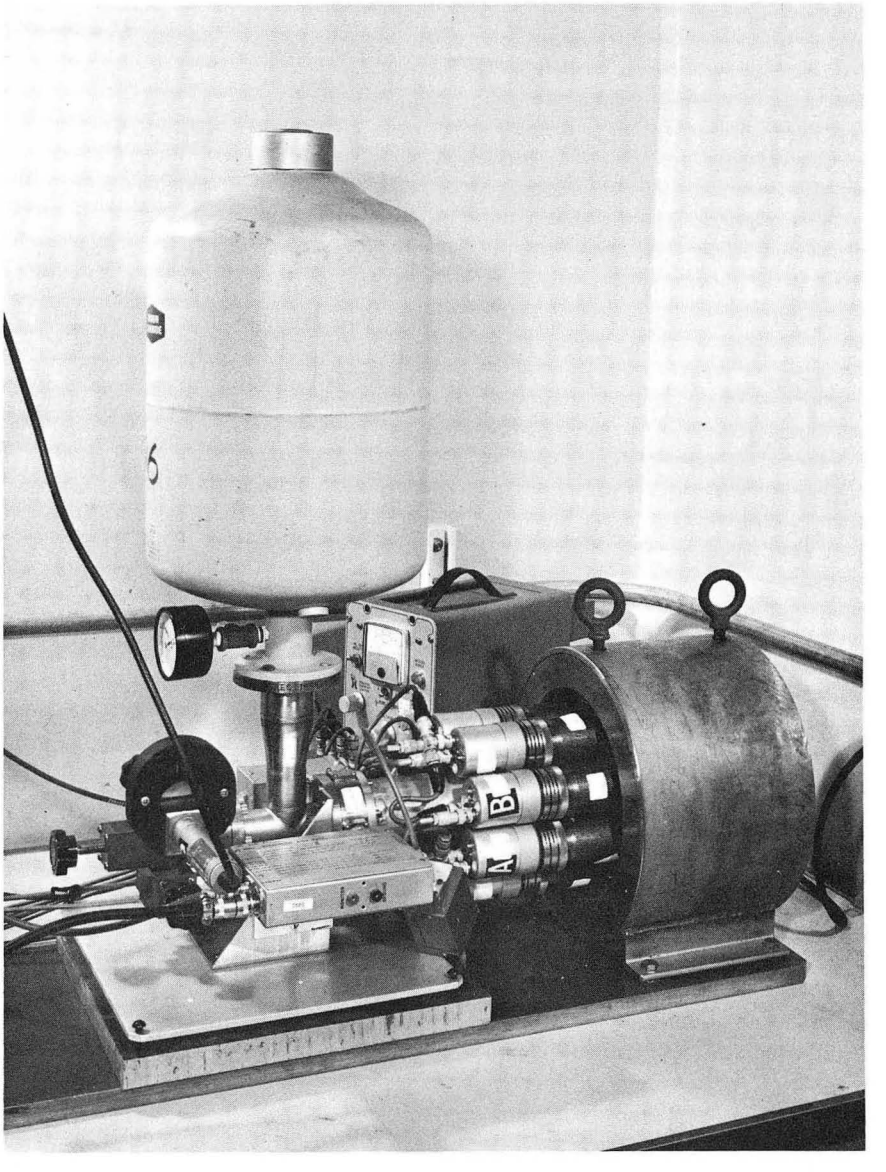

XBB 6811-7295

Fig. 20-b. The pair-spectrometer with the Ge(Li) detector in position.

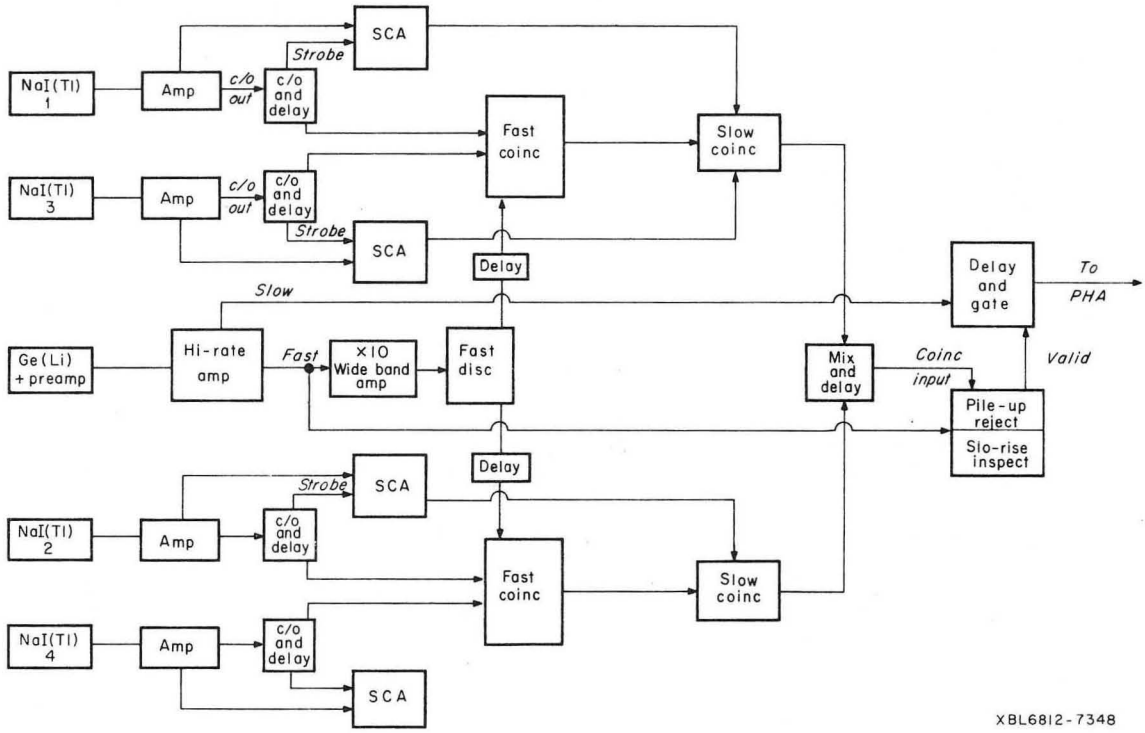

Fig. 20-c. Block diagram of the pair spectrometer.

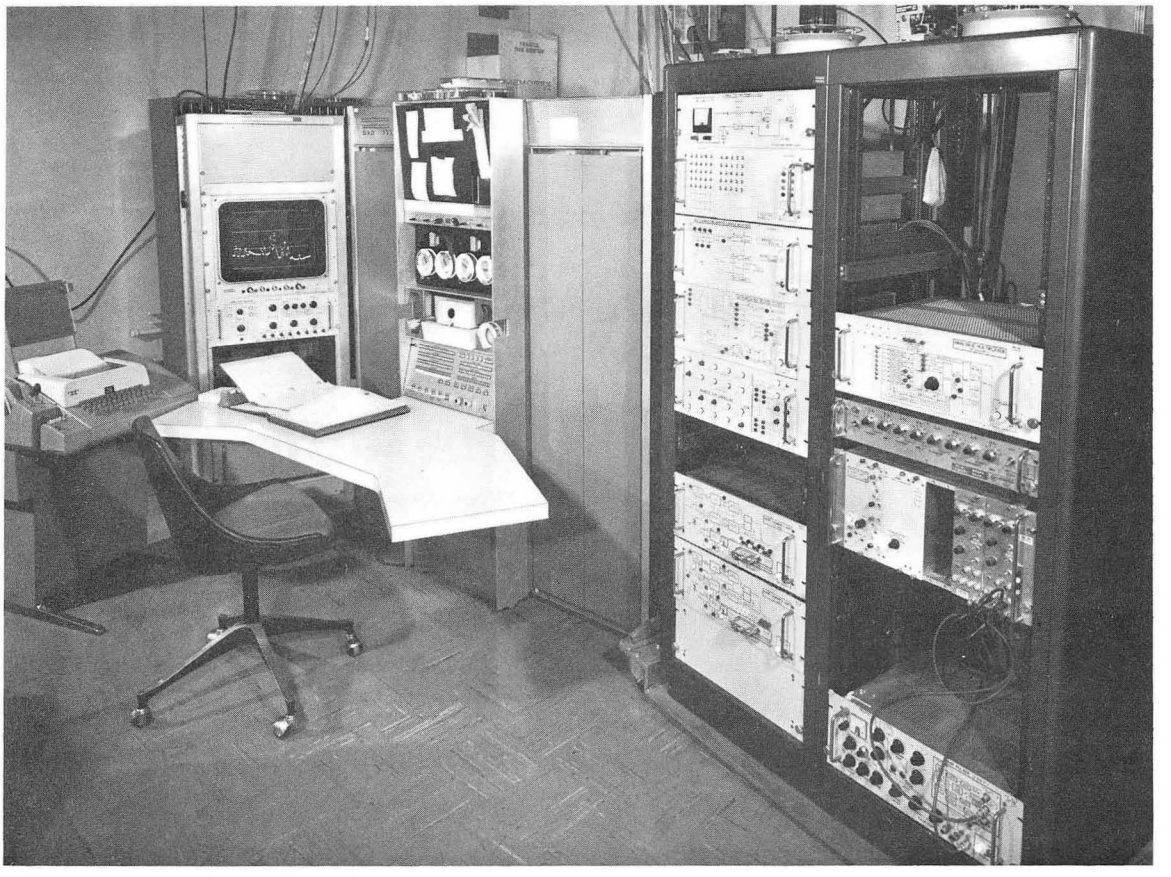

XBB 688-5165

Fig. 21-a. The PDP-7 data system.

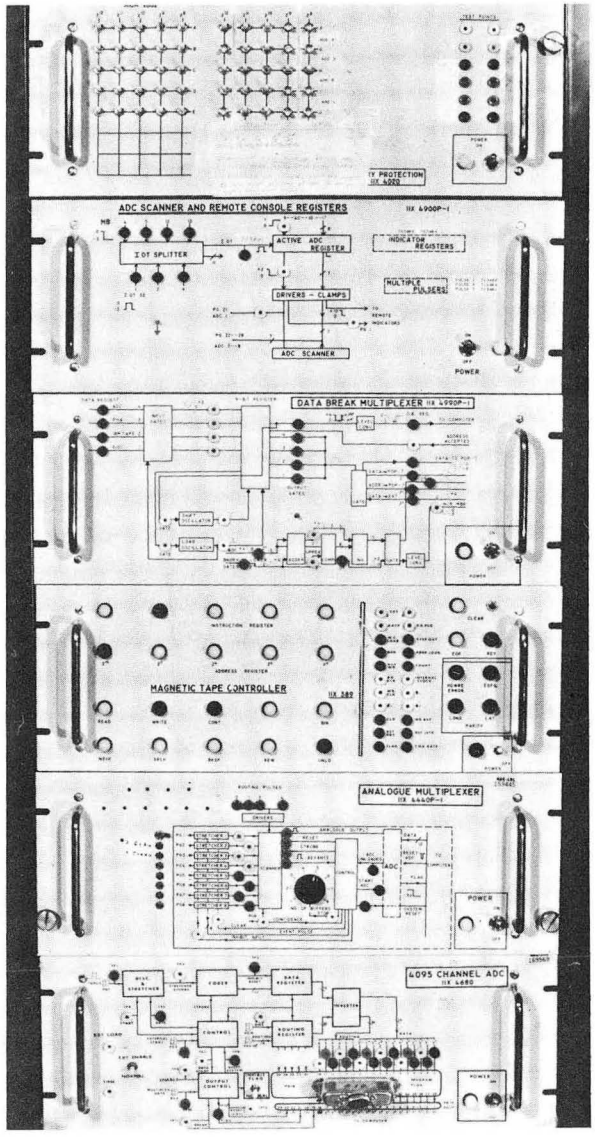

XBB 688-5311

Fig. 21-b. The PDP-7 peripheral hardware used in acquiring multiparameter coincidence data.

can be obtained from Ref. 94, but we will discuss briefly a few salient points of particular interest to the experimenter. In its present form the multiparameter system is capable of accepting four-parameter coincidence data, although provision has been made for expansion of this capability to handle eight-parameter input. For simple γ-γ coincidence work of the type we have carried out, two Ge(Li) energy signals and a timing signal generated by a conventional start-stop time-to-amplitude converter (TAC) are fed into the analogue storage and multiplexer unit. If a "valid event" coincidence pulse is received, the analogue pulses are stretched for several hundred microseconds until they can be individually encoded by the single ADC. Two points ought to be mentioned in connection with this highly important phase of the data-taking process: 1) we have found in practice that the stability and reproducibility of the analogue stretchers is remarkably good. In fact, we have been unable to discern any loss in system resolution when the Ge(Li) signals are subjected to stretching. 2) It is not unreasonable to expect that if the ADC employed were of the "rundown" or Wilkinson variety this exceptionally favorable condition might be altered because of the variable analysis time characteristic of that type of ADC. And although the potential problem itself ought not to be insurmountable (e.g., by inserting a rather long fixed dead-time before encoding each pulse), it must at least be conceded that the SBA-type ADC introduces to the system welcome speed and simplification, if not indispensable precision.

The total time required by the multiplex unit and ADC to process each coincidence event is of the order 200 μsec, so that the multiparameter

system is capable of handling about 1000 four-parameter coincidence events per second. We have found this to be more than adequate in all our work to data; the rate limitation is normally found to be in the Ge(Li) detector system itself, not in the multiparameter data handling system.

The PDP-7 computer is used for buffer storage of the incoming coincidence data and for generating a live display of the amplitude distributions for each of the input analogue signals. When full, the 512-word record in the data buffer is dumped on magnetic tape via an AMPEX TM-7 unit. In this way, all of the experimental information from an entire run is preserved serially in a 4096 × 4096 × 512 × 512 channel matrix for later analysis.

A second program, MULTIS, is complementary to the actual data accumulation program MULTIDR, and allows the user to do simple 4-parameter "coincidence" sorts on the PDP-7. It is not, however, practical as a rule to use the small computer for extensive multiparameter data analysis, since about 20 minutes is required for each pass over a 2400' IBM tape. All of our data have been sorted on the CDC-6600 computer at LRL using the code MSB (with minor modifications) written by Don Lebeck at LRL. This program allows one to sort and manipulate simultaneously data describing coincident photopeaks, backgrounds, and random coincidence events so that the resulting output presumably represents only "true" photopeak coincidences. The only real limitation of the sorting procedure on the 6600 is the size of the 6600 memory. We presently can sort up to 23 4096-channel coincidence spectra simultaneously. (A proportionately

larger number of compressed 1023- or 2048-channel spectra can be obtained instead, if desired.) A practical limitation, however, is the basic 6600 circuit speed. A large number of sorts with a high density of valid events may require 10 - 12 minutes of central-processor time per 2400' tape.

The triumphs and frustrations associated with "computerized science" are well-known by now; the topic is interesting but extremely time-consuming. Therefore we return at this point to the subject at hand--the decay of Ta^{176}--and refer the interested reader to the several references already cited for additional details.

In Fig. 22 then, we show the block-diagram of the experimental γ-γ coincidence system, with the computer and peripheral equipment again reduced to a single box. As indicated, we have employed a leading-edge discriminator in conjunction with a conventional stop-start TAC to extract timing information from the detector pulses. The apparatus shown is not atypical for this type of experiment, except perhaps for the logarithmic pulse-height compensation unit indicated at the TAC output. We have found this module to be capable of reducing the width of a typical Ge(Li)-Ge(Li) time distribution by a factor of two. The method of effecting this reduction is simple. Leading edge timing introduces an approximately exponentially increasing centroid shift of the time distribution as a function of decreasing energy, i.e. pulse height (cf. Fig. 23). By mixing appropriately attenuated energy analogue signals with their corresponding timing signal, one can roughly compensate for the "energy walk" of the timing pulses. The details of this simple but effective technique have

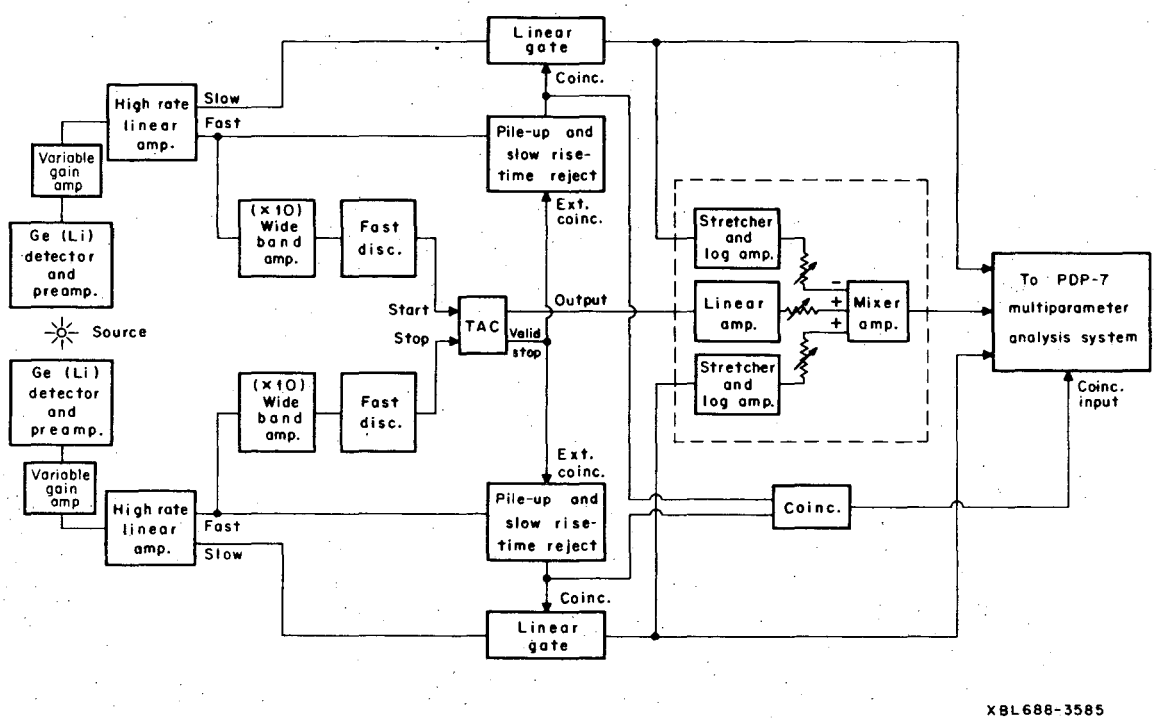

Fig. 22. Block diagram of a typical γ-γ coincidence data-acquisition system.

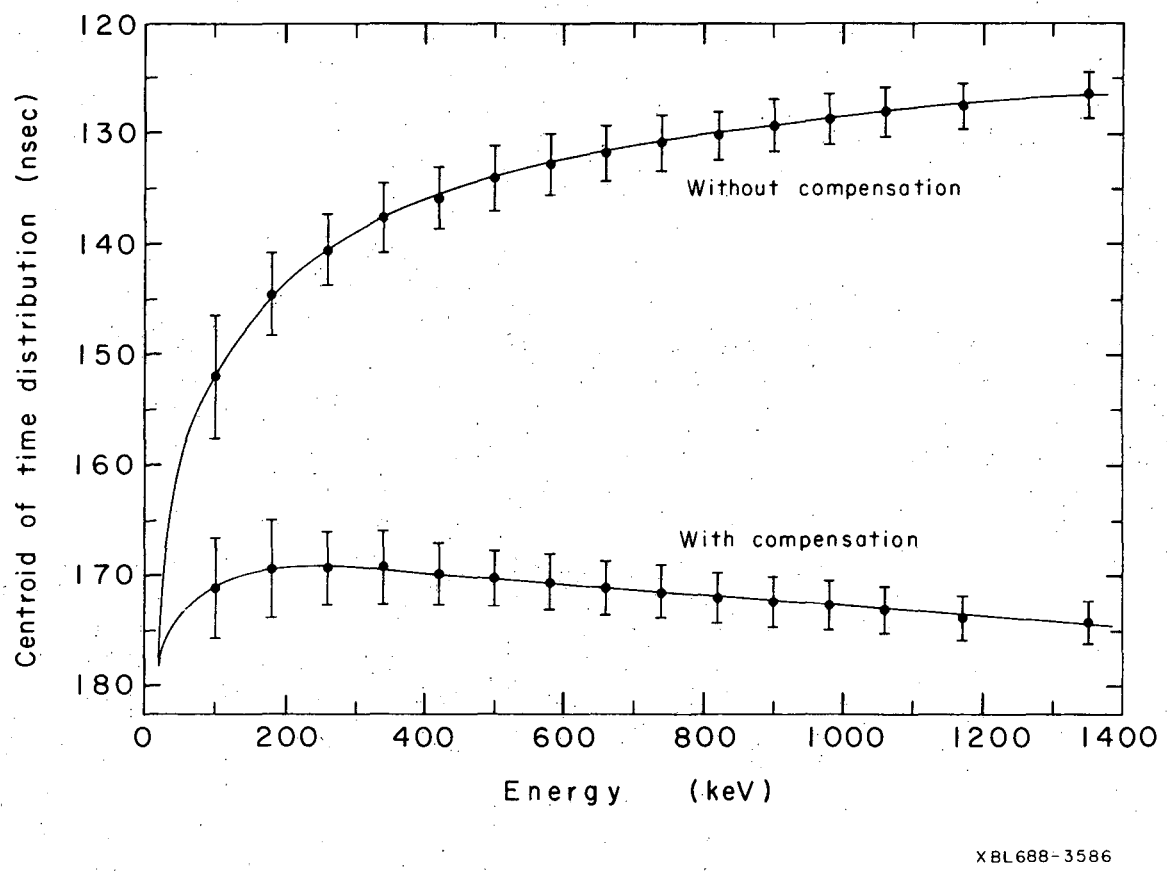

Fig. 23. Plot of the centroid position as a function of energy for a 13-mm depletion depth planar Ge(Li) detector. The "error" bars are used to indicate the full width at half maximum (FWHM) of the time distribution. The lower curve shows the effect of mixing the log E_γ compensation signal with the TAC output.

been discussed in Ref. 95. It is also possible to achieve somewhat more crudely a fairly effective pulse height compensation by simply employing two linear amplifiers having a flat, stretched pulse output (e.g., two "bias amplifiers") saturating at about 600 keV, above which the "energy walk" is relatively small. The two linear amplifiers then replace the logarithmic amplifiers in Fig. 22.

The γ-γ coincidence data on the decay of Ta^{176} have been taken using a 35 cm^3 "5-sided" coaxial drift Ge(Li) detector with resolution 3.4 keV at 1333 keV in conjunction with the 10 cm^3 planar detector described earlier. In Figure 24 is shown the time distribution curve for Ta^{176} γ-γ coincidences measured with these two detectors. The FWHM resolving time is 24 nsec. This allows one to set a digital time gate of about 65 nsec for the purpose of sorting. The large "spike" to the left of the main time distribution peak represents events arising from the coincident pulses fed into the two Ge(Li) preamplifiers for the purpose of gain stabilization.

3. Experimental results--the decay of Ta^{176}

The Compton-suppressed singles γ-ray spectrum of the decay of Ta^{176} has allowed us to identify over 300 transitions associated with the energy levels of Hf^{176}. Many of the transitions are, to be sure, weak, but the interfering activities from Ta^{178}, Ta^{177}, Ta^{175}, and its daughter, Hf^{175} were also found to be relatively weak, and in any case none of these nuclei has lines of significant intensity above about 1 MeV. In Figs. 25 and 26 we show the γ-ray singles spectrum obtained with the Livermore apparatus described earlier. The data shown represent two separate runs,

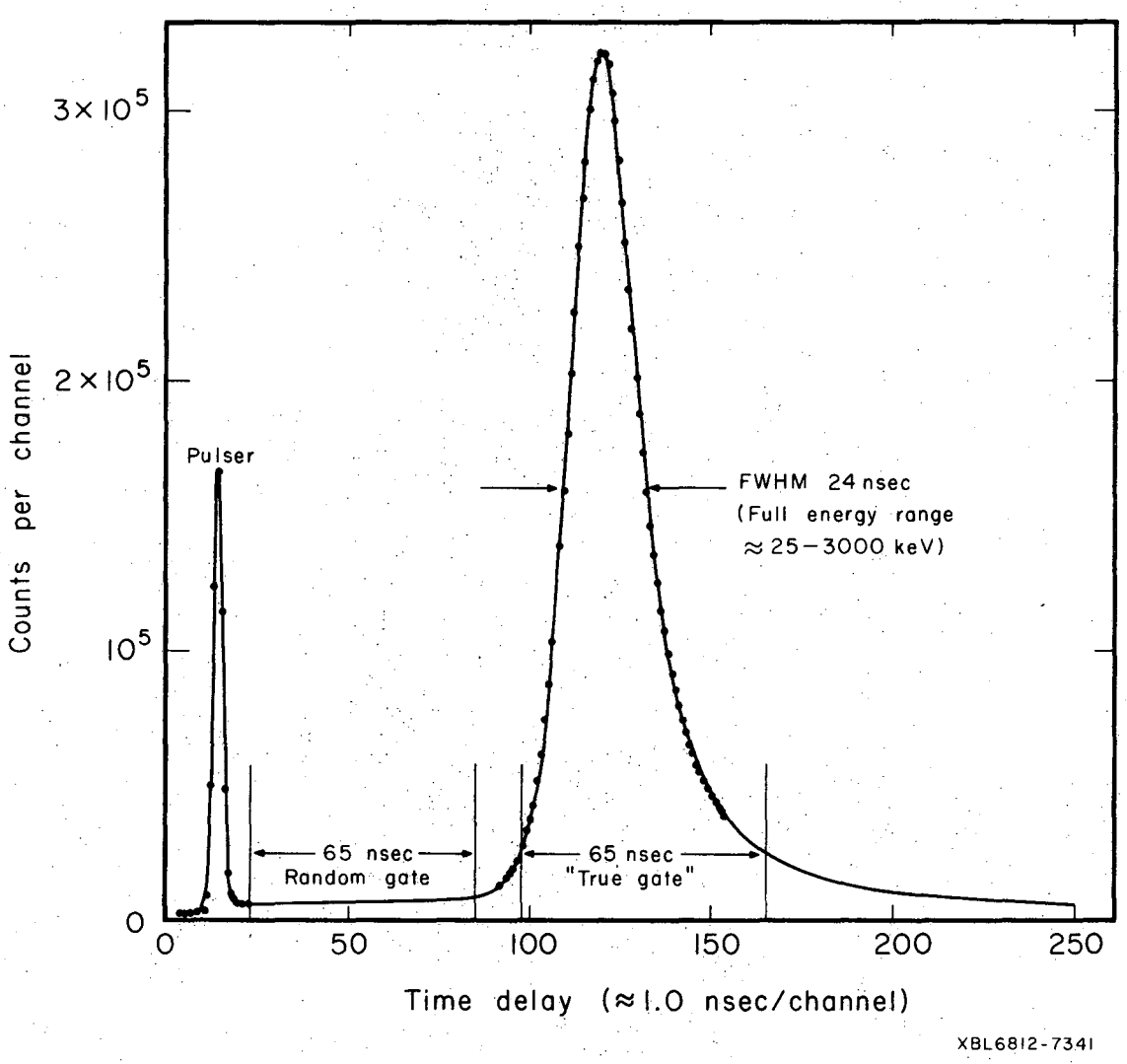

Fig. 24. Time distribution for Ta^{176} γ-γ coincidence data. Taken with a 35 cm^3 coaxial "U-drift" Ge(Li) detector in conjunction with a 10 cm^3 planar Ge(Li) detector.

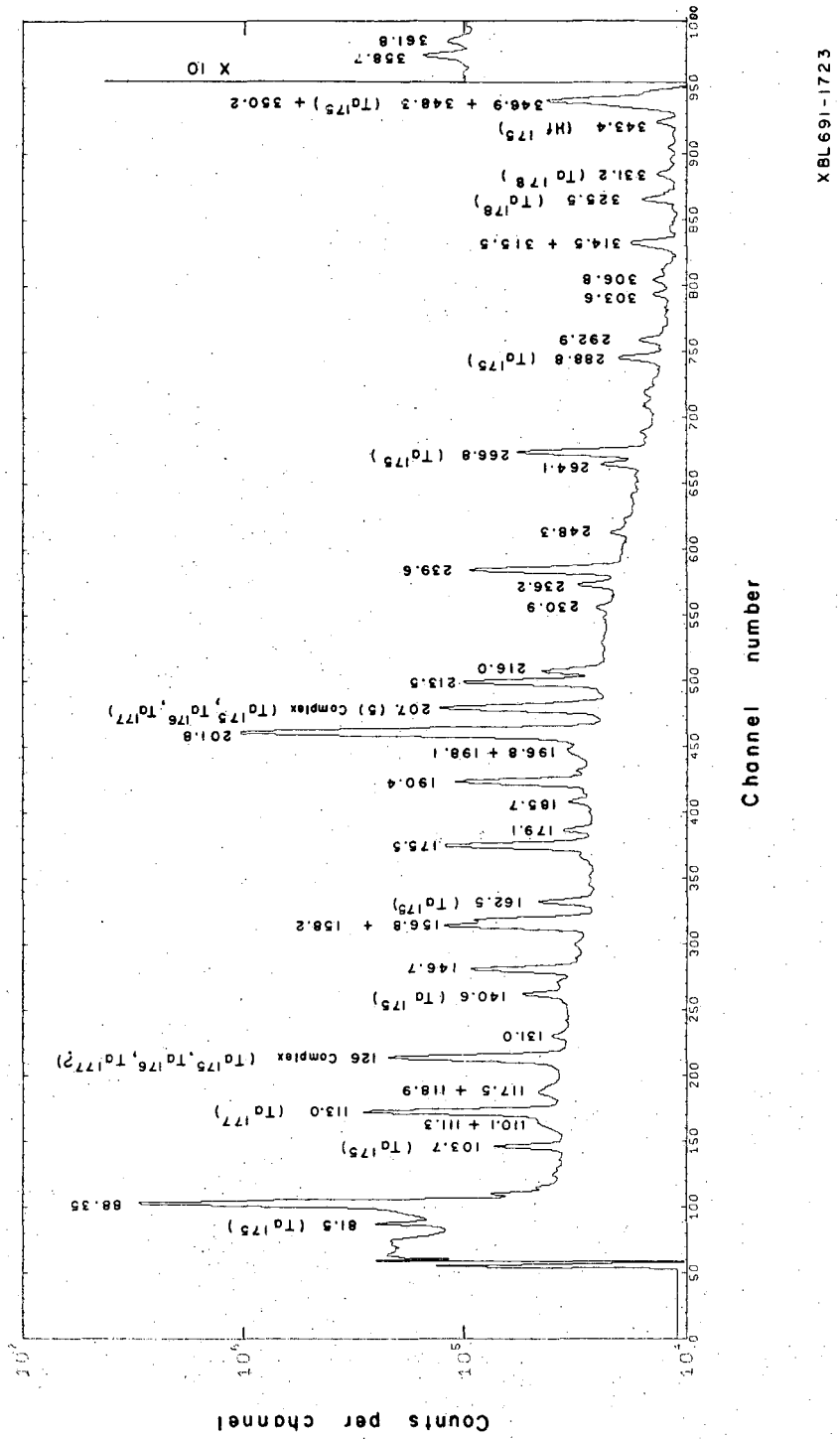

Fig. 25-a. The Compton-suppressed Ge(Li) γ-ray singles spectrum of Ta^{176} in the region 80 - 365 keV.

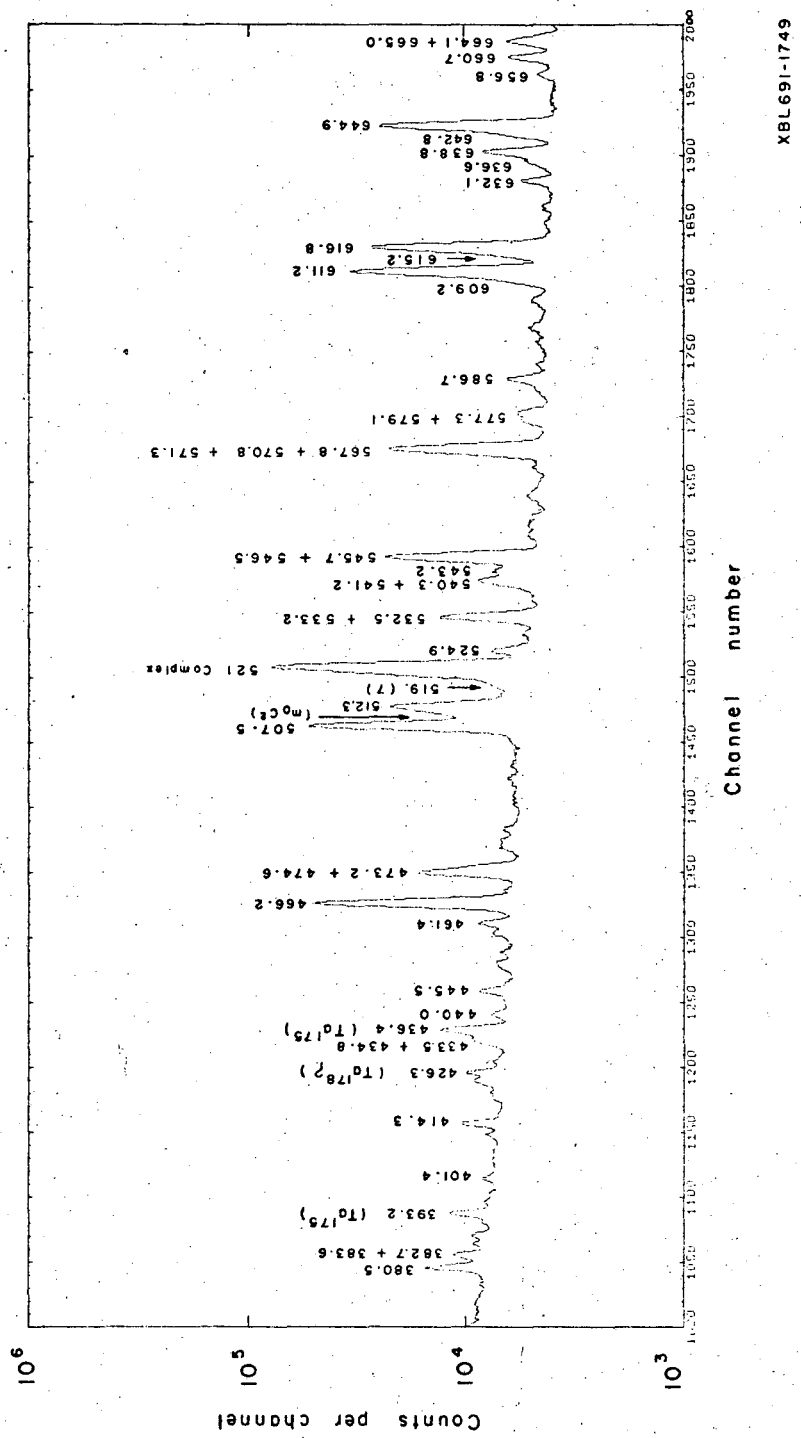

Fig. 25-b. The Compton-suppressed Ge(Li) γ-ray singles spectrum of Ta^{176} in the region 365 - 667 keV.

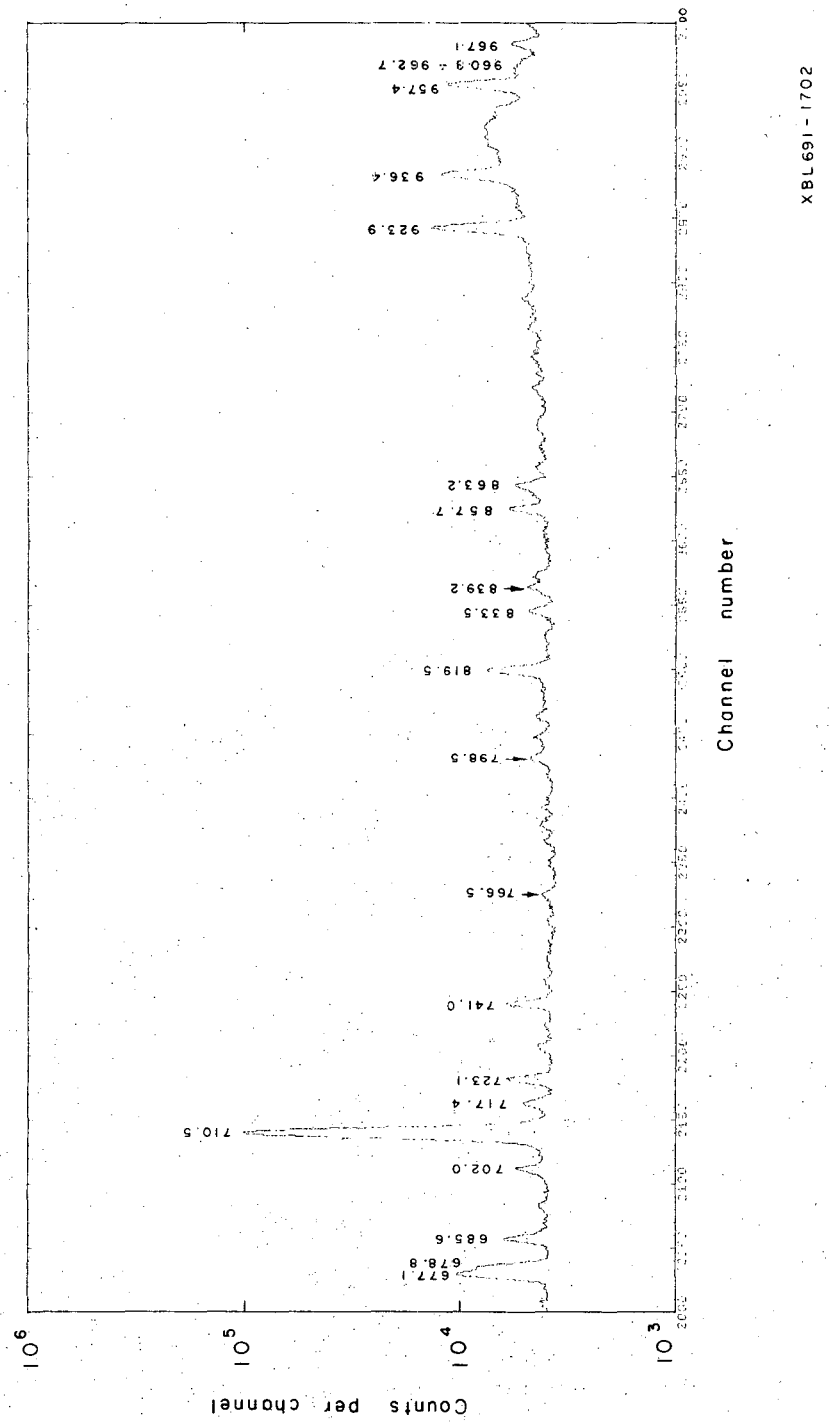

Fig. 25-c. The Compton-suppressed Ge(Li) γ-ray singles spectrum of Ta^{176} in the region 667 - 970 keV.

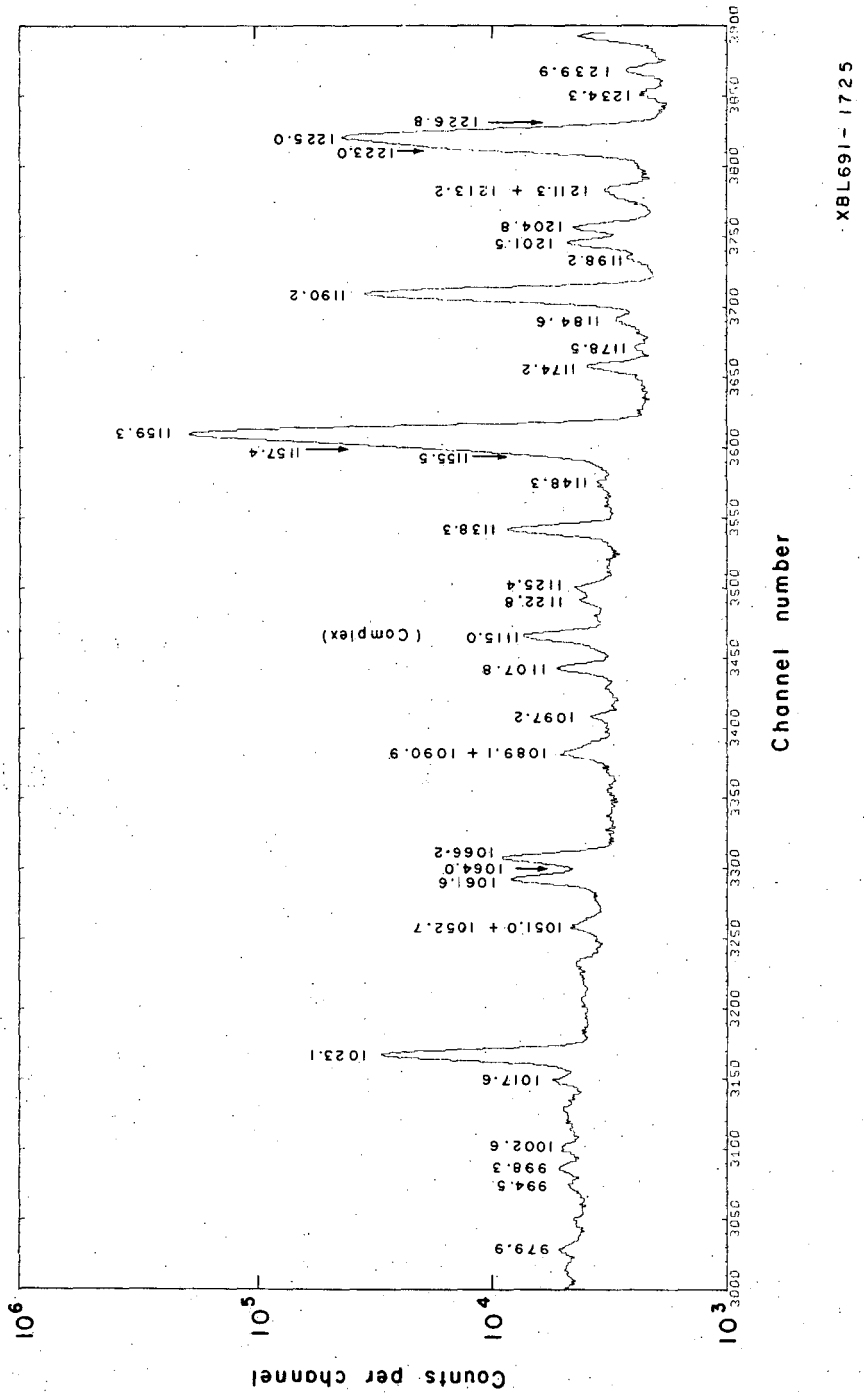

Fig. 25-d. The Compton-suppressed Ge(Li) γ-ray singles spectrum of Ta^{176} in the region 970 - 1245 keV.

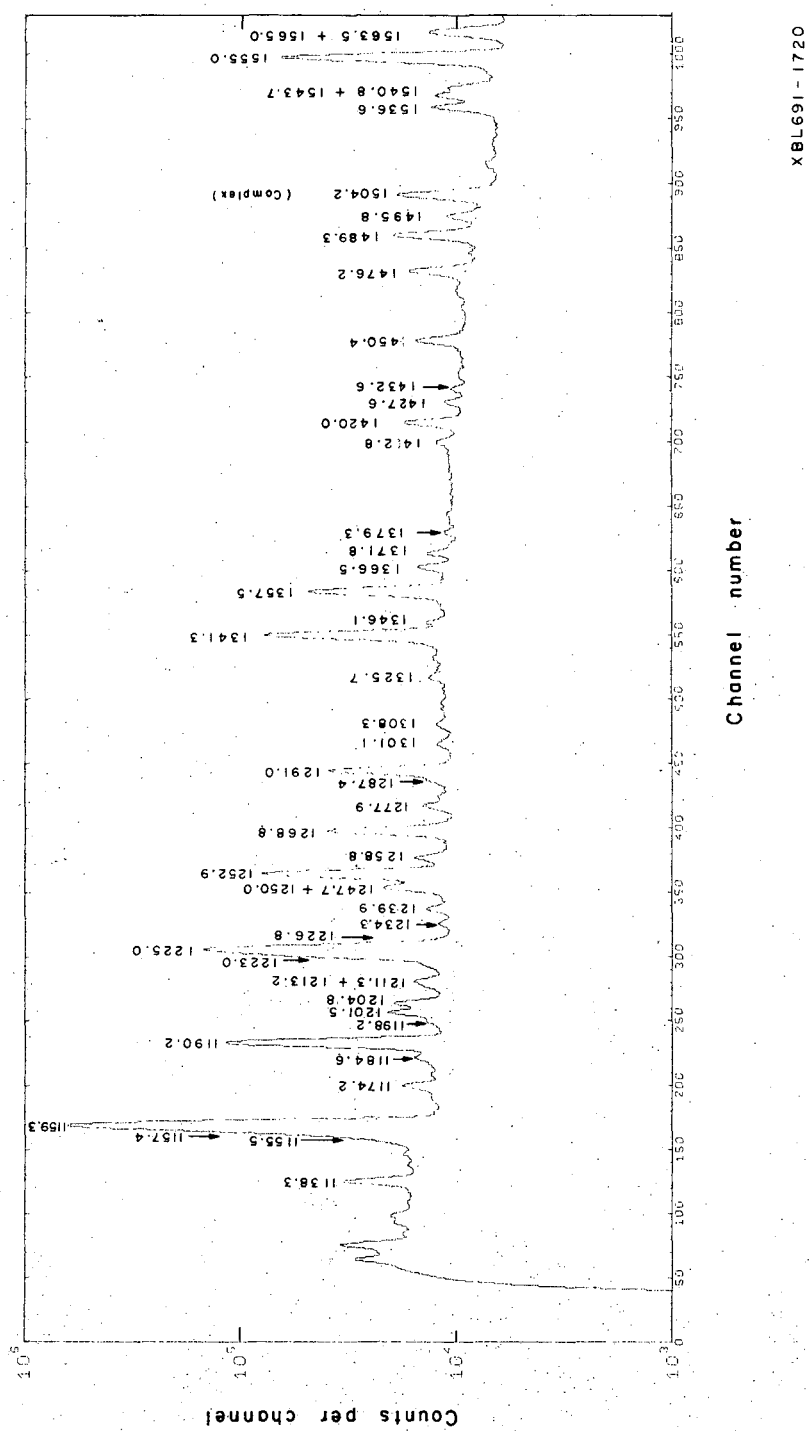

Fig. 26-a. The Compton-suppressed Ge(Li) high-energy γ-ray singles spectrum of Ta^{176} in the region 1060 - 1570 keV.

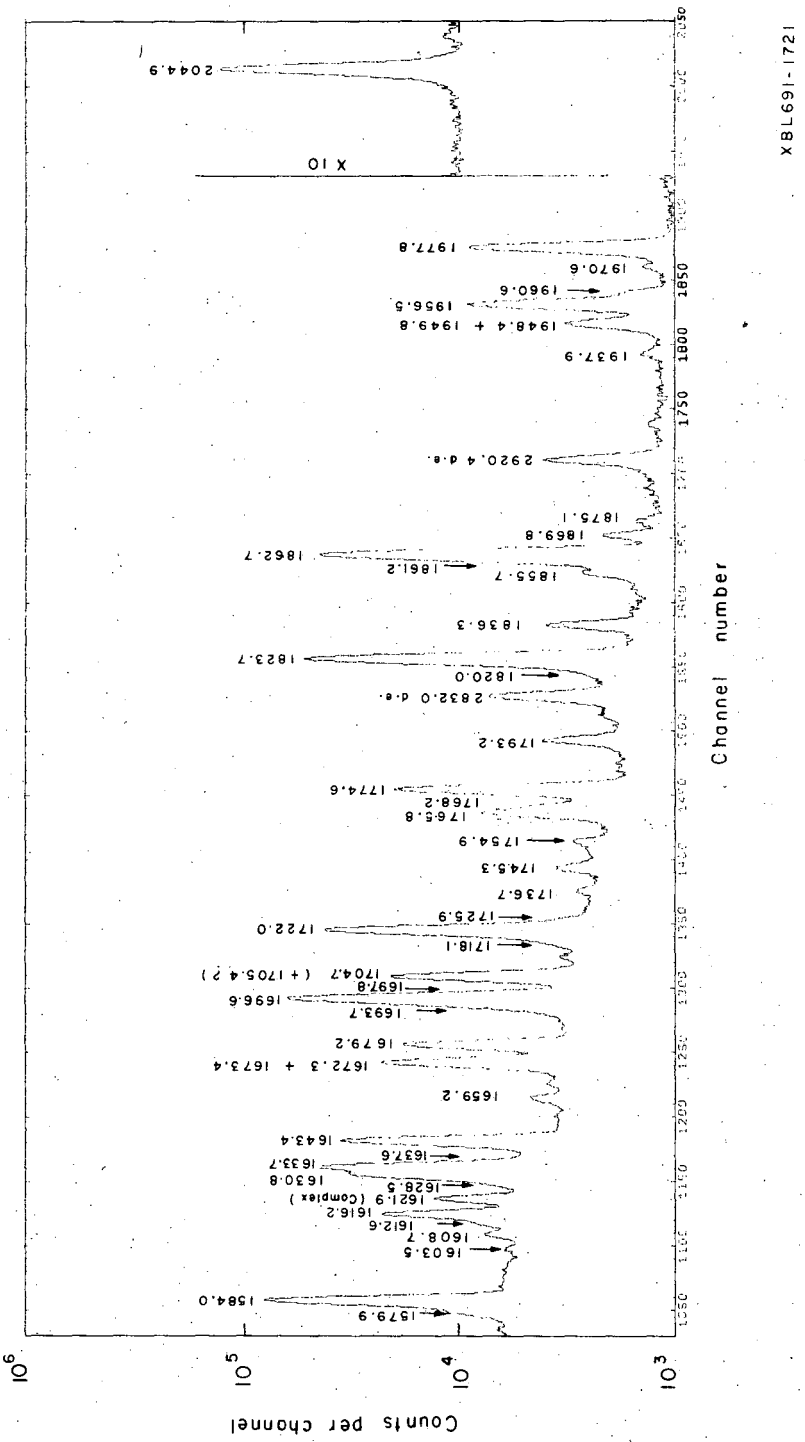

Fig. 26-b. The Compton-suppressed Ge(Li) high-energy γ-ray singles spectrum of Ta^{176} in the region 1570 - 2060 keV.

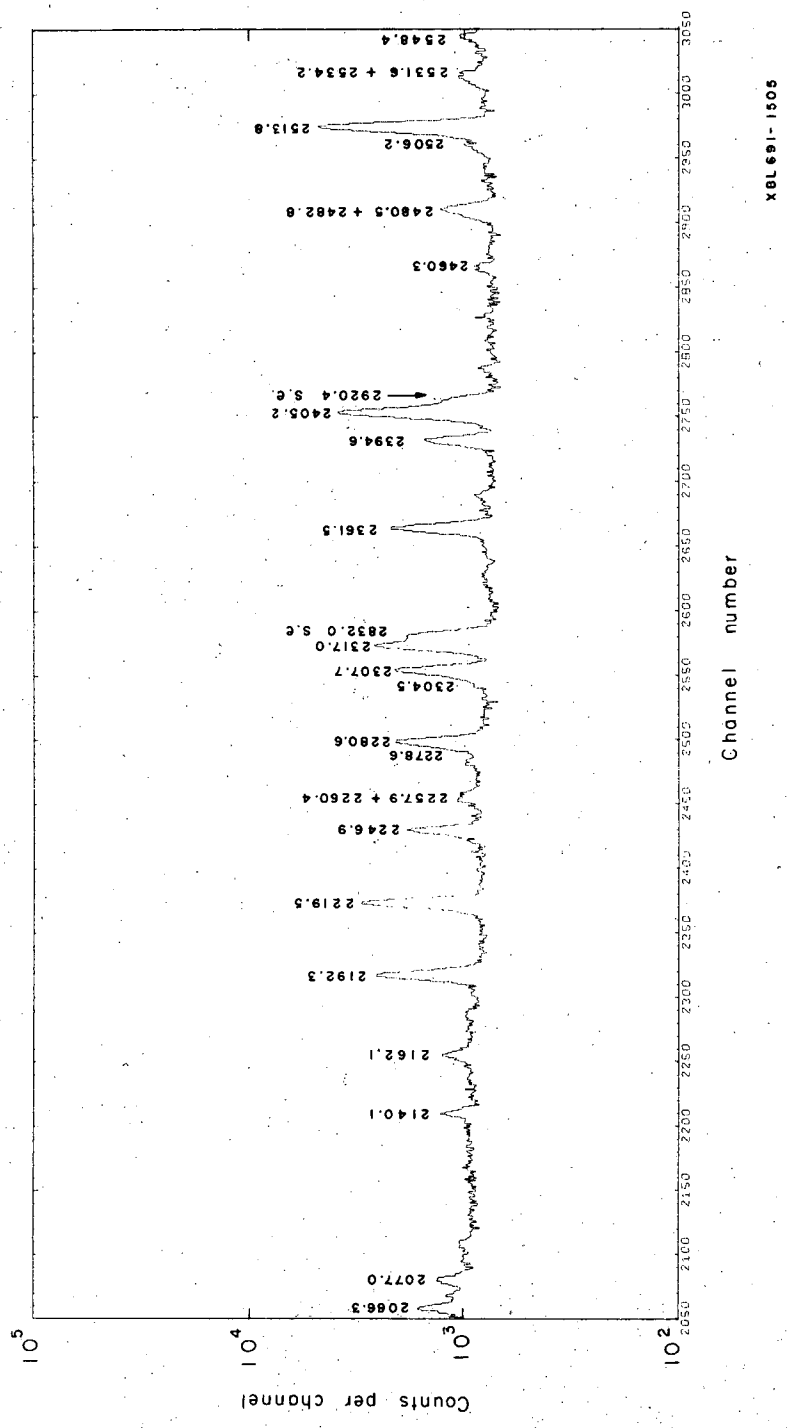

Fig. 26-c. The Compton-suppressed Ge(Li) high-energy γ-ray singles spectrum of Ta^{176} in the region 2060 – 2550 keV.

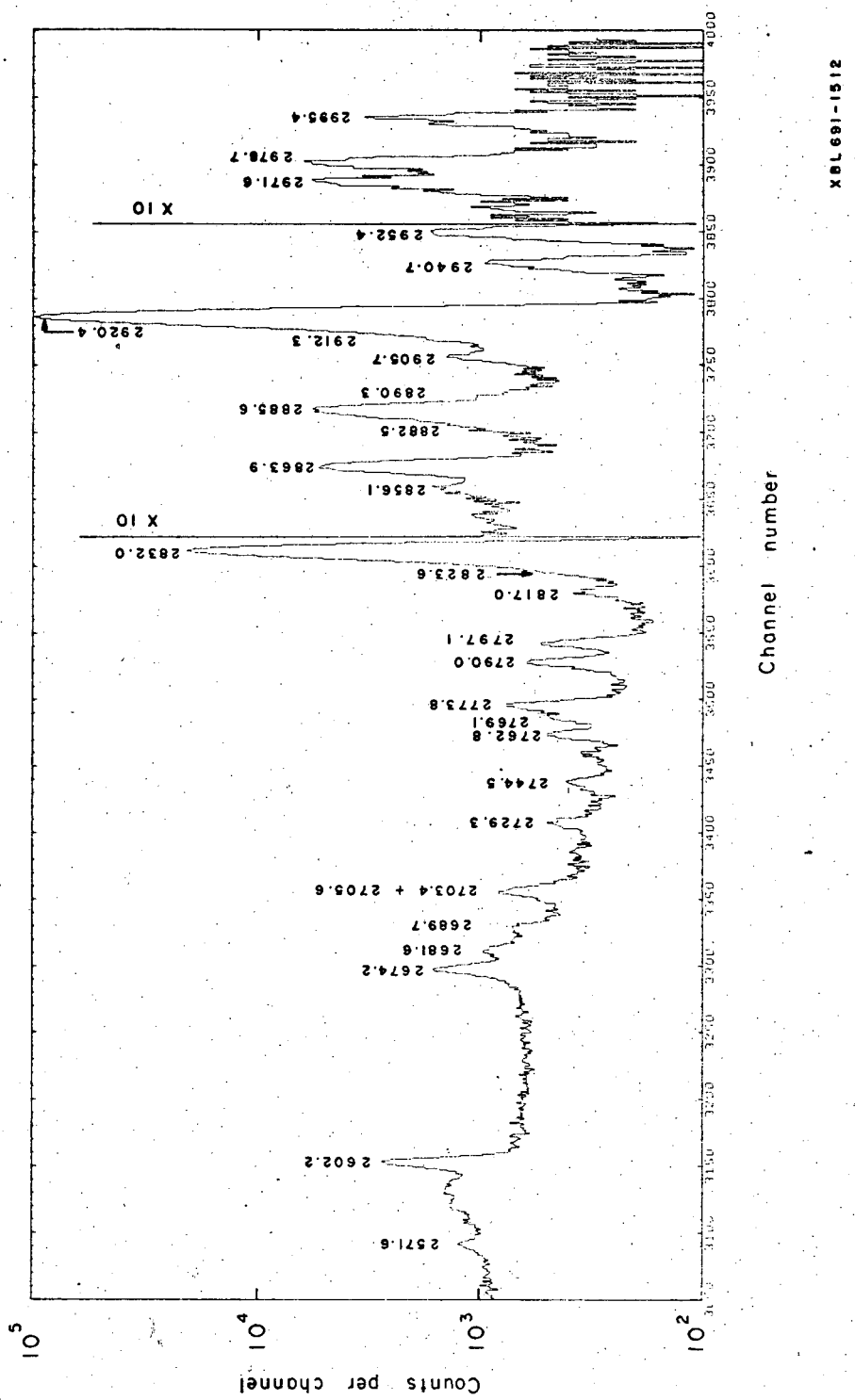

Fig. 26-d. The Compton-suppressed Ge(Li) high-energy γ-ray singles spectrum of Ta^{176} in the region 2550 - 3020 keV.

one from ≈ 75 - 1250 keV, the other a high energy run from 1.06 - 3.00 MeV. The lines from Ta^{175}, Ta^{177}, Ta^{178}, and Hf^{175} contamination are appropriately labeled. It should be noted that one does not expect to see the escape peaks appearing prominently in the Compton-suppressed spectrum, since single-escape peaks will presumably be suppressed just as efficiently as are Compton-scattered events, while the double-escape lines will be even further suppressed. To illustrate the point, we offer for comparison in Figs. 27 the low energy Ta^{176} singles spectrum taken with the 10 cm^3 planar detector in our laboratory. Note that the double-escape lines measured at 801.7 and 840.6 keV arising from the very strong 1823.8- and 1862.8-keV transitions show up prominently in the spectrum, whereas they are hardly to be seen in the anti-Compton spectrum, if indeed they are present at all. We therefore feel confident that escape peaks are essentially deleted from the low energy anti-Compton spectrum. Unfortunately this is not quite so for the high energy Compton-suppressed spectrum in Figs. 26. A glance at the background in the region around 1200 keV reveals on comparison with Fig. 25d the fact that the Compton-suppression anti-coincidence unit was operating intermittently during this run. Therefore the strong double-escape lines from the 2832- and 2920-keV transitions, though sharply reduced in Fig. 26b, are still prominent. We did not consider it worthwhile to retake the data, however, since we were able in our laboratory to obtain a pair spectrum to resolve any ambiguities in the high-energy portion of the Ta^{176} spectrum.

Energy calibration has been carried out employing both "internal" and "external" techniques. Numerous appropriate standards (cf. Appendix B)

have been used at energies less than 1.35 MeV, and primarily Co^{56} has been used at higher energies. The recent excellent standardization work by Gunnink, et al.[96] has been especially valuable in this regard. In Appendix B, the details of the energy determinations are discussed.

An aid to both the energy measurements and to resolving stronger multiplets in the low energy region of the spectrum were the high resolution data shown in Fig. 28. This spectrum was obtained with the "thin window" 1 cm^3 crystal described in Appendix A.

Finally, in Figs. 29 we show the "pair" spectrum of Ta^{176}. The resolution here is considerably better than in any of the other high-energy spectra, and from about 1600 - 2700 keV the peak-to-background ratio is also more favorable. Unfortunately, the low rate at which the data can be gathered does not in this case enable one to exploit fully the advantages of the pair technique other than for the stronger lines in the spectrum.

We have combined the data from these several sources to determine the energies and intensities of the γ-ray transitions following decay of Ta^{176}. In general, the intensities are derived from the Compton-suppressed data, checked against the data taken in our own laboratory. Where the "thin-window" and "pair" spectra provide better information, we have made use of those data.

Analysis of the Ta^{176} spectra for peak centroids (energies) and intensities posed no small problem. For the past 18 months we have been fortunate in having at our disposal for this purpose the spectral analysis computer code, SAMPO, developed by Routti and Prussin[97]

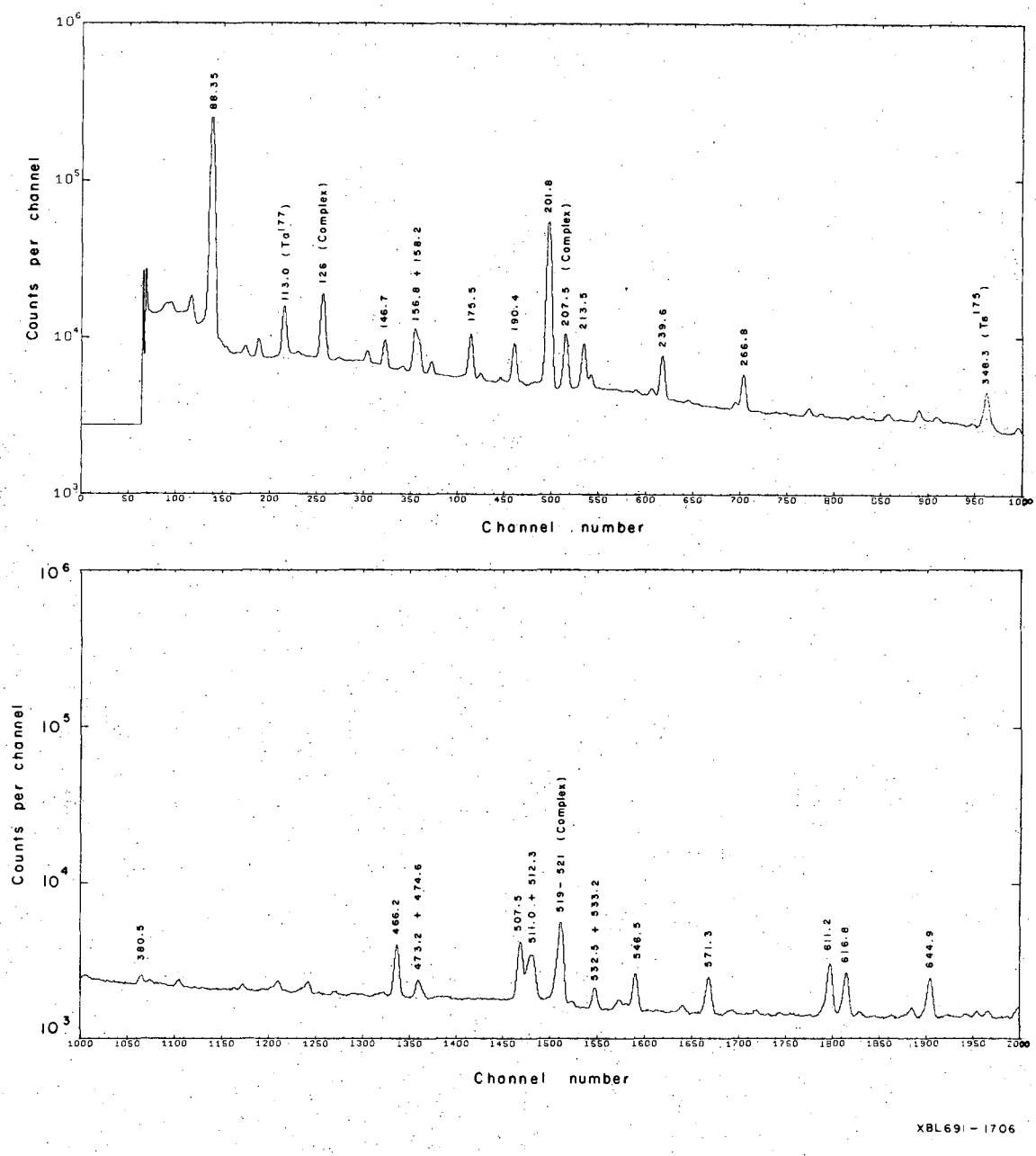

Fig. 27-a. The γ-ray singles spectrum of Ta^{176} in the region 70 - 680 keV taken with the 10 cm^3 planar Ge(Li) diode.

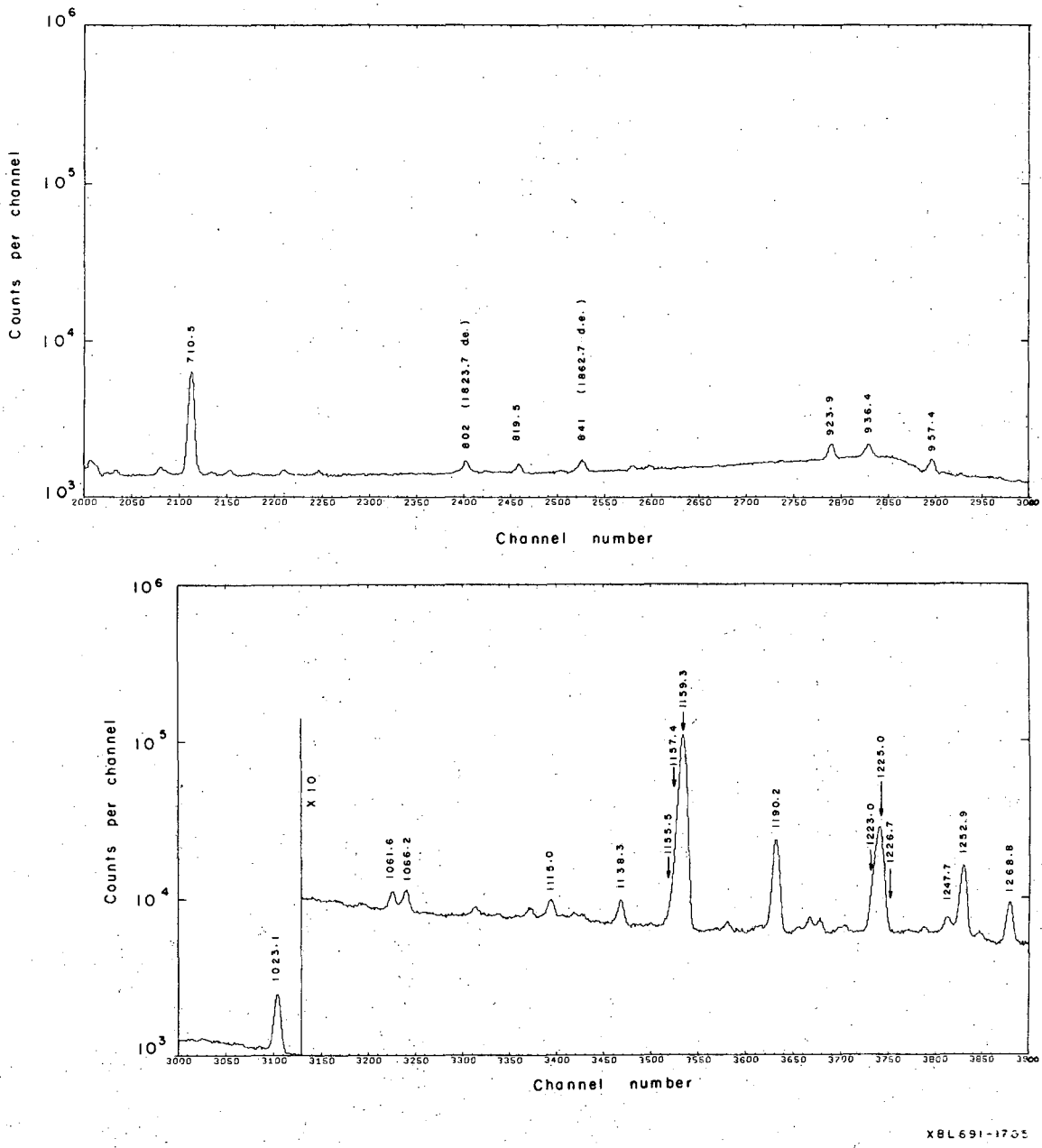

Fig. 27-b. The γ-ray singles spectrum of Ta^{176} in the region 680 - 1270 keV taken with the 10 cm^3 planar Ge(Li) diode.

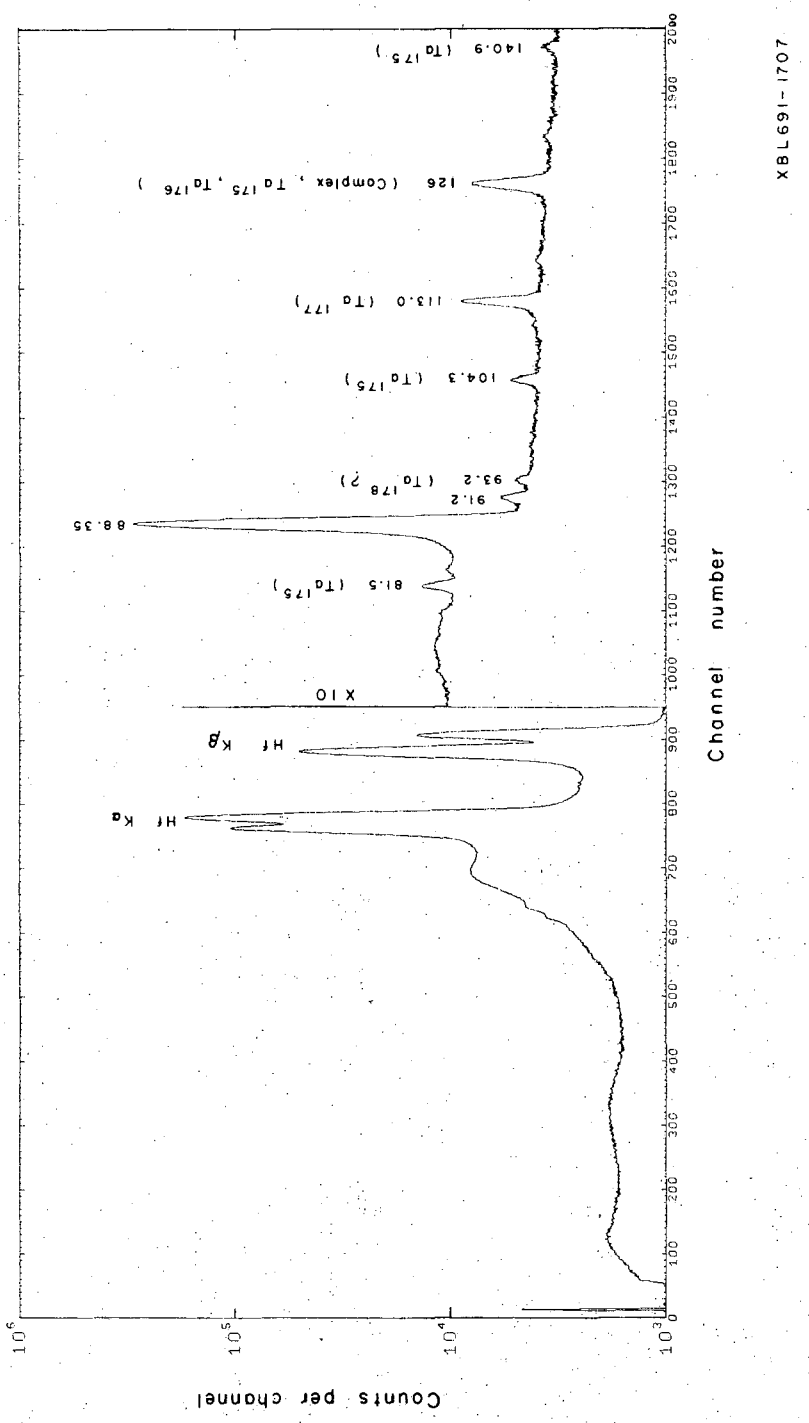

Fig. 28-a. The low energy γ-ray singles spectrum of Ta^{176} taken with a 1-cm^3 "thin window" Ge(Li) diode. 0 - 142 keV.

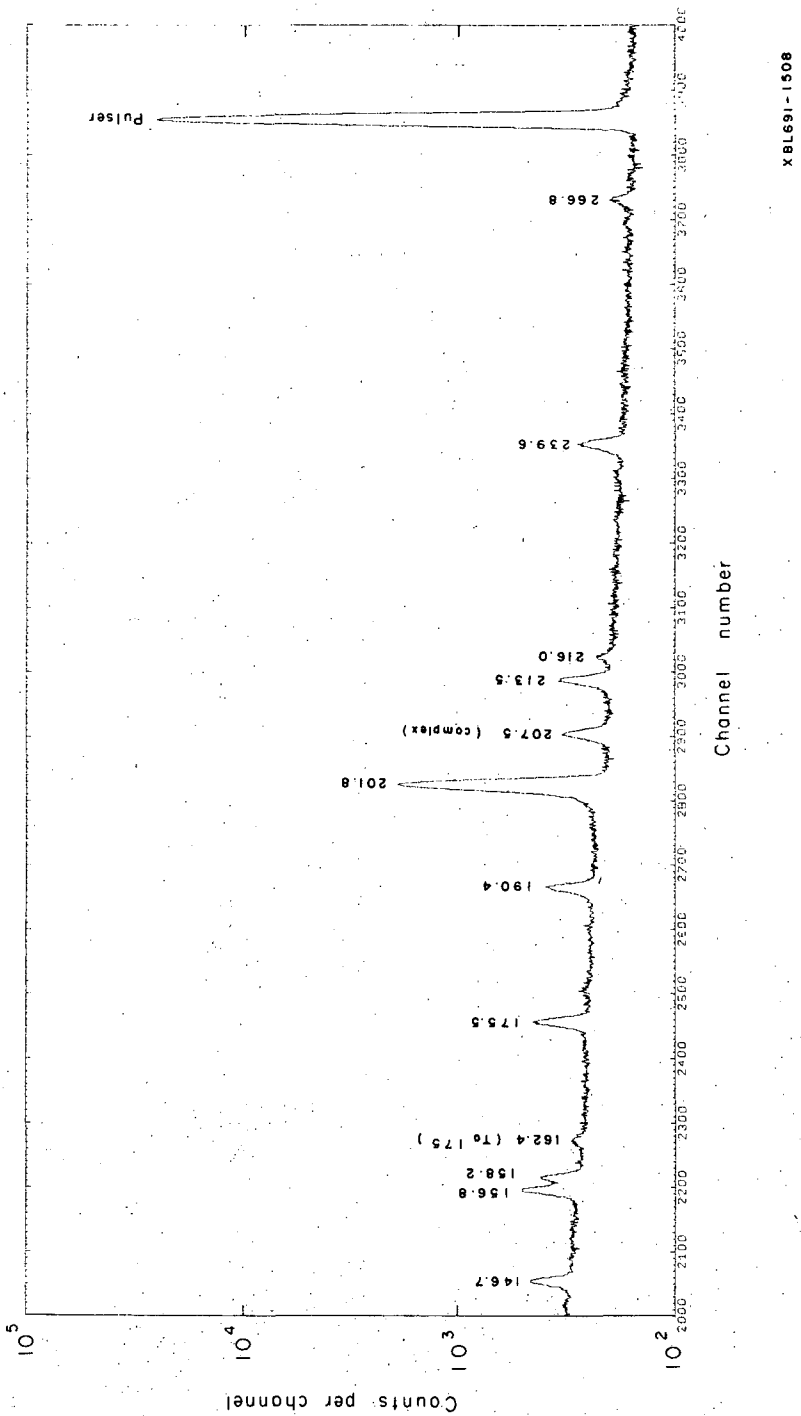

Fig. 28-b. The low energy γ-ray singles spectrum of Ta^{176} taken with a 1-cm^3 "thin-window" Ge(Li) diode. 142 - 270 keV.

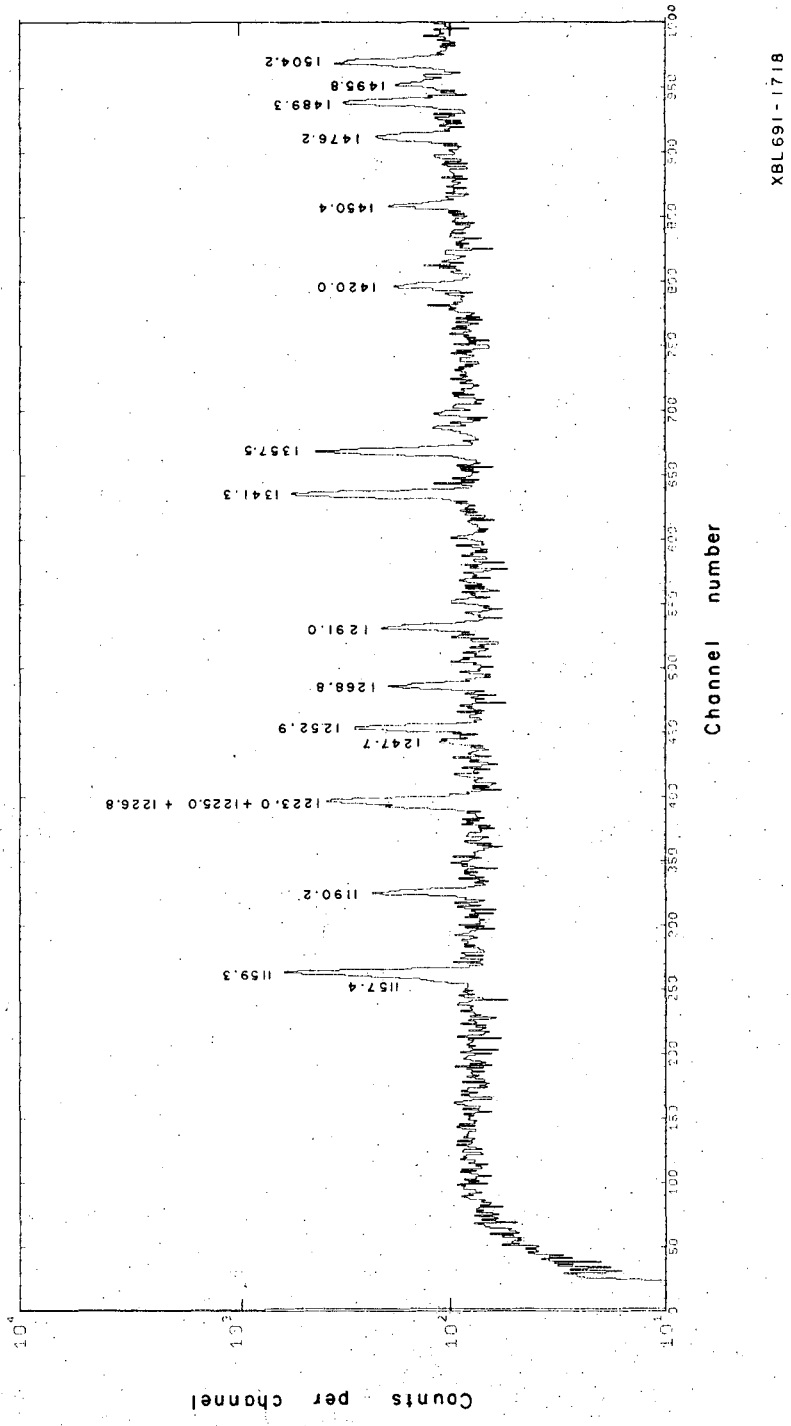

Fig. 29-a. The Ta^{176} "pair spectrum" taken with the five-crystal pair spectrometer of Fig. 20. All energies represent γ-ray transition energies. 1025 - 1520 keV.

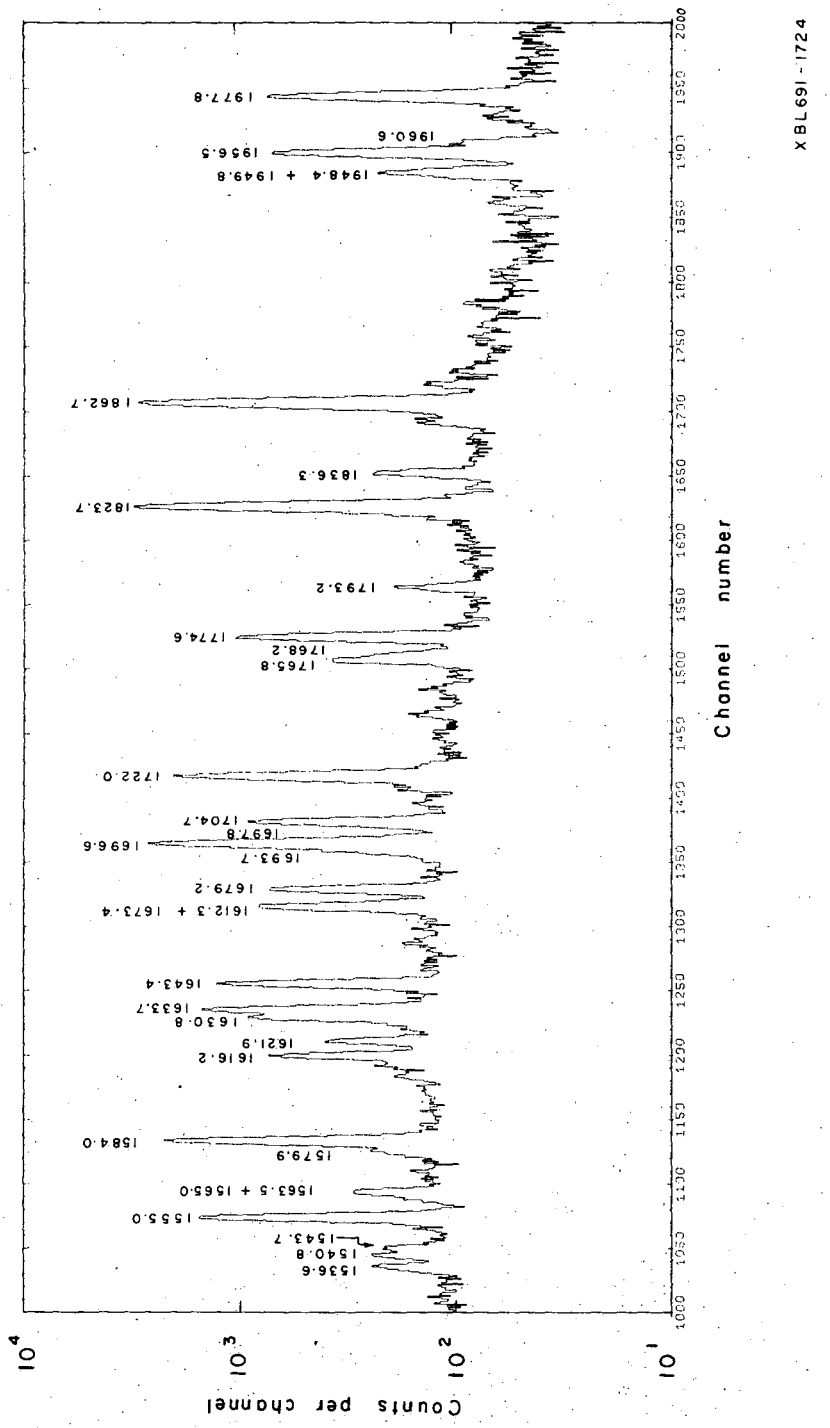

Fig. 29-b. The Ta^{176} "pair spectrum" taken with the five-crystal pair spectrometer of Fig. 20. All energies represent γ-ray transition energies. 1520 - 2000 keV.

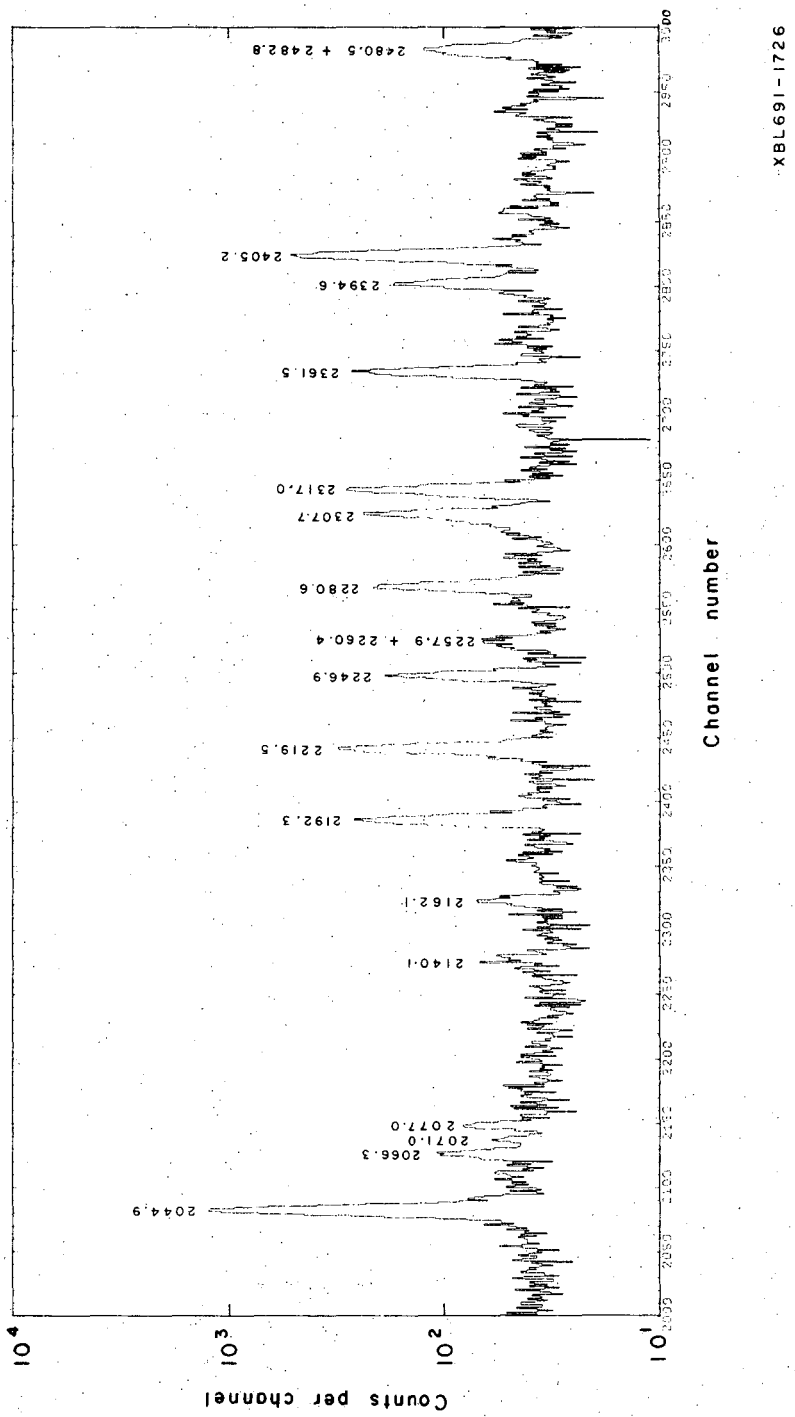

Fig. 29-c. The Ta^{176} "pair spectrum" taken with the five-crystal pair spectrometer of Fig. 20. All energies represent γ-ray transition energies. 2000 - 2490 keV.

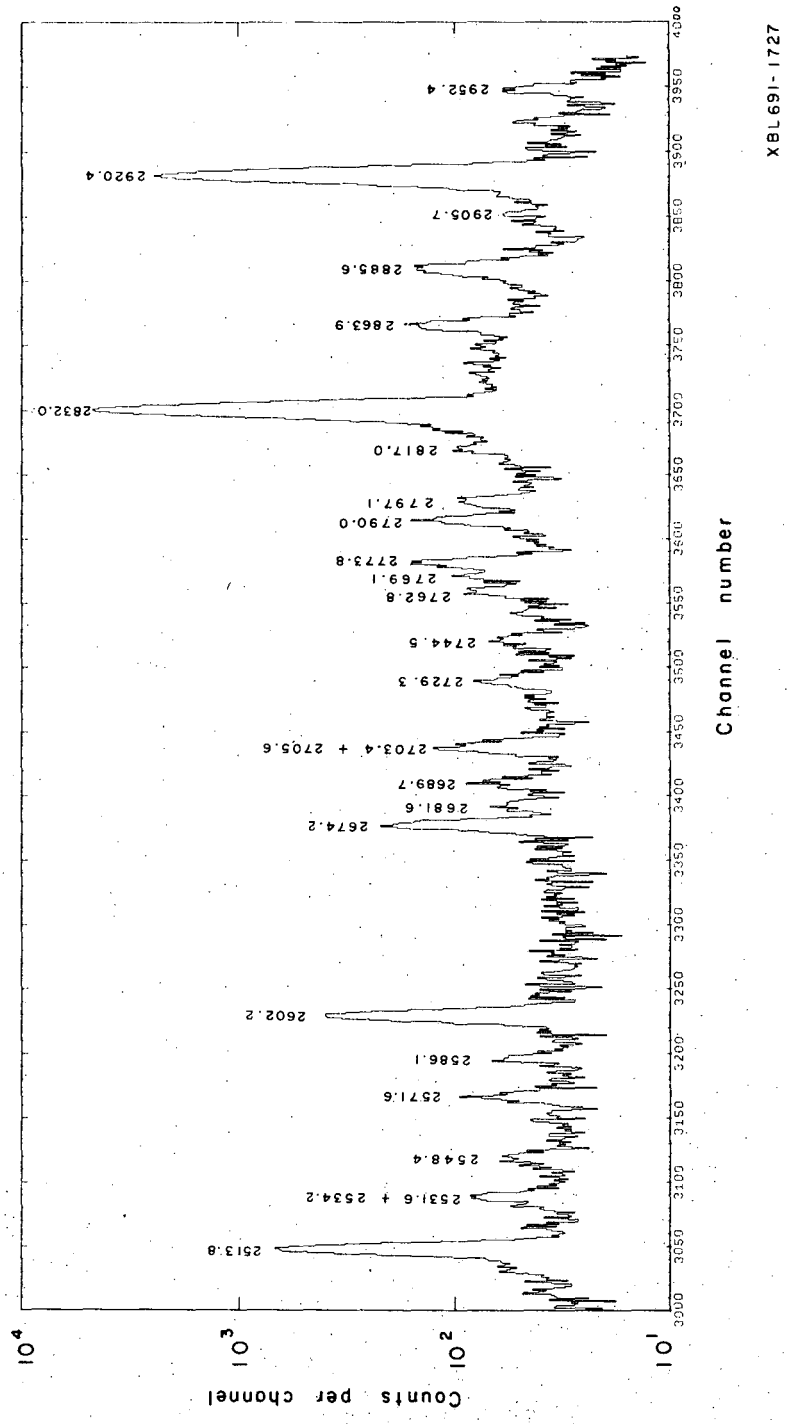

Fig. 29-d. The Ta^{176} "pair spectrum" taken with the five-crystal pair spectrometer of Fig. 20. All energies represent γ-ray transition energies. 2490 – 3000 keV.

and now in extensive use at LRL. To bring the interested reader up to date on our present "state of the art" in reduction of nuclear spectroscopic data we present a brief discussion of the topic in Appendix B.

In Tables 13, then, we list the observed γ-rays from the decay of Ta^{176} to levels in Hf^{176}. We have chosen to classify the γ-rays into two categories depending on their intensity. In Table 13a are listed only those lines observed to have intensity ⩾ 1% relative to the 710.5-keV line. Table 13b lists those lines having intensity < 1% of the 710-keV intensity. With very few exceptions, we have been unable to definitely place in the decay scheme any of the transitions in the latter category. Although we believe the energies (of the stronger lines) to be precise to 0.2 keV or less over the entire energy range of the spectrum, because of the extreme complexity of the spectrum we have not considered that simple energy sums and differences alone provide sufficient information for definite placement of a transition in the decay scheme.

As a consequence of the ease with which complete and, for the most part, statistically satisfying coincidence data can now be gathered using the PDP-7 multiparameter data system, it is no longer unreasonable and in the case of Ta^{176} it is necessary to require γ-γ coincidence confirmation of all assignments to a proposed level scheme. The data we present in Appendix C were gathered with the 10 cm^3 planar and 35 cm^3 coaxial detectors described earlier. The two detectors were placed in 90° geometry with a lead absorber between the detectors to minimize scattering effects. Calibrated absorbers of ≈ 15 mil Cd and ≈ 5 mil Cu were placed before each detector to reduce the number of low energy

Table 13-a. γ-ray transitions observed in the decay of Ta^{176}: a) Transitions observed with intensity ⩾ 1% of the 710.5-keV γ-ray intensity.

E_γ(keV)[a,d]	I_γ[b]	α_K[c]	$\alpha_K/\alpha_{\Sigma L}$	Multipole	Level[e] placement
88.35 (4)	230.	>8.(-1)	>0.2	E2	88.35
91.23 (4)	1.1	>6.0†	<3.7†		1404.5
*125.(4)[f]	⩽4.				1912.0
146.74 (5)	3.9	8.8(-1)†			1856.9
156.84 (7)	6.6	3.7(-1)†			1404.5
158.19 (7)	4.2	8.6(-1)†			1862.8
175.50 (7)	7.8	5.1(-1)†	5.6		1819.0
190.36 (7)	7.6	4.3(-1)	7.2		1862.8
201.84 (6)	102.	1.65(-1)[g]	2.0	E2	290.2
*207.(5)[h]	⩽1.5				1912.0
213.50 (6)	9.8	2.9(-1)			1856.9
216.00 (7)	2.2				1793.7
236.19 (7)	1.5	2.2(-1)			1958.1
239.62 (6)	10.0	2.5(-1)	⩾5.7		1912.0
264.13 (6)	1.4				1577.6
315.50 (15)	1.5 (2)				[2265.2]
346.90 (20)	2.1				1924.6
350.18 (20)	1.5	8.9(-2)			2308.3
358.72 (20)	1.8				2308.3
380.48 (20)	2.4	1.8(-2)			1958.1
414.34 (15)	1.4	6.2(-2)			[1793.6],[1819.0]
426.34 (15)	1.2 (2)	4.7(-2)			[1767.5]
445.52 (8)	1.0				[2308.3],[1672.3]
461.41 (8)	1.1 (2)				[(2944.1)]
466.16 (7)	20.6				1912.0
473.21 (7)	5.1				2944.1
474.64 (8)	1.6				[(2066.2)],[1854.0]

(continued)

Table 13-a. Continued

E_γ(keV)[a,d]	I_γ[b]	α_K[c]	$\frac{\alpha_K}{\alpha_{\Sigma L}}$	Multi-pole	Level[e] placement
507.46 (9)	26.7	3.8(-2)	6.4	M1	2432.0
512.34 (10)	9.5	3.1(-2)	7.0	M1	1958.1
*519.7 (2)	(6.)				1924.6
*520. (6) (2)	(5)				
*521.3 (1)	(5.)	≈3.6(-2)	≈8		2470.7
*521.6 (1)	(45.)				1862.8
524.90 (11)	1.1 (25)				
532.54 (11)	4.5 (7)	3.3(-2)			1912.0
533.23 (16)	1.2 (4)				[(2482.9)]
540.27 (13)	1.1 (2)				2307.8
541.24 (12)	1.7 (2)				
543.18 (11)	1.5				2265.2
545.74 (11)	4.1 (7)				
546.53 (10)	9.8	⩽4.5(-2)			2470.7
569.77 (11)	2.1 (3)				1862.8
570.76 (10)	8.5	3.5(-2)			1912.0,[(2482.9)]
571.30 (9)	4.9				[1819.0]
579.08 (15)	1.1				1958.1
586.72 (9)	1.6				
609.25 (9)	1.4 (2)				[1856.9]
611.16 (8)	23.4	2.6(-2)	6.8	M1	1924.6
615.22 (9)	1.9 (3)				[1862.8]
616.79 (8)	18.6	4.4(-3)		E1	1958.1
632.12 (9)	1.3				
638.83 (8)	3.7	⩽2.2(-2)			2432.0
642.85 (8)	1.8	⩽4.3(-2)			
644.86 (8)	18.4	2.1(-2)			1958.1
660.67 (8)	2.2				[2969.0]

(continued)

Table 13-a. Continued

E_γ(keV)[a,d]	I_γ[b]	α_K[c]	$\frac{\alpha_K}{\alpha_{\Sigma L}}$	Multi-pole	Level[e] placement
664.07 (10)	1.6 (2)				[(2482.9)]
665.01 (12)	1.1 (3)				[2308.3]
677.09 (8)	5.9	≤2.1(-2)			1924.6
678.85 (8)	3.8	1.9(-2)			2944.1
685.55 (8)	2.2	1.5(-2)			
701.96 (9)	1.3				[1949.7]
710.50 (8)	100.	1.8(-2)	6.0	M1	1958.1
717.45 (8)	1.2				
723.10 (8)	2.4	2.1(-2)			[1949.7]
740.97 (9)	2.5	3.1(-2)			
819.49 (10)	4.8				2265.2
833.50 (10)	1.4 (2)				[2791.5],[2878.2]
839.25 (11)	1.3 (2)				[2905.6]
857.66 (10)	2.6				
863.19 (10)	2.2				
923.94 (8)	13.5	≈1.3(-3)		E1	2265.2
936.42 (8)	10.4	5.0(-3)			1226.6
951.86 (10)	1.3 (2)				2265.2
957.40 (8)	10.6	9.2(-3)			1247.7
960.77 (12)	1.4 (2)				2817.6
962.74 (14)	1.0 (2)				[2912.2],[2921.0]
967.06 (9)	2.4 (3)				[2308.3]
979.94 (22)	1.1				
994.46 (12)	1.0 (2)				[2307.8],[2944.1]
998.30 (10)	1.8 (3)				
1002.62 (11)	1.3 (2)				
1017.58 (11)	2.2 (3)				[2265.2]

(continued)

Table 13-a. Continued

E_γ(keV)[a,d]	I_γ[b]	α_K[c]	$\frac{\alpha_K}{\alpha_{\Sigma L}}$	Multi-pole	Level[e] placement
1023.10 (10)	49.4	1.6(-3)		E1	1313.3
1043.29 (11)	1.1 (2)				
1051.03 (11)	2.0 (3)				1341.3
1061.61 (9)	10.0	5.4(-3)			1149.9
1064.03 (12)	1.6 (2)	≤1.5(-2)			2921.0
1066.20 (9)	11.9	3.7(-3)			2470.7
1089.06 (10)	3.7				1379.3
1090.94 (13)	1.4 (2)				[2432.0]
1097.24 (10)	1.2 (2)				
1107.81 (9)	4.7	6.1(-3)			
*1115.0 (9)	9.2	6.3(-3)			1404.5,2969.0
1122.80 (9)	1.9 (3)				[1413.0]
1125.45 (9)	2.6				
1138.26 (8)	12.6	2.8(-2)	≈4	E0+E2	1226.6
*1155.5 (2)	11.2 (1.8)	≈3 (-3)			1445.8
1157.41 (10)	62.9	5.6(-3)	4.2		2470.7
1159.30 (10)	458.	2.9(-3)	6.2	E1+M2	1247.7
1174.17 (10)	3.8				2817.6
1184.55 (13)	2.0 (3)	≤1.4(-2)			[2432.0]
1190.22 (10)	84.1	5.4(-3)			2912.2
1198.15 (11)	1.2 (2)				[2920.4]
1201.48 (10)	6.7	7.3(-3)			2969.0
1204.85 (10)	6.1	4.7(-3)			1293.2
1211.30 (13)	1.5 (2)				
1213.20 (11)	2.7				[2885.5]
1222.95 (10)	37.0	[3.3(-2)]	[≥5.9]	M1	2470.7
1224.96 (10)	105.	[6.4(-4)]		E1	1313.3

(continued)

Table 13-a. Continued

E_γ(keV)[a,d]	I_γ[b]	α_K[c]	$\frac{\alpha_K}{\alpha_{\Sigma L}}$	Multi-pole	Level[e] placement
1226.85 (25)	5.5 (1.0)				1226.6
1234.26 (15)	1.2 (2)				
1239.86 (12)	2.1 (3)				[2817.6],[2912.2]
1247.68 (15)	8.5 (9)	1.1(-2)	≈5	M2	1247.7
1250.01 (18)	2.3 (3)				
1252.90 (10)	57.1	3.4(-3)	7.6	(M1+E2)	1341.3
1258.75 (11)	3.5 (5)	≤6.2(-3)			2969.0
1268.78 (10)	24.6	2.5(-3)			2912.2
1277.90 (11)	2.9				
1287.40 (12)	1.7				1577.6
1291.01 (10)	24.6	≤1.9(-2)	≈6	(E0+E2)	1379.3
1301.10 (11)	1.4				[1591.3]
1308.30 (12)	1.2				
1325.67 (13)	1.5 (2)				[2969.0]
1341.33 (10)	61.9	2.6(-3)	6.3	(M1+E2)	1341.3
1346.08 (25)	1.3 (3)				2791.5
1357.52 (10)	37.0	≈3(-3)			1445.8
1366.49 (11)	4.0				2944.1
1371.75 (12)	2.8				2817.6
1379.29 (15)	1.0 (3)				[1379.4]
1412.84 (11)	2.1				[2817.6],[(1413.0)]
1420.04 (10)	8.4				1710.2
1427.64 (11)	2.2				
1432.56 (11)	1.6				2878.2
1450.40 (10)	6.7				2791.5
1476.18 (10)	8.8	1.6(-3)			2817.6
1489.33 (10)	13.5				1577.6
1495.85 (15)	3.5				1786.1
*1503.(7)	≤2.				1793.7
1504.24 (10)	14.1				2817.6

(continued)

Table 13-a. Continued

E_γ(keV)[a,d]	I_γ[b]	α_K[c]	$\frac{\alpha_K}{\alpha_{\Sigma L}}$	Multi-pole	Level[e] placement
1515.56 (13)	1.0				[2920.4]
1536.62 (11)	7.1				2878.2
1540.82 (11)	6.5				2920.4
1543.73 (15)	4.7				2791.5
1555.05 (10)	74.1	7.8(-4)	≥3.6	E1	1643.4
1563.53 (13)	3.6 (6)				1854.0
1564.95 (11)	7.6				2878.2
1579.9 (2)	5.2 (5)	1.8(-3)			2921.0
1584.02 (10)	97.6	1.7(-3)			1672.3
1603.46 (18)	1.0 (3)				
1608.68 (11)	2.7				
1612.63 (12)	3.2				2762.6
1616.18 (10)	23.8	2.4(-3)			1704.6
*1621.87 (10)	10.7				1710.2,1912.0
1628.53 (30)	2.5 (6)				
1630.83 (10)	32.8	2.2(-3)			2944.1
1633.74 (10)	54.3	6.0(-4)		E1	1722.0
1637.60 (18)	1.5 (3)				[2885.5]
1643.45 (10)	44.4	6.5(-4)		E1	1643.4
1659.21 (11)	2.0				
1672.32 (12)	22.0	2.4(-3)	≈8		1672.3
1673.40 (16)	8.3 (2.0)				2921.0
1679.18 (11)	22.3	5.7(-4)		E1	1767.5
1693.7 (2)	9.6	2.3(-3)	8.3		2920.4
1696.55 (13)	85.8	2.2(-3)			2944.1
1697.8 (2)	≤8.				1786.1
1704.70 (12)	25.9	1.4(-3)	≥3.4		1704.6
*(1705.4)	≤3				1793.7

(continued)

Table 13-a. Continued

E_γ(keV)[a,d]	I_γ[b]	α_K[c]	$\frac{\alpha_K}{\alpha_{\Sigma L}}$	Multi-pole	Level[e] placement
1718.1 (4)	1.8 (6)				
1722.04 (13)	60.6	6.0(-4)		E1	1722.0
1725.9 (4)	1.2 (4)				
1745.29 (14)	2.1				
1754.94 (16)	1.3				
1765.75 (15)	8.8	1.2(-3)			1854.0
1768.22 (16)	3.4				
1774.56 (15)	28.9	1.9(-3)	10	M1	1862.8
1793.17 (15)	3.7				
1820.0 (3)	1.6 (3)				
1823.70 (15)	83.4	1.6(-3)			1912.0
1836.34 (16)	4.0				1924.6
1855.69 (16)	2.2				
1861.15 (25)	4.8 (1.2)				1949.7
1862.74 (15)	74.0	1.6(-3)	7.6	M1	1862.8
1869.78 (16)	1.5				1958.1
1948.40 (18)	2.2 (5)				
1949.80 (17)	2.4 (5)	1.5(-3)			1949.7
1956.48 (15)	15.9	1.1(-3)			2044.8
1960.60 (16)	1.1				
1977.85 (15)	16.2	9.8(-4)			2066.2
2044.87 (15)	25.0	9.4(-4)			2044.8
2066.28 (16)	1.3				2066.2
2192.33 (20)	4.2	4.3(-4)		[E1(+M2)]	2280.7
2219.49 (20)	5.4	5.7(-4)			2307.8
2246.92 (20)	2.4				
2280.6 (2)	3.3				2280.7
2307.7 (2)	3.7	7.7(-4)			2307.8

(continued)

Table 13-a. Continued

E_γ(keV)[a,d]	I_γ[b]	α_K[c]	$\frac{\alpha_K}{\alpha_{\Sigma L}}$	Multi-pole	Level[e] placement
2317.0 (2)	4.6	4.3(-4)		[E1(+M2)]	2405.4
2361.5 (2)	3.8				
2394.6 (2)	2.3				[2482.9]
2405.2 (2)	9.1	4.6(-4)		[E1(+M2)]	2405.4
2482.8 (2)	1.6				[2482.9]
2513.82 (20)	12.4				2602.2
2602.15 (20)	6.5 (7)				2602.2
2674.2 (2)	3.4				
2703.4 (3)	1.3 (3)				
2773.8 (2)	2.1 (3)				
2789.98 (20)	1.5				--
2797.14 (20)	1.2				[2885.5]
2823.60 (40)	1.0 (2)				[2912.2]
2832.00 (20)	80.5	8.8(-5)		E1	2920.4
2863.88 (20)	2.0				
2885.55 (22)	2.0	4.5(-4)			[2885.5]
2920.41 (20)	40.6	7.1(-5)		E1	2920.4

[a]The energy errors indicated reflect the combined statistical uncertainty associated with the peak centroid, and the systematic errors expected from system non-linearity and from uncertainties in the standard calibration energies.

[b]Except where otherwise indicated, the errors in the relative intensities are about 8%, an error arising largely from the uncertainty of the detector efficiency. Where the indicated errors exceed this figure, they reflect the statistical uncertainty, σ, associated with the computer least squares fit to the photopeak.

[c]Conversion coefficients marked with a dagger (†) have been computed from the data of Harmatz, et al. (Ref. 81).

[d]The starred (*) lines are complex groups we have been unable to resolve.

(continued)

Table 13-a. Continued

[e]Level assignments are indicated by three notations, depending on the basis (and relative confidence) of the assignment:

1247.7 ⟹ consistent coincidence and singles data. Placement in the level scheme will be found in Fig. 34.

[2265.2] ⟹ assigned on the basis of energy difference only. Placement is in Fig. 35.

[(2482.9)] ⇒ assigned by energy difference, and feeding or de-exciting a probable level indicated in Fig. 35.

[f]Obscured by the Ta^{175} lines at 125.9 and 126.6 keV. We assign a Ta^{176} line on the basis of coincidence data.

[g]Theoretical value. Assumed pure E2 for normalization.

[h]Obscured by the Ta^{175} line at 207.4 and the Ta^{177} line at 208.4 keV. Assignment of the Ta^{176} line is made on the basis of coincidence data.

Table 13-b. The γ-rays following decay of Ta^{176} to levels in Hf^{176}: Transitions observed with intensity 0.20 - 0.99% of the 710.5-keV intensity.

E_γ(keV)	I_γ	Level Placement
110.1 (2)	0.36 (5)	
111.3 (2)	0.31 (5)	
117.5 (2)	0.23 (5)	
118.93 (2)	0.22 (4)	[(1710.2)]
131.0 (15)	0.40 (10)	[1924.6], [1949.7]
140.9 (10)	0.97 (10)	
173.00 (7)	0.28 (4)	[1577.6]
179.10 (6)	0.72 (7)	
185.72 (6)	0.50 (6)	
192.80 (8)	0.24 (4)	[1445.8]
196.82 (14)	0.46 (12)	[2602.2]
198.07 (12)	0.70 (15)	
230.88 (8)	0.49 (4)	
248.29 (8)	0.52 (5)	
271.58 (9)	0.24 (4)	
277.74 (8)	0.20 (4)	
280.77 (7)	0.22 (4)	
292.88 (10)	0.73 (7)	
303.55 (15)	0.42 (4)	[2905.6]
306.79 (20)	0.50 (5)	
314.53 (20)	0.57 (7)	
318.83 (30)	0.21 (4)	[2921.0]
327.05 (30)	0.26 (4)	
337.51 (20)	0.23 (3)	
343.38 (20)	0.69 (7)	
361.76 (20)	0.62 (9)	[2066.2]
362.71 (30)	0.38 (9)	[1767.5]

(continued)

Table 13-b. Continued

E_γ(keV)	I_γ	Level Placement
366.20 (25)	0.24 (3)	
382.71 (25)	0.44 (8)	
383.60 (20)	0.97 (10)	[2308.3]
386.10 (20)	0.45 (5)	[2791.5]
388.06 (20)	0.56 (5)	[1767.5]
401.44 (20)	0.36 (4)	[2044.8]
411.67 (20)	0.34 (5)	
421.08 (30)	0.33 (7)	
423.15 (30)	0.32 (8)	
424.48 (15)	0.92 (10)	[1672.3]
428.85 (20)	0.27 (4)	[1722.0]
433.51 (9)	0.80 (9)	
434.85 (10)	0.89 (9)	[2905.6]
440.01 (8)	0.41 (5)	
450.94 (13)	0.31 (5)	[2307.8]
452.18 (10)	0.45 (6)	[1793.6], [1856.9]
454.63 (9)	0.32 (5)	[2762.6]
459.10 (9)	0.60 (7)	[2265.2]
479.14 (10)	0.55 (7)	
480.83 (9)	0.54 (7)	[2405.4]
483.28 (9)	0.50 (6)	
494.98 (13)	0.26 (4)	
517.4 (4)	0.60 (30)	
529.08 (17)	0.26 (10)	
550.4 (5)	0.81 (20)	
551.4 (2)	0.35 (6)	[2405.4]
553.5 (2)	0.40 (6)	[1958.1]
555.2 (2)	0.27 (5)	[2265.2]
560.0 (2)	0.51 (7)	

(continued)

Table 13-b. Continued

E_γ(keV)	I_γ	Level Placement
561.6 (3)	0.25 (6)	
566.6 (2)	0.23 (4)	
577.3 (1)	0.83 (9)	[(2885.5)]
583.5 (2)	0.24 (4)	[1924.6]
584.9 (2)	0.36 (5)	
589.9 (1)	0.30 (4)	
594.9 (2)	0.23 (4)	
598.6 (2)	0.46 (8)	[1912.0]
604.6 (1)	0.48 (6)	[2885.5], [2912.2]
626.1 (2)	0.31 (5)	[(2482.9)]
636.6 (1)	0.95 (10)	[1949.7], [2944.1]
656.8 (1)	0.64 (7)	
670.2 (2)	0.22 (5)	
693.2 (1)	0.38 (5)	
730.7 (1)	0.60 (7)	[2308.3]
735.9 (2)	0.30 (6)	
760.4 (2)	0.31 (5)	[2470.7]
766.5 (1)	0.56 (7)	
774.0 (3)	0.24 (6)	
779.3 (1)	0.54 (6)	
782.7 (1)	0.62 (7)	
784.2 (2)	0.34 (7)	
787.1 (1)	0.53 (6)	
789.4 (2)	0.26 (4)	
798.5 (2)	0.87 (15)	[2470.7]
799.5 (3)	0.39 (20)	
801.7 (2)	0.26 (5)	
803.8 (1)	0.65 (7)	

(continued)

Table 13-b. Continued

E_γ(keV)	I_γ	Level Placement
808.6 (1)	0.68 (8)	
837.7 (3)	0.35 (10)	
841.5 (2)	0.78 (18)	[2791.5]
842.6 (5)	0.38 (20)	
861.0 (1)	0.75 (9)	[2265.2], [2905.6], [(2452.3)]
867.4 (1)	0.63 (8)	[2912.2]
872.3 (2)	0.31 (5)	
876.6 (2)	0.46 (6)	
878.4 (2)	0.45 (6)	
884.7 (3)	0.26 (10)	
886.3 (2)	0.72 (9)	
893.3 (2)	0.48 (12)	[2470.7]
900.3 (1)	0.69 (8)	
907.3 (1)	0.89 (10)	
971.8 (1)	0.89 (10)	
975.1 (2)	0.81 (10)	
977.0 (2)	0.91 (11)	
981.0 (3)	0.92 (35)	[2905.6]
986.7 (2)	0.60 (12)	
1011.1 (3)	0.57 (20)	[2969.0]
1021.0 (5)	0.66 (30)	[2878.2]
1035.0 (2)	0.46 (9)	
1052.7 (2)	0.80 (12)	[2432.0]
1112.9 (2)	0.94 (10)	[2817.6]
1148.3 (2)	0.85 (15)	[2791.5]
1178.5 (2)	0.70 (12)	[2405.4]
1281.2 (2)	0.87 (13)	
1333.1 (2)	0.69 (18)	[(2482.9)]

(continued)

Table 13-b. Continued

E_γ(keV)	I_γ	Level Placement
1438.1 (3)	0.55 (12)	[2817.6]
1462.6 (2)	0.49 (10)	
1467.5 (2)	0.80 (9)	
1470.0 (2)	0.93 (20)	
1482.8 (3)	0.54 (14)	
1573.3 (2)	0.66 (16)	
1665.0 (2)	0.91 (14)	
1712.0 (3)	0.82 (20)	
1736.7 (2)	0.71 (8)	
1751.1 (3)	0.51 (9)	
1875.1 (3)	0.47 (9)	
1911.6 (3)	0.24 (5)	[1912.0]
1937.9 (2)	0.45 (7)	
1970.6 (2)	0.57 (7)	
2042.7 (5)	0.65 (22)	
2049.2 (4)	0.52 (11)	
2057.4 (3)	0.32 (5)	
2071.0 (2)	0.31 (5)	
2077.0 (2)	0.76 (9)	
2090.6 (3)	0.26 (5)	
2140.1 (2)	0.72 (8)	
2162.1 (2)	0.72 (8)	[2432.2]
2257.9 (4)	0.44 (12)	
2260.4 (3)	0.57 (10)	
2272.1 (3)	0.32 (5)	
2278.6 (3)	0.49 (7)	
2304.5 (4)	0.50 (22)	
2314.8 (5)	0.50 (25)	

(continued)

Table 13-b. Continued

E_γ(keV)	I_γ	Level Placement
2374.2 (3)	0.35 (7)	
2421.7 (3)	0.37 (6)	
2460.3 (3)	0.54 (7)	
2480.5 (4)	0.80 (10)	
2506.2 (3)	0.51 (9)	
2531.6 (5)	0.40 (12)	
2534.2 (3)	0.65 (12)	
2548.4 (3)	0.63 (10)	
2571.6 (2)	0.85 (9)	
2586.1 (3)	0.63 (10)	
2681.6 (3)	0.60 (15)	
2689.7 (3)	0.85 (20)	
2705.6 (3)	0.45 (17)	
2729.3 (2)	0.65 (10)	
2744.5 (3)	0.48 (7)	
2755.3 (3)	0.25 (7)	
2762.8 (2)	0.90 (12)	
2769.1 (3)	0.85 (9)	
2817.0 (4)	0.85 (12)	[2905.6]
2845.1 (3)	0.12 (3)	
2854.1 (9)	0.10 (7)	
2856.1 (5)	0.22 (9)	[2944.1]
2882.5 (4)	0.57 (11)	
2890.3 (4)	0.15 (5)	
2905.7 (4)	0.40 (6)	[2905.6]
2912.3 (6)	0.39 (6)	[2912.2]
2940.7 (3)	0.34 (4)	
2952.4 (2)	0.69 (8)	

(continued)

Table 13-b. Continued

E_γ(keV)	I_γ	Level Placement
2971.6 (3)	0.21 (3)	
2978.7 (3)	0.34 (3)	
2995.4 (3)	0.092 (14)	

NOTE: The convention followed for noting level assignments is the same as in Table 13-a.

events. Nine 2400' tapes of serial data were gathered in a single 36-hour run. At the completion of the run, a 65 nsec gate was set on the timing curve (Fig. 24) and three tapes of data were initially sorted on the PDP-7 in order to obtain a gross coincidence spectrum for each of the two detectors. The higher resolution "planar" data were used to select digitally the coincidence gates of interest. In Fig. 52 we show the gross coincidence spectrum for the planar detector and in Table 21 we indicate the location of the coincidence "gates" which were set. The background windows have been selected immediately adjacent to the peak windows on the high energy side whenever possible. In Fig. 54 are shown for reference the gross "coaxial" coincidence data. These data were used as an energy calibration for later computer analysis of the sorted coincidence spectra. Intensity data for the sorted spectra were obtained with use of the efficiency curve for the coaxial detector + absorber shown in Fig. 53. (Figures and tables relevant to the coincidence data are in Appendix C.)

Subtraction of background and random events has been carried out by the computer code during the sorting process, so that the spectra shown presumably represent only "valid" photopeak coincidences. The appropriate relation describing the spectra is just

$$N_{coinc} = (P_T - P_R) - (B_T - B_R)$$

where

P_T = total coincidences in the peak gate

P_R = random coincidences in the peak gate

B_T = total coincidences in the background gate

B_R = random coincidences in the background gate.

In Fig. 55 (Appendix C) we display the 81 γ-γ coincidence spectra we have obtained from the decay of Ta^{176}. The quality of the data can perhaps best be estimated by examining each spectrum in the region of the "gate" peak. In nearly every case, there is little perturbation of that region to suggest departure from a normal background continuum.

Finally, in Figs. 30 - 32 we show the conversion electron data gathered with the 3 mm × 1 cm^2 Si(Li) detector. Figures 30 display the low energy conversion spectrum up to 1.6 MeV. In Fig. 31 is shown a high-gain spectrum of the region up to about 300 keV, and Fig. 32 shows the high-energy (1.0-3.0 MeV) electron spectrum. These latter data for the most part represent electron energies beyond the supposed range (ignoring scattering) of electrons incident upon a 3 mm thick Si wafer. The statistics are consequently quite poor above ≈ 2.0 MeV, and only gross features of the electron spectrum can be discerned. An unusual feature of this spectrum is the appearance of a pair of rather strong lines at 1811 and 1899 keV. These lines have no counterpart in the photon spectrum. Moreover, they were not observed by either Harmatz, et al.,[73] or by Verheul, et al.[74] though both groups should easily have seen the lines if they were present with the intensity seen in Fig. 35. We note that the energy separation between the two spurious "electron" lines is exactly 88 keV. These facts coupled with the observed ≈ 2:1 intensity ratio of the lines leads us to believe

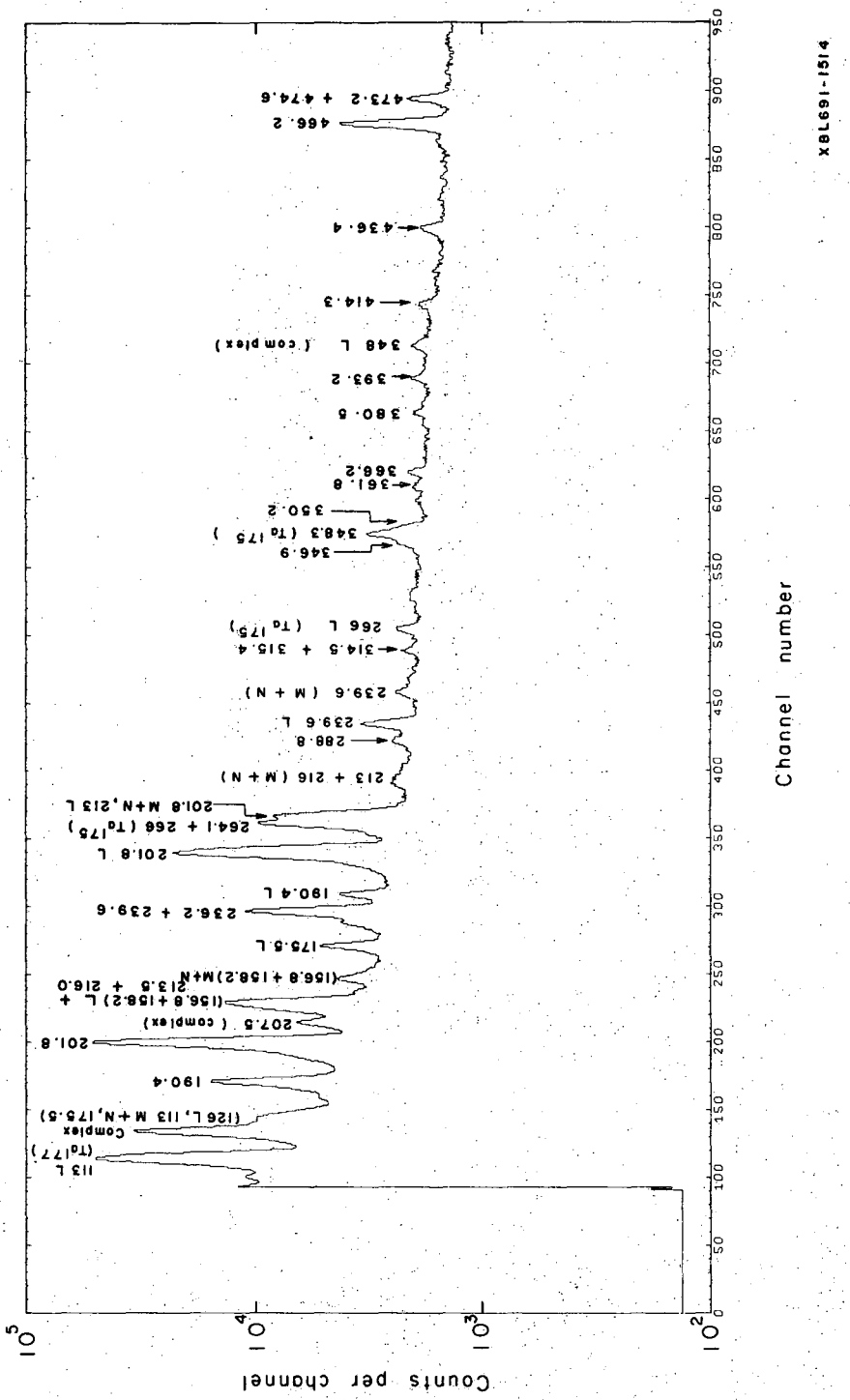

Fig. 30-a. Conversion-electron spectrum from decay of Ta^{176} (160 –495 keV). Taken with a 1 cm^2 × 3 mm deep Si(Li) detector. Unless otherwise noted, peaks are K-shell conversion lines corresponding to the indicated (photon) transition energy.

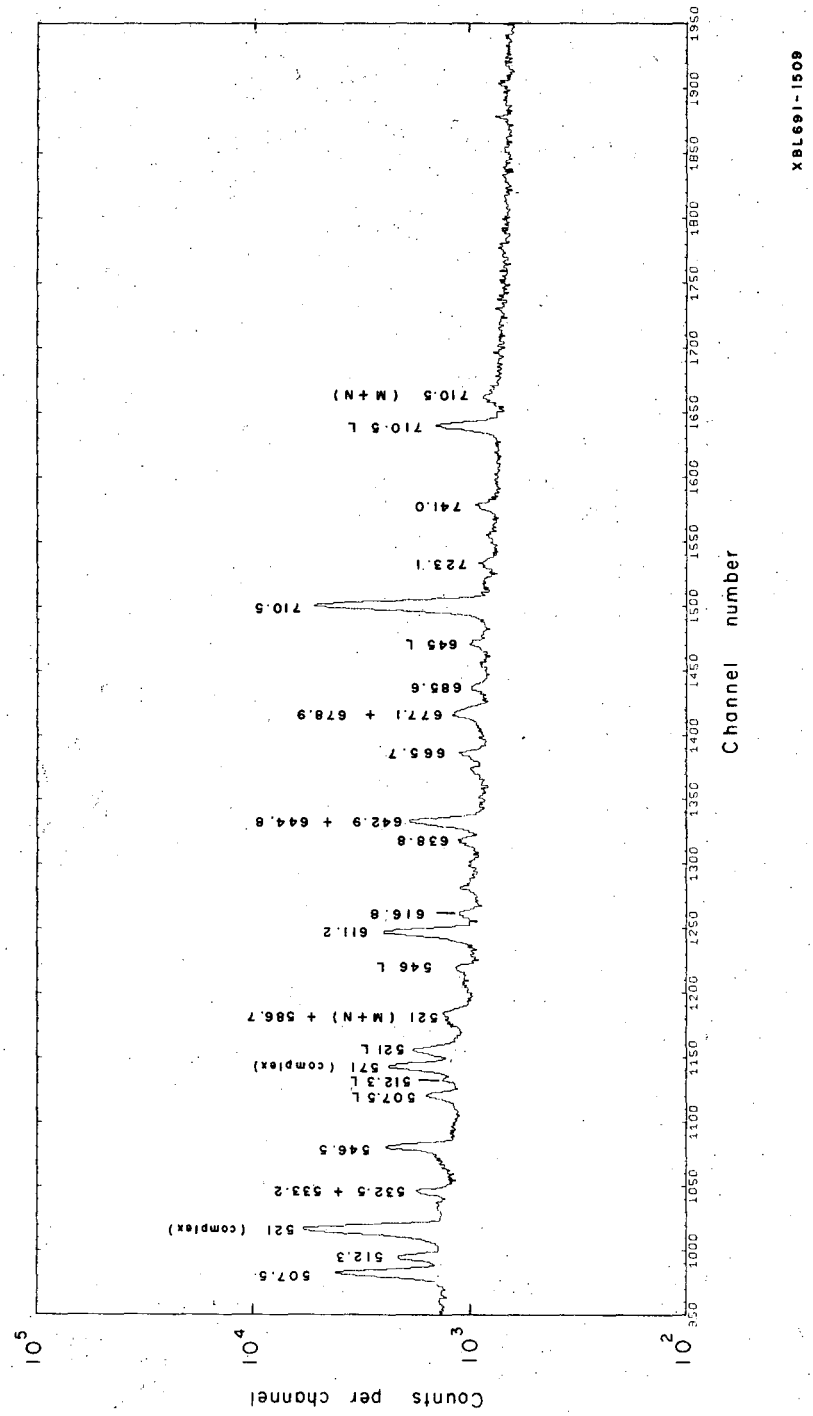

Fig. 30-b. Conversion-electron spectrum from decay of Ta^{176} (495 - 890 keV). Taken with a 1 cm^2 × 3 mm deep Si(Li) detector. Unless otherwise noted, peaks are K-shell conversion lines corresponding to the indicated (photon) transition energy.

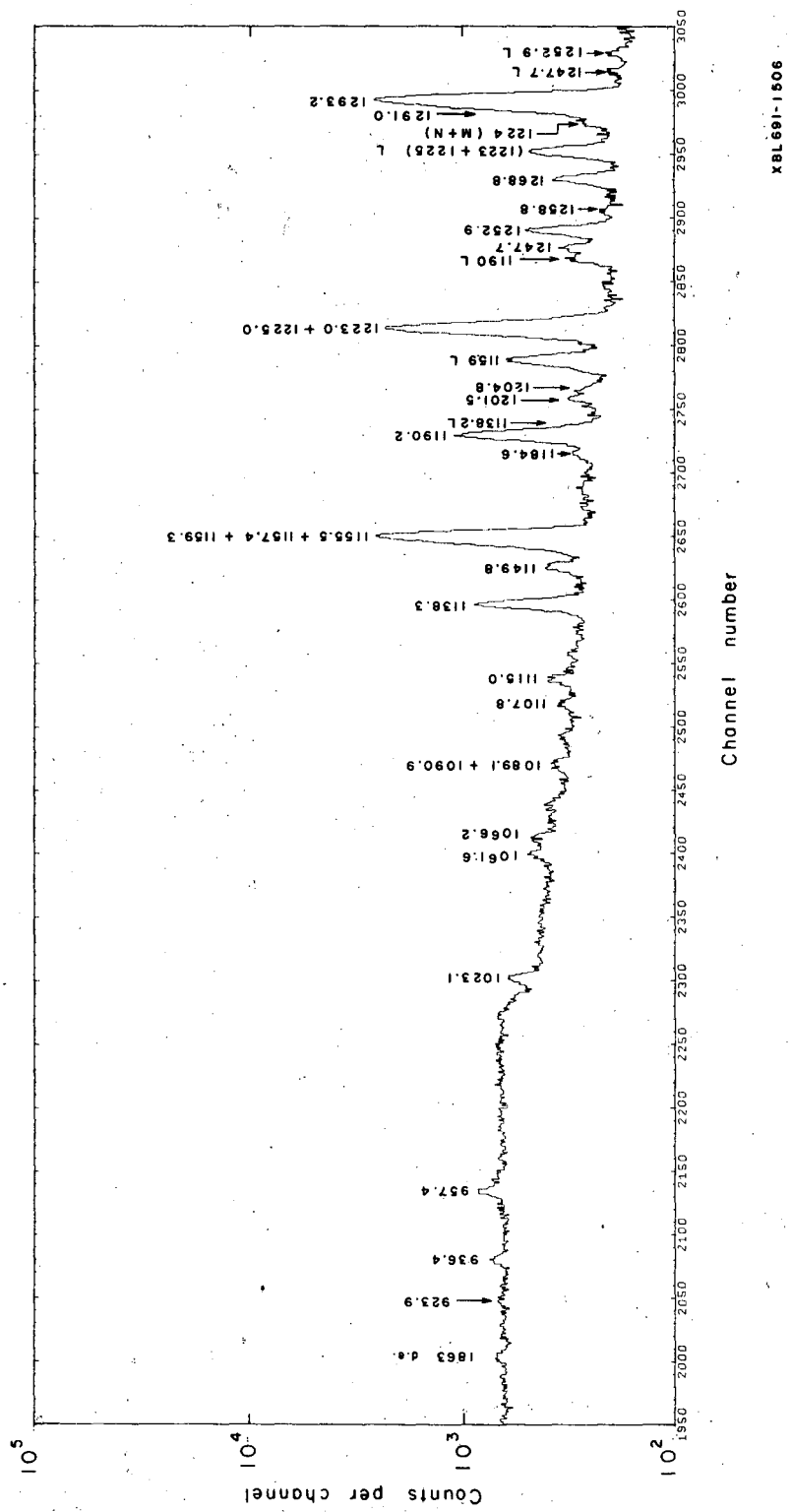

Fig. 30-c. Conversion-electron spectrum from decay of Ta^{176} (890 - 1310 keV). Taken with a 1 cm^2 × 3 mm deep Si(Li) detector. Unless otherwise noted, peaks are K-shell conversion lines corresponding to the indicated (photon) transition energy.

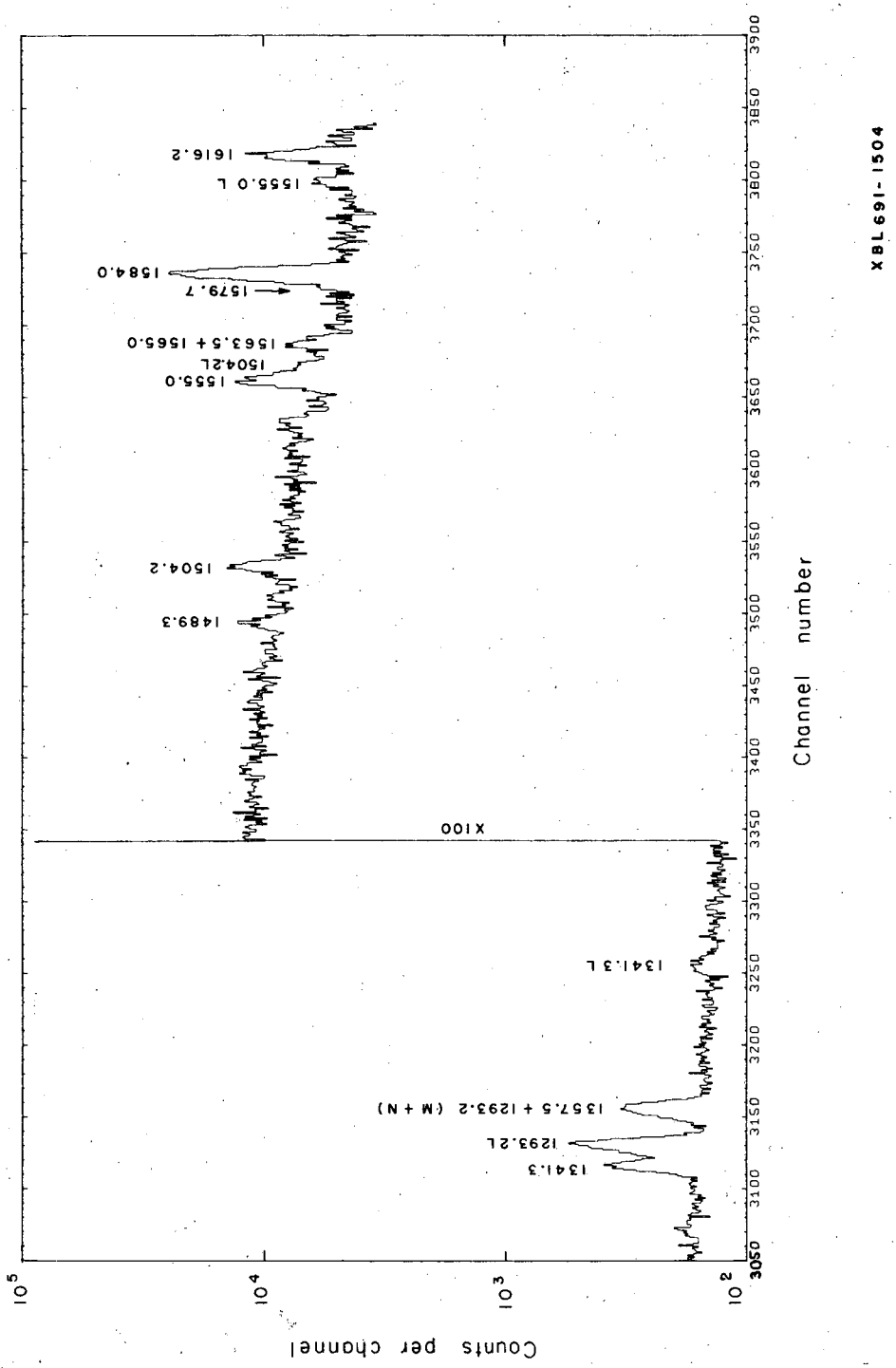

Fig. 30-d. Conversion-electron spectrum from decay of Ta^{176} (1310 - 1620 keV). Taken with a 1 cm^2 × 3 mm deep Si(Li) detector. Unless otherwise noted, peaks are K-shell conversion lines corresponding to the indicated (photon) transition energy.

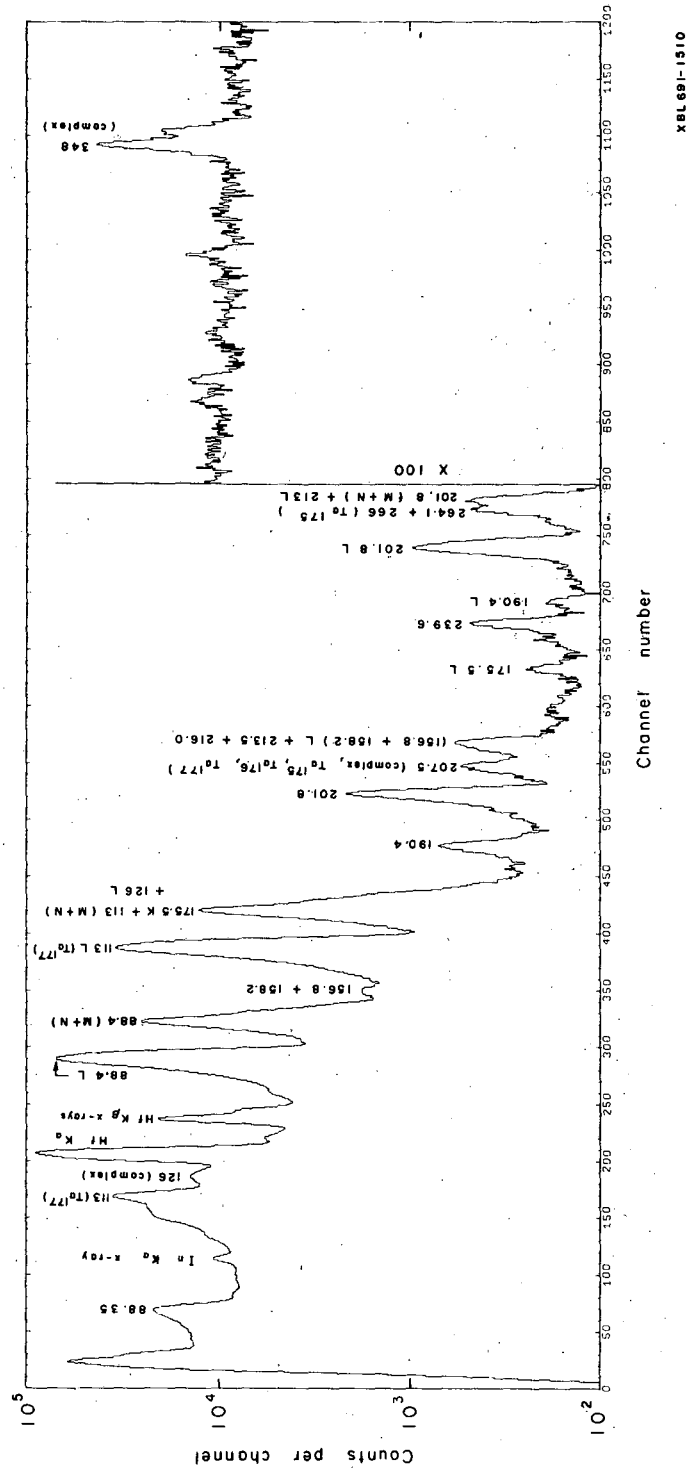

Fig. 31. Low energy conversion-electron spectrum of Ta^{176} (0 - 350 keV). The labeling is consistent with that in Figs. 30.

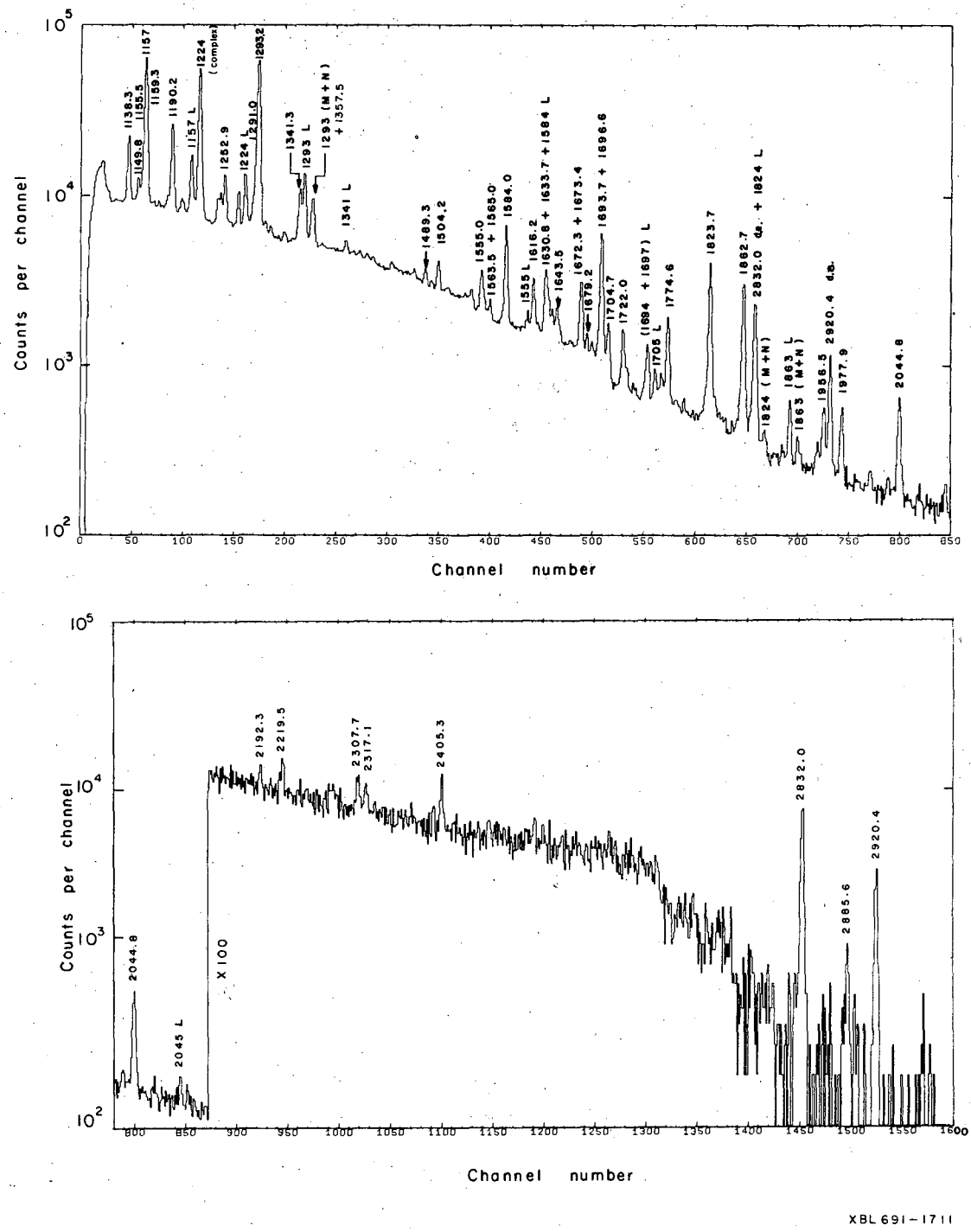

XBL 691-1711

Fig. 32. High energy conversion-electron spectrum of Ta^{176} (1 - 3 MeV). Labeling is consistent with that in Figs. 30.

that they are caused by the strong photon transitions at 2832.0 and 2920.4 keV, a belief that is supported by the observation that both lines are just 1022 keV ($2m_0c^2$) below the corresponding photon energies. We conclude, then, that the spurious "electron" lines in fact are the 2832.0- and 2920.4-keV photon double-escape peaks, representing a feature we are not accustomed to seeing in Si(Li) spectra. The observation is not surprising, however, when one considers that at 2.0 MeV the silicon pair-production cross-section is already equal to the germanium photoelectric cross-section at that energy, and at 3 MeV is a factor of five greater (see Fig. 33).

The Si(Li) conversion electron spectra have been primarily useful in 1) revealing the locations of E0 transitions present in Ta^{176} decay, and 2) providing rather clear indication of those transitions which are essentially E1 <u>or</u> M2 in character. Unfortunately, most of the observed transitions in the Ta^{176} spectrum are undoubtedly of M1, E2, or mixed M1-E2 or E1-M2 character because there is little or no population of states with spins exceeding 3 units of angular momentum (with the exception, of course, of the 4+ member of the ground band). Little information on transition multipolarity can be gleaned from K-conversion coefficients alone in such cases. This fact, and the complexity of the Ta^{176} spectrum severely restrict the usefulness of the Si(Li) conversion data. We have indicated in Table 13 the meaningful and unambiguous information provided by the electron spectra. Conversion coefficients have been determined by normalization to the conversion coefficient[98] of the presumably pure E2 ground rotational band transition at 202 keV.

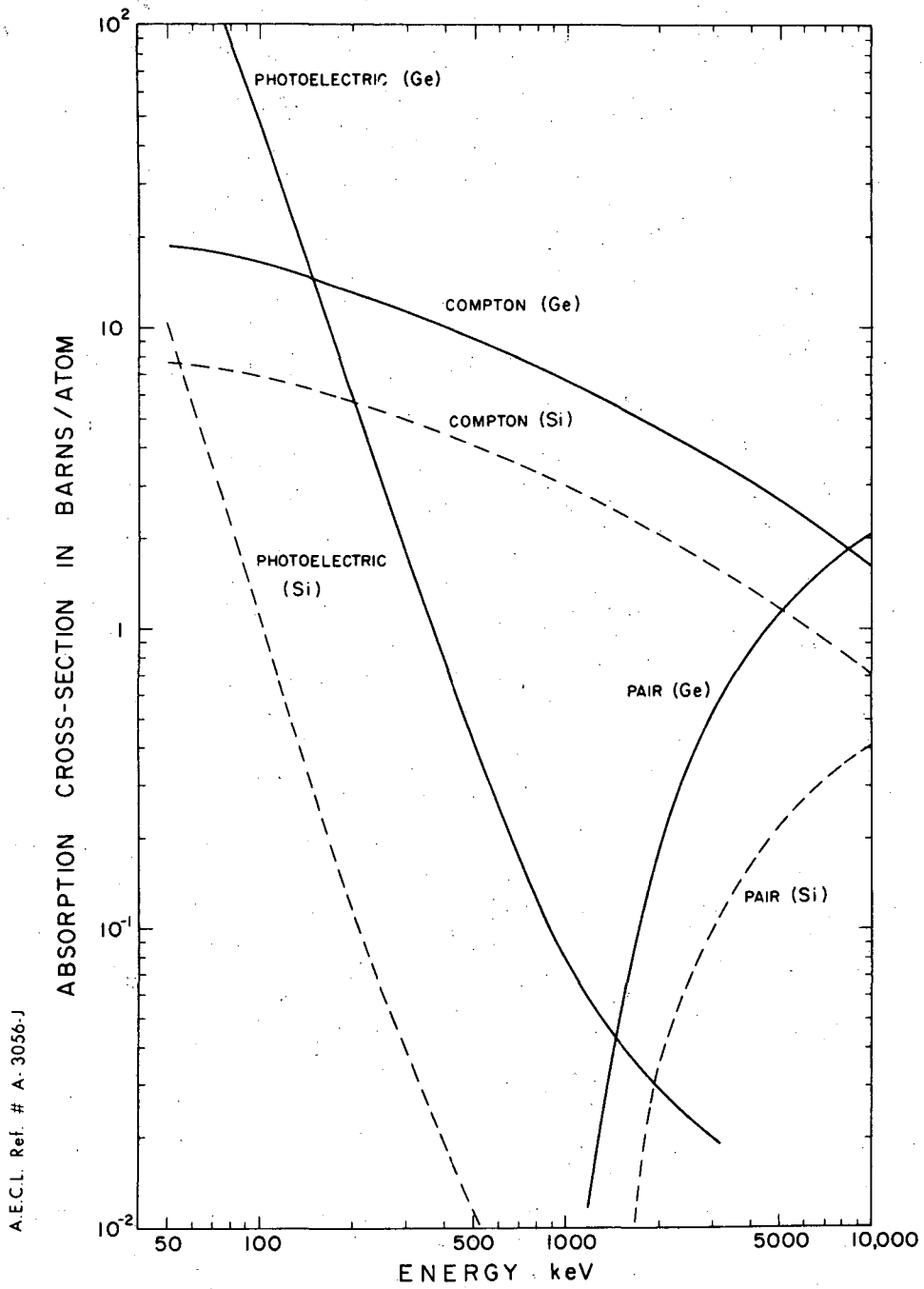

XBL 691-137

Fig. 33. Energy variation of the photoelectric, Compton, and pair-production cross-sections in silicon and germanium.

In Table 14 we list the conversion electron lines observed from the decay of Ta^{176}. Because the electron detection efficiency of the Si(Li) crystal is poorly known above 1.6 MeV, the relative intensity errors indicated reflect the rather large uncertainty associated with extrapolating the curve of Fig. 18 to 3 MeV.

Table 14. Conversion electron lines observed following decay of Ta^{176} to levels in Hf^{176}.

Transition Energy (keV)	Conversion Electron Intensity[a,b] K_{e-}	$\sum L_{e-}$	$\sum (M+N)_{e-}$
88.4	$>1.0 \times 10^4$	$\approx 4.8 \times 10^4$	$\approx 1.4 \times 10^4$
91.2	>66†	180†	
131.1	40†		
146.7	190†		
156.8	135†		
158.2	200†		
175.5	220†	39.	
190.4	180	25.	
201.8	960	471.	
213.5	156		
236.2	18.5		
239.6	138	⩽24.	
288.8	7.4		
314.5 + 315.4	4.5		
346.9	⩽7.2		
350.2	7.4		
361.8	3.7		
366.2	5.5		
380.5	2.4		
382.7 + 383.6	5.7		
393.2	4.9		
414.3	4.8		
436.4	6.7		
466.2	53.8		
473.2 + 474.6	⩽13.4		

(continued)

Table 14. Continued

Transition Energy (keV)	Conversion Electron Intensity[a,b] K_{e^-}	$\sum L_{e^-}$	$\sum (M+N)_{e^-}$
507.5	55.9	8.7	
512.3	16.2	2.3 (5)	
519.7	≤20.4		
521 (complex)	89.4	≤10.9	
532.5 + 533.2	10.3		
546.5	≤24.2		
571 (complex)	26.0		
611.2	33.8	≤5.0	
616.8	4.5		
638.8	≤4.6		
642.9	4.3		
644.8	21.3		
665.7	≤5.1		
677.1	≤6.8		
678.9	4.1		
685.6	3.4		
710.5	100.	16.6	3.2 + 1.3
723.1	2.9		
741.0	4.3		
923.9	1.0 (5)		
936.4	2.9		
957.4	5.4		
1023.1	4.5		
1061.6	3.0 (5)		
1064.0	≤1.5		
1066.2	2.4 (5)		
1089.1	≤2.0		
1107.8	1.6 (3)		

(continued)

Table 14. Continued

Transition Energy (keV)	Conversion Electron Intensity[a,b] K_{e^-}	$\sum L_{e^-}$	$\sum (M+N)_{e^-}$
1115.0	3.2		
1138.3	19.6	≤6.	
1149.8	5.0		
1155.5	2.0 (4)		
1157.4	19.6	4.7	
1159.3	72.8	11.8	
1184.6	1.5 (3)		
1190.2	25.0		
1201.5	2.7		
1204.8	1.6 (5)		
1223.0	67.	11.3	
1225.0	3.7		
1247.7	≤5.0	1.0	
1252.9	10.7	1.4	
1258.8	≤1.2		
1268.8	6.1		
1291.0	≤25.5	≤4.1	
1293.2	87.3	13.9	
1341.3	8.8	1.4	
1357.5	≤6.4		
1476.2	0.8		
1489.3	1.3		
1504.2	2.4	0.8	
1555.0	3.2	≤0.9	
1563.5 + 1565.0	1.2		
1579.7	0.5		
1584.0	9.4		
1616.2	3.1		

(continued)

Table 14. Continued

Transition Energy (keV)	Conversion Electron Intensity[a,b] K_{e-}	$\sum L_{e-}$	$\sum (M+N)_{e-}$
1630.8	4.0		
1633.7	1.8		
1643.5	1.6		
1672.3 + 1673.4	4.1	0.5 (2)	
1679.2	0.71 (13)		
1693.7	1.2 (3)	1.4	
1696.6	10.4		
1704.7	2.0	⩽0.6	
1722.0	2.0		
1765.8 + 1768.2	0.81 (20)		
1774.6	3.0 (5)	0.3	
1820.0	0.4 (1)		
1823.7	7.5 (1.3)	0.8 (3)	
1862.7	6.4 (1.1)	0.84 (17)	0.3
1949.8	0.21 (05)		
1956.5	1.0 (2)		
1977.9	0.88 (16)		
2044.8	1.3 (3)		
2192.3	0.10 (3)		
2219.5	0.17 (4)		
2307.7	0.15 (3)		
2317.1	0.11 (3)		
2405.3	0.23 (6)		
2832.0	0.39 (10)		
2885.6	0.05 (2)		
2920.4	0.16 (5)		

[a]Except as otherwise indicated, relative intensity errors may be taken to be ≈ 15%. These errors reflect the combined systematic uncertainties arising from the following: 1) normalization to the 710.5-keV K-conversion line; 2) the efficiency of the Si(Li) device and of the Ge(Li) detector used to determine the Si(Li) e^- detection efficiency by the method described in Ref. 79.

[b]Intensities marked with a (†) are from Ref. 81, normalized to the 201.8-keV K-conversion line.

D. Data Analysis and Construction of the Hf^{176} Level Scheme

In Fig. 34 we show schematically the decay of Ta^{176} to levels in Hf^{176} as derived from our data. We have been able on the basis of coincidence, singles γ-ray, and conversion electron data to place in the level scheme all transitions with intensity ⩾ 4% of the 710.5-keV photon intensity. The transitions placed in Fig. 34 represent only those lines for which definite assignments could be made on the basis of γ-γ coincidence data. As we mentioned previously, we have not considered simple energy sums and differences to provide sufficient information for placement of a transition in the level shceme. There are numerous weak lines which could be placed on the basis of energy information alone, and undoubtedly some of these placements would be correct. Therefore in Fig. 35 we show again the Hf^{176} level scheme, this time indicating those weak transitions which can be fit to the established levels on the basis of energy information alone. We emphasize that there are not sufficient coincidence data to support the assignments in Fig. 35. We also show a few low energy transitions (dotted lines) whose presence is indicated by coincidence data, but which we are unable to observe in either the photon or electron spectrum.

A detailed exposition on the assignment of each transition to its proper place in the level scheme seems impractical in this case, and since we have included for inspection all of the γ-γ coincidence data (Appendix C), we feel such a discussion would be more confusing than enlightening. We do, however, wish to comment on a few key assignments of particular interest and importance to the correct construction of the level scheme.

Fig. 34. (1 of 2) The decay of Ta^{176}, Lu^{176}, and Lu^{176m} to levels in Hf^{176}.

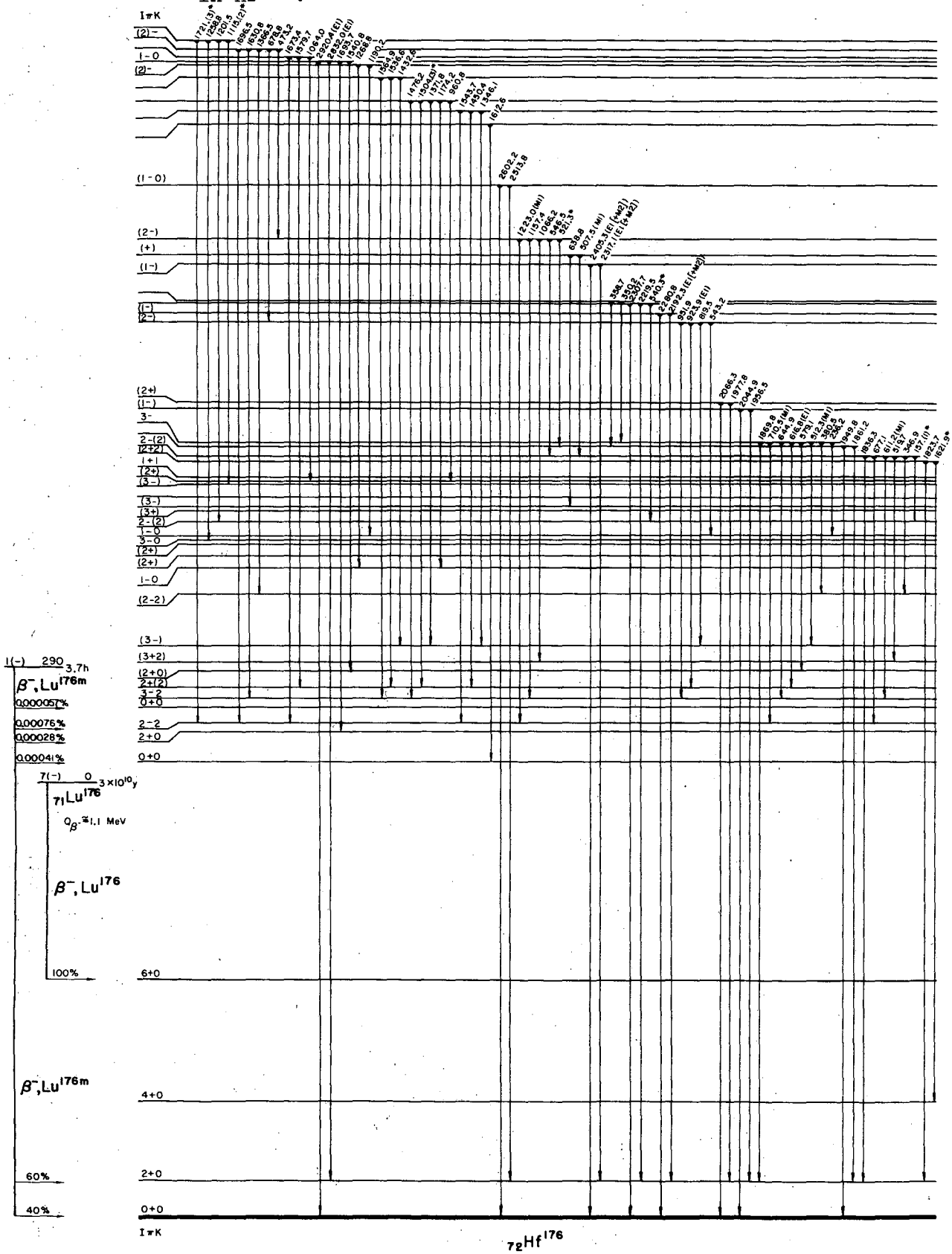

Fig. 34. (continued, 2 of 2) The decay of Ta^{176}, Lu^{176}, and Lu^{176m} to levels in Hf^{176}.

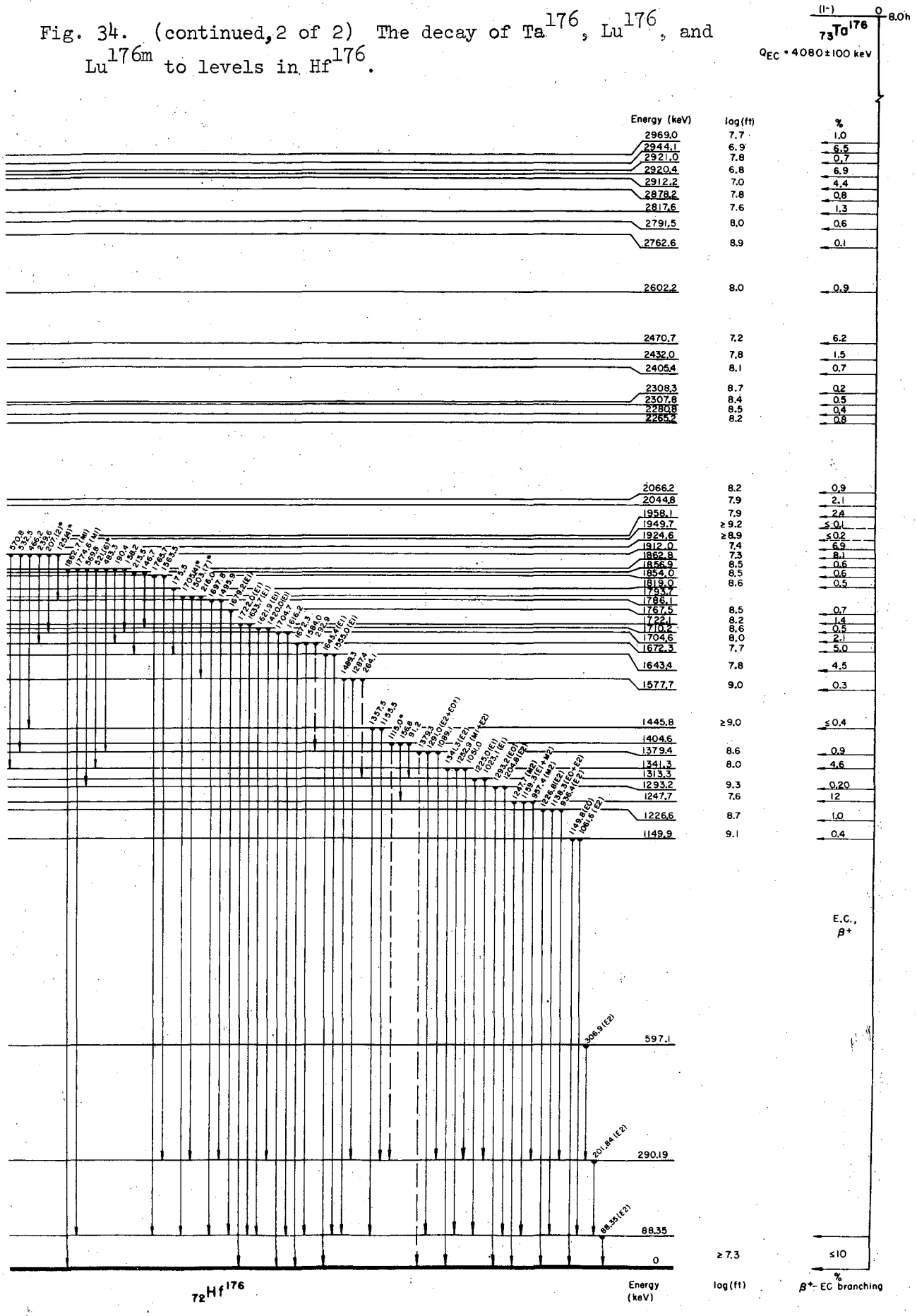

Notes on Figure 34:

1) We have recently investigated the decay of Lu^{176m} (3.7 h). The results of that study have been included in the figure and are in agreement with the earlier assignments made on the basis of Ta^{176} decay data. In Appendix D we present a brief discussion of the Lu^{176m} decay.

2) The assignments shown in this figure are all supported by γ-γ coincidence data.

3) Starred (*) transitions indicate lines not resolved in singles data, but expected to be complex on the basis of coincidence data.

4) Where energies are in parentheses [e.g., 207.(5)], this indicates the singles data are complicated by the presence of other lines, and energy assignments have been made using coincidence spectra or level scheme systematics.

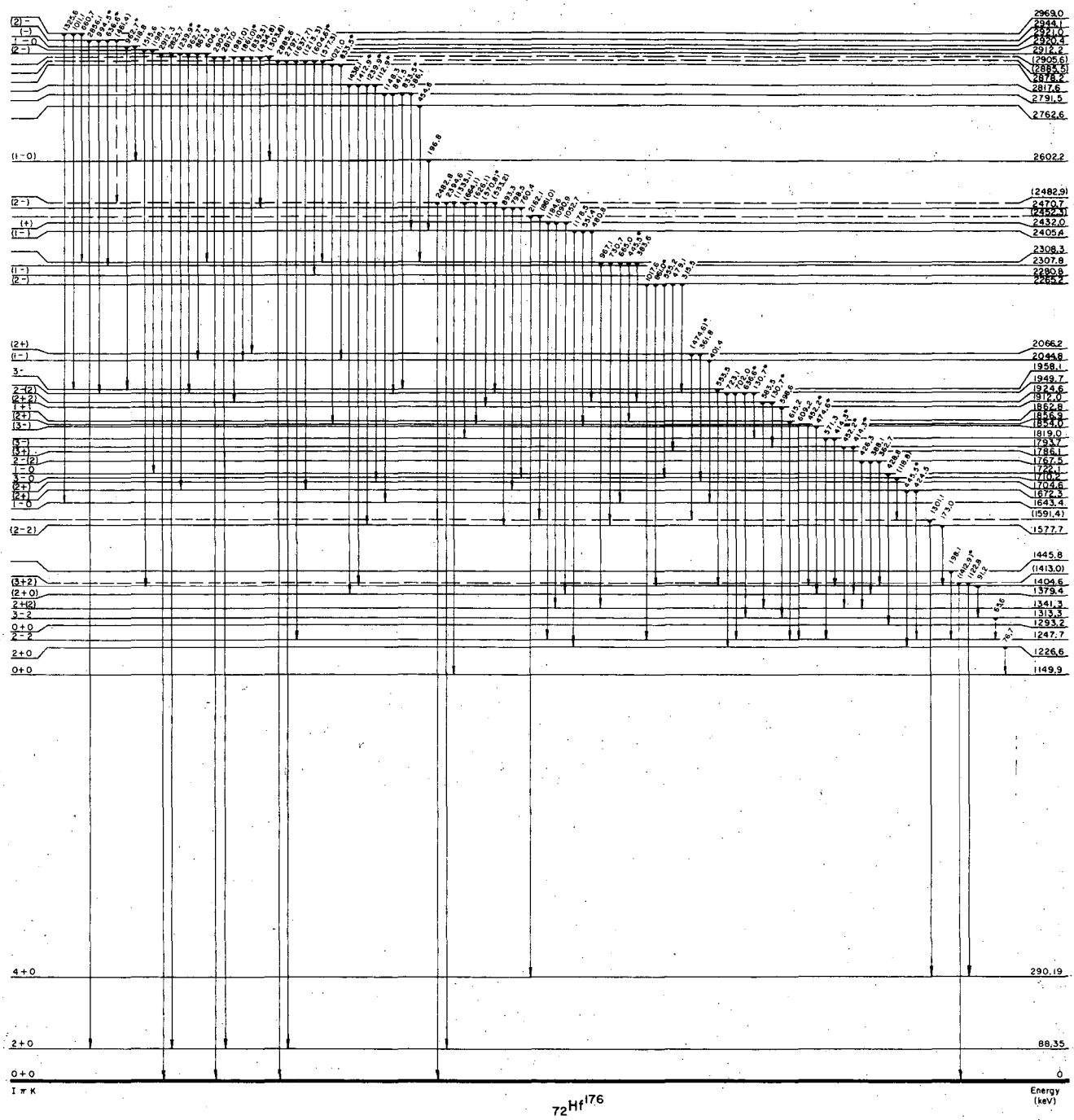

Fig. 35. The level scheme of Hf^{176} showing additional transitions from Ta^{176} decay which could be placed on the basis of energy sums and differences alone.

Notes on Figure 35:

1) The transitions shown in this figure are neither supported nor refuted by coincidence data. They are assigned solely on the basis of energy sums and differences, and include all possible combinations falling within one standard deviation of the combined transition- and level-energy errors.

2) A few additional levels are assigned (broken lines) on the basis of rather tenuous data, or on the basis of the 88.35-keV energy difference.

3) Parentheses [e.g., (533.2)] here indicate a transition populating or de-exciting one of the tentative added levels; therefore these assignments are quite uncertain.

4) Starred transitions fit between more than one pair of levels.

5) A very few low energy transitions not observed but indicated by coincidence data to be likely assignments are shown as dashed lines.

1. Sample data analyses

a. The 1159-keV multiplet

A deceptive stumbling block that has consistently plagued all previous attempts to properly interpret the decay of Ta^{176} has been the strong "line" at 1159 keV. On the basis of centroid shifts in coincidence data we first concluded that this line was in fact a triplet of close-lying lines arranged in such a way as to make them extremely difficult to detect in γ-ray singles data displaying resolution poorer than about 2.8 keV at Co^{60}. Analysis of the three spectra coincident with the 466-, 710-, and 1023-keV transitions reveals the following:

Gate line (keV)	"1159" centroid location (chan)	Centroid energy (keV)
466.2	1469.3	1155.2 ± 0.2
1023.1	1472.2	1157.6 ± 0.2
710.5	1474.6	1159.4 ± 0.1

Consideration of the singles Compton-suppressed data in this region (Fig. 25d) would certainly suggest that the line is a doublet, but the intensity ratios $I_{1155}:I_{1157}:I_{1159} = 11:65:476$ make it extremely difficult to visually detect the presence of a third line. The power of computer data analysis here becomes evident. Using experimental peak shape parameters obtained from strong "clean" singlets in the spectrum (cf. Appendix B) the resolution of the 1159-keV multiplet shown in Fig. 36 is obtained. The three gates set on the multiplet confirm the analysis as can be seen from the 1155-, 1157-, and 1159-keV coincidence spectra (Appendix C). Finally, the pair spectrum (Fig. 29) clearly shows the 1157-keV component, and indicates its intensity is 13.3% that of the

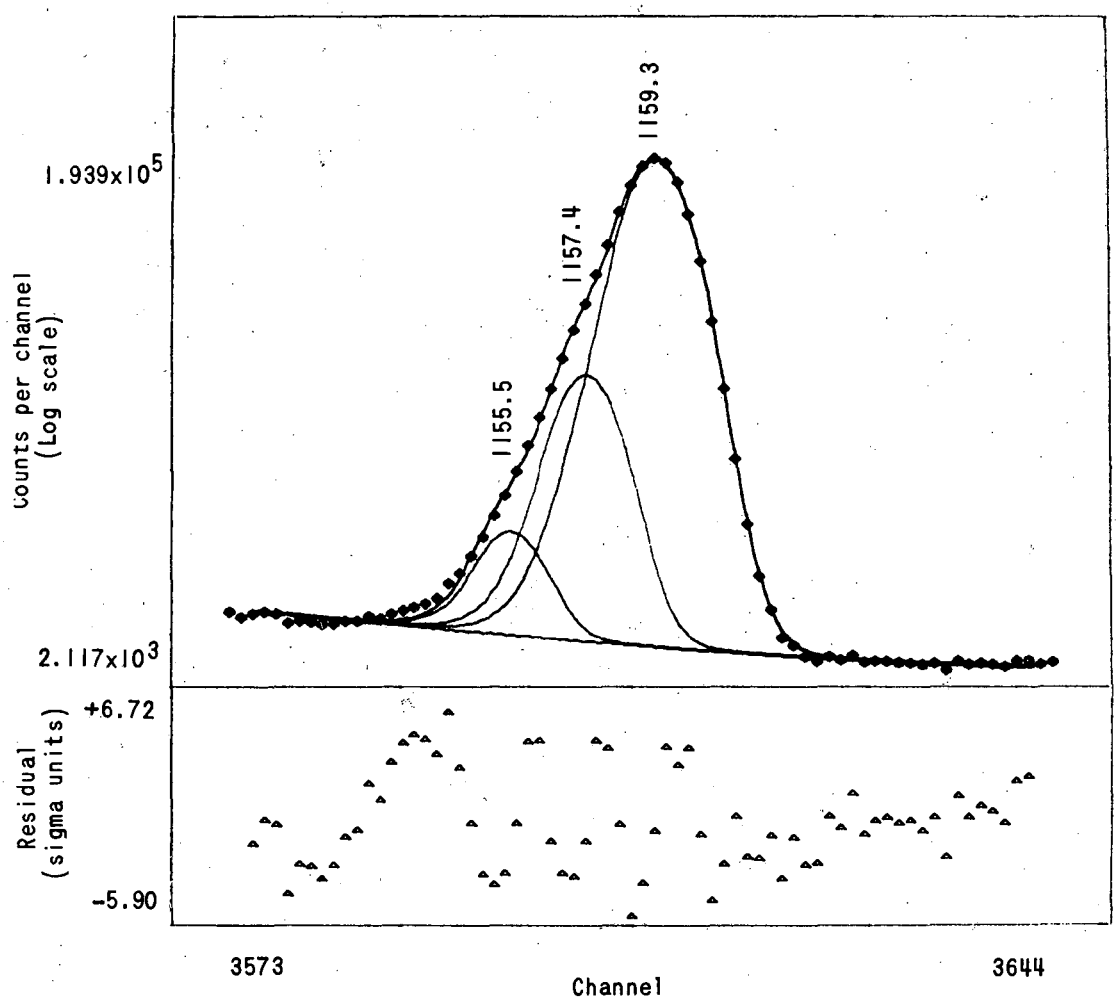

XBL 691-143

Fig. 36. The 1159-keV γ-ray multiplet resolved into three components. There is even some evidence for a weak fourth component at about 1152 keV.

1159-keV line, in excellent agreement with the 13.7% value obtained from the fit in Fig. 36.

The difficulties in analysis exemplified by the above case are repeated many times in the Ta^{176} spectrum. We have discussed this case in detail because of its importance to proper construction of the level scheme, and because it yielded rather unambiguous results in the end. In other cases we were not so fortunate.

b. The 508-, 511-, 512-, 521-keV complex

Analysis of this region for both energies and intensities is severely complicated by several factors. Firstly, the presence of the 511-keV annihilation peak between two bona-fide transition lines at 508 and 512 keV complicates the computer fit to the data because of the abnormal width of the 511-keV peak. Fortunately the electron spectrum provides some help here. Secondly, the dimensions of our peak analysis program, SAMPO, presently allow us to handle multiplets containing up to only six components. And finally, the line at 521-keV, it seems evident from coincidence data as well as from singles data, is quite complex. It appears certain there are components at 519.7, 521.3, and 521.6 keV. We have assigned these transitions to the level scheme and estimated their energies and intensities from coincidence and singles data. There may also be other components at ≈ 517 and ≈ 521 keV. The former possibility seems quite likely, but it is difficult for us to draw further conclusions from the data. We simply are limited by the resolution of the detection systems.

c. Other complex lines of interest

The 541 - 547 keV complex is another case similar to the one just discussed. Coincidence data allow us to fit two transitions at 543.2 and 546.5 keV with some certainty, and a third at about 540.3 keV with less certainty. As nearly as we can tell from singles analysis (cf. Fig. 37) there are five lines present.

At 1224 keV the presence of a doublet is quite evident. However, the assignment of the line at 1226.7 keV is much less obvious. We have noted a slight asymmetry in all the computer fits of the 1223 - 1225 doublet indicating the presence, albeit weak, of a high-energy shoulder with intensity $\approx 6\%$ compared to the 1225-keV line intensity. This fact, coupled with rather tenuous evidence from the 1694-keV coincidence spectrum seemed to justify assignment of the 1225.7-keV transition from the level of that energy to ground, an assignment consistent with the 2+ spin and parity we proposed from K-conversion electron data for the 936- and 1138-keV transitions. Figure 38 compares the doublet and triplet analyses of the complex at 1224 keV. The Lu^{176m} decay data later confirmed the presence of the line at 1226.7 keV, and verified the computer fit to the Ta^{176} data.

There are several other instances where the Compton-suppressed data show weak lines in the region of much stronger lines (cf. e.g., Fig. 39, the low energy side of the 611 - 617 keV "doublet"), but in general the presence of these lines does not seem to introduce ambiguities into our interpretation of the more prominent data. A factor of two improvement in resolution (impossible, of course, with Ge(Li) devices)

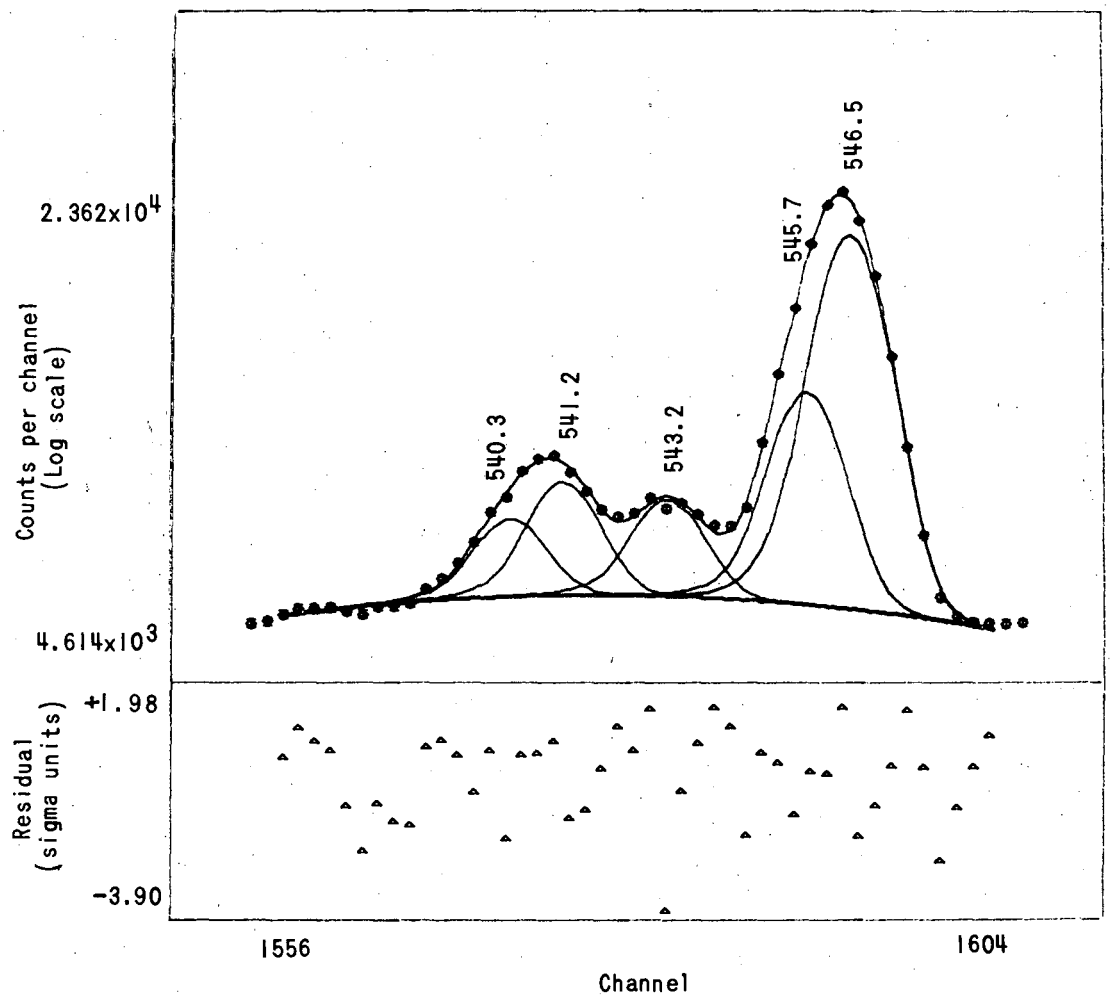

XBL 691-139

Fig. 37. The computer fit to the γ-ray complex at 541 - 547 keV.

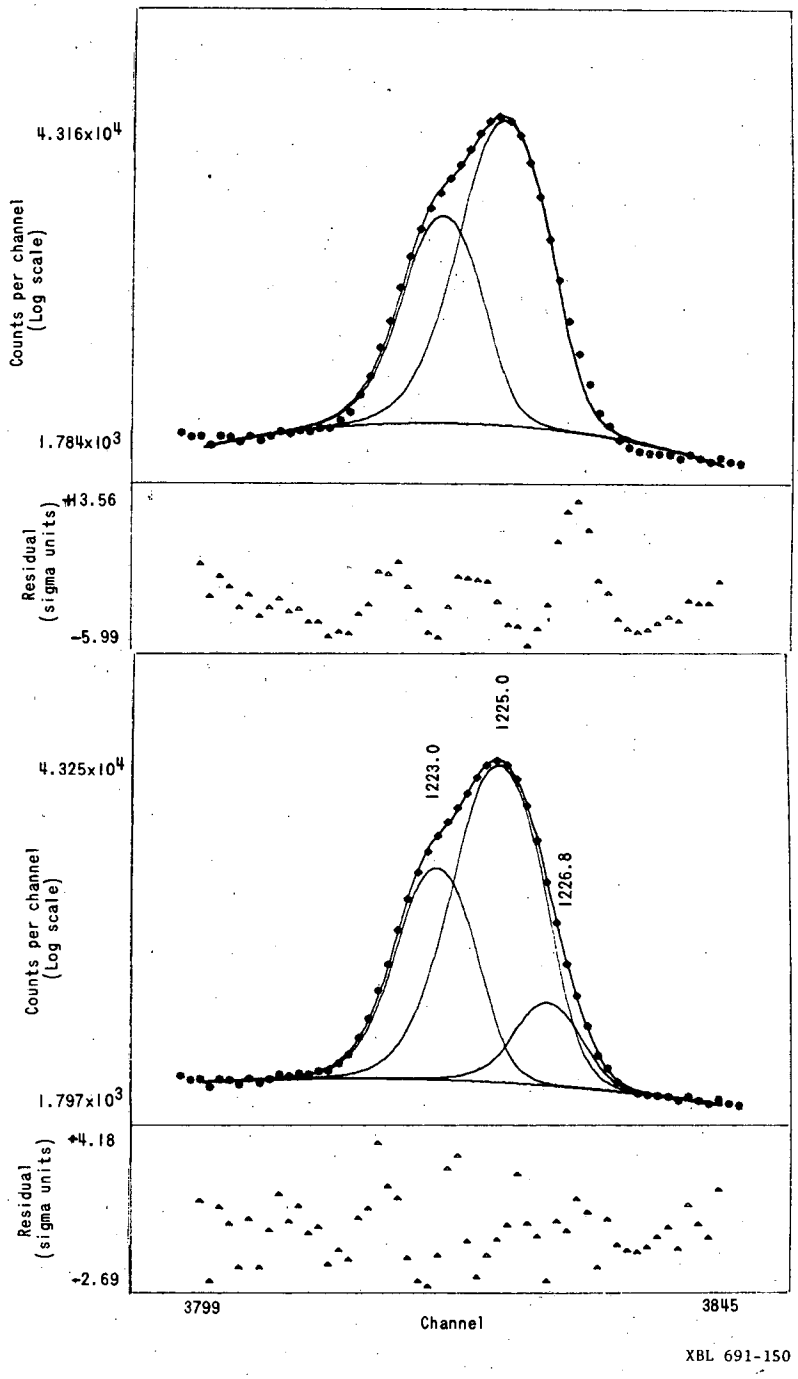

Fig. 38. The γ-ray multiplet at 1225-keV fitted as a doublet (top) and a triplet (bottom).

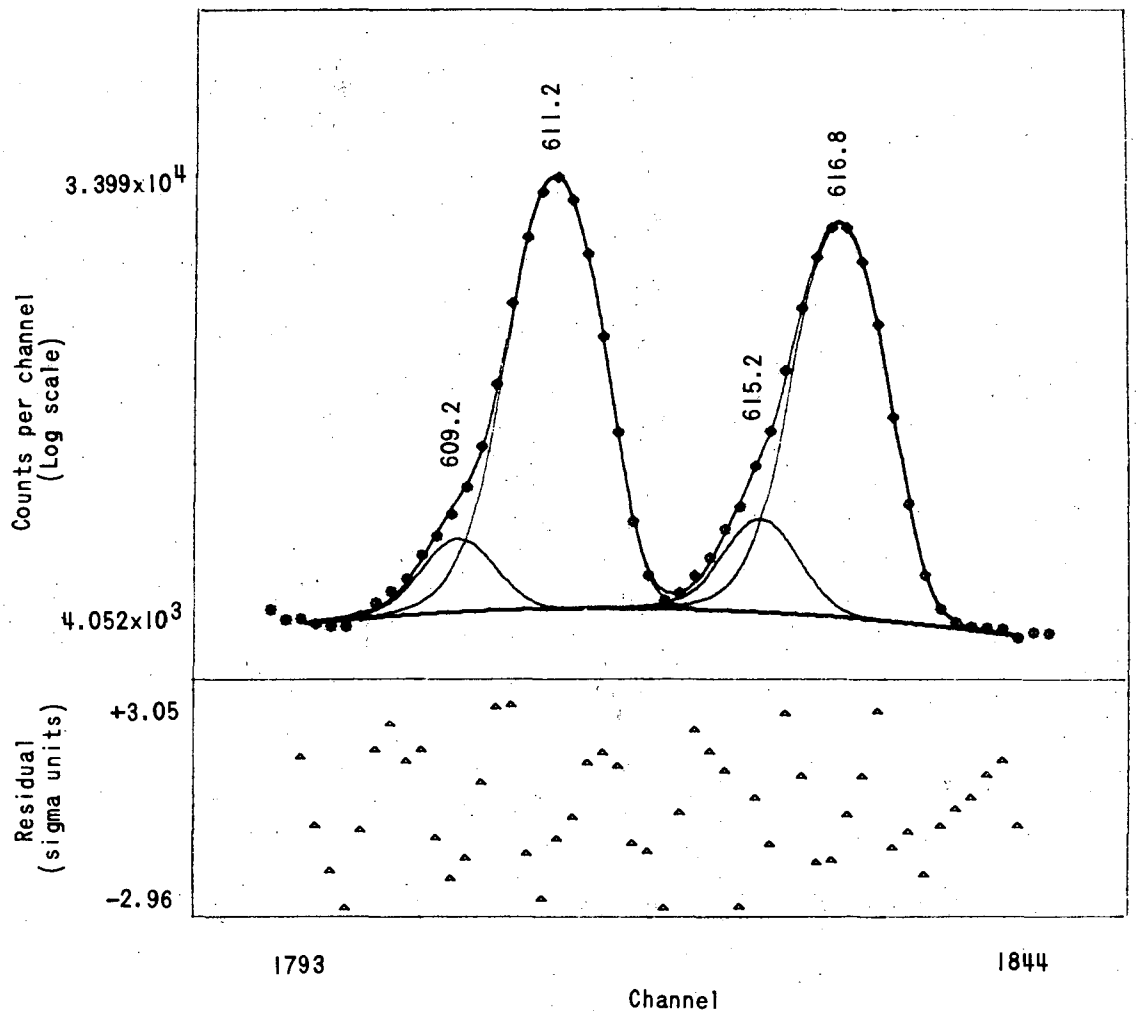

XBL 691-147

Fig. 39. Computer fit to the γ-rays at 610 - 618 keV.

would undoubtedly unveil many lines in addition to the ones we have presently identified, but for now we shall have to be content to confine our consideration to the stronger lines in the spectrum.

d. The 1149.9- and 1293.2-keV E0 transitions

The conversion electron spectrum (Fig. 30) reveals the presence of two lines that have no counterpart in the photon emission spectrum. These transitions, at 1149.9 and 1293.2 keV, presumably arise from pure E0 conversion processes, and indicate the presence of two low-lying (K = 0+0) states in the Hf^{176} level structure. We shall comment further on this interesting occurrence during our discussion of the level scheme.

e. The evidence for the low energy transition at 91.2 keV

We find evidence for the presence of a 91.2-keV transition in the "thin-window" high resolution spectrum (Fig. 28). Harmatz et al.[81] reported the line in their conversion electron spectrum, and indicated a likely E2(+M1) multipolarity. We shall discuss this latter point more fully later on. For now it is sufficient to cite the experimental evidence we find for the presence of the line. Although we are hard-pressed to definitely assign the line to Ta^{176} on the basis of singles data, there is strong circumstantial evidence in the coincidence data that also indicates its presence. The 1066-keV coincidence spectrum clearly shows the presence of the 1225-keV line in coincidence, as well as some indication for the presence of the weaker 1023-keV line. This analysis is corroborated by the 1023-keV coincidence spectrum showing the 1066-keV line, and the 1225-keV coincidence spectrum showing the same

1066-keV transition in coincidence. Thus, in this instance we are able by careful analysis to establish fairly conclusively the presence of a transition on the basis of coincidence data. We also point to this case as an example of analysis performed on data that we consider very near the statistical limits of significance, i.e., in few cases have we assigned a transition on the basis of less reliable information. Since we have not discussed the "coincidence matrix" for each transition, we trust that the above analysis will serve as a criterion by which the reader can attach some sort of "confidence rating" to the proposed decay scheme.

2. Spin and parity assignments

Assignment of the spins and parities to levels on the basis of K-conversion electron data and γ-ray relative intensities alone is a hazardous endeavor, and it is principally for this reason that the work described here must be considered incomplete, for it is exactly those nuclear parameters that are of primary interest to the theoretician. Still, we are able to draw some definite conclusions in this regard from our data, and it is worthwhile to indicate the basis on which we arrive at those conclusions.

To begin with (cf. Fig. 34), the two lowest levels above the ground rotational band almost certainly are themselves members of a single elementary rotational band. As we have indicated, the E0 transition at 1149.9 keV confirms unambiguously the assignment of a $(K = 0+0)$ level at that energy. The level at 1226.7 is designated $K = 0+2$ on the basis of: 1) the enhanced K-conversion coefficient associated with

the 1138-keV line ($\alpha_K = 2.3 \times 10^{-2}$) indicates either an E0 component or, alternatively, a pure M2 transition; 2) the presence of the 936.4- and 1226.7-keV transitions identifies the spin as 2, therefore the parity is necessarily positive. Branching ratios to the ground band indicate K = 0 as most likely (cf. Table 15).

The level at 1247.7 keV can be definitely assigned as 2- on the basis of conversion coefficient data and γ-ray branching. The 1159-keV transition to the ground-band 2+ state is very strong and the K-conversion indicates a probable E1 multipolarity. Moreover, the 957.4- and 1247.7-keV lines can be identified fairly certainly as M2 in character (cf. Fig. 40) from the conversion data. Not so certain is the K quantum-number assignment. Although K = 2 is most likely, the M2 branching ($I_{957}:I_{1248} = 11:9$) seemingly contradicts this designation. But a K = 1 assignment, though certainly otherwise acceptable, immediately raises the question of the spin 1 member of the band, a member which ought to be strongly populated if it is present at all.

The level at 1313.3 keV is definitely spin 3 and negative parity from conversion data and from the absence of a transition to ground. Again, the K quantum-number is less certain, though it is likely the same as that of the 1247.7-keV level. We thus prefer to consider these two levels as members of a K = 2- band.

The (K = 0+0) designation for the state at 1293.2 keV is, on the basis of the conversion data, again an obvious assignment. It is of particular interest, for reasons we will discuss at length later on,

Table 15. Squares of Clebsch-Gordan coefficients for low angular-momentum coupling of interest in Ta^{176} decay.

K_i	K_f	I_i	λ	$(I_i \lambda K_i \Delta K \mid I_f K_f)^2$		
				$I_f = 0$	$I_f = 2$	$I_f = 4$
0	0	2	2	0.200	0.286	0.515
		4	2		0.286	0.260
1	0	1	1	0.334	0.167	
		2	2	0.200	0.072	0.229
		3	1		0.286	0.215
		4	2		0.239	0.020
2	0	2	2	0.200	0.286	0.015
		4	2		0.120	0.351

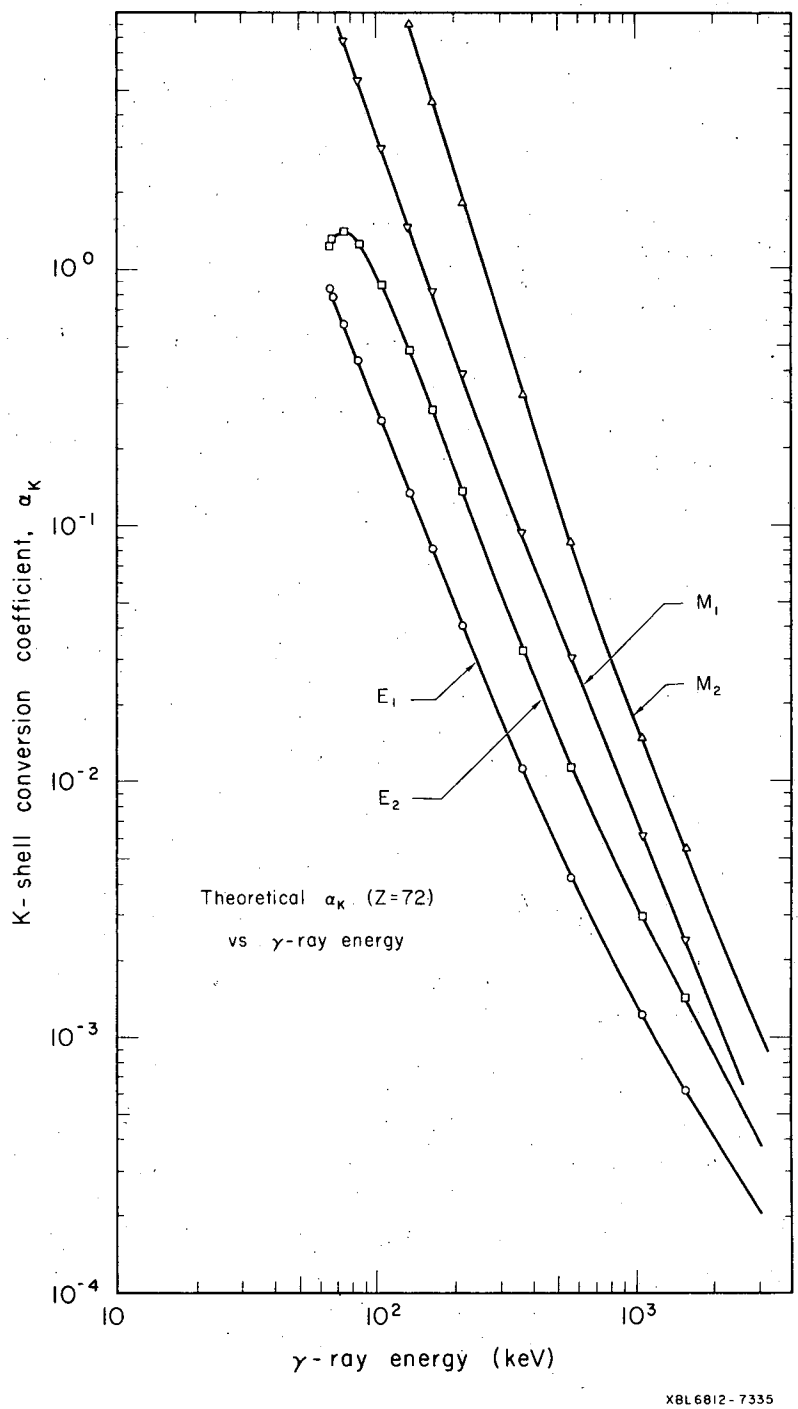

Fig. 40. Theoretical K-conversion coefficients for Hf (Z=72). From Hager and Seltzer (Ref. 98).

to be able to identify the 2+ member of this second 0+ band. Unfortunately, though we have two candidates for the position, we are not able to unambiguously assign a definite (K = 0+2) classification to either one. The first possibility might be the level at 1341 keV, but it seems likely both from γ-ray branching and from the relatively "normal" 1253-keV K-conversion coefficient, that this state is (K = 2+2) K-conversion and the K/L ratio for the 1253-keV transition seem to indicate that it is (M1 + E2) in character. With this 2+ state apparently thus accounted for, we are next left to contemplate the 1379.4-keV level, a level that could be a relatively innocuous 2- state with anomalously large branching to the 4+ member of the ground rotational band. At least if we adhered to this interpretation we would be in a less embarrassing position than if we were to propose any of the alternatives. However, one most unsettling discrepancy remains if the 2- assignment is made--the K-conversion coefficient of the presumed E1-(M2) 1291-keV transition may turn out in fact to be far too large for even a predominantly M2 transition. Our fit (Fig. 41) to the electron complex at 1290 - 1293 keV indicates a K-conversion coefficient of perhaps 1.9×10^{-2} for the 1291-keV line--a number that would seem to classify the transition as being M2 or E0 - E2 in nature. But we must emphasize that the complication of the 1223 - 1225 (M+N) lines and the very strong 1293-keV E0 K-electron line in this region may have compromised the reliability of the computer fit to the 1291-keV component. The 1089-keV conversion coefficient is also uncertain, but it appears to be large enough to be compatible with an M2 assignment. The γ-ray branching, though often anomalous for

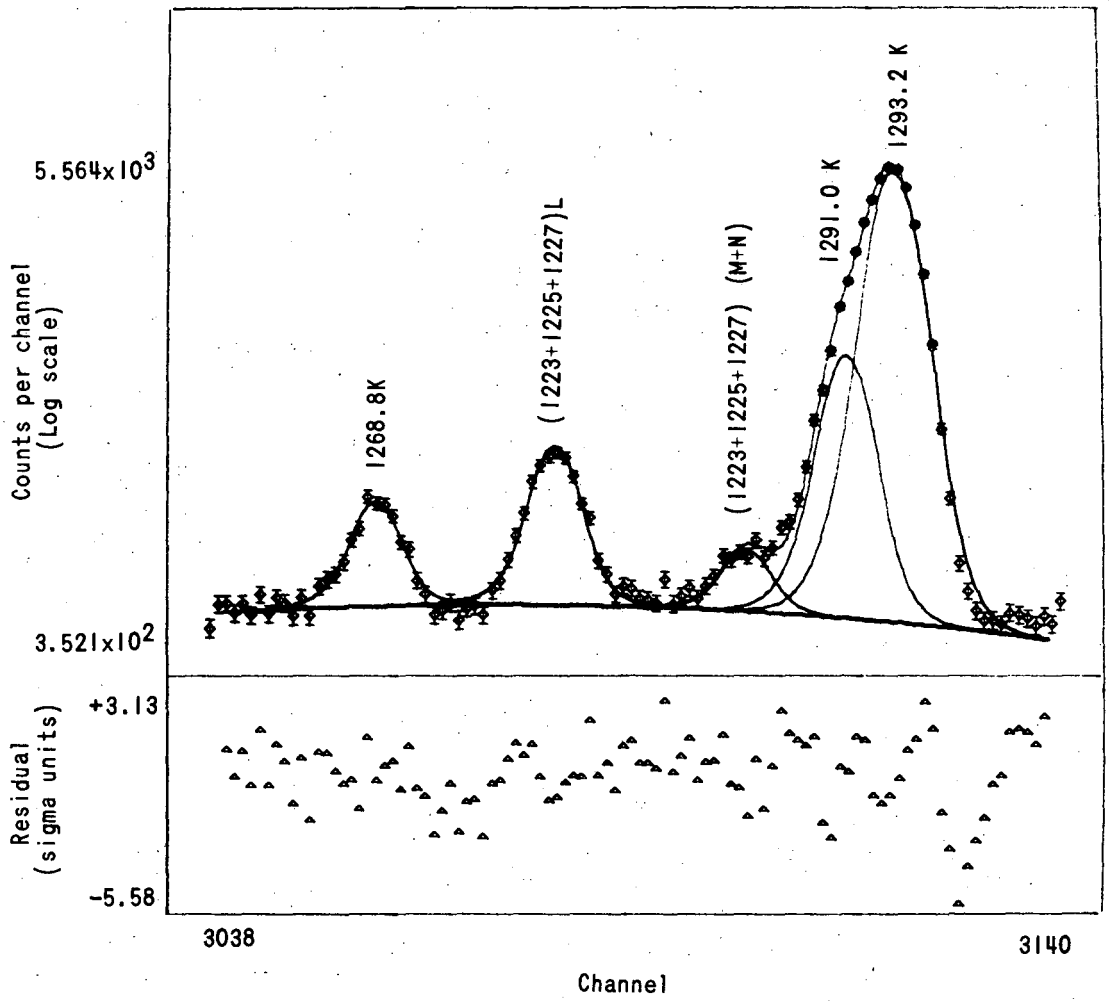

XBL 691-142

Fig. 41. The conversion electron spectrum in the region about 1290 keV resolved into its component peaks.

transitions from (K = 0, 2+) excited states, is in this case so far removed from what one would expect that a 2- assignment would seem most likely if the electron data were ignored.

Thus, the evidence is strong that, despite our protestations to the contrary, the fit to the electron data for the 1291-keV K-conversion line is correct (cf. Fig. 41), in which case we are compelled to propose a (K = 0+2) assignment for the level in question. The weak 1379.3 keV transition has (because of its importance) in this single instance been included in the level scheme (Fig. 34) even though it is too weak to be identified in the coincidence data. If it does not belong to the level at 1379.4 keV, then of course alternative assignments of spin and parity that would not be offensively inconsistent with the electron data could be made (e.g., 3+, 4+). If, on the other hand, the 1379.3-keV transition is properly placed, then we are obliged to accept the (K = 0+2) assignment, a startling development for reasons we shall discuss in section E.

The level at 1404.5 keV may be the 3+ member of the K = 2 band ostensibly beginning at 1341 keV, but we are unable to see the transition to the 2+ member of the ground band. In view of our earlier discussion placing the 91.2-keV transition from this level to the 1313.4-keV level, it would be most pleasing to be able to label the level at 1404.5 keV as the 4- member of the K = 2 band with other members presumably at 1247.7 and 1313.3 keV. This would be particularly satisfying because then we could call the 156.8-keV line the 4- → 2- crossover E2 transition, and the 91.2- and the proposed 65.7-keV (unobserved in singles) lines would fit in nicely as the cascade M1 - E2's. But unfortunately, tempting as it is

to try to impart this bit of orderliness to an otherwise chaotic situation, there are several reasons why we cannot be certain about the assignment. First of all, the K-conversion of the 1115-keV transition seems too high for it to be pure E1; but this evidence is insufficient since there may be M2 admixture, and the 1115-keV line is itself apparently complex. The 156.8-keV transition and its conversion coefficient give us little additional help; the conversion coefficient is almost exactly what one would expect for pure E2--or mixed E1 - M2. The same conclusions could apply to the 91.2-keV transition, although Harmatz et al.[81] propose an E2 assignment on the basis of L-subshell ratios. There is little feeding of the 1405-keV level from above, and about all one can say from branching is that we do not see a 1316.4-keV transition that one might expect from a 3+ or 4+ level.

One additional comment should be made with regard to the appreciable discrepancy in the energy measured for the 115.0-keV transition thought to de-excite the 1404.5-keV state. The following energy sums apply:

1114.96	1247.64	1313.30
+ 290.19	+ 156.84	+ 91.23
1405.15	1404.48	1404.53

We are not accustomed to tolerate errors this large, particularly at such relatively low energies, and if it were not for the 1115-keV coincidence data coupled with the known complexity of the 1115-keV peak we would be inclined to propose two separate levels at 1405.2 and 1404.5 keV. Such a proposal would seem in many respects to be more satisfactory, but we are unable to prove this hypothesis.

Finally, we prefer the 3- assignment at 1446 keV, although the K-conversion coefficients are here quite uncertain since both the 1155.5- and 1357.5-keV K-conversion lines are complex. Some additional support to the assignment is afforded by the 466.2-keV transition, which is essentially E1 in character (from K-conversion data). We prefer the 2+ assignment for the 1912-keV level, which would be consistent with negative parity for the 1446-keV level.

For levels above 1450 keV the information on spins and parities is for the most part meager. We quickly mention a few of the assignments that seem fairly certain, and the basis for each assignment:

1643.4 keV: 1- on the basis of K-conversion coefficients and branching. Branching indicates K = 0. The 3- member of the band is likely at 1710.4 keV.

1722.1 keV: Transitions from this level are almost certainly E1 from electron data, and the branching indicates (K = 0-1).

1767.5 keV: The 1679.2-keV transition to the ground 2+ state is apparently E1 from conversion data. One would suspect that one of the lines in the region around 1767 keV might belong to this level and represent the transition to ground, but coincidence data seem to rule out that possibility. We therefore assign the level as 2-.

1862.8 keV: Conversion coefficients indicate the transitions from this level to the ground band are probably M1 in character, and branching indicates K = 1. In the absence of the transition to the ground 4+ member, we prefer (K = 1+1).

1924.6 keV: K-conversion coefficient data indicate the 1836-keV transition is E1. Moreover, γ-ray feeding to other levels and associated conversion lines (e.g., 611.2 keV) seem to make the 2- assignment here fairly certain.

1958.1 keV: The 616.8-keV transition is essentially pure E1, indicating the parity of this level is negative. We prefer the spin 3 assignment from feeding to other levels and perhaps also because of the near-lying 2- level, although spin 2 cannot be ruled out entirely.

2920.4 keV: This level is fed strongly by the Ta^{176} EC decay [log (ft) = 6.8] and in turn decays predominantly to the ground and first excited states of Hf^{176}. Branching to the ground band unambiguously indicates (K = 0-1) to be the likely assignment. The parity is somewhat less certain, although we favor a negative assignment, both because of the strong EC decay to this level and because of the apparent weakness of the conversion lines. We are uncertain of the electron counter efficiency at 3 MeV, but our estimates of the efficiency at that energy would have to be off by about an order of magnitude for the K-conversion coefficient to be raised enough to place the E1 assignment in doubt.

Finally, after much vacillation and with great reluctance we have arrived at the conclusion that nature, in a pique, has seen fit to populate a level at 2921.0 keV. Consistent inconsistencies in the energy calibrations for the high-lying 2832.0 - 2920.4 doublet and consideration of the feeding that would be required of a single level at 2921 keV have forced this conclusion. Coincidence data indicate the 1064.0-, 1579.7-, and 1673.4-keV transitions feed the 1856.9, 1341.3

(K = 2+2), and 1247.7 (K = 2-2) levels, while the 1540.8- and 1693.7-keV transitions feed the 1379.4 (possible K = 0+2) and 1226.7 (K = 0+2) levels. These data are consistent with a (K = 0-1) state at 2920.4 keV, and a second probably higher-spin state at 2921.0 keV. The energy data also support this conclusion.

We have indicated a number of other possible spin and parity assignments for the various Hf^{176} levels, but they are for the most part quite uncertain. The cases we have discussed above represent those levels for which we have felt definite spin and parity assignments could be made on the basis of the available information.

3. EC- β^+ branching

It will be noticed in Fig. 34 that we have indicated absolute EC-β^+ feeding to the various Hf^{176} levels from Ta^{176} decay. These estimates have been obtained by using the preliminary results of Fominikh, et al.[99] which indicate the ratio of total positron emission resulting from Ta^{176} decay to K-conversion electron emission resulting from the 1159-keV complex is $I_{\beta^+}/I_{K_{1159}} = 26$. By combining this information with our conversion electron data and by then summing the observed γ-ray (and conversion electron, where significant) intensity feeding and de-exciting each level, we were able to obtain the indicated branchings. The branching to the ground and first excited states must be considered a limit, since the authors in Ref. 99 indicate only that the (3000 ± 80)-keV positron component carries about 27% of the total positron intensity. In addition, we have been unable to place in the decay scheme γ-rays representing about 7% of the total observed photon

emission intensity from Ta^{176} decay. The errors arising from this source should be relatively small, however, compared to the ≈ 10-15% error resulting from the combined individual γ-ray intensity errors, provided we are correct in presuming the unplaced photons to be about evenly distributed throughout the level structure.

E. Discussion of the Hf^{176} Level Scheme

1. K = 0+ excited states

Of the Hf^{176} levels for which we have definitive information, by far the most interesting from the standpoint of contemporary nuclear theory are the two excited K = 0+ levels at 1150 and 1293 keV. We have been able to identify the 2+ rotational band member of the lower state, and as we have earlier indicated, it is possible that the level at 1379.4 keV is the 2+ member of the second K = 0+ band.

These K = 0+ states are deserving of special attention for two reasons: 1) γ-ray branching from members of the excited K = 0+ bands to members of the ground state rotational band is a phenomenon of particular interest at the present time, primarily because of rather large observed deviations from Alaga's branching rules for the $K = 0_2 I_2 \rightarrow K = 0_1 I_1$ transitions from presumed β-vibrational bands to the ground bands of deformed even-even nuclei; 2) the nature of the first excited K = 0+ bands themselves, interpreted in the microscopic superfluid model, is a question of theoretical significance that has also recently evoked considerable discussion.

The first subject has lately been considered experimentally in studies performed on the nuclei Gd^{154} and Hf^{178}.[100,101] The important theoretical ramifications associated with the problem have been discussed by Mottelson.[102]

The second topic may be related to the first. It has recently been proposed that some of the low-lying K = 0+ states in even-even deformed nuclei may be essentially characterized as pairing-vibrational excitations,[103] particularly near the middle of the rare-earth region of deformation. In addition, it has also been suggested that such states may be significantly influenced by spin-quadrupole interactions.[104,105] The possibility would seem to exist, then, that pairing vibrations and/or spin-quadrupole interactions may influence the relative transition rates for the K = 0+ states in such nuclei. We shall consider these two possibilities separately, bearing in mind that they may in fact turn out to be intimately related.

a. <u>γ-ray branching from the K = 0+ excited states</u>

In the relatively few deformed nuclei in the rare-earth region for which excited K = 0+ bands have been reported, γ-ray branching from the 2+ members of the presumed β-vibrational bands to the 2+ ground band members has generally been found to disagree with theory. It is now thought that because of the mixing of the excited K = 0+ bands with other K = 0+ bands, notably the ground band, the E2 branching is not expected to follow the intensity rules of Alaga, but rather should be given by the general expansion of the transition matrix elements in terms of the total angular momentum, I.[102] To first order this

expansion is, for E2 transitions of the type $K = 0_2 I_2 \rightarrow K = 0_1 I_1$:

$$B(E2;\ K = 0_2 I_2 \rightarrow K = 0_1 I_1) = (I_2\ 200|I_1 0)^2 \times |M_1 + M_2[I_2(I_2+1) - I_1(I_1+1)]|^2 \quad . \tag{36}$$

The matrix elements M_1 and M_2 are related to the familiar Z_0 parameter by $Z_0 = M_2/M_1$. In general, the linear expansion (36) and similar forms (e.g., for the Hf^{177} E1's we have discussed in part I) ought to be valid to the extent that first order perturbation theory is applicable.

However, significant departures from even the form (36) have been noted for all excited K = 0+ (β-vibrational) bands thus far observed. The discrepancies between experiment and theory can in every case be attributed to an apparent enhancement of the $0_2 2_2 \rightarrow 0_1 2_1$ transition intensity. It has been suggested that the presence of appreciable M1 admixture could account for this enhancement. Mottelson[102] has pointed out that although such radiation is forbidden in the I-independent approximation, if the nuclear rotational g-factor, g_R, is deformation dependent, the transition operator

$$M(M1,\ \mu) = \sqrt{\frac{3}{4\pi}} \left[g_R(\beta_0) + (\beta-\beta_0) \frac{\partial g_R(\beta_0)}{\partial \beta} + \ldots \right] \times I_\mu \left(\frac{e\hbar}{2Mc} \right)$$

obtains, and the transition matrix element for the M1 decay of a β-vibrational state can be written:

$$B(M1;\ n_\beta=1,\ I_2 \rightarrow n_\beta=0,\ I_1) = \frac{3}{4\pi}\left(\frac{e\hbar}{2Mc}\right)^2 \times \frac{\hbar\omega_\beta}{2C_\beta}\left(\frac{\partial g_R}{\partial\beta}\right)^2 \delta(I_1,I_2)I_1(I_1+1) \tag{37}$$

where $\frac{\hbar\omega_\beta}{2C_\beta}$ is the amplitude of the β-vibrational motion, obtainable from the E2 transition matrix elements between the ground and β-vibrational bands. If $\left(\frac{\partial g_R}{\partial\beta}\right)$ is of the order unity, the observed enhancements could be explained.[102] (Recent theoretical calculations by Krumlinde suggest $\left(\frac{\partial g_R}{\partial\beta}\right)$ may indeed be near unity.[106])

The obvious test for the presence of M1 mixtures in the $\Delta I = 0$ transitions in question is to perform a direct experimental measurement of the M1 - E2 mixing ratio, for example by γ-ray angular correlation studies on the nuclei of interest. Such measurements have recently been carried out for Gd^{154} by Hamilton, et al.[100] and for Hf^{178} by Nielsen, et al.[101] The results of the two experiments are apparently contradictory--Hamilton et al. find the $0_2 2_2 \rightarrow 0_1 2_1$ transition in Gd^{154} to be essentially pure E2, while Nielsen, et al. find only (17 ± 10)% E2 character in the corresponding transition in Hf^{178}.

Mottelson has emphasized the important implications of the problem for the valid application of the rotational model in general to deformed nuclei; it seems clear that if indeed the postulated M1 mixture is found to be absent, then the commonly accepted picture of the K = 0+ excited

states as symmetric vibrations in the quadrupole field of these nuclei will have to be substantially modified.

Because of the serious implications the problem bears for the collective model, we summarize in Table 16 not only the experimental results we have obtained for Hf^{176}, but also the information presently to be found in the literature. The literature data in some cases represent a weighted mean of data from the indicated sources.

It is significant that we apparently do <u>not</u> observe for the (K = 0+2) state at 1226.7 keV in Hf^{176} the spectacular departures from Alaga's rules observed in, e.g. Hf^{178}. However, it should be noted that the error on the 2'+ → 0+ transition intensity is fairly large, and the only precise indicator we have of the relative branching is the 2'+ → 4+/2'+ → 2+ intensity ratio. We also recall that the nature of the 1379.4-keV state is still in doubt. If this state turns out to be the 2+ member of the K = 0+ band beginning at 1293.2 keV, the following remarkable departures from Alaga's rules will obtain: (see Table 17 following Table 16)

Table 16. Summary of experimental data on γ-ray branching from excited K = 0+ bands in even-even deformed rare-earth nuclei.

Nucleus	$\frac{E_{\gamma_1}\ (keV)}{E_{\gamma_2}\ (keV)}$	$\frac{I\pi K_n \xrightarrow{\gamma_1} I_1\pi K_1}{I\pi K_n \xrightarrow{\gamma_2} I_1'\pi K_1}$	$\frac{B(E2)I \to I_1}{B(E2)I \to I_1'}$	Ref.
Sm^{152}	$\frac{444}{811}$	$\frac{2+0_2 \to 4+0_1}{2+0_2 \to 2+0_1}$	2.5 (7)	107-109
	$\frac{811}{689}$	$\frac{2+0_2 \to 0+0_1}{2+0_2 \to 2+0_1}$	0.19 (5)	
	$\frac{444}{811}$	$\frac{2+0_2 \to 4+0_1}{2+0_2 \to 0+0_1}$	13 (4)	
Gd^{154}	$\frac{444}{693}$	$\frac{2+0_2 \to 4+0_1}{2+0_2 \to 2+0_1}$	3.0 (5)	107, 108
	$\frac{816}{693}$	$\frac{2+0_2 \to 0+0_1}{2+0_2 \to 2+0_1}$	0.14 (3)	
	$\frac{444}{816}$	$\frac{2+0_2 \to 4+0_1}{2+0_2 \to 0+0_1}$	18 (3)	
	$\frac{925}{678}$	$\frac{4+0_2 \to 2+0_1}{4+0_2 \to 4+0_1}$	0.11 (11)	
Gd^{156}	$\frac{841}{1040}$	$\frac{2+0_2 \to 4+0_1}{2+0_2 \to 2+0_1}$	0.54 (24)	109, 110
	$\frac{1129}{1040}$	$\frac{2+0_2 \to 0+0_1}{2+0_2 \to 2+0_1}$	0.074 (29)	
	$\frac{841}{1129}$	$\frac{2+0_2 \to 4+0_1}{2+0_2 \to 0+0_1}$	7.2 (3.7)	

(continued)

Table 16. Continued

Nucleus	$\frac{E_{\gamma_1}\text{(keV)}}{E_{\gamma_2}\text{(keV)}}$	$\frac{I\pi K_n \xrightarrow{\gamma_1} I_1\pi K_1}{I\pi K_n \xrightarrow{\gamma_2} I_1'\pi K_1}$	$\frac{B(E2)I \to I_1}{B(E2)I \to I_1'}$	Ref.
Er^{164}	$\frac{(1340)}{1242}$	$\left(\frac{2+0_2 \to 0+0_1}{2+0_2 \to 2+0_1}\right)$	(0.48 (35))	111
	$\frac{1785}{1698}$	$\frac{2+0_3 \to 0+0_1}{2+0_3 \to 2+0_1}$	0.14 (8)	
Yb^{170}	$\frac{1534}{1450}$	$\frac{2+0_2 \to 0+0_1}{2+0_2 \to 2+0_1}$	0.30 (6)	112
Yb^{172}	$\frac{858}{1039}$	$\frac{2+0_2 \to 4+0_1}{2+0_2 \to 2+0_1}$	2.5 (6)	113, 114
	$\frac{1120}{1039}$	$\frac{2+0_2 \to 0+0_1}{2+0_2 \to 2+0_1}$	1.3 (4)	
	$\frac{858}{1120}$	$\frac{2+0_2 \to 4+0_1}{2+0_2 \to 0+0_1}$	2.0 (6)	
Hf^{176}	$\frac{936}{1138}$	$\frac{2+0_2 \to 4+0_1}{2+0_2 \to 2+0_1}$	2.2 (2)	This work
	$\frac{1227}{1138}$	$\frac{2+0_2 \to 0+0_1}{2+0_2 \to 2+0_1}$	0.30 (6)	
	$\frac{936}{1227}$	$\frac{2+0_2 \to 4+0_1}{2+0_2 \to 0+0_1}$	7.3 (1.6)	
Hf^{178}	$\frac{969}{1183}$	$\frac{2+0_2 \to 4+0_1}{2+0_2 \to 2+0_1}$	0.45 (14)	101

(continued)

Table 16. Continued

Nucleus	$\frac{E_{\gamma_1}\text{ (keV)}}{E_{\gamma_2}\text{ (keV)}}$	$\frac{I\pi K_n \xrightarrow{\gamma_1} I_1\pi K_1}{I\pi K_n \xrightarrow{\gamma_2} I_1'\pi K_1}$	$\frac{B(E2)I \to I_1}{B(E2)I \to I_1'}$	Ref.
	$\frac{1276}{1183}$	$\frac{2+0_2 \to 0+0_1}{2+0_2 \to 2+0_1}$	0.066 (29)	
	$\frac{969}{1276}$	$\frac{2+0_2 \to 4+0_1}{2+0_2 \to 0+0_1}$	6.8 (1.6)	

Table 17. E2 branching from the 1379.4-keV proposed (K = 0+2) State.

	Experiment	Alaga's Rule
$\frac{B(E2)2'+ \rightarrow 4+}{B(E2)2'+ \rightarrow 2+}$	0.35 ± .04	1.80
$\frac{2'+ \rightarrow 0+}{2+ \rightarrow 2+}$	0.031 ± .06	0.699
$\frac{2'+ \rightarrow 4+}{2'+ \rightarrow 0+}$	11.4 ± 2.2	2.58

These data appear to have more in common with the Hf^{178} data of Ref. 101 than do the data for the other (1227-keV)2'+ state in Hf^{176} listed in Table 16. But the question of the proper assignment of the 1379.4-keV state is not yet resolved, so the data in Table 17 may not be applicable at all.

Finally, we consider what appears to be an anomalously fast E0 (or slow E2) transition in Hf^{176}. It is convenient, for the purpose of comparing E0 - E2 branching from a given state, to be able to write a sort of "reduced" E0 transition strength analogous to the familiar B(E2) reduced photon transition moment. Church and Weneser[115] have expressed the electric monopole transition probability, W, as the product of an electronic factor Ω, and a nuclear strength parameter, ρ,

$$W = \Omega \rho^2 .$$

The electronic factor, Ω, is to a first approximation independent of the intrinsic and collective nuclear properties, while ρ^2 describes the nuclear monopole matrix elements. Reference 115 contains in graphic form the values of Ω as a function of atomic number and transition energy.

Rasmussen[116] has shown that for the case of a spheroidal nucleus undergoing quadrupole vibrations, the ρ^2 of Church and Weneser can be written to first order as

$$\rho^2 = \frac{9}{8\pi^2} Z^2 \beta^2 \hbar (BC)^{-1/2} \quad . \tag{38}$$

The reduced E2 strength from the 0+ β-vibrational state to the 2+ ground state is[117]

$$B(E2;\ 0'+ \rightarrow 2+) = \frac{9}{32\pi^2} Z^2 e^2 R_0^4 \hbar (BC)^{-1/2} \quad . \tag{39}$$

Then a dimensionless ratio of the reduced E0 and E2 transition strengths can be given from (38) and (39),

$$X \left(\frac{B(E0;\ 0'+ \rightarrow 0+)}{B(E2;\ 0'+ \rightarrow 2+)} \right) = \frac{\rho^2 e^2 R_0^4}{B(E2;\ 0' \rightarrow 2)} \tag{40}$$

without knowledge of the nuclear "spring constant" C, or the mass parameter, B, i.e. the dependence of the E0 and E2 transition strengths on the zero-point vibrational amplitude $(BC)^{-1/4}$ is the same.[116]

Experimentally, if the relative E0 and E2 transition probabilities are known, with Ω obtained from Ref. 115 the parameter X may be calculated and compared with the theoretical

$$X = 4\beta^2 \tag{41}$$

of Rasmussen for a vibrating spheroid.

To this end, we summarize in Table 18 the available experimental data on E2/E0 branching ratios from K = 0+ excited states in the rare-earth region of deformation. It ought to be noted while considering the calculated values for X in column 5 that from Eq. (41) we would expect in general, for the deformed nuclei in this region, $0.15 \leqslant X \leqslant 0.50$. And indeed, Table 18 indicates that this is approximately true, with two remarkable exceptions: Hf^{176} and probably Yb^{170}. Even more noteworthy is the fact that in Hf^{176}, one of the E0 transitions behaves in "normal" fashion, while the other is in disagreement with theory by at least an order of magnitude. And although the data for Yb^{170} are preliminary,[122] and we have no error limits for the indicated measurements, a similar observation seems to apply to that nucleus.*

There are also large values of X reported for Er^{164}, but these are for 0+ states above 2 MeV, not likely to qualify as primarily β-vibrational in character. In fact, the authors suggest that they may represent the two-phonon K = 0+ "γ-vibrations" of Davydov and Rostovsky[124] expected at perhaps 1.5 - 2.0 MeV.

Rasmussen[116] also early derived an alternative formulation for the E0 matrix elements based on a microscopic model of the nuclear β-vibration. Here, using an asymptotic anisotropic harmonic-oscillator representation for the appropriate Nilsson orbitals, the quadrupole oscillations were described as coherent superpositions of individual

---

*Detailed work on the decay of Lu^{170} to levels in Yb^{170} is in progress at Livermore.

Table 18. $X = \frac{e^2 R_0^4 \rho^2}{B(E2)}$ for E0-E2 branching in even-even deformed rare-earth nuclei.

Nucleus	Ref.	Transition	Energy (keV)	Rel. Int.	X
Gd^{154}	118, 119	$0_2^+ \rightarrow 0_1^+$	682	$(2.1\pm0.4)\times10^{-2}$	0.071 ± 0.023
		$0_2^+ \rightarrow 2_1^+$	557	1.1 ± 0.3	
Gd^{156}	120	$0_2^+ \rightarrow 0_1^+$	1040	0.011	0.27
		$0_2^+ \rightarrow 2_1^+$	951	1.4	
Dy^{156}	121	$0_2^+ \rightarrow 0_1^+$	676		0.06
		$0_2^+ \rightarrow 2_1^+$	538		
		$2_2^+ \rightarrow 2_1^+$	829		0.15 ± 0.07
		$4_2^+ \rightarrow 4_1^+$	1088		0.20 ± 0.07
		$6_2^+ \rightarrow 6_1^+$	1437		0.12 ± 0.06
Er^{164}	111	$0_2^+ \rightarrow 0_1^+$	1246	9.6×10^{-3}	0.15 ± 0.03
		$0_2^+ \rightarrow 2_1^+$	1157	2.84 (40)	
		$0_3^+ \rightarrow 0_1^+$	1698	2.9×10^{-3}	0.39 ± 0.06
		$0_3^+ \rightarrow 2_1^+$	1614	1.36 (19)	
		$0_4^+ \rightarrow 0_1^+$	1766	6.4×10^{-3}	0.78 ± 0.11
		$0_4^+ \rightarrow 2_1^+$	1677	1.55 (22)	
		$0_5^+ \rightarrow 0_1^+$	2171	4.5×10^{-3}	1.76 ± 0.25
		$0_5^+ \rightarrow 2_1^+$	2080	1.14 (16)	

(continued)

Table 18. Continued

Nucleus	Ref.	Transition	Energy (keV)	Rel. Int.	X
		$0_6^+ \rightarrow 0_1^+$	2185	2.5×10^{-3}	5.6±1.8
		$0_6^+ \rightarrow 2_1^+$	2094	0.21 (8)	
Yb^{170}	122	$0_2^+ \rightarrow 0_1^+$	1479	0.6	9.1
		$0_2^+ \rightarrow 2_1^+$	1395	4.8	
		$0_3^+ \rightarrow 0_1^+$	1565	0.1	0.96
		$0_3^+ \rightarrow 2_1^+$	1481	10	
Hf^{176}	Present work	$0_2^+ \rightarrow 0_1^+$	1150	0.091 (14)	0.16±0.03
		$0_2^+ \rightarrow 2_1^+$	1062	10.0 (9)	
		$0_3^+ \rightarrow 0_1^+$	1293	1.58 (24)	7.3±1.2
		$0_3^+ \rightarrow 2_1^+$	1205	6.1 (5)	
Hf^{178}	123	$0_2^+ \rightarrow 0_1^+$	1199	$(3.5\pm0.7)\times10^{-3}$	0.18±0.05
		$0_2^+ \rightarrow 2_1^+$	1106	0.44±0.09	
		$0_3^+ \rightarrow 0_1^+$	1434	$(1.9\pm0.4)\ 10^{-3}$	0.10±0.03
		$0_3^+ \rightarrow 2_1^+$	1341	0.95±0.19	
		$0_4^+ \rightarrow 0_1^+$	1444	$(8.4\pm1.7)\ 10^{-3}$	0.38±0.11
		$0_4^+ \rightarrow 2_1^+$	1351	1.1±0.2	

excitations of the easily polarizable protons in orbitals near the Fermi surface. The result of this treatment predicts a first order branching

$$X \left(\frac{B(E0;\ 0'+ \rightarrow 0+)}{B(E2;\ 0'+ \rightarrow 2+)} \right) = 9\beta^2 ,$$

somewhat more than twice as large as that predicted by the vibrating spheroid model, but still far too small to explain the value 7.3 for the transitions from the Hf^{176} 1293-keV 0+ state.

The prediction of Davydov and Rostovsky[124] for the E0 transition strength from the β-vibrational state does not differ appreciably from that of Rasmussen:

$$X = 4\beta_0^2(1 + \frac{1}{s}) \quad .$$

Here, "s" is the ratio of the energy of the first member of the "anomalous" K = 2+ band (normally called the γ-vibrational band) to the energy of the 2+ ground rotational band member. For Hf^{176}, 1/s can hardly be greater than 0.1. Further, it seems unlikely that the 1293-keV level of Hf^{176} could be the (normally higher energy) K = 0+ two-phonon "γ-vibrational" state of Davydov, but verification of this point requires knowledge of the zero-point amplitudes of the nuclear β- and γ-vibrations that we do not possess.

It is clear that more experimental data are required for other rare earth nuclei before we can correctly label the 1293.2-keV 0+ state in Hf^{176} as "anomalous", but nevertheless on the basis of the information

in Table 18, perhaps some guarded speculation about the factor of 20 difference in the two E0 branching ratios in Hf^{176} would be in order.

b. The nature of the K = 0+ excited states

Since the early and successful treatment by Bohr and Mottelson of collective nuclear motion in terms of quadrupole shape oscillations and nuclear surface rotations, there have been numerous attempts to provide a microscopic description of these so-called collective nuclear motions in terms of long-range (quadrupole) and short-range (pairing) nucleon-nucleon interactions. The first of these has been generally treated by incorporating the major portion of the quadrupole force into an ellipsoidal binding field, while the pairing interaction has been successfully described, as we saw earlier, by the BCS superconductivity theory applied to nuclei. Thus the picture has evolved of the nucleons moving in a deformed, axially symmetric potential and exhibiting certain properties analogous to those associated with superconducting systems of particles.

There remain, however, residual quadrupole and pairing interactions which have been used to explain a number of the properties of low-lying nuclear energy levels in deformed nuclei. The earliest descriptions of the collective β- and γ-vibrations (and also rotations) were carried out assuming an adiabatic separation of particle and collective nuclear motion. In particular, the collective nuclear motions were first treated by Bohr and Mottelson in terms of a classical vibrating, rotating liquid drop model. The collective and the single particle models were treated as essentially separate entities in this

early picture, although it was certainly known that they were intimately related.

It has thus been common to treat the residual quadrupole interactions as perturbations caused by slow fluctuations in the shape of the average nuclear quadrupole field. More recently, however, after the development of the superconductive theory of nuclear pairing interactions, the method of variations, now commonly referred to (for the nuclear problem) as the quasi-boson approximation has been applied to describe the collective nuclear vibrations in a kind of nuclear Hartree-Fock treatment.

A number of authors have investigated the problem of the β-vibrational states in deformed nuclei; we refer the interested reader to the work of Marshalek,[125] Bes,[51] and Soloviev,[126] and references cited therein. The most recent investigations have primarily been concerned with the effects of the non-adiabatic couplings of collective and intrinsic nuclear motion, and of vibrational and rotational collective modes. The presumed interaction of the β- and γ-vibrational states with the ground state of deformed nuclei and their consequent contribution to the familiar B coefficient of the second-order term in the rotational energy expansion

$$E_I = \frac{\hbar^2}{2\mathcal{J}} I(I+1) + BI^2(I+1)^2 + \ldots$$

has recently been discussed by Pavlichenkov,[127] Bes, et al.,[52] and Marshalek.[128] References 127 and 128 contain predicted numerical values for the z_0 parameters thought to describe the mixing of the ground and

β-vibrational bands, and Ref. 52 predicts similarly the z_2 parameters for γ-vibrations.

Thus, the more refined treatments of the quadrupole and pairing interactions have proved quite successful in explaining a large number of nuclear properties, such as trends in deformation, odd-even mass differences, observed trends in momenta of inertia, energy gaps in intrinsic spectra of even-even nuclei, etc. However, it was suggested by Bohr and Mottelson[129] that, in a manner exactly analogous to the way in which fluctuations in the average quadrupole field of the nucleus give rise to the β-vibrational excitations, so also can similar fluctuations in the average pairing field give rise to other collective excitations, now commonly referred to as pairing vibrations. Instead of a distortion in the shape of the nucleus, a distortion in the superconducting property of the nucleus can be considered to occur. This distortion is registered by fluctuations in the energy gap, Δ. Whereas the β-vibrations are interpreted as arising from changes in the average quadrupole moment of the nucleus, the pairing vibrations are associated with variations in the "diffuseness" of the Fermi surface, or alternatively, with the coherent transfer of particles from states below to states above the nuclear Fermi surface. Although the superconducting solutions require that the nucleus have a fixed average number of particles, the non-conservation of the particle number now becomes a fundamental descriptive feature of the nucleus, just as the non-conservation (except on the average) of angular momentum in the deformed field is fundamental to the Nilsson "particle" description of the nucleus. The development of superconducting character in the

nucleus due to pair interactions is found to be exactly analogous to the development of a stable quadrupole shape deformation due to the quadrupole interactions of the nucleons. An excellent discussion of the physical and formal analogies between the pairing- and quadrupole-field vibrations is given by Bes and Broglia in Ref. 130.

Bes and Broglia conclude that a new set of K = 0+ collective excitations may be generated by the superconductivity fluctuations in nuclei. These fluctuations are thought likely to appear as low energy excitations, provided the nucleus is sufficiently close to the transition point between the single-particle (spherical) and superconducting system, and provided there exist at least two well-defined groups of particle levels such that the energy gap separating the two groups is large compared to the energy separation of the particles within each group.

Experimentally, the most effective method for exciting the pairing vibrational modes ought to be by use of the (t,p) reaction. The cross-sections in the rare-earth region for these reactions are predicted to fluctuate rather substantially with the appearance and disappearance of small gaps in the Nilsson single-particle spectrum.

It is of particular interest to our study of ${}_{72}Hf^{176}_{104}$ that a decrease in the single-particle level density has been found experimentally and reported by Burke, et al.[131] in this nucleus. Of parallel interest is the recent extension of Mikoshiba, et al.[103] of the calculations of Bes and Broglia to include the effects of quadrupole field fluctuations on the pairing excitations. The calculations of Mikoshiba include consideration of what are thought to be the most important non-adiabatic couplings,

namely, centrifugal stretching and the Mottelson-Valatin[132] or Coriolis anti-pairing (CAP) effect. The properties of the ten lowest excited K = 0+ states for a number of nuclei in the rare-earth region are investigated, and the contribution of the β- and pairing-vibrations to these states is estimated.

Particularly relevant here are the specific results reported for Hf^{176}. Although for most rare-earth nuclei, the K = 0+ excited states are predicted to be primarily β-vibrational in character, notable exceptions are the predictions for Er^{170}, Yb^{172}, Hf^{176}, and W^{182}. In these cases, the calculations of Mikoshiba et al. indicate that the β-vibrations ought to appear at higher energies than the neutron pairing vibrational states (for the same reasons cited earlier by Bes[130]), and the lowest energy (K = 0+ 0) excitations should have significant pairing-vibrational character. For Gd^{154} and Hf^{178} the results of Ref. 103 indicate that the pairing- and β-vibrational states coincide.

If we assume for the moment that the calculations of Mikoshiba et al. provide an approximately correct description of a significant pairing vibrational contribution to the lowest-lying K = 0+ state in Hf^{176}, then the question arises, how can one distinguish these K = 0+ states from those with predominantly β-vibrational character (other than by (t,p) reactions)? Unfortunately, the answer to this question does not augur favorably for our chances of being able to relate the experimental measurements we possess for Hf^{176} to any kind of pairing-vibration picture at this time. Udagawa[133] has pointed out that the predictions for γ-ray branchings from members of a state postulated to

be strongly pairing-vibrational in nature are not significantly different from the predictions of Bohr and Mottelson for branching from β-vibrational states. One might speculate that the pairing vibrations ought to give a smaller contribution to E0 matrix elements since they presumably provide for monopole (volume-change) processes primarily when the pairing excitations involve orbitals from oscillator shells with appreciably different nuclear volumes. But our data simply do not allow us to draw any definite conclusions regarding the possible pairing-vibrational nature of the K = 0+ states in Hf^{176}.

We can make some observations based on the Hf^{176} data, however:

1) Mikoshiba et al. predict that the first three K = 0+ excited states in Hf^{176} should lie at about 1400, 1550, and 1700 keV. We shall include their energy level predictions in a later table along with other theoretical calculations for Hf^{176}. For now, it is important to note that the first and third of these states are predicted to be predominantly composed of neutron pairing vibration. The second (presumably the β-vibrational state, in this picture) is calculated to be somewhat more β-vibrational than pairing-vibrational in nature, and to carry a large fraction (perhaps 40%) of the "collectivity" of the β-vibration.

2) We observe in Hf^{176} K = 0+ excited states at 1150 and 1293 keV, considerably lower in energy than the above theoretical values would indicate. However, the state at 1150 keV has a transition intensity ratio $\frac{I(E2)}{I(E0)} = 120$, while for the state at 1293 keV the corresponding ratio is only 4 (cf. Table 18).

3) We find only moderate disagreement between the $0+0_2 \rightarrow 2+0_1$ branching from the 1227-keV member of the lower K = 0+ band and the predictions of Alaga (cf. Table 16).

4) The E2/E0 branching from the lower K = 0+ state (1150 keV) in Hf^{176} is in approximate harmony with other experimental data available for the rare-earth nuclei; however the relative weakness of this E0 compared to the 1293-keV E0 is qualitatively consistent with what one might expect of the E2/E0 intensities if the lower state is primarily a pairing vibration and the upper state a quadrupole vibration, that is if one assumes the pairing vibrational mode has a relatively small E0 transition strength.

For the sake of completeness, we also must mention the recent considerations of Belyaev.[134] Here, another mechanism is proposed whereby the pairing fluctuations are seen to result in the formation of two types of 0+ states principally distinguished by their different E0 transition probabilities. The two types of pairing excitations are derived by requiring gauge-invariance of the pairing interaction, and are of opposite time parity. The spectrum of T-even 0+ excitations begins above the pairing gap, 2Δ, and these states are expected to have E0 transitions to ground much weaker than the T-odd 0+ excitations, the lowest of which lies below the two-quasiparticle limit, 2Δ. Though it is difficult to make specific comparisons between experiment and the qualitative calculations of Belyaev, if we assumed the 1150-keV 0+ state to lie below 2Δ (T-odd?) and the 1293-keV state to lie above 2Δ (T-even?) (a rather fine distinction to begin with), then the relative

E0 strengths to ground for the two Hf^{176} 0+ excitations would seem to be at variance with what is expected from Belyaev's preliminary investigation. But we are not, to be sure, able to draw any definite conclusions in this regard on the basis of the limited data we possess for Hf^{176}.

A second rather different contribution toward the interpretation of low-lying K = 0+ states in deformed nuclei has recently come from Pyatov et al.[104] The work of these authors seems to provide a more plausible explanation for the disparate characteristics of the two K = 0+ states in Hf^{176}.

It is suggested in Ref. 104 that the spin-quadrupole interactions, though relatively unimportant in spherical nuclei, become very effective in regions of permanent nuclear deformation and lead to significant qualitative changes in the behavior of collective excitations in such nuclei. They may, it is thought, give rise to secondary K = 0+ and K = 2+ collective states at energies below the two-quasiparticle excitations. The proposed effect basically results from the fact that spin-quadrupole forces manifest themselves primarily between shells, whereas the quadrupole-quadrupole interactions are very important within shells. Since the degeneracies of the subshells are split in deformed nuclei and the single-particle levels are only doubly-degenerate, the spin-quadrupole interaction is thought likely to become quite significant in such nuclei. Inclusion of the spin-quadrupole interactions can substantially reduce the predicted electric quadrupole transition probabilities from the second excited 0+ states and generally, for nuclei well within the region of deformation, will favor creation of relatively long-lived 0+ states at energies of the order $\approx$ 1 MeV. Accordingly, if there were

no mixing between the spin-quadrupole and the quadrupole-quadrupole interactions, two distinct types of collective excitations with different decay characteristics would be expected. However, mixing between the two modes does occur, and is thought likely to vary significantly within the region of deformation, and perhaps even from nucleus to nucleus. This is because of the great sensitivity of the spin-quadrupole interaction constant to the details of the average single-particle field levels.[104]

Pyatov and co-authors conclude that it is necessary to consider both spin-quadrupole and quadrupole-quadrupole interactions to explain the observed low-lying 0+ excitations in deformed even-even nuclei, and they present results of their theoretical calculations for the energies, reduced electric quadrupole transition strengths, and wave functions of the low-lying 0+ states in nuclei with mass 150 - 174. Unfortunately, they do not, then, provide explicit results for Hf^{176}, so we are unable to make a direct comparison between their theoretical predictions and our experimental data. Nevertheless, it is significant that we do observe in Hf^{176} two K = 0+ excitations at or below the Fermi surface, and the decay characteristics of the two states are indeed markedly different. Moreover, the relative E0/E2 branching from the 1150- and 1293-keV 0+ states observed is in qualitative agreement with that predicted by Pyatov, et al., if we assume the lower-energy state to be predominantly quadrupole, and the upper state to be strongly influenced by the spin-quadrupole interaction. The anomalous branching of the upper state would in this picture be seen to arise from a retardation

of the E2 de-excitation mode, rather than from an enhancement of the E0 mode, i.e. the 1293-keV 0+ state would be expected to have a longer lifetime than the 0+ state at 1150 keV. We ought also to point out that the tentative (K = 0+2) assignment for the state at 1379.4 keV now becomes of even greater importance since significant E2 retardation (perhaps as much as an order of magnitude) may be expected to result in the anomalous branching we apparently observe. It is thus conceivable that the 2+ member of this higher-lying band may have a very large M1 component, a possibility that warrants further investigation. Moreover, confirmation of the 1379.4-keV state as ($K = 0_3+2$) would provide strong evidence for the collectivity of the second 0+ excited state, since the moment of inertia would then be nearly identical to that of the ground band. We conclude that the Hf^{176} data may provide tentative confirmation of the predicted strength of the spin-quadrupole interactions in deformed nuclei.

It is clear that much more detailed systematics of the K = 0+ excitations in rare-earth nuclei are needed to clarify both the nature of the collectivity of these states, and the multipole composition of radiative transitions between the ground and excited K = 0+ band members. The Hf^{176} nucleus offers a most interesting case for further study, because of the appearance, 150 keV apart, of two low-lying K = 0+ states exhibiting such markedly different characteristics. Whether the one state is predominantly pairing-vibrational in nature and the other essentially a quadrupole vibration, or whether, as we think more likely, the state at 1293-keV is longer-lived and is identified by retarded

E2 strengths as being strongly influenced by spin-quadrupole interactions remains to be seen. But this latter possibility is exciting enough to warrant immediate further study of the low-lying 0+ levels in Hf^{176}.

2. Comparison of the known Hf^{176} levels with theory

Because of the uncertainty associated with the majority of the Hf^{176} spin assignments, in the hope that more definitive data (perhaps in the form of careful γ-γ and e^--γ angular correlation studies) will become available at a later date, we shall at this point quickly summarize the Hf^{176} levels for which we have been able to make definite spin and parity assignments, and compare the experimental data with several extant theoretical calculations. In Fig. 42 we show the relevant experimental and theoretical data. The most recent of the calculations shown are those of Malov and Soloviev,[135] and in general their calculations for the first excited states of indicated $I\pi K$ appear to be in good agreement with experiment. We have not been able to identify the 1-1 level predicted to lie at ≈ 1.4 MeV, but we find at least probable experimental counterparts to all of the other indicated theoretical states. The 2+2 state predicted at 1700 keV could be either of the 1672.5- or the 1704.7-keV experimental levels we tentatively assign as 2+, but we also observe a likely 2+2 state at the somewhat unexpectedly low energy, 1341 keV. The calculations of Malov and Soloviev were carried out using single particle energies and wave functions from a Saxon-Woods potential for A = 181. The results obtained using these energies and wave-functions are reported to generally be in better agreement with experiment than the earlier results of Soloviev.[61]

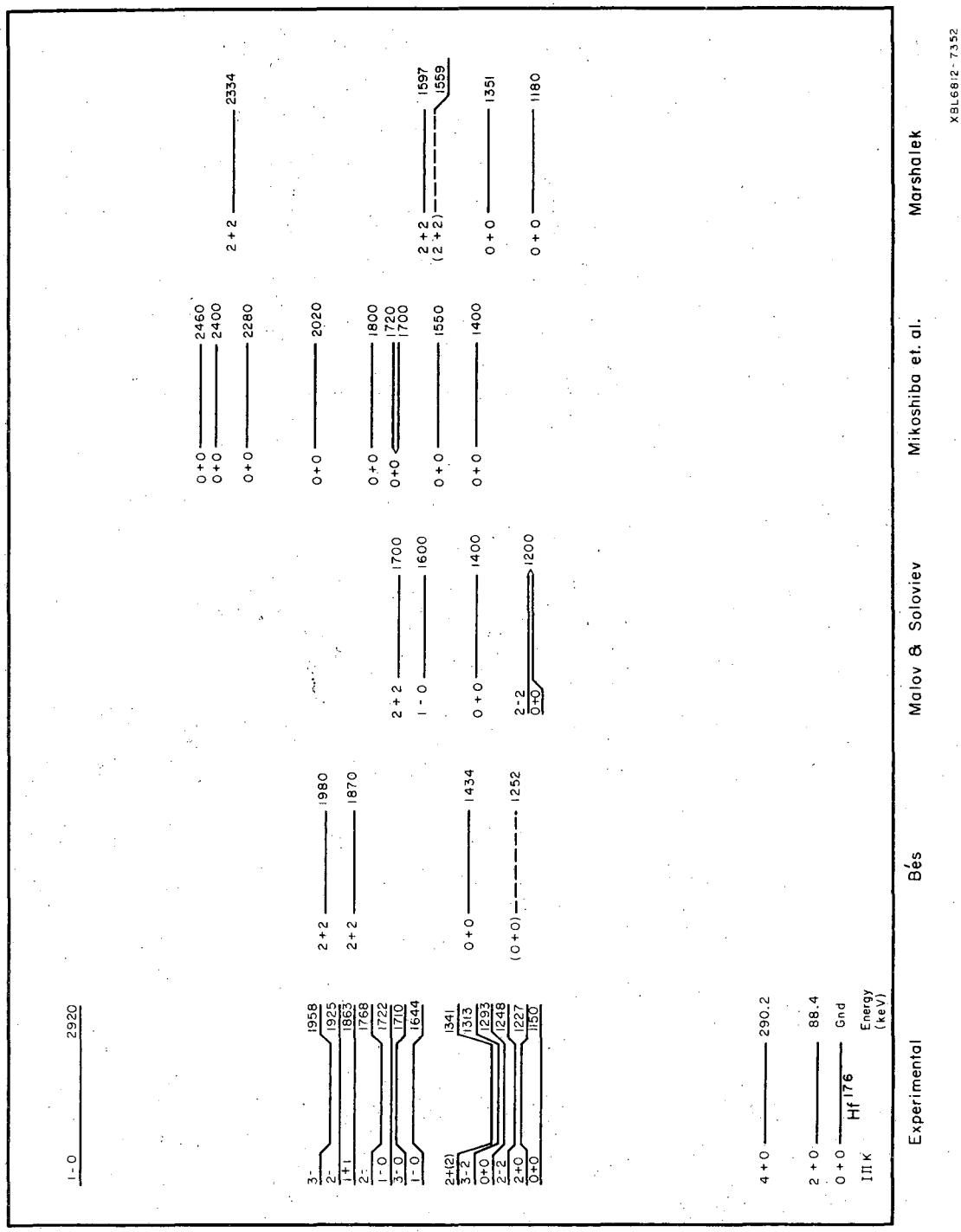

Fig. 42. Comparison of Hf^{176} experimental levels with theory from Bes,[51,52] Malov and Soloviev,[135] Mikoshiba, et al.,[103] and Marshalek.[125]

The calculations of Bes[51,52] for the β- and γ-vibrational states are not very recent, and they did not include the non-adiabatic effects that the most recent calculations of this type include; nevertheless, Bes' prediction for the location of the β-vibrational state seems very good, if we can assume the experimental 0+ level at 1293 keV represents the β-vibration of Hf^{176}. As we mentioned above, we are uncertain of the location of the γ-vibrations in Hf^{176}. The solid lines in Fig. 42 indicate Bes' calculations for deformation $\delta = 0.25$, while the single dashed β-vibrational level is calculated for $\delta = 0.30$. The deformation of Hf^{176} is thought to lie between these limits.[52]

We have already discussed at some length the recent calculations of Mikoshiba et al. for the excited K = 0+ states. We reproduce here all ten of the states indicated in Ref. 103.

Lastly we have included for completeness the early results of Marshalek[125] which, although obtained with a pure harmonic oscillator potential and Nilsson asymptotic wave functions, nevertheless appear to show good agreement with experiment for Hf^{176}. Unfortunately, however, the effects of the so-called spurious states (zero-energy K = 0+ roots corresponding to each of the three rotational degrees of freedom) that arise from the quasi-boson treatment of the quadrupole force were not considered in Ref. 125, therefore the results for the K = 0+ states should be considered as only of qualitative interest.

The results shown are those obtained by Marshalek from solutions of a dispersion equation similar to that usually associated with the random phase approximation, but in this case deduced using a generalized

version of the Inglis "cranking model". Two sets of solutions (both assuming deformation $\epsilon = 0.24$) were reported corresponding to slightly different single-particle energy shifts. For Hf^{176} the two results do not differ significantly, except for the predicted location of the K = 2+ γ-vibration state, for which we have indicated both solutions.

For the K = 0+ and the K = 2+ excitations, the higher lying state corresponds to the predicted first intrinsic state. For the 0+ state, this implies excitation of a pair of nucleons above the Fermi surface, an excitation that may be viewed as an elementary pairing vibration of the type discussed earlier. It is interesting that, in spite of the assumptions used to obtain these results, the predicted energies of the two 0+ states are in remarkably good agreement with experiment. Moreover, in this case the lower of the two states predicted represents the β-vibration, and corresponds most closely to the "well-behaved" K = 0+ state we observe at 1150 keV. The upper (intrinsic) 0+ excitation, presumably lies approximately at an excitation corresponding to the energy gap 2Δ, and could represent the notorious K = 0+ state we observe, with all its apparent anomalies, at 1293 keV.

F. Proposed Further Study

One needs only to glance at Table 13 and Fig. 34 to arrive at the inescapable conclusion that much work remains to be done on the decay of Ta^{176}. The spectre of some 200 γ-rays listed as unassigned is perhaps awesome, but we suspect that many years will pass before the last of those transitions is properly placed in the Hf^{176} level scheme.

The task of assigning unambiguous spins and parities to each of the levels in Fig. 34, though it might seem hopeless at first thought, is nevertheless not only feasible but for the most part practical with the on-line multiparameter data acquisition system (and others like it elsewhere) described in this paper. And since it is essential to the purpose of establishing detailed nuclear systematics that this phase of the work be completed, we would like to dwell on this topic at least briefly.

The short (8 hours) half-life of Ta^{176} renders a complete high-resolution electron spectroscopic study of the decay an extremely impractical if not impossible proposition in view of the single-channel limitation on the momentum scan of the best magnetic electron spectrometers now in use. And if the determination of transition multipolarity by measurement of internal conversion coefficients must thus be discarded as an unworkable option, there remains only the method of directional correlations as a means of attacking the problem.

Yamazaki and Hollander[136] designed and built at LRL as early as 1965 an apparatus whose purpose was to allow the simultaneous, multi-channel, semi-automated acquisition of e^--γ and γ-γ angular

correlation data. The device consisted of a fixed Si(Li) detector for use as an electron spectrometer, a fixed Ge(Li) detector for use as a γ-ray spectrometer, and a 2" dia. by 2" NaI(Tl) spectrometer on a movable mount for use as the second γ-ray spectrometer. The NaI(Tl) spectrometer was to be eventually replaced by an array of four large-volume Ge(Li) detectors. Unfortunately, a severe practical limitation on the usefulness of this elegantly conceived device was imposed by the strictly "hard-wired" data recovery systems available at that time for extracting the information the apparatus was capable of producing. Two sets of 10 single-channel analyzers were employed to set the desired electron and γ-ray pulse-height windows. The singles counts and two-dimensional coincidence counts for each of the four angular positions of the NaI(Tl) detector were stored in a 400-channel analyzer--a total of 10 × 10 × 4 bits of information for each scan!

The results from the multiparameter experiments we have carried out on the Ta^{176} decay indicate conclusively that, with the on-line computer systems now in operation, the serious data-recovery limitations on such a directional-correlation device have been removed. The apparatus of Yamazaki and Hollander, coupled with the 8-parameter analysis capability of the system in Figs. 21 could, in a single run of duration comparable to the 36 hours we required to accumulate γ-γ coincidence data alone, yield the entire $4096^6 \times 512 \times 512$ matrix of information describing in detail <u>all</u> of the e^--γ and γ-γ coincidences and their respective angular correlations and timing distributions. That such an experiment is now feasible goes without question. The statistical quality of the data

that could be expected can be judged to some extent by simply considering the conversion electron and γ-γ coincidence data we have obtained for Ta^{176}.

However, since in angular correlation work one often wishes to measure accurately anisotropies of 10% or less, correlation data ought ideally to have a precision of the order 1%. Then the calibration of the correlation apparatus becomes crucially important. Although many of the electronic problems with regard to stability, resolving time, etc. are substantially reduced by the digital time and energy analysis made possible by the computerized multiparameter system, nevertheless certain of the old problems familiar to experimenters performing angular correlation measurements remain. Potentially the most limiting of these problems is perhaps that of determining the solid angle attenuation factor of the counters. The design of the correlation apparatus must be optimized by considering two factors: 1) the true-to-random coincidence ratio and 2) the accuracy with which solid-angle corrections can be determined, and thereby the extent to which the ideal point-detector information can be approximated by correcting the raw data. Needless to say, if (1) is optimized by placing the detectors in the closest possible geometry, (2) suffers, and the anisotropies may be "washed out" entirely. On the other hand, if (2) is favored by separating the detectors, then the random coincidence rate will be increased substantially, and the statistics of the coincidence data will suffer because of the large corrections for random events that will be necessary.

In practice then, the quality of the angular correlation data finally depends to a large degree upon the accurate determination of the solid angle correction factor for the detectors. For this reason, it must be carefully considered whether the factor-of-N decrease in time required to accumulate data with an array of N detectors is worth the manifold increase in problems that would be associated with trying to determine unique solid-angle and photopeak efficiency characteristics for each of the N detectors. Naturally, the argument in favor of the N-detector array is that it would facilitate the study of isotopes with half-life 1/N times the half-life that could be meaningfully studied with a single movable detector.

Assuming that the experimental problems are surmountable (and they are) then the procedure that would in principle allow one to uniquely determine the spins and parities of nearly all the Hf^{176} states indicated in Fig. 34 is clear. The usual expression

$$W(\Theta) = \sum_{K=0}^{K_{max}} A'_{2K} P_{2K} (\cos \Theta)$$

for the angular distribution of a γ-γ cascade of pure multipolarity is generally expanded to the fourth-order term

$$W(\Theta) = 1 + A_{22} \cos^2\Theta + A_{44} \cos^4\Theta \qquad (42)$$

where the A_{22} and A_{44} now are normalized coefficients so that $A_{00} = 1$.

This is sufficient to describe all of the radiations for which angular correlations have to date been measured. If one of the radiations is of mixed multipolarity, then the simple expression (38) becomes more complicated, and the $E\lambda$-$M(\lambda+1)$ or $M\lambda$-$E(\lambda+1)$ mixing ratio δ must be determined, where δ is the ratio of the reduced matrix elements for the two multipole transitions $I_1 \xrightarrow{\lambda_1} I_2$, $I_1 \xrightarrow{\lambda_2} I_2$. This mixing ratio can normally be uniquely determined if only one of the correlated γ-rays is mixed (cf. e.g. the discussion of Frauenfelder and Steffen in Ref. 137 and references cited therein). The additional information necessary for determining spins and parities is obtainable from the conversion coefficient measurements, and, more importantly, from the e^--γ angular correlations. For e^--γ correlations, (38) becomes

$$W_{e^-\text{-}\gamma}(\Theta) = 1 + b_{22}\, A_{22} \cos^2\Theta + b_{44}\, A_{44} \cos^4\Theta \qquad (43)$$

where the so-called particle parameters, b_{22} and b_{44} are the coefficients expressing the dependence of the correlation on the same factors that influence the internal-conversion process. Hager and Seltzer[98] have also calculated and tabulated the particle parameters b_{2K} for K, L, and M shell conversion.

It now is possible to outline exactly what information could be expected from e^--γ and γ-γ angular correlation studies of Ta^{176} decay. In the most general case, the expression (38) depends on seven parameters: I_1, λ_1, δ_1, I_2, λ_2, δ_2, and I_3. It is usually safe to assume, and in

particular for Hf^{176} it is certainly safe to assume (except in the few cases for which E0-M1-E2 mixtures occur) that the quantity λ in the ratio of dipole to quadrupole reduced matrix elements

$$\delta = \frac{\langle f \| \lambda+1 \| i \rangle}{\langle f \| \lambda \| i \rangle} \quad .$$

is always 1, i.e. that quadrupole is the highest multipolarity radiation present. This reduces to five the number of unknown quantities in the general case. If we know I_2 and I_3 (as we would in nearly every case for Ta^{176}), and if we can select λ_2 to be a pure transition of known multipolarity (as we can in most cases), and if further the A_{22} and A_{44} parameters are then determined experimentally, knowledge of these five quantities in principle allows us to uniquely determine the unknown quantity of interest, namely δ_1. In Hf^{176} the pure E2 ground-band transitions would thus provide a useful starting point by providing δ for a number of the stronger transitions feeding the 2+ and 4+ ground-band states.

Now in contradistinction to γ-γ correlations, e^--γ correlations depend not only on the multipolarities of the radiations involved, but also on the parity changes of the converted transitions. Therefore the final bit of information necessary to the unique determination of spins and parities is provided by the e^--γ correlation data--provided δ_1 can be obtained from the γ-γ correlations.

To balance the argument, however, in more gloomy and realistic terms, the complexity of the Ta^{176} spectrum ought to be recalled. There

is little doubt that in many critically important cases the presence of a near-lying line might seriously compromise the results one could in theory expect to obtain for every strong line in the spectrum. Nevertheless, the prospects for the measurements proposed above being carried out simultaneously literally by the score are indeed now excellent.

G. Summary and Conclusions

Considering the plethora of data we have just presented, it seems desirable to recap briefly the results of this work. Of some 350 transitions that we have observed to be associated with the decay of Ta^{176}, about 140 have, on the basis of coincidence data, been placed with relative certainty in the proposed Hf^{176} level scheme (Fig. 34). Approximately 90 additional transitions have been tentatively placed (Fig. 35) on the basis of energy sums and differences, though coincidence data are not sufficient to confirm (or refute) these assignments. The level scheme for Hf^{176} deduced from the data consists of nearly 50 energy states, for which the spins and parities of 14 (in addition to the ground rotational band members) have been definitely established. There is reason to believe, as we have shown in the previous section, that most of the remaining levels could be assigned appropriate quantum numbers if the proposed angular correlation experiments were carried out.

Perhaps the most interesting feature of the level scheme, at least for contemporary nuclear theory, is the presence of the two low-energy K = 0+ excitations at 1150 and 1293 keV, both ostensibly "collective", but each displaying distinctly different decay characteristics. Further work to elucidate the nature of these states is certainly called for.

In conclusion, it seems that by exploiting fully the precision inherent to carefully controlled studies of natural radioactivity, finely detailed second-order systematics of nuclear properties can now be obtained simply and quickly by using the many advantages and capabilities

of the on-line computer for data acquisition and analysis. In this section, we hopefully have not just deduced in a considerably more efficient way some properties of the nucleus Hf^{176}, but have also shown the form if not the substance of the remarkably complete information on nuclear structure that contemporary spectroscopic studies should provide.

ACKNOWLEDGMENTS

There must literally be scores of persons who have contributed toward the successful conclusion of this work. We mention here several of those to whom special thanks are due:

We are deeply indebted to Drs. Joseph M. Jaklevic, A. Judd Haverfield, Stanley G. Prussin, C. Michael Lederer, and to the many others who have been associated with the spectroscopy group, and particularly to Dr. Jack M. Hollander under whose guidance much of this work has been carried out.

To Dr. David C. Camp we are grateful for assistance in obtaining several spectra with the anti-Compton spectrometer at Livermore, and for many stimulating discussions.

We also wish to acknowledge the major contribution of Drs. Lloyd B. Robinson and Fred S. Goulding and their associates in designing, building, programming, and maintaining the PDP-7 data system, without which the latter half of this work would not have been possible. The advice and assistance of Don A. Landis and the several members of the Chemistry Technical Support Group is also gratefully acknowledged. The timely comments and assistance of Mich Nakamura and Dr. Emmanuel Elad have been of particular importance to certain phases of this work.

Special thanks must go to Dr. Richard H. Pehl for his continuing interest and helpful comments, and to the other members of the Semiconductor Instrumentation Group for their constant support and cooperation in providing us with "state-of-the-art" semiconductor detection systems, and for enduring our ceaseless badgering for the past two years.

The data-analysis phase of this work would perhaps never have been completed without the sustained "extra-curricular" effort Mr. Jorma T. Routti put forth in developing the 6600 computer code for on-line spectral analysis, while himself working on his doctoral thesis.

To Mrs. Ruth-Mary Larimer we proffer our thanks for her tireless juggling of cyclotron schedules and exceptional diplomatic skills that so often produced our targets on such short notice and under the most trying circumstances.

We also wish to note our most enjoyable and, intellectually if not pecuniarily most profitable association with Drs. Rand Watson, John Cooper, and Arnold Gilbert, and Messrs. Jerry Wilhelmy, Jim Lamb, and Marty Holtz.

The largest measure of thanks, however, we owe to Prof. John O. Rasmussen under whose direction this work was carried out. His patient advice, unflagging enthusiasm, and genuine humanity have been a constant source of professional and personal inspiration throughout the course of our graduate study.

And finally, we affectionately thank Miss Judy Holzhauer for contributing in her gentle way the unfailing confidence and support that have meant so much during the past 1000 days, and also our parents for providing through the years the Gift of Freedom we again celebrate this

Christmas Day 1968

APPENDIX A

Precision Spectroscopy of Lu^{177m} Decay

In the high-resolution γ-ray spectroscopic study of Lu^{177m} decay by Haverfield, et al.,[20] the authors reported 12 of the 16 $\Delta K = -1$ E1 transitions presumably arising from this decay. A simple analysis of the data at that time revealed the likelihood that two more of the E1 transitions of interest could be observed and their intensities measured by using somewhat better detection systems. Because of the importance of obtaining precise experimental information for as many of these transitions as possible, we expended considerable effort in an attempt to obtain the best possible measurements for the relative intensities of the E1's accompanying the decay of the unique nucleus, Lu^{177m} to Hf^{177}.

Samples of 161-d Lu^{177m} were prepared by neutron irradiation of natural Lu_2O_3 powder. The samples were allowed to decay for six months to insure the absence of 6.8 d. Lu^{177}. The Lu_2O_3 powder was then dissolved in 3N HCl and the Lu activity was separated by ion exchange using α-hydroxy-isobutyric acid as the eluant for a room-temperature Dowex 50W-X4 resin column. The procedure for the chemical separation is described in Ref. 138.

Singles spectra of Lu^{177m} decay were taken using the Ge(Li) Compton-suppression spectrometer at Livermore (resolution 1.1 keV at 122 keV) and a 1-cm^3 high resolution (0.77 keV at 122 keV) Ge(Li) crystal in our own laboratory. The latter spectrometer was carefully

calibrated using absolute γ-ray standards and Hf^{180m} as a relative intensity standard. In Fig. 43 we reproduce the efficiency curve for this 1-cm^3 "thin window" device. We are confident that the curve is accurate to ≈ 3% in the region of interest (75 - 500 keV).

In Fig. 44 we display a portion of the Lu^{177m} γ-ray spectrum taken with the anti-Compton device. The favorable peak-to-background ratio obtainable with this device has enabled us to identify the 242.5-keV M1 - E2 cascade transition leading from the 21/2 to the 19/2 spin level of the K = 7/2- band. More importantly, Fig. 45 shows the observed 88.4-keV E1 transition leading between the spin 19/2 members of the two Hf^{177} rotational bands.

The high-resolution spectra taken with the 1-cm^3 crystal have facilitated the confirmation of the 69.2-keV E1 transition tentatively assigned earlier[20] and have allowed more accurate measurement of relative intensities for several of the previously reported weak E1 transitions. In Fig. 46 we show the linear plot for the 69.2-keV line. Figures 47 show two particularly interesting regions of the Lu^{177m} high-resolution spectrum. The 117.2-and 145.8-keV E1 transitions seen earlier[20] as only poorly defined shoulders on the 116.0-and 147.2-keV lines are now resolved. The second partial spectrum shows that the very weak 283.4-keV E1 is nearly resolved from the 281.8-keV photopeak, and the E1 doublet at 292 keV now clearly shows the 292.5-keV line to be weaker than the 291.4-keV E1.

The experimental results representing our "best values" for the Hf^{177} E1 transition intensities have been derived from a number of independent measurements and are shown in Table 8. Deduction of the

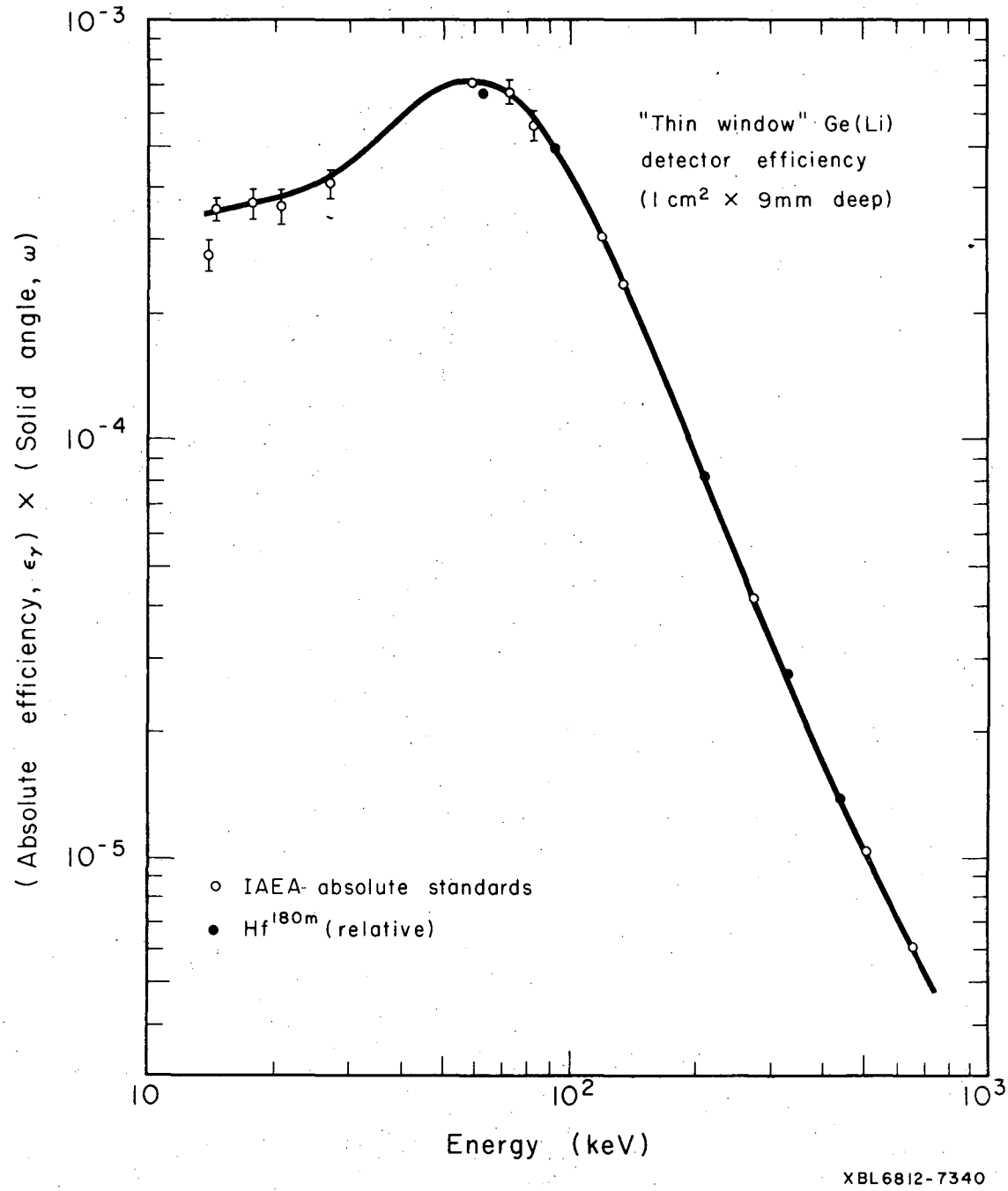

Fig. 43. Absolute photopeak efficiency vs. γ-ray energy for the 1-cm^3 "thin-window" Ge(Li) detector.

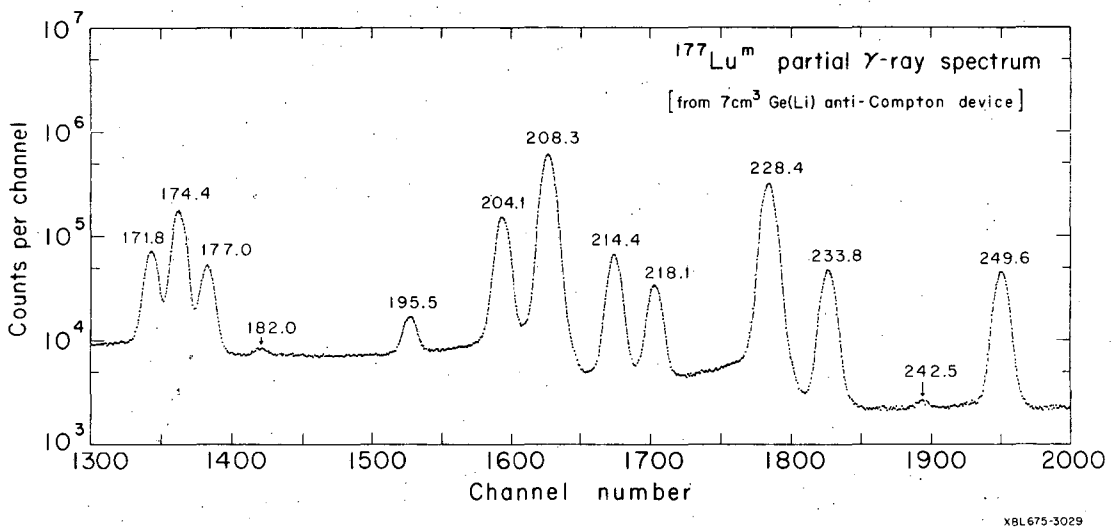

Fig. 44. The Compton-suppressed γ-ray spectrum of Lu^{177m} in the region 170-250 keV showing the location of the 242.5-keV transition.

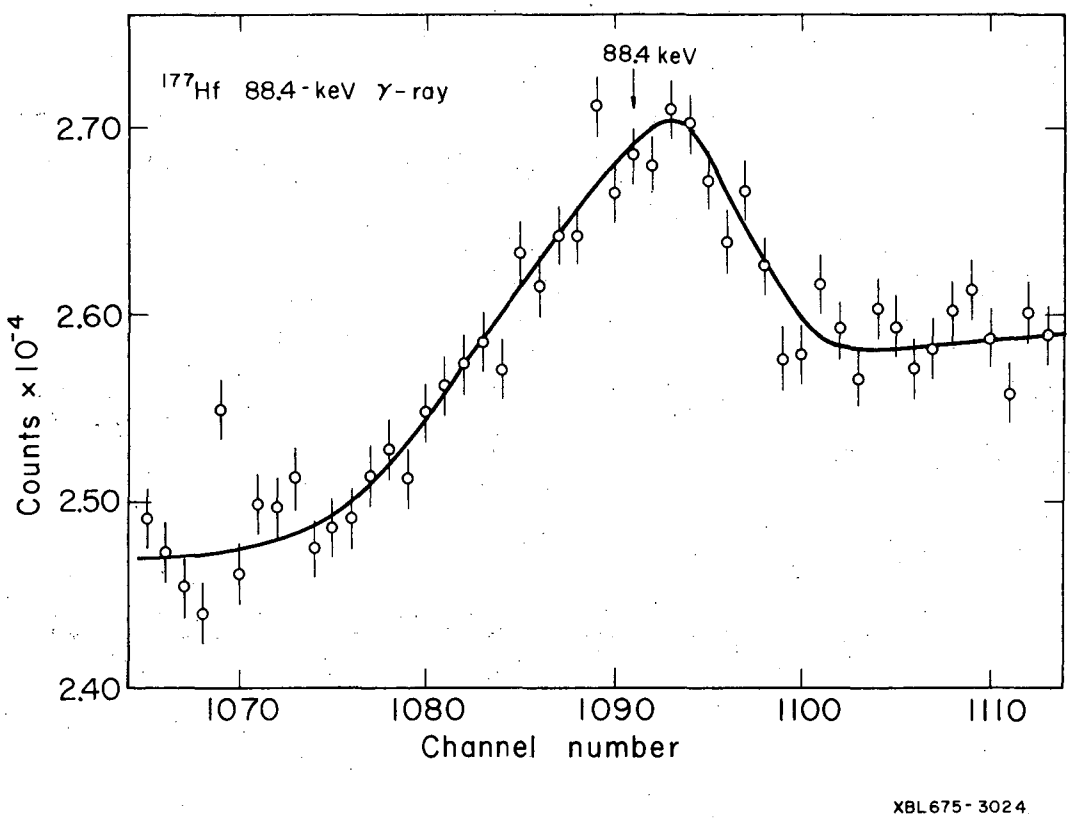

Fig. 45. Linear plot of the 88.4-keV E1 γ-ray from a Compton-suppressed spectrum of Lu^{177m} decay. (scale: 0.080 keV/chan)

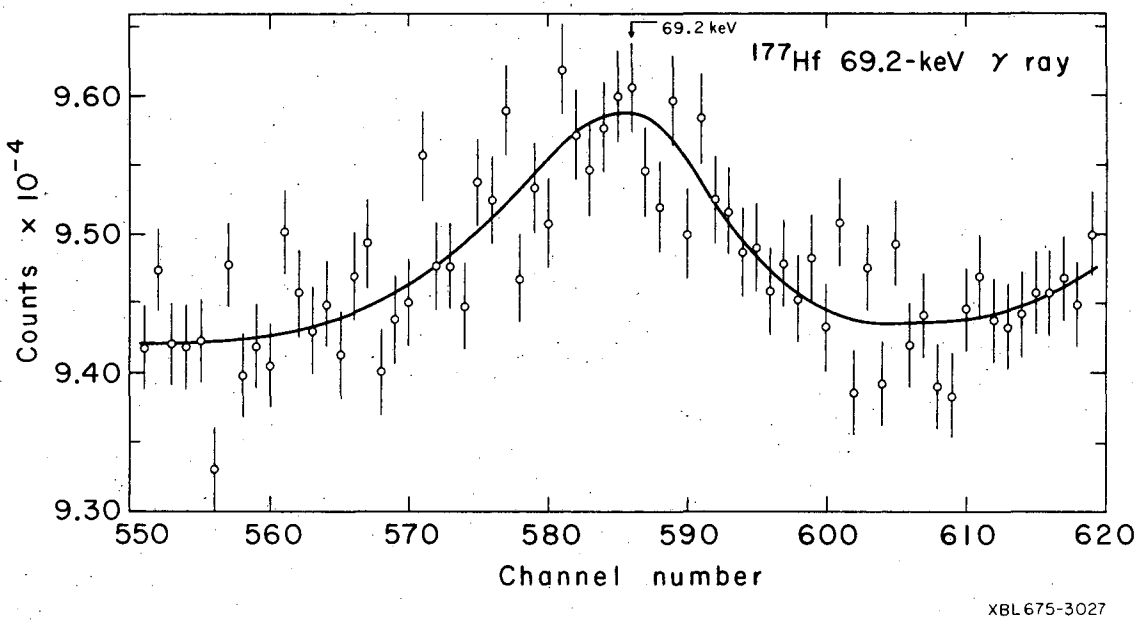

Fig. 46. Linear plot of the 69.2-keV E1 γ-ray from Lu^{177m} decay. (scale: 0.038 keV/chan)

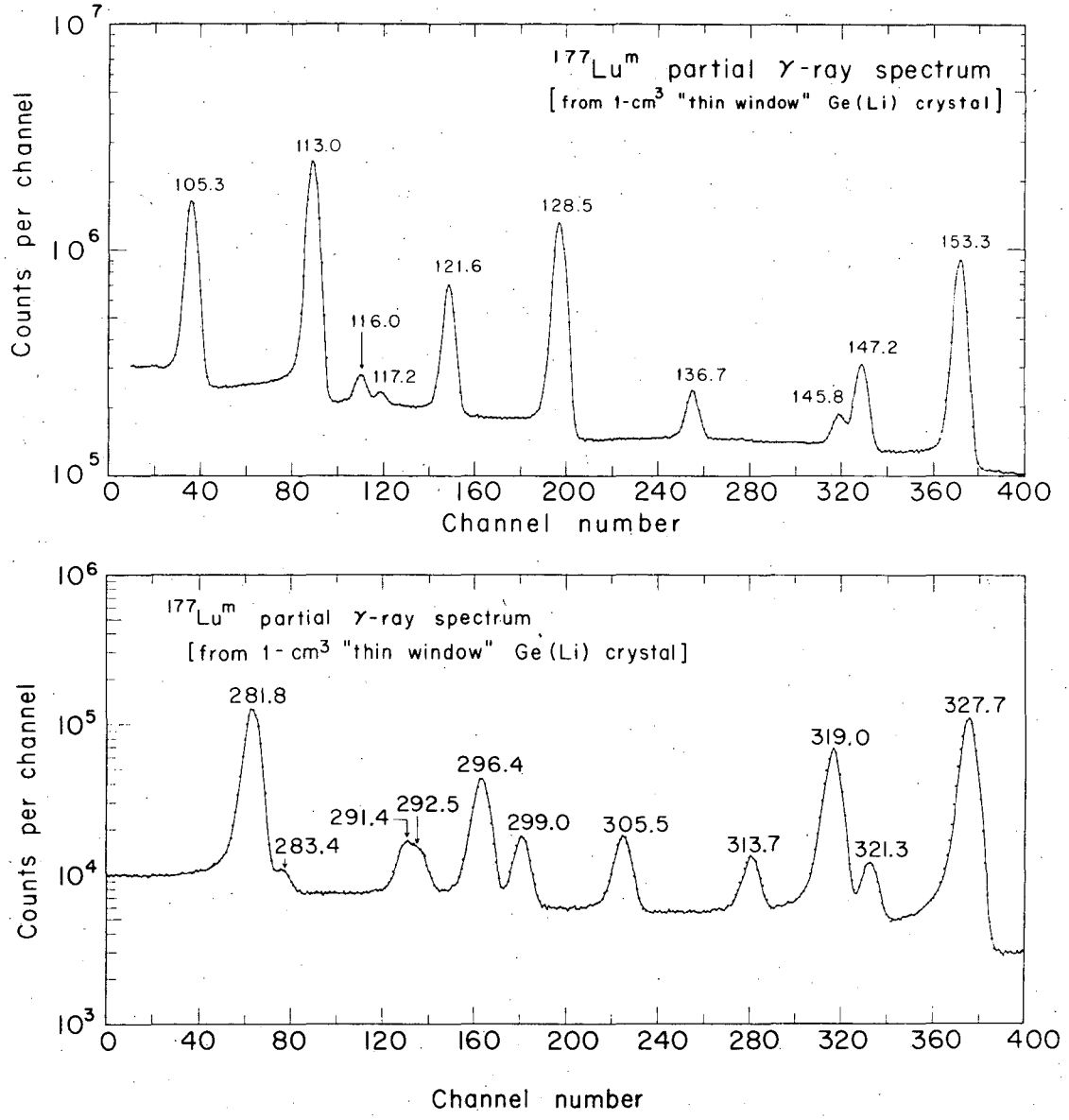

XBL 691-95

Fig. 47. High-resolution γ-ray spectrum of Lu^{177m} in the regions 100-150 and 275-330 keV.

absolute E1 lifetimes from the rotational model also required precise knowledge of the K = 9/2+ intraband transition intensities. The results of these measurements seemed to indicate a small (maximum ≈ 10%) systematic error in the earlier published intensities for the higher energy Lu^{177m} γ-rays.[20] Because of the usefulness of Lu^{177m} as a low-energy relative intensity standard, we feel it worthwhile to compile a corrected list of relative intensities for the most prominent singlet lines in the spectrum. Table 19 shows that listing, together with the new error limits. A word of caution to the user is included as a footnote.

Finally, in connection with this experimental work we had hoped to be able to carry out conversion-electron spectroscopy studies on Lu^{177m} using the iron-free magnetic spectrometer at Berkeley. The feasibility of the experiment depends to a large extent on being able to obtain a strong, "mass-free", line source of Lu^{177m}. The only way to meet these requirements is to produce the source with a high quality isotope separator equipped with a device for ion deceleration at the target position. The paper by Bergstrom, et al.[139] provides an excellent discussion of the method and problems involved in preparing such sources for precision electron spectroscopy.

We planned to use the Berkeley isotope separator to carry out the all-important source-preparation phase of this project, but unfortunately, repeated delays have forced us to abandon the undertaking. However, since one must allow at least six months for the Lu^{177} + $Lu^{177m}(n,\gamma)$-produced activity to decay so that the 6.8 day Lu^{177} fraction has

Table 19. Relative intensities for selected prominent Lu^{177m} γ-rays.

Lu^{177m} Relative Intensities	
Energy (keV)	Intensity†
71.7	7.2 (4)
105.3	100 (4)
113.0	184 (7)
128.5	131 (5)
153.3	144 (6)
204.1	117 (5)
208.3	512 (20)
228.4	310 (12)
281.8	118 (5)
327.7	152 (6)
378.5	240 (10)
413.6	135 (5)
418.5	172 (8)
466.0	20 (1)

†Normalized to 105.3-keV line = 100.

CAUTION: The user should take care that the Lu^{177m} source is sufficiently distant from his detector so that the probability for sum-coincidence events is negligible. For reasons that are obvious from Fig. 6, it is generally not advisable to employ complex relative intensity standards such as Lu^{177m} if calibrations very near the detector surface are desired. The experimenter has only to place the Lu^{177m} standard at ≈ 0 source-to-detector distance and compare the relative intensities of the 413.6- and 418.5-keV lines for this geometry with the intensities for a very small solid angle to convince himself of this fact.

entirely disappeared, the irradiation of 70% enriched Lu^{176} samples had already been carried out before the project was dropped. Therefore we shall report the results of our preliminary work so that the requirements for the experiment will be better defined for possible future work on the problem.

The thermal neutron cross-section for the desired $Lu^{176}(n,\gamma)Lu^{177m}$ reaction has recently been measured by Nethaway and Mendoza to be 7 ± 2 barns.[22] The competing reaction $Lu^{176}(n,\gamma)Lu^{177}$(6.8 d) has a much larger 2100 ± 150 barn cross section.[140] This unfavorable ratio for the production of the desired 161-day isomer becomes an important consideration, the question being whether one can prepare a sample with high enough specific activity to make isotope separation practical. Since the efficiency of the electron spectrometer is roughly 0.1%, source strengths of at least 10 μCi would be required to achieve reasonable counting rates. Fortunately, no Lu^{177m} β^--decays directly to the ground state of either Lu^{177} or Hf^{177}, so all of the decays strengthen the desired conversion electron spectrum. However, the isotope separator can be expected to operate with only about 1% efficiency; therefore, to produce a 10 μCi source of Lu^{177m}, $\approx$ 1 mCi of activity is required.

We have found that, using 70% enriched Lu^{176} samples, this requirement can be just met. Five mg. samples of the enriched $Lu_2{}^{176}O_3$ were irradiated for 9 days with a thermal neutron flux $> 10^{15}$ $cm^2 sec^{-1}$ at the Savannah River test reactor. One year after the end of the irradiation, the samples were counted to estimate the Lu^{177m} activity. The total activity at that time was found to be about 5×10^7 disint/sec,

or $\approx$ 1.4 mCi. Satisfactory results were also obtained by irradiating a similar sample for 21 days at the lower flux ($\phi \approx 5 \times 10^{14}$ $cm^{-2}sec^{-1}$) MTR reactor at the Idaho Falls site. Counts on this sample six months after irradiation showed 7×10^{7} disint/sec, or 1.9 mCi Lu^{177m} to be present. These results show that sufficient Lu^{177m} activity was present to prepare the electron sources as planned.

However, it would be desirable to enhance further the Lu^{177m}/Lu^{177} production ratio. The large Lu^{177} cross section arises primarily from a thermal neutron capture resonance at $\sim$ 0.15 eV.[140] Unfortunately, no comparable cross-section vs. energy data are available for Lu^{177m}. We have therefore carried out a simple experiment to see whether the ratio of Lu^{177m} to Lu^{177} production might be enhanced by effectively eliminating the thermal neutron flux in an irradiation.

The procedure used was as follows: Two 50 mg. samples of natural Lu_2O_3 powder were sealed in quartz tubing. One of the quartz tubes was wrapped in 25 mil Cd foil to eliminate the thermal neutron component. The samples were then irradiated for several days in the LRL research reactor at Livermore ($\Phi = 5 \times 10^{13}$ $cm^{-2}sec^{-1}$). The Cd ratio (thermal/epithermal) for the unprotected sample was $\approx$ 7:1, while for the Cd-wrapped sample the effective Cd cutoff energy should have been about 4.5 eV.[141]

The results of this crude experiment indicated that the ratio $\sigma_{177^m}/\sigma_{177}$ was indeed effectively enhanced by about a factor of three for the Cd-wrapped sample, though the production rate of the Lu^{177m} was decreased by a factor of 10. Still, this enhancement may be most welcome to the experimentalist interested in preparing a Lu^{177m} sample for electron

spectroscopy, since the huge 6.8 d Lu^{177} cross-section makes Lu^{176} "burn-up" a major consideration for preparing Lu^{177m} samples of high specific activity. The proposed experiment is certainly feasible, and if carried out would provide an abundance of data of particular importance to nuclear theory.

APPENDIX B

Techniques of Precision Spectroscopy

The extreme complexity of the Ta^{176} decay makes it imperative that one be able to obtain very precise energy measurements for all lines in the spectrum. This in turn requires: 1) highly stable electronics; 2) a consistent and accurate method of photopeak analysis; 3) a way of estimating the departure of the data-taking system from ideal linear response to photon energy; and 4) precise energy calibration standards spanning the region of interest. These requirements are perhaps generally well-recognized, but we suspect that what is not so well appreciated is the difficulty of satisfying all four of the requirements consistently and reproducibly to yield experimental energies within what ought ideally to be only statistical deviation from the calibrated standard values. Consequently, we would like to devote some time to a discussion of the problem, and recount both our attempts to contribute toward its satisfactory solution, and the timely and welcome recent contributions from other quarters.

The prime ingredient essential to producing precision spectroscopic data has already been discussed. We have described in section (II.C.1) the feed-back gain and base-line stabilization control system that we have employed for nearly all of our measurements. The stabilization system has been a comforting bit of insurance during many 48-hour counts, but significant improvements in the long-term stability of the primary pulse amplification and analysis systems have also imparted to the

experimenter a new confidence in the likelihood (as opposed to the possibility) of his system remaining stable during extended measurements. The "weak link" in our feedback stabilization system is still the pulser that must be employed as a stability reference if no strong peaks convenient for the purpose appear in the spectrum, or alternatively, if one wishes to perform an energy calibration before and/or after an extended count of an unknown spectrum. We will discuss this problem further under point 3.

Considering the four points in order, we ought next to recall that until very recently there was appreciable error associated with the presumably simple operation of finding peak centroids. Particularly in the case of complex peaks, hand analysis was a tedious and often inaccurate process, and the assumption of a simple Gaussian peak shape for computer analysis of Ge(Li) spectra was of questionable validity since peak shapes can vary significantly from detector to detector, and small gain shifts may make such a simple routine inconsistent even within a single spectrum.

Then of course there was the related knotty problem of subtracting properly the background to obtain the correct peak area. Haverfield[79] discussed this problem in some detail and pointed out that the "standard" Ge(Li) photopeak has the approximate functional form of a Gaussian with exponential tail. Routti and Prussin[97] have made use of this model and have developed a rather sophisticated FORTRAN IV computer code for the analysis of Ge(Li) γ-ray spectra. We have for some 18 months now made extensive use of the routine, and can report increasing satisfaction with

the consistency and the reliability of the results we are able to obtain with the code. All of our spectra have been analyzed "on-line" to the LRL CDC-6600 computer using this code. A CRT light pen program option allows the user to visually define the peaks to be fitted and the fitting interval, and to immediately inspect the results of the fit for accuracy and statistical precision. In Fig. 48 we display another complex portion of the Ta^{176} singles γ-ray spectrum which has been fitted by the code. The impressive consistency and reliability of the analysis has been described in detail in Ref. 97. Although the method of fitting Ge(Li) photopeaks to a function consisting of a Gaussian with high and low-energy exponential tails has doubtless been tried with varying degrees of success elsewhere, we would like to comment briefly on the philosophy behind the specific method followed in Ref. 97 for the all-important determination of "standard" response functions for each region of a given γ-ray spectrum.

The parameters that ostensibly define the single γ-ray photopeak are: 1) the Gaussian width, 2) the joining distance of the exponential tail on the low energy side, and 3) the joining distance of the exponential on the high energy side of the Gaussian centroid. Experimentally each of these parameters will be variable, even for a single given detection system, as a result of count rate effects and system instability. And certainly it is well known that not only the peak width, but also the tailing characteristics can vary significantly from one detector to another. Consequently, Routti and Prussin have chosen the only possible method for accurately determining the variation with energy of the detector

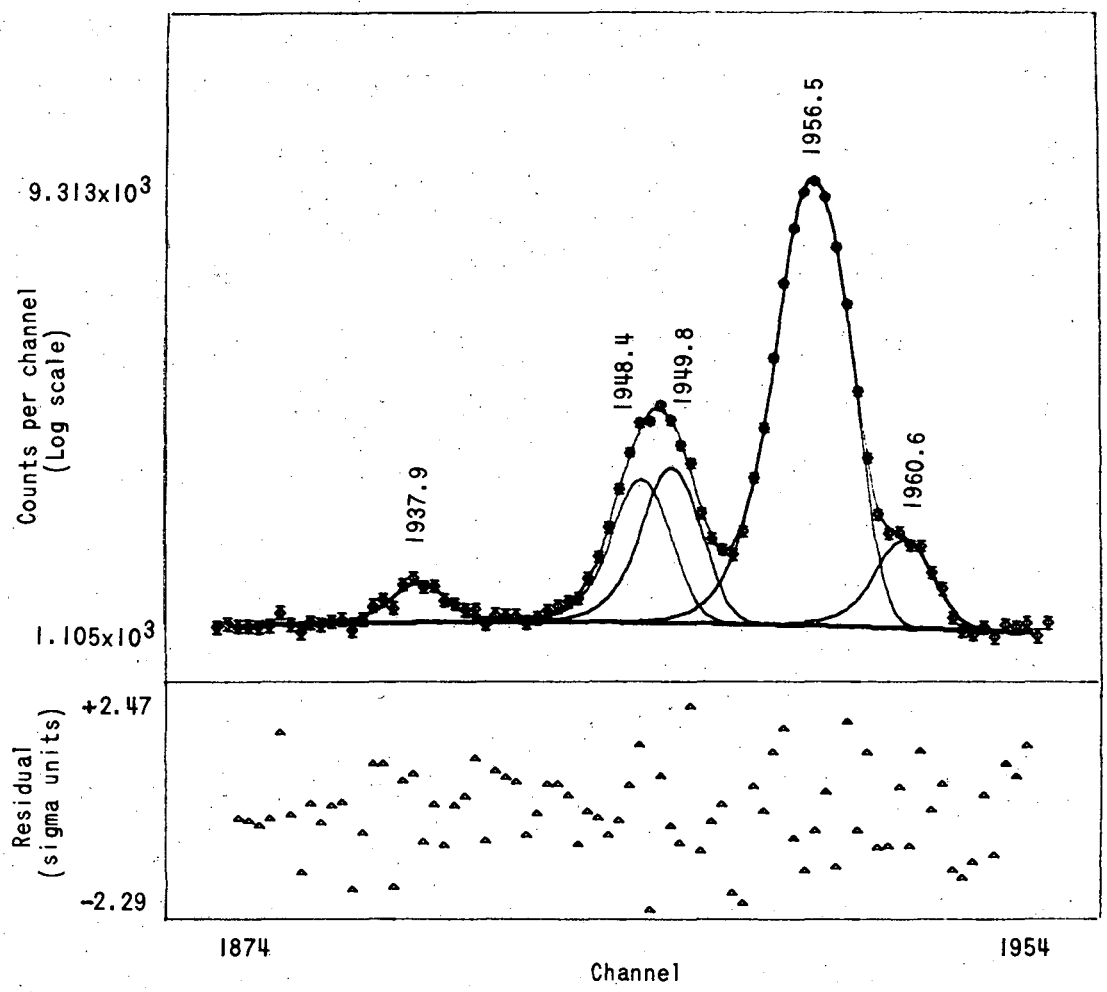

XBL 691-141

Fig. 48. Region of the Ta^{176} γ-ray spectrum around 1950 keV fitted with the spectrum analysis code SAMPO.

response function--direct empirical calibration of "clean" (preferably strong) single lines internal to the spectrum. The resulting parameters (CW, CL, CH) obtained by this method ideally form a series of curves, smoothly-varying with channel number (energy), and providing within the limits of experimental error the exact parameters required to properly fit each line in the spectrum. Plots of the peak shape parameters obtained from functional fits to a number of single lines in one of the Ta^{176} spectra are shown in Figs. 49 and 50. The values CW and CL read from the curves were used to define (by interpolation) the standard peak shapes at each point in the spectrum. (CH is quite large for these data, and is not plotted since it does not significantly affect the analysis.)

The principal advantage (other than speed) afforded by computerized spectral analysis using standard line shapes generated as described above is the mathematical consistency required of each fit. This greatly reduces if it does not eliminate entirely the deviations that necessarily are always introduced by the subjectivity of the "hand" analyst. The old problem of performing properly the background subtraction under a photopeak, a critically important procedure if accurate relative intensities are to be obtained, is substantially solved, if not by accuracy, by consistency. And finally, we have shown in the text of this paper illustrations of the indispensible ability of the computer code to analyze not only multiplets, but to reveal apparent singlets to be multiplets. In summary then, we now feel that we indeed do possess a reasonably consistent and accurate method of photopeak analysis.

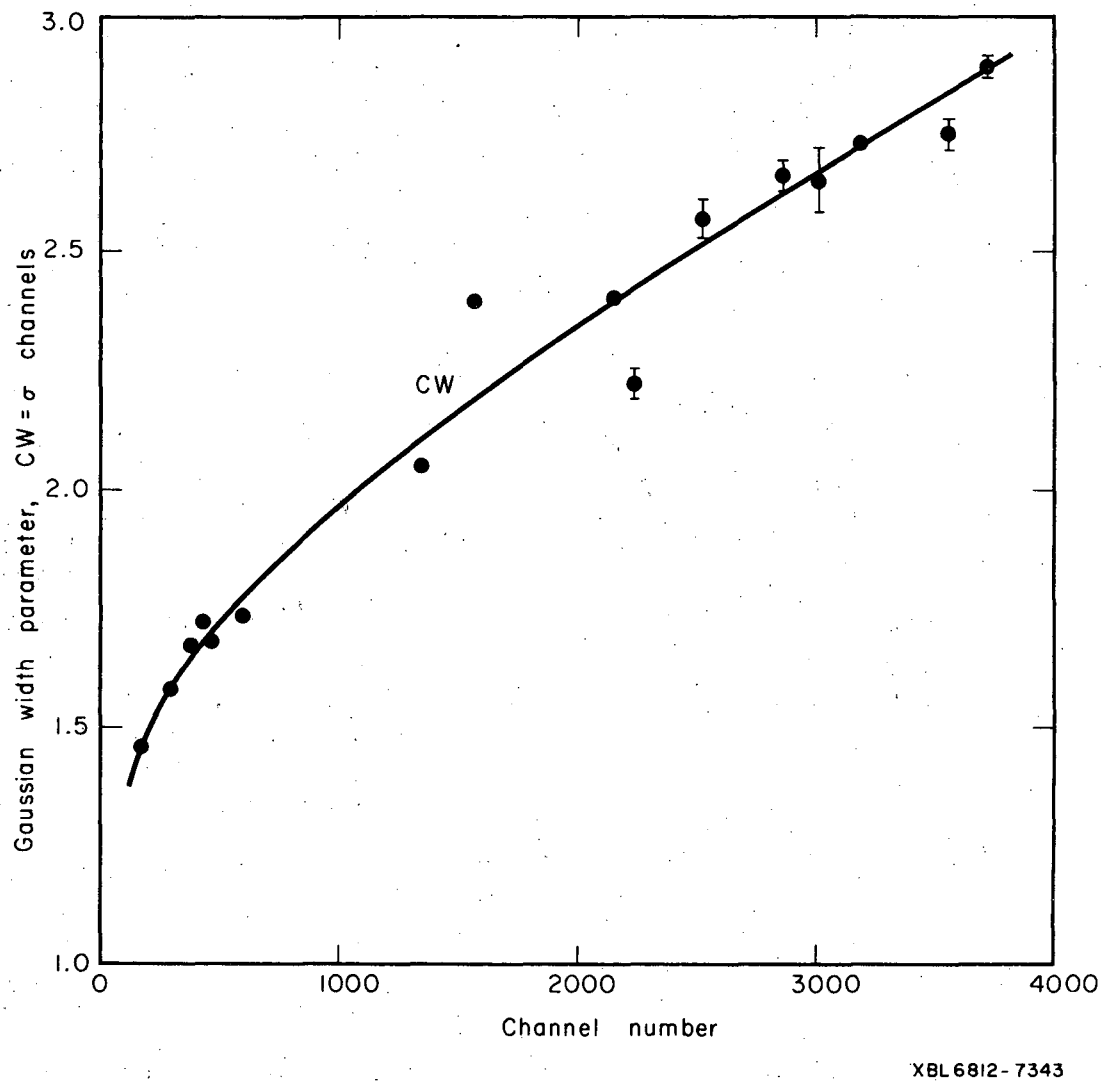

Fig. 49. Plot of the empirically determined parameter CW defining the Gaussian portion of the Ge(Li) photopeak response function for the Ta^{176} Compton-suppressed spectrum (80-1240 keV). (FWHM = 2.355CW = 2.355σ)

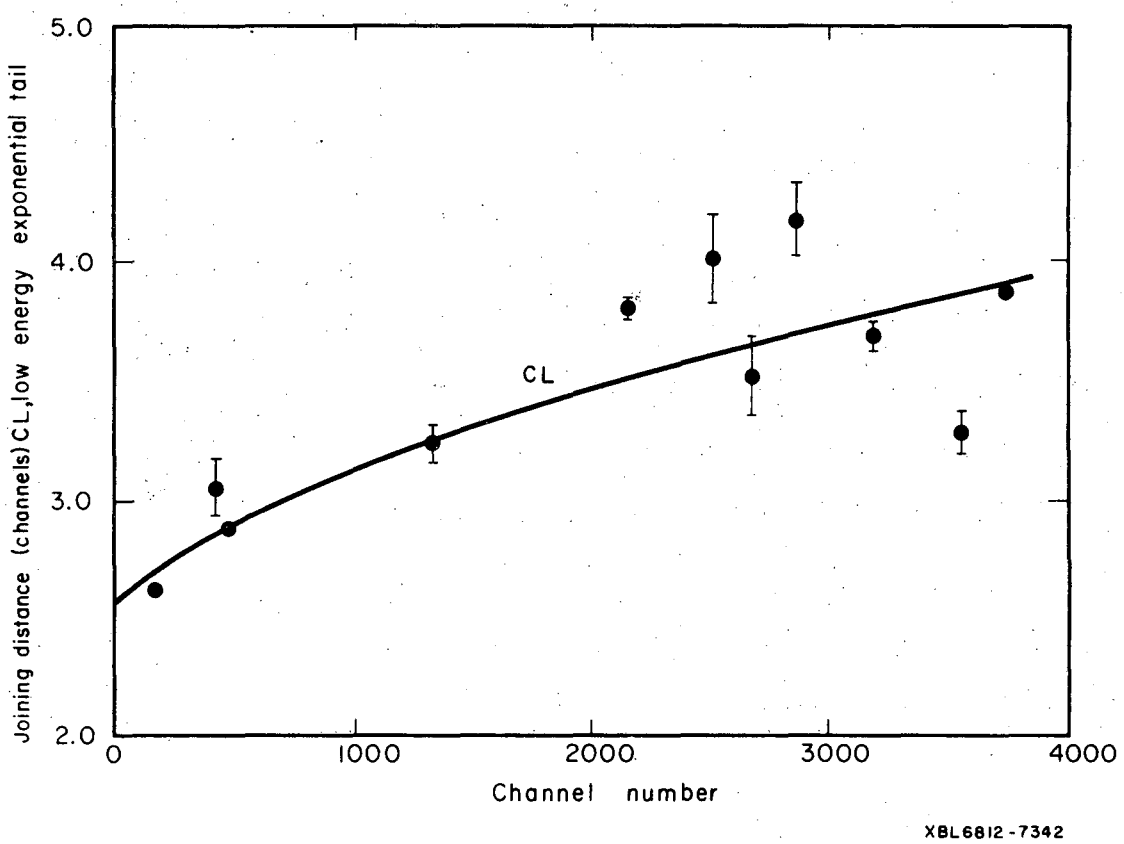

Fig. 50. Plot of the empirical parameter CL defining the joining distance of the low-energy exponential tail for the Ge(Li) response function.

It is unnecessary to stress again the importance of being able to obtain precise photopeak energies if one intends to resolve a decay as complex as that of Ta^{176}. We are now confident that we can reproducibly determine the location of peak centroids to less than one percent of the peak FWHM, and the peak areas to within three percent This statement holds for all cases except those where counting statistics or spectrum complications (e.g. multiplets) are dominant. An equally important and related problem is defining the deviation of the detection system from the ideal linear response to pulse height. This is the third subject we now treat--the method we have employed to obtain precise energy calibrations and an estimate of system integral linearity. (The differential SBA ADC linearity may be inferred from the specification in Ref. 88 which states that the counting rate is equal to within 1% for all channels above channel 60 when the ADC is fed with a source of randomly distributed pulses.)

In general, either of two methods can be easily used to determine unknown photopeak energies. Both methods require the use of well-known γ-ray energy standards, and which method is to be preferred depends only on the form of the unknown spectrum. If the spectrum to be determined is not overly complex, it is often preferable to just count a number of standard sources simultaneously with the unknown sample, so that calibration lines internal to the spectrum can be used to determine the unknown photopeak energies. This very simple procedure is attractive because no gain or baseline stabilization is in theory required, provided the "unknown" count rate is maintained to be relatively constant, and provided no severe drifts occur in the system during the counting time.

Unfortunately, in very complex spectra, the above method is often impractical, because of the likelihood that "unknown" photopeaks will interfere with standard peaks. In this case, the only alternative is to employ a gain and base-line stabilization system in conjunction with either pulser-generated reference peaks, or possibly with two mono-energetic γ-ray sources (for obvious reasons it is highly undesirable to enlist a γ-ray source as the gain reference at the high-energy end of the spectrum). In principle, the only limitation to absolute reproducibility using this method ought to be the stability of the reference pulses; it is essential that the pulsers be stable to 50 ppm. We do not consider that we have yet achieved in the system described in section (III.C.1) the pulser stability that is both desirable and feasible. The pulsers employed in our work have been of two varieties: 1) a dual "pulse train" generator with transistorized choppers at the preamplifier input;[142] 2) a Hg-switch relay pulser of the type described in Ref. 143. The DC reference level supply (section II.C.1) used with both of these pulsers is easily stable to the desired 50 ppm. (specification, < 25 ppm/year). But the active stages in the tail-pulse generator (1) have not yet been optimized for maximum stability; therefore we at this point can only quote an empirical long term stability $\leqslant 0.01\%$. The Hg-switch relay pulser (2) ought to have better stability characteristics than the system (1), but we are in this case not yet equipped with the dual system including appropriate delays required for generating independent gain and base-line stabilization reference pulses.

Ideally, in order to properly check system linearity, three pulsers are necessary--two to insure continuous base-line and gain stability and the third to generate the variable, precisely known pulses for the linearity check itself. We presently do not have a convenient way to feed a third pulser into the detector test capacitor, although the necessary pre-amp modification is certainly simple. This capability is essential if reproducible linearity checks are to be performed, since small level shifts of the order of those being measured can easily occur during the linearity check if the gain and baseline levels are not stabilized.

Despite the above-noted deficiencies of our experimental system, we were able to obtain what we felt were adequate system linearity checks in a usually reproducible way. The switch-settable precision reference voltage source was used to "step" the pulser amplitude in ≈ 0.1 V increments over the entire range of the spectrum. The pulser peaks were computer analyzed for centroid positions using the code SAMPO described earlier. Enough counts were accumulated in each pulser peak so that the error in the centroid location was < 0.01 channel. In Fig. 51 we show a typical curve displaying the deviations from linearity for a Ge(Li) detector system. It is seen that (without bias amplifier) the deviations are generally $< 0.015\%$ over the region from channel 350-4000. Similar integral linearity characteristics have been observed in other amplifier-ADC systems of this type in use at LRL.

In all of the non-linearity measurements we have made, the singularity at about channel 2048 appears. This presumably represents

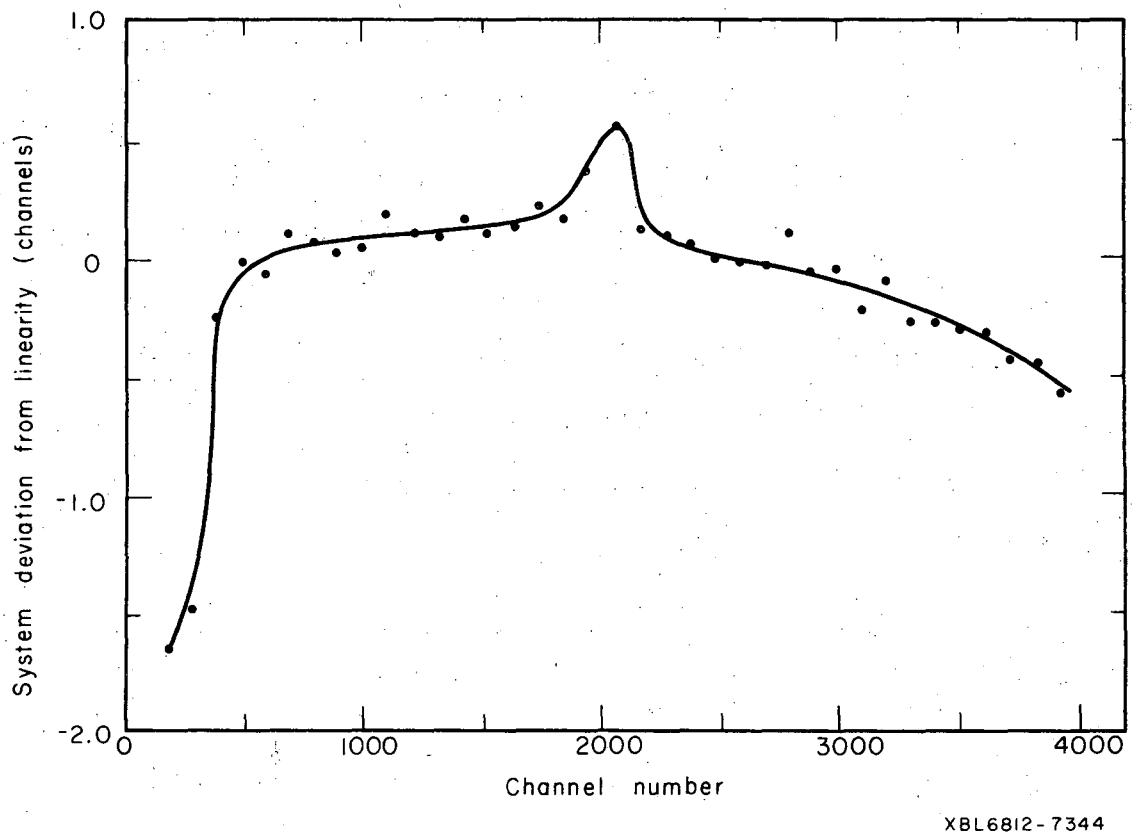

Fig. 51. Typical non-linearity curve for a Ge(Li) detector system in conjunction with the SBA-type ADC used in this work.

the differential non-linearity expected for the SBA ADC at the "binary channel" locations (2047-2048, and to a lesser degree, 1023-1024, 511-512, etc.[88]). Our curves indicate that the most important of these differential non-linearities (2047-2048) has been successfully smoothed to < 0.01% by the method described in Ref. 88.

In principle, a precision pulser could be used to calibrate an entire spectrum, given only two standard energy peaks; the feasibility of this calibration technique being performed under computer control is currently being explored at our laboratory.[144] The problems of such an undertaking are well-known.[145] Not the least of the uncertainties is that inherent to any attempt to simulate with a pulser an actual photoelectric event occurring in the bulk germanium. Even though the pulsers we employ inject charge directly onto a test capacitor at the Ge(Li) diode input, we still cannot be absolutely certain that the simulation is exact. The "safest" way to check linearity and obtain precision energy data in practice is still then to simply have a large number of standards that essentially define the non-linearities of the system. We must concede that, despite our attempts to develop more precise and sophisticated methods for determining non-linearity, this is the method we have had to resort to in our work because we do not yet consider the "pulser" techniques reliable enough to merit our complete confidence.

An additional note should also be included regarding the analysis of calibration and linearity data once it has been obtained. It is customary in many laboratories to use a least-squares polynomial fit to the experimentally determined detector system non-linearities, and thereby

to correct the energy calibration. In general, this is no doubt an acceptable procedure, particularly for routine work carried out on a single well-calibrated apparatus maintained at constant gain. However, when numerous detectors and a variety of system components are employed for independent, unrelated measurements, as is usually the case in the typical laboratory, it is a hazardous practice to employ as a matter of course a polynomial fit to the energy calibration data without examining very closely the behavior of the polynomial function. Consider as a case in point the data shown in Fig. 51A. Clearly, it is possible in some instances for a polynomial fit to "pass through" all of the energy calibration points, but behave in a most unrealistic fashion in regions between the points. In such cases, a simple linear interpolation between successive calibration points can be more accurate than a polynomial fit to the points. Alternatively, small portions of the data can be fitted separately to appropriate polynomial functions. The obvious conclusion is simply this: If one wishes to measure photopeak energies to less than 0.01% precision, as is now possible, the utmost care must be employed to properly correct for the non-linear response of the detection system, an effect that can easily introduce errors an order of magnitude greater than the errors associated with the standard calibration energies.

Finally, what precision we were able to obtain in the Ta^{176} energy determinations we owe in large measure to the recent standardization results from two sources: Gunnink, et al.[96] and J. B. Marion.[146] The former have carried out precise γ-ray energy determinations for a number

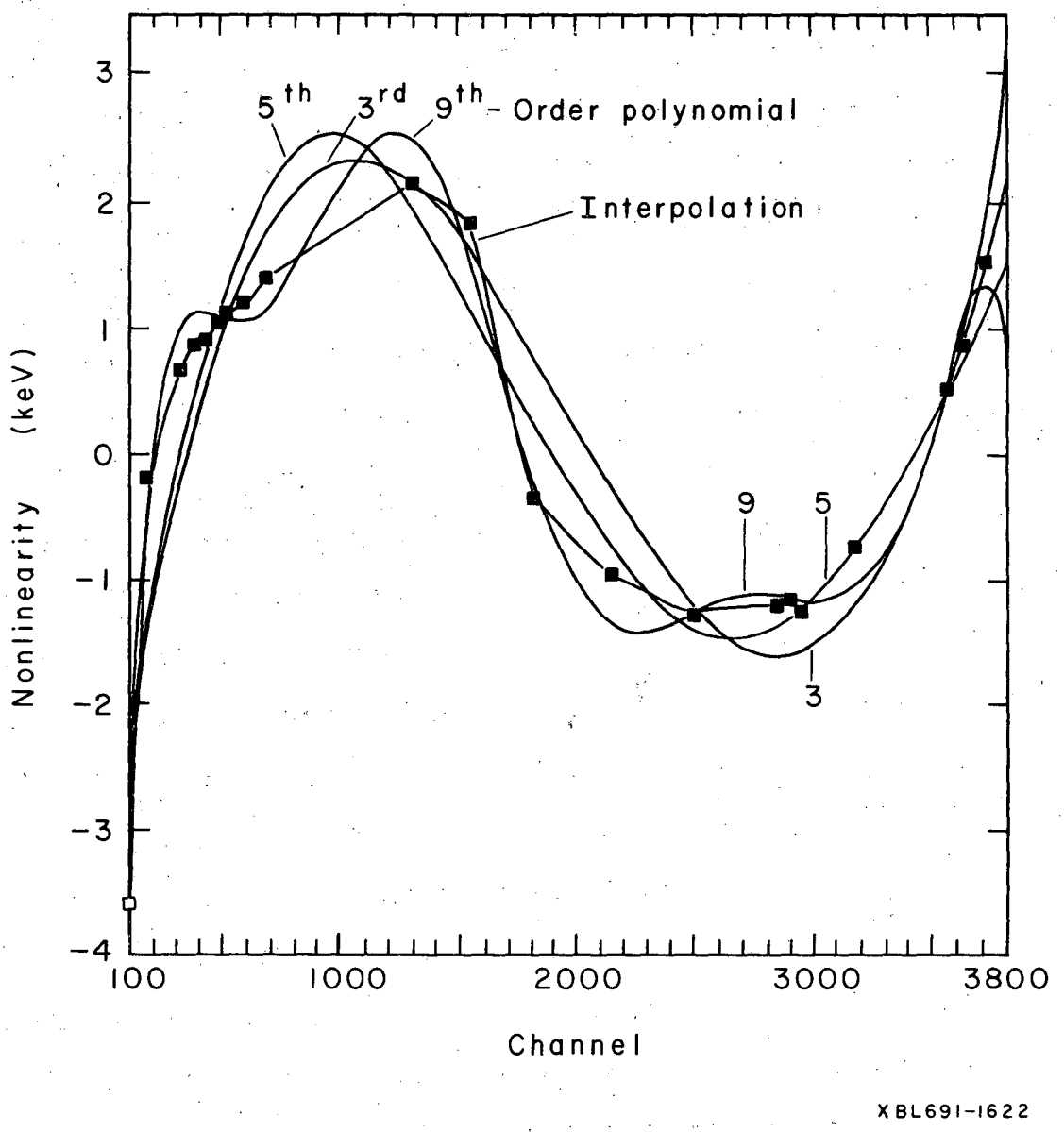

Fig. 51-a. Comparison of polynomial fits and linear interpolation between energy calibration points for the non-linearities in one Ge(Li) detector system.[97] (The data are for the Ta^{176} low-energy Compton-suppressed γ-ray singles spectrum.)

of isotopes, most notably Co^{56}, Th^{228} and its equilibrium daughters, and Ra^{226}. Of particular interest is the discussion in Ref. 96 of the hazards involved in using "escape" peaks for energy calibration. The point of this discussion is worth repeating. If the experimenter wishes to employ "escape" peaks as standard calibration lines, he must position his source so that the photons impinge on the detector at an angle perpendicular to the electric field set up in the diode by the high voltage bias. A moment's reflection about the difference between the pair and photoelectric interactions reveals the reason for taking this precaution: The positron produced by a pair event experiences an acceleration exactly opposite to that affecting a photoelectron. At the electric field strengths up to 350 V/mm now commonly associated with Ge(Li) diodes, it is easy to imagine that the opposing effect of this acceleration can be appreciable. For the 13 mm deep, 10 cm^3 planar detector which we operate at 365 V/mm bias, we observe shifts of almost 0.3 keV for the Ta^{176} 2832.0- and 2920.4-keV double-escape peaks when measurements made with the source perpendicular to the electric field are compared to those taken with the source parallel to the electric field in the diode.

In Table 20 we list the energy standards we have employed in our work. This tabulation has been compiled from Refs. 96, 146, and 147.

Table 20. Energy calibration standards for γ-ray spectroscopy. Compiled from Refs. 96, 146, and 147.

Source	$t_{\frac{1}{2}}$	γ-ray Energy	Source	$t_{\frac{1}{2}}$	γ-ray Energy
Am^{241}	458y	26.348±.010	Hg^{203}	47d	279.191±.008
		59.543±.015	Sn^{113}	115d	391.712±.050
Ta^{182}	115d	65.722±.001	Th^{228} and daughters	698d	39.85 ±.01
		67.747±.002			238.624±.009
		100.106±.001			510.723±.020
		152.435±.004			583.139±.023
		179.393±.003			*1592.696±.050
		222.110±.003			*2103.70 ±.07
		264.072±.006			2614.708±.053
		1121.40 ±.09			
		1221.53 ±.11	m_oc^2		511.005±.002
Cd^{109}	453d	88.010±.030	Bi^{207}	30y	569.65 ±.05
					1063.60 ±.05
Co^{57}	270d	122.03 ±.03			1769.71 ±.13
		136.44 ±.04	Cs^{137}	30y	661.615±.030
Ir^{192}	74d	136.333±.010	Mn^{54}	303d	834.810±.030
		201.282±.010	Y^{88}	108d	*814.12 ±.06
		205.782±.014			898.03 ±.04
		295.938±.009			1836.13 ±.04
		308.435±.010			
		316.488±.010	Zn^{65}	245d	1115.46 ±.05
		377.44 ±.04	Co^{60}	5.3y	1173.22 ±.03
		468.060±.010			1332.505±.025
		588.557±.017			
		604.385±.017	Na^{22}	2.6y	1274.55 ±.04
		612.435±.017	Co^{56}	77d	846.782±.060
					1037.851±.060

(continued)

Table 20. Continued

Source	$t_{\frac{1}{2}}$	γ-ray Energy
Co^{56}(cont)		1175.085±.070
		1238.290±.040
		1360.219±.040
		*1576.561±.050
		1771.33 ±.06
		2015.33 ±.07
		2034.90 ±.06
		*2180.17 ±.07
		*2231.60 ±.06
		*2251.15 ±.07
		*2429.28 ±.10
		*2598.52 ±.05
		*2691.17 ±.08
		*2742.60 ±.07
		*2762.15 ±.08
		3202.18 ±.07
		3253.61 ±.06
		3273.16 ±.07
		3451.29 ±.10
		3548.11 ±.18

*Escape peak energy. The user should read the caution in Appendix B and in Ref. 96 concerning the use of escape peaks for energy calibration. We have added certain single-escape energies to the listing of Gunnink, et al.[96] for Co^{56} and Th^{228} by assuming the value for m_0c^2 listed above.

APPENDIX C

The γ-γ Coincidence Data for the Decay of Ta^{176} to Levels in Hf^{176}

In the following pages we display in its entirety the Ta^{176} γ-γ coincidence data on the basis of which we have constructed the level scheme of Fig. 34. A few comments about the Figs. 52-55 are necessary to aid the reader in interpreting the data.

Figure 52 shows the gross coincidence spectrum for the 10 cm^3 Ge(Li) planar crystal which was used as the "gate" side of the coincidence data. The gates for the coincidence spectra (Figs. 55) are all keyed by channel number to Fig. 52, and the reader can determine the exact channels included in each gate. For example, above the first coincidence plot, (Fig. 55) we find the numerical identification (1 134 137 0 0). The second and third numbers are of interest, and define the gate channels 134-137 for the 88-keV transition, as can be verified in Fig. 52. Similarly, the second spectrum is identified as that arising from a gate set on channels 283-286 in Fig. 52, i.e. on the 201.8-keV transition. The remaining spectra are ordered according to the gate energy. For convenience we include in Table 21 a summary of the peak and background gates and their approximate corresponding peak energies.

Figure 54 shows the gross coincidence spectrum from the 35-cm^3 coaxial detector. This spectrum serves to identify the peaks in the coincidence spectra 55. The efficiency curve in Fig. 53 can be used to obtain qualitative relative intensities for the coincidence spectra.

We have not attempted to label every peak appearing in the coincidence plots, but have generally noted only the stronger lines, and those lines

which have been used to deduce the decay scheme in Fig. 34. Where we have not accounted for the presence of a prominent line, we so indicate with a question mark (?).

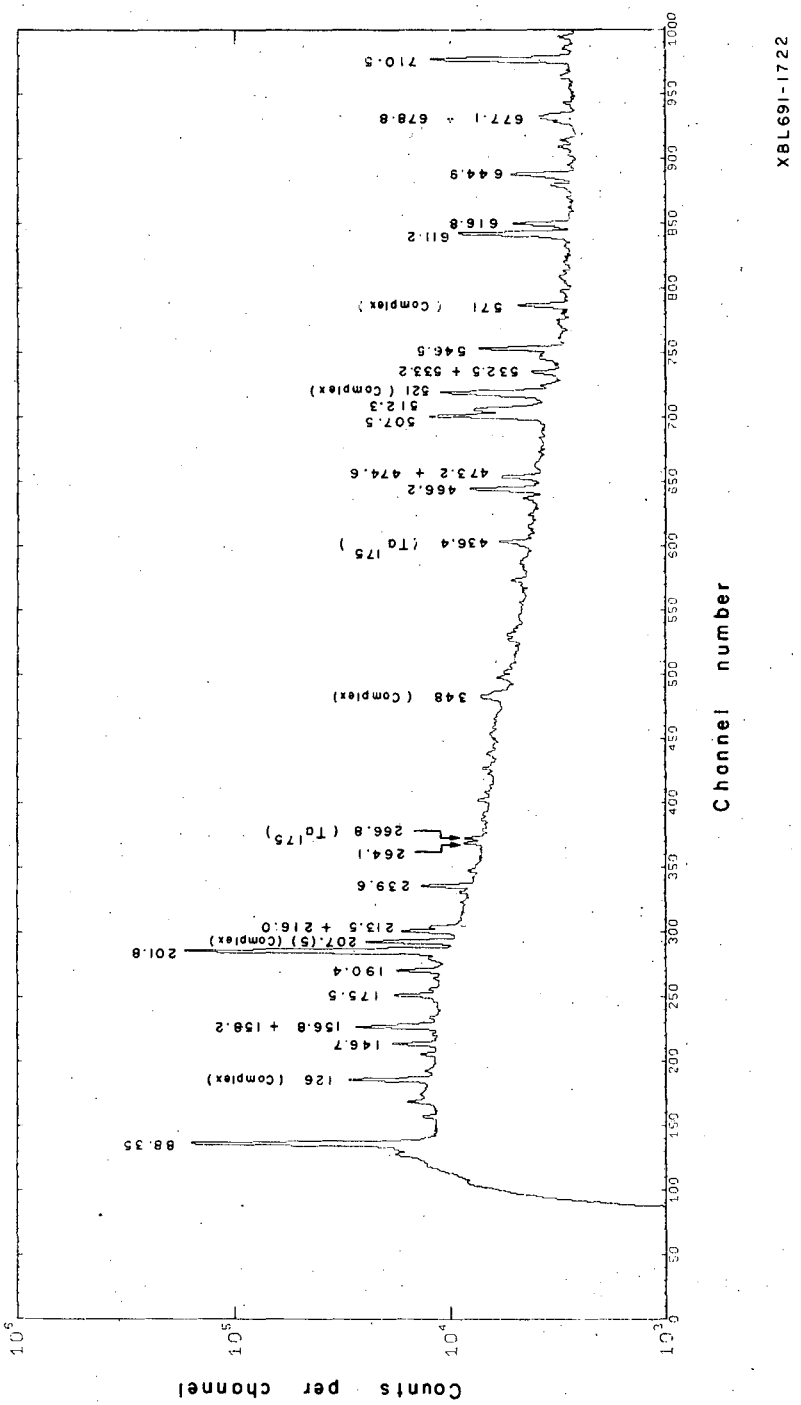

Fig. 52-a. Gross γ-γ coincidence spectrum of Ta^{176} for the 10 cm^3 planar detector. (Resolving time, 65 nsec) 85 - 725 keV.

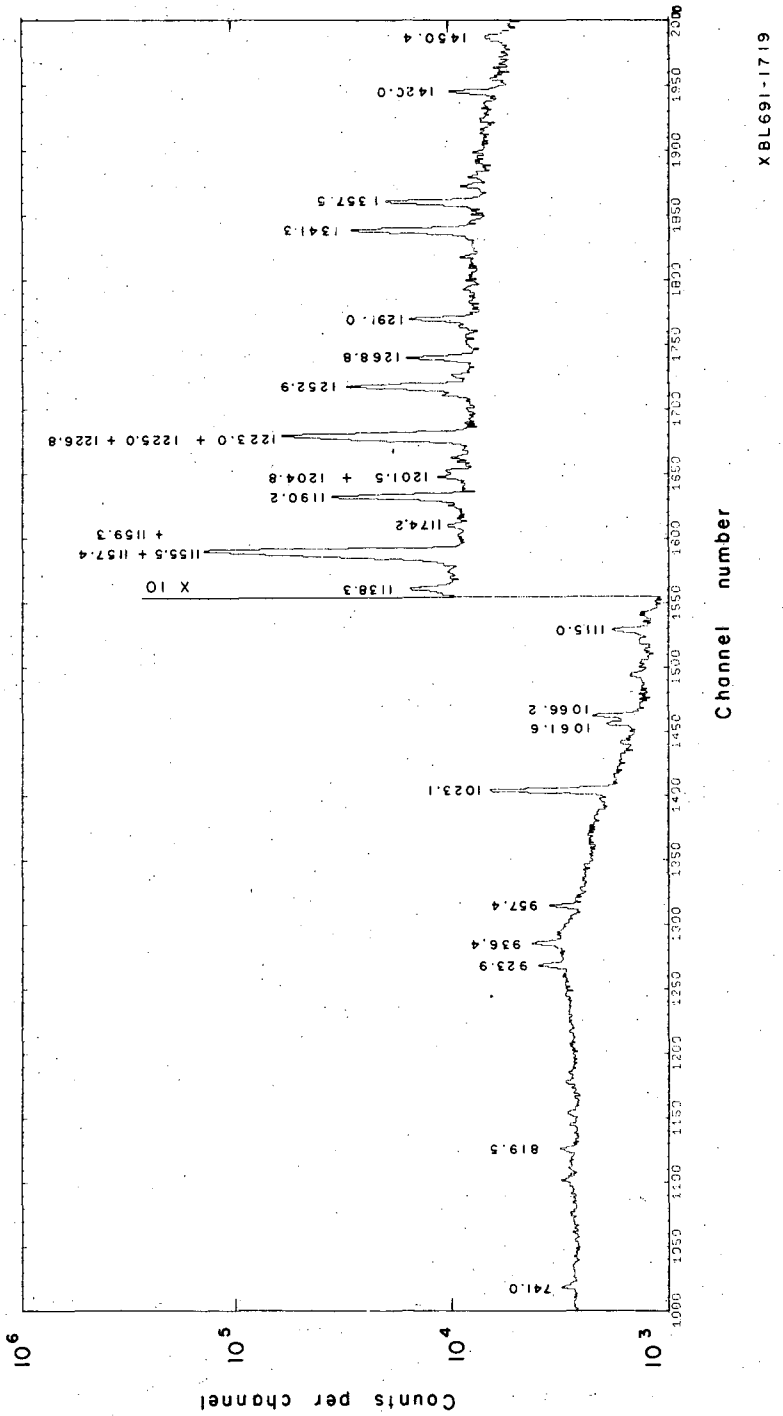

Fig. 52-b. Gross γ-γ coincidence spectrum of Ta^{176} for the 10 cm^3 planar detector. (Resolving time 65 nsec) 725 - 1455 keV.

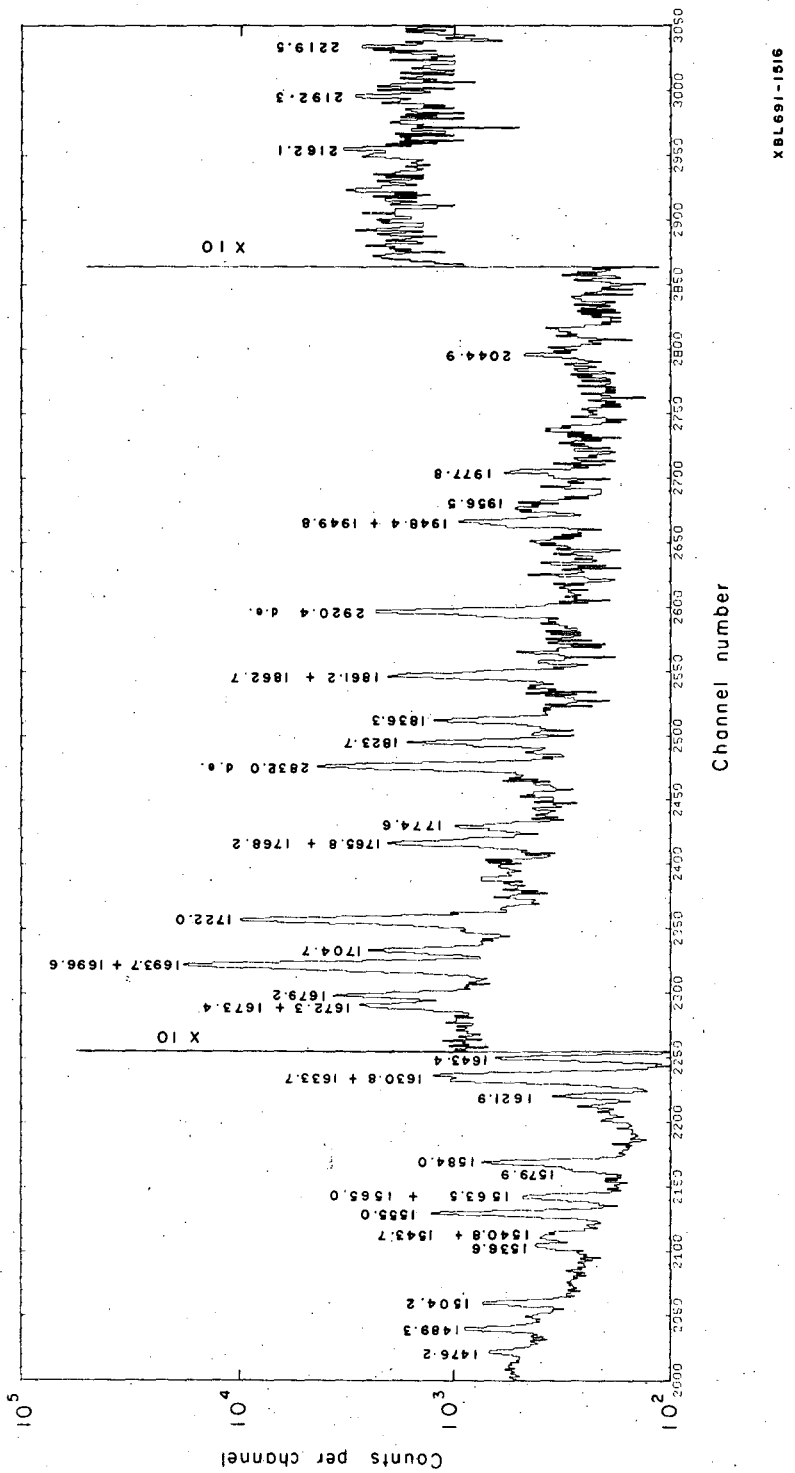

Fig. 52-c. Gross γ-γ coincidence spectrum of Ta^{176} for the 10 cm^3 planar detector. (Resolving time, 65 nsec) 1455 - 2230 keV.

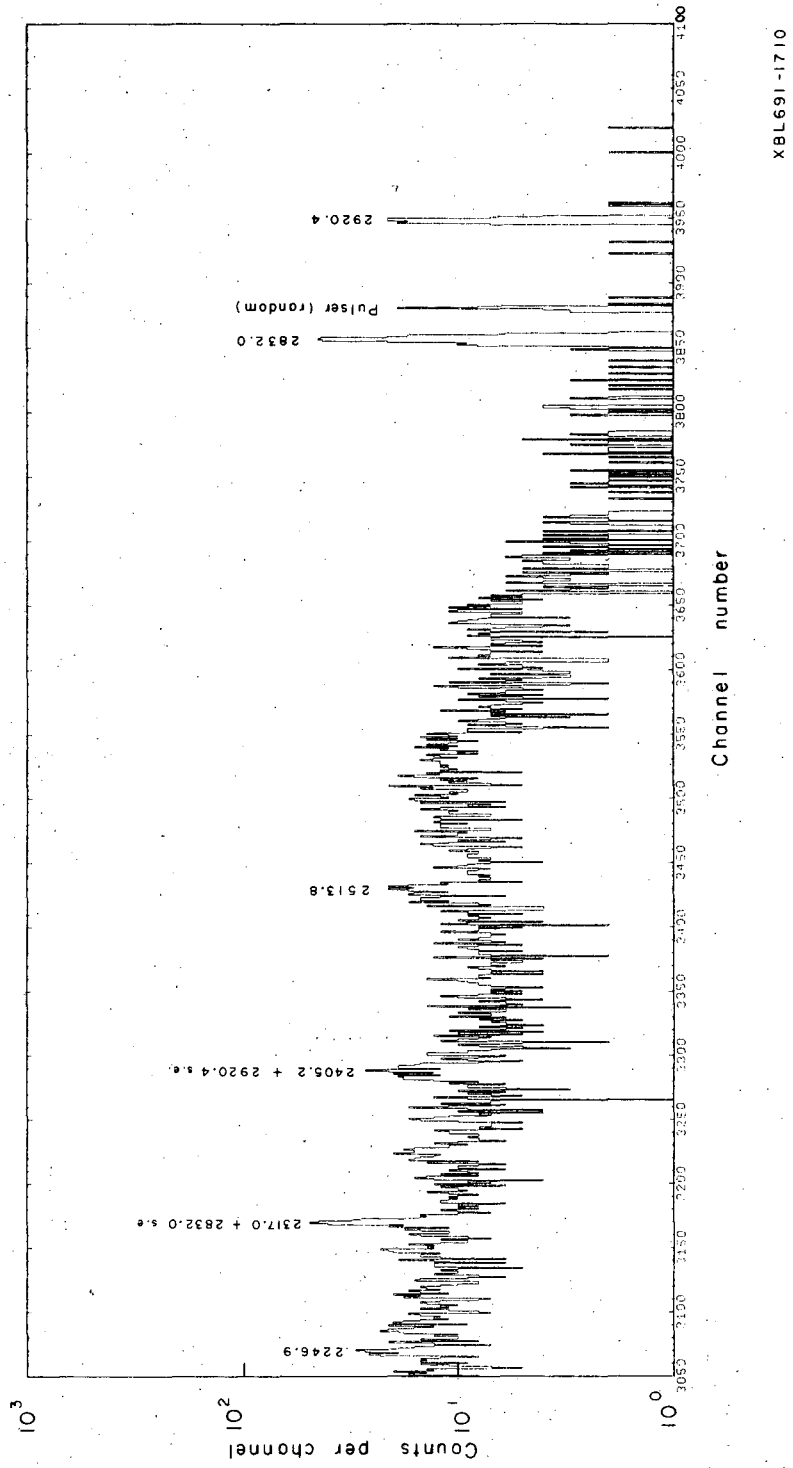

Fig. 52-d. Gross γ-γ coincidence spectrum of Ta^{176} for the 10 cm^3 planar detector. (Resolving time 65 nsec) 2230 - 30000 keV.

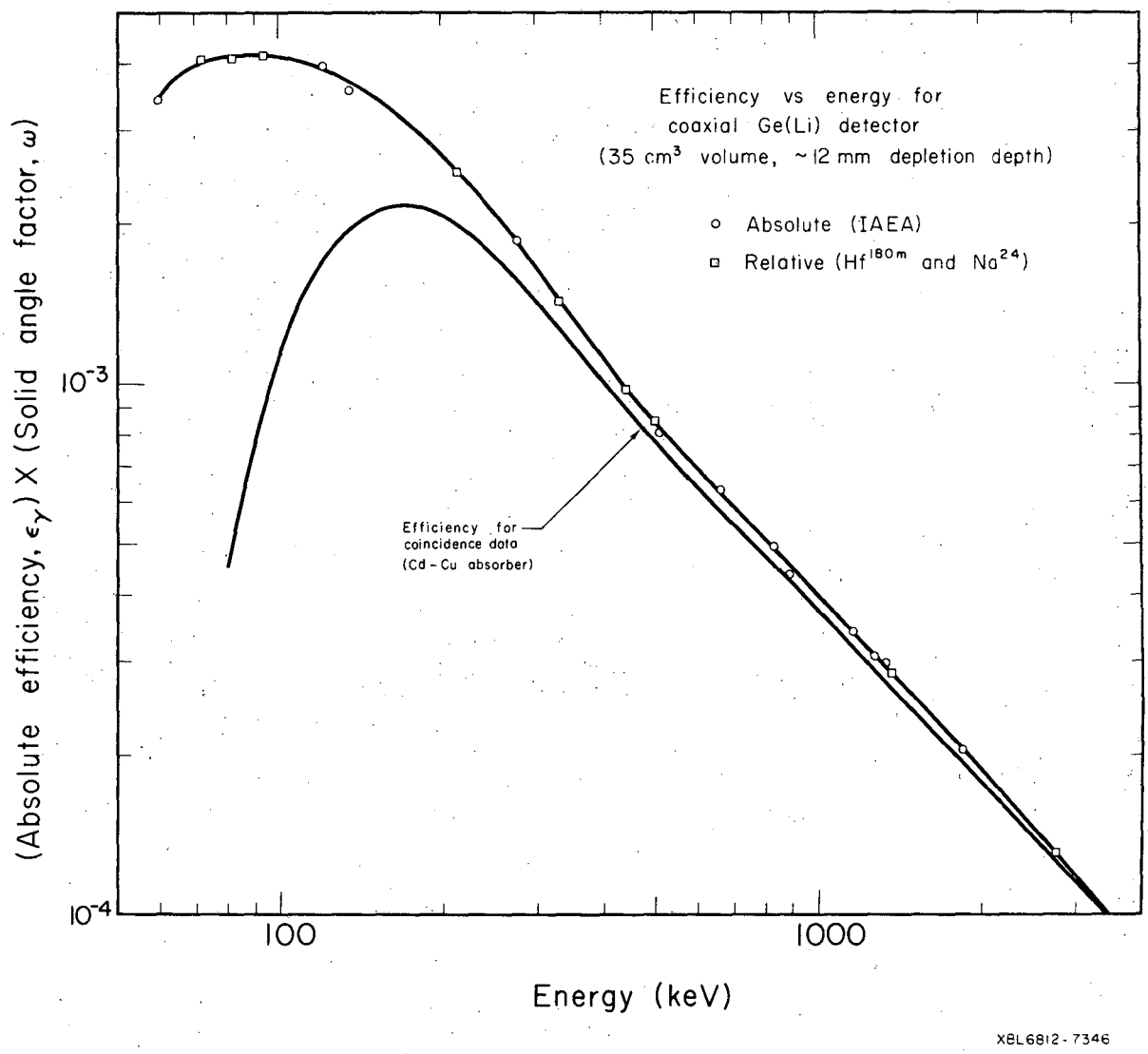

XBL6812-7346

Fig. 53. Absolute photopeak efficiency vs. energy for the 35-cm^3 coaxial detector used for obtaining the γ-γ coincidence spectra of Ta^{176} shown on the following pages. The lower curve (Cd-Cu absorber) applies.

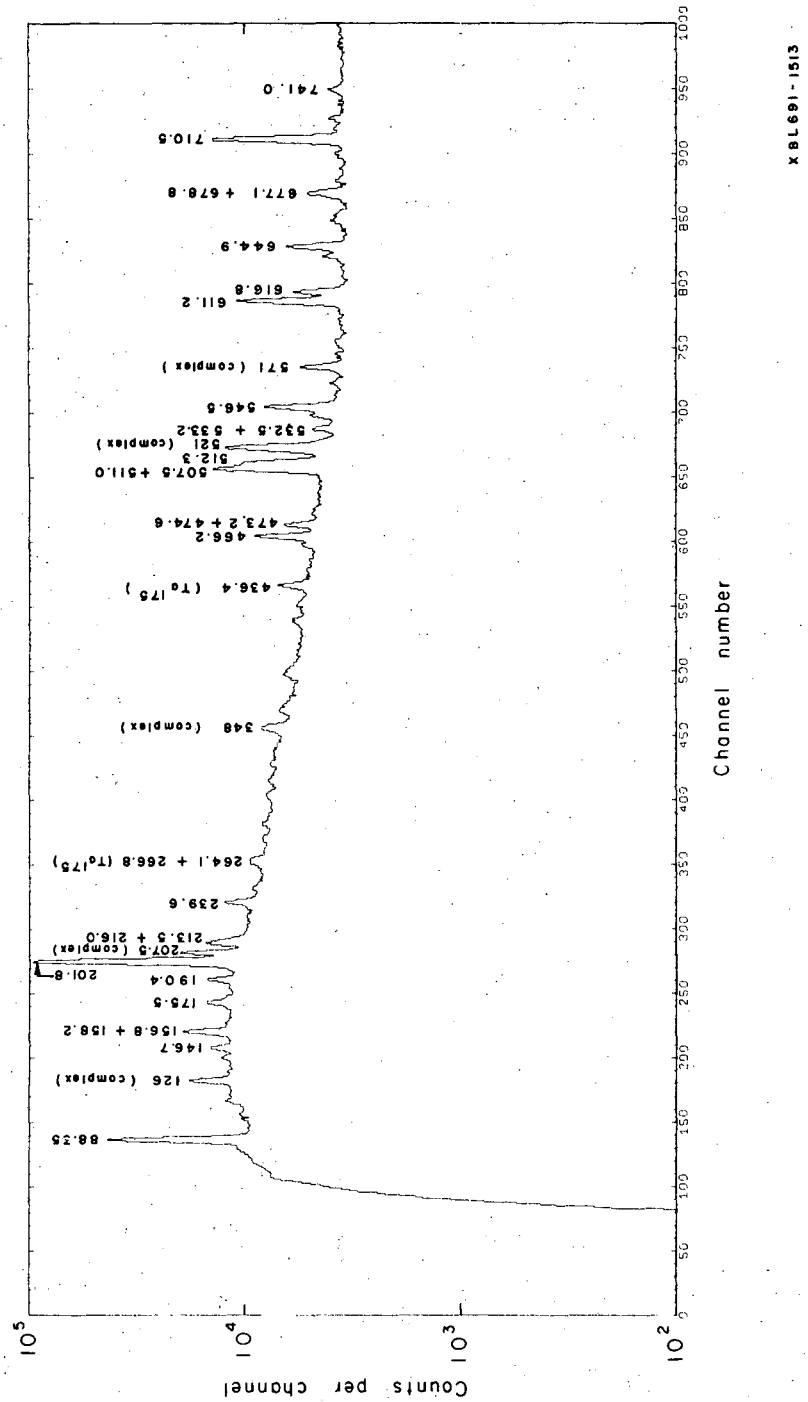

Fig. 54-a. Gross γ-γ coincidence spectrum for the 35 cm^3 coaxial detector. (Resolving time, 65 nsec) 85 – 775 keV.

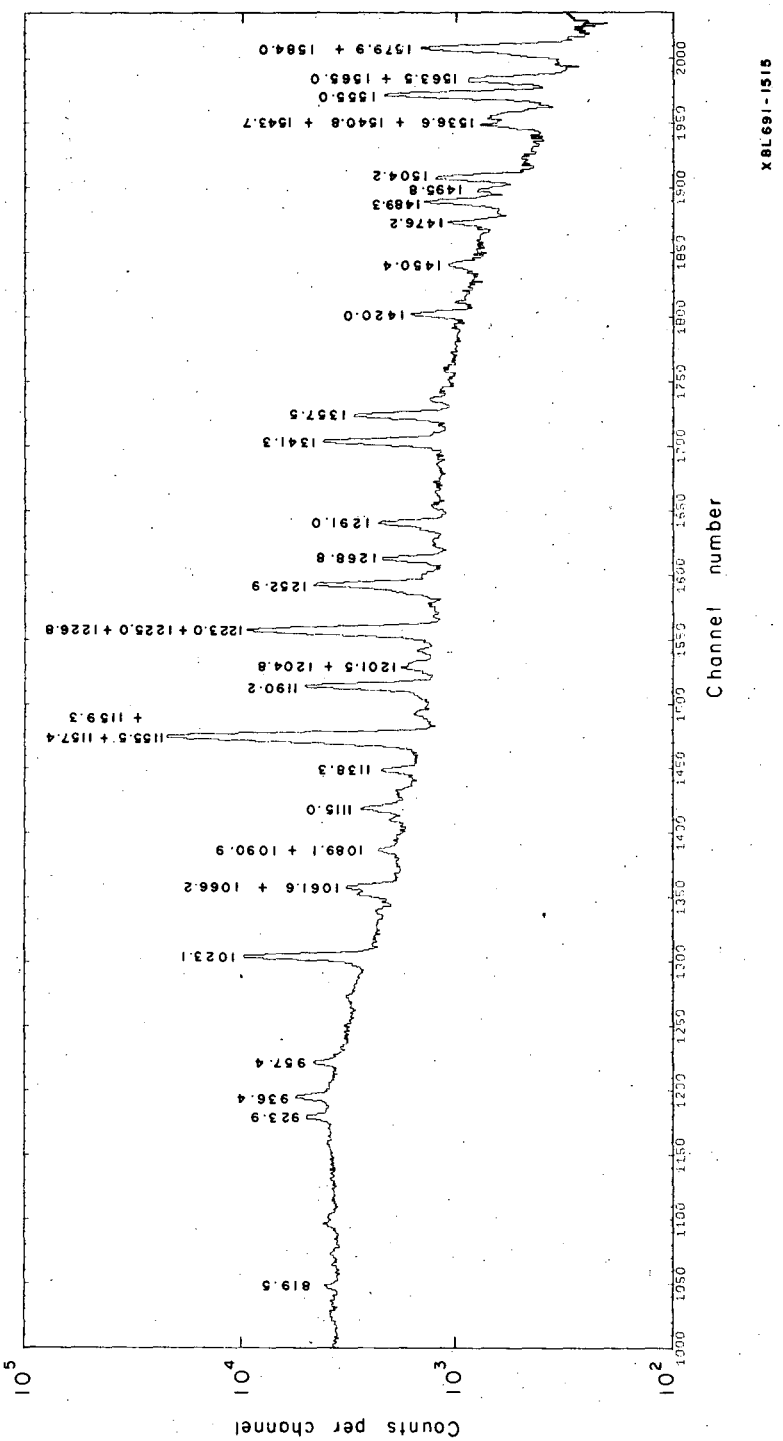

Fig. 54-b. Cross γ-γ coincidence spectrum for the 35 cm^3 coaxial detector. (Resolving time, 65 nsec) 775 - 1600 keV.

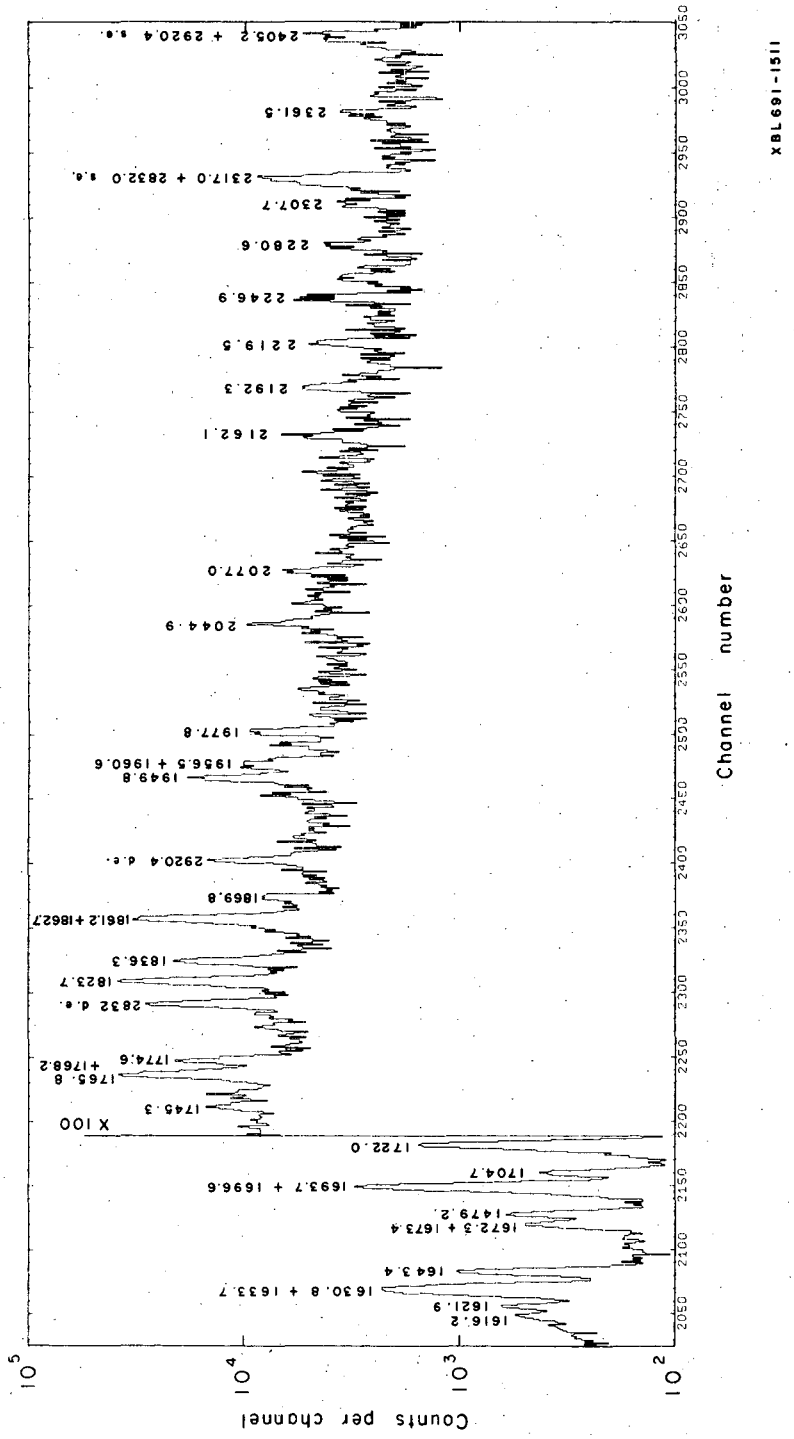

Fig. 54-c. Gross γ-γ coincidence spectrum for the 35 cm^3 coaxial detector. (Resolving time, 65 nsec) 1600 - 2410 keV.

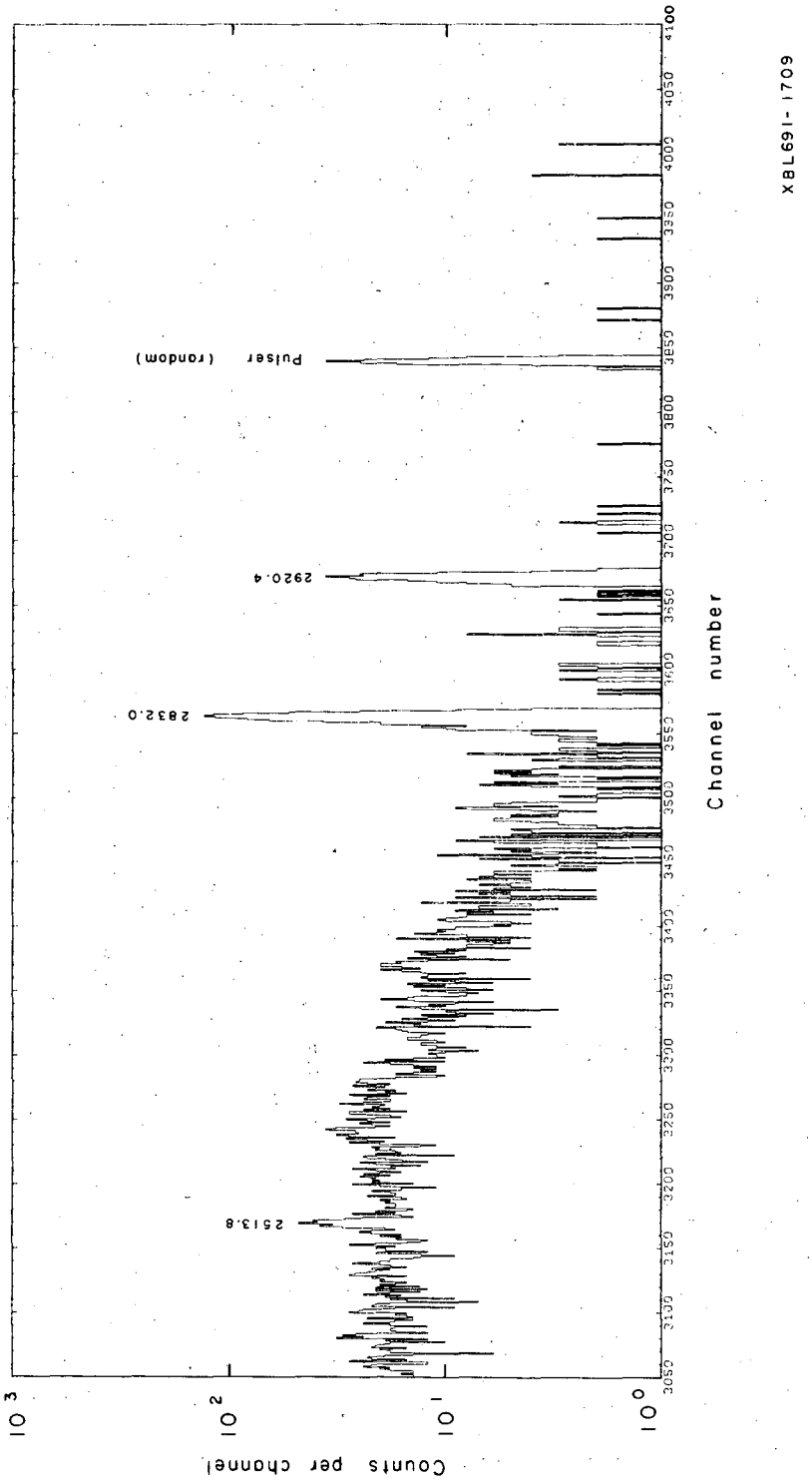

Fig. 54-d. Gross γ-γ coincidence spectrum for the 35 cm^3 coaxial detector. (Resolving time, 65 nsec) 2410 - 3150 keV.

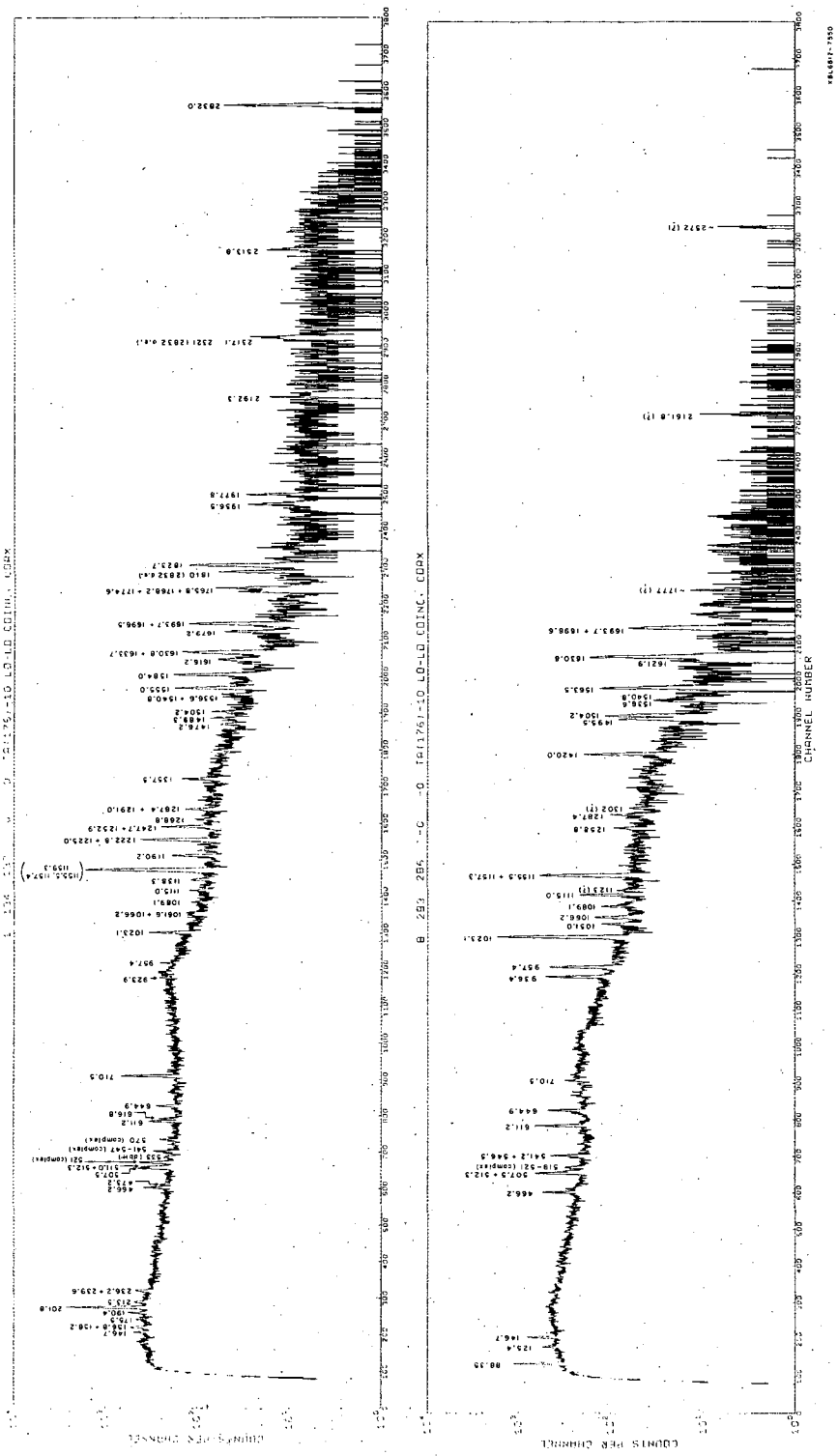

Fig. 55. The γ-γ coincidence spectra from Ta^{176} decay (90° geometry). Left: 88-keV; Right: 202-keV. (continued)

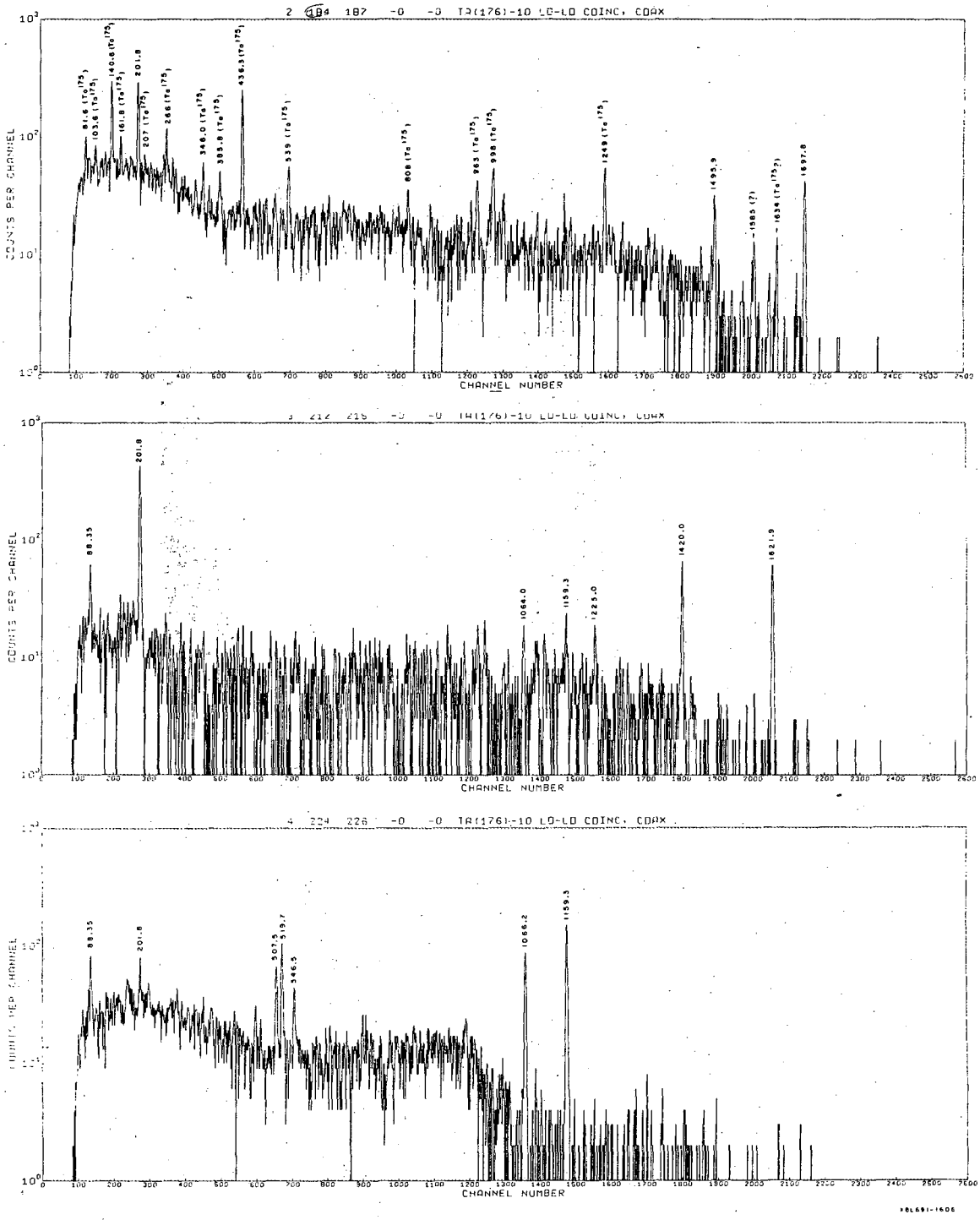

Fig. 55. (continued) The γ-γ coincidence spectra from Ta^{176} decay (90° geometry). Top: 126-keV; Middle: 147-keV; Bottom: 156-keV.

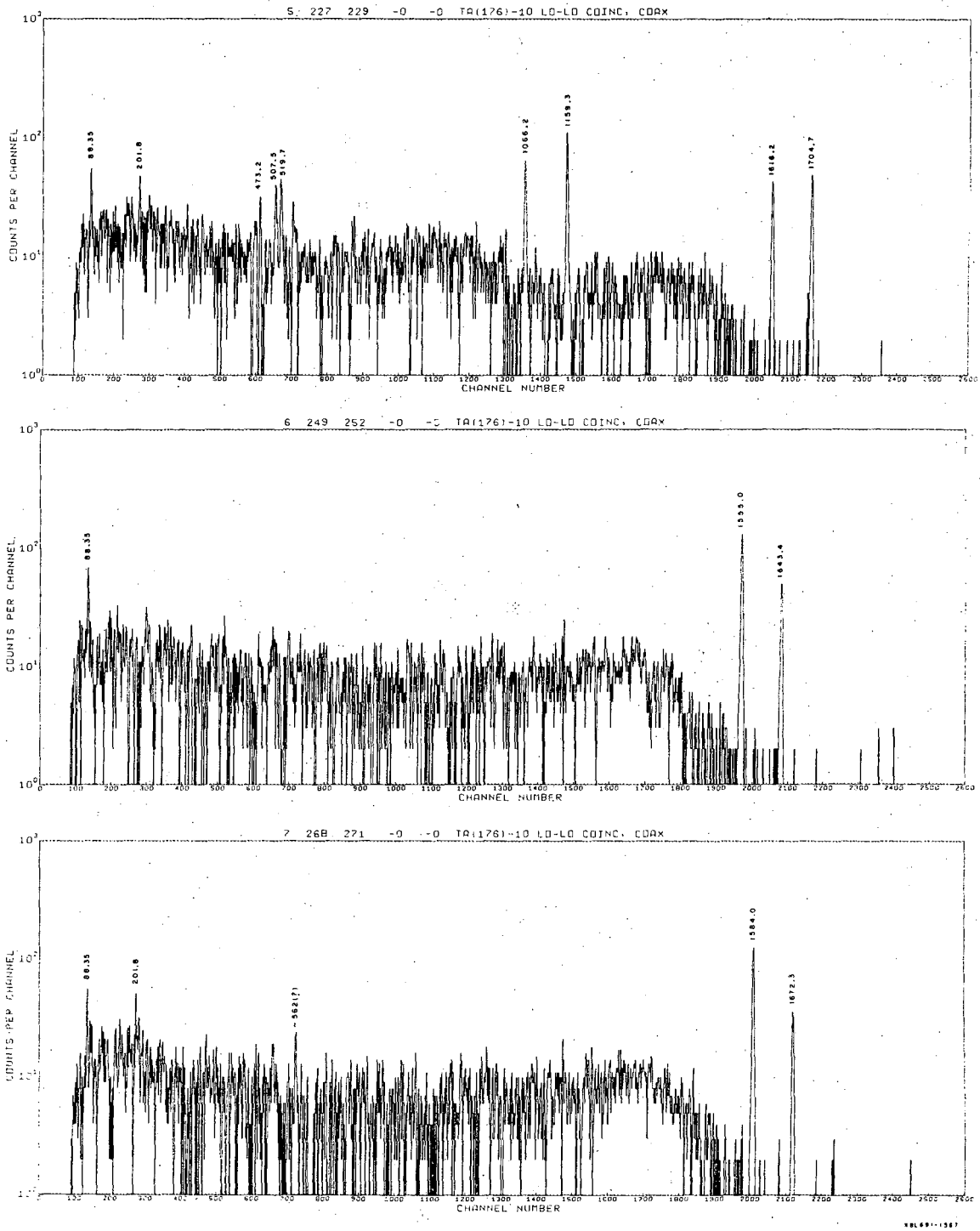

Fig. 55. (continued) The γ-γ coincidence spectra from Ta^{176} decay (90° geometry). Top: 158-keV; Middle: 175-keV; Bottom: 190-keV.

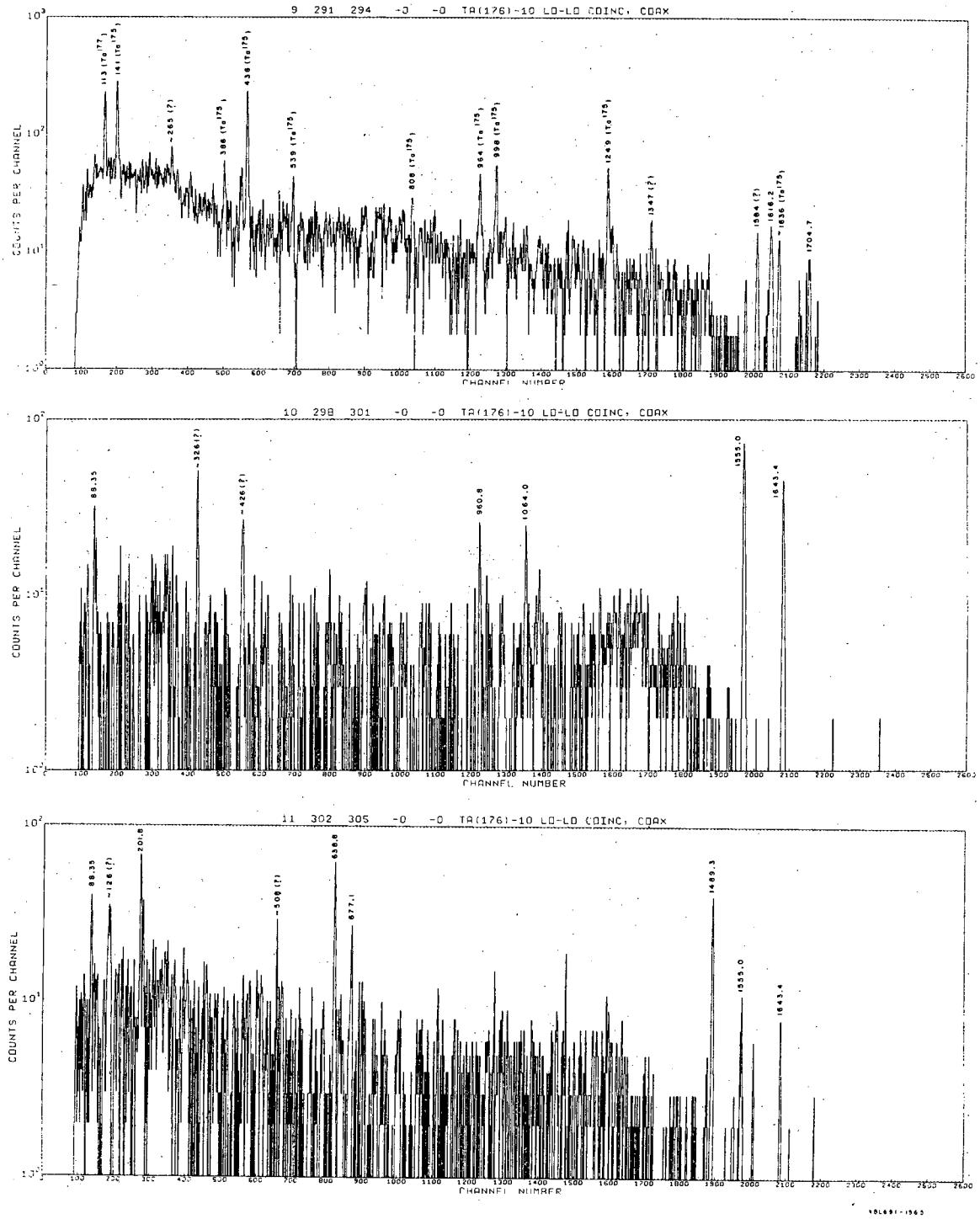

Fig. 55. (continued) The γ-γ coincidence spectra from Ta^{176} decay (90° geometry). Top: 207-keV; Middle: 213-keV; Bottom: 216-keV.

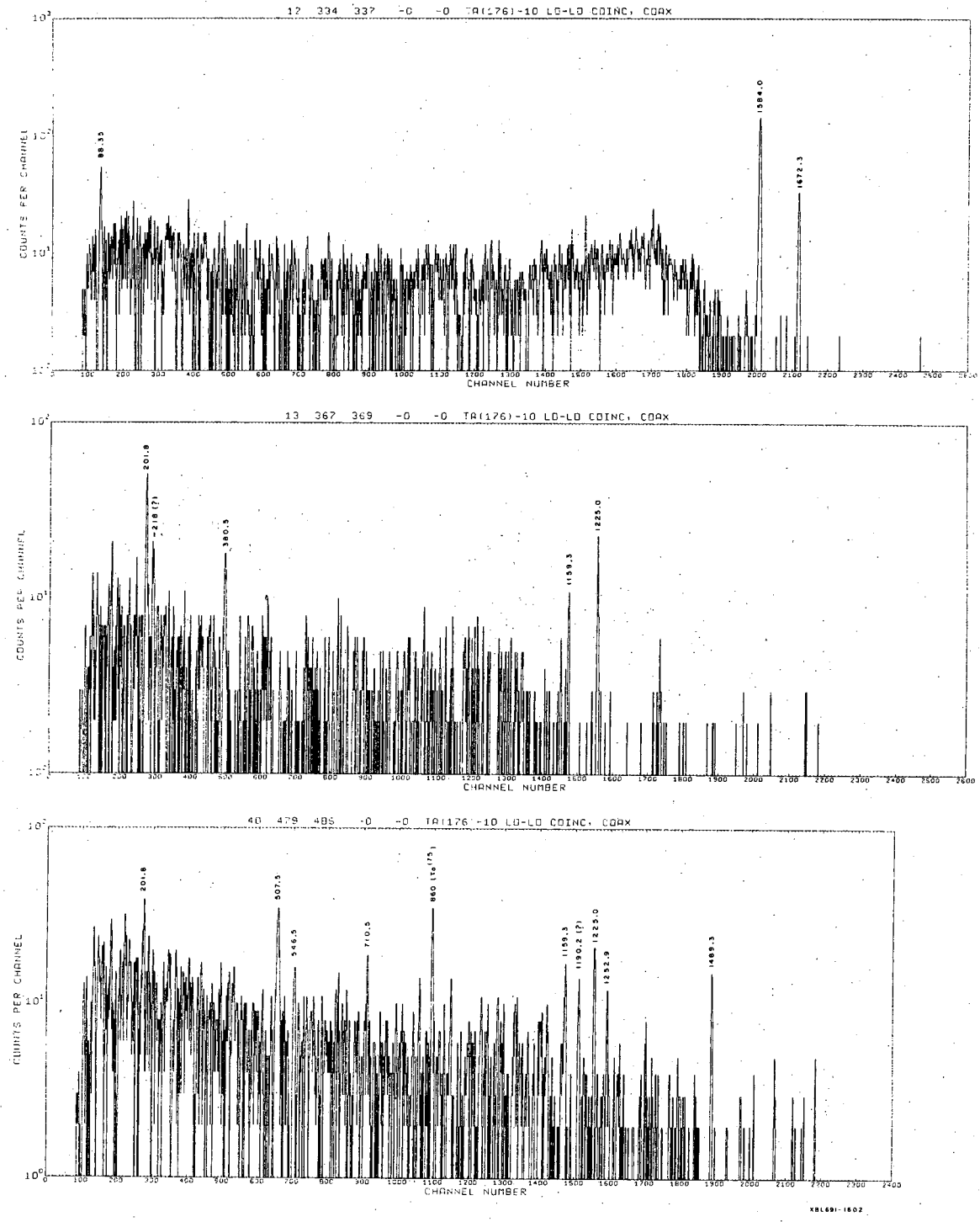

Fig. 55. (continued) The γ-γ coincidence spectra from Ta^{176} decay (90° geometry). Top: 240-keV; Middle: 264-keV; Bottom: 348-keV.

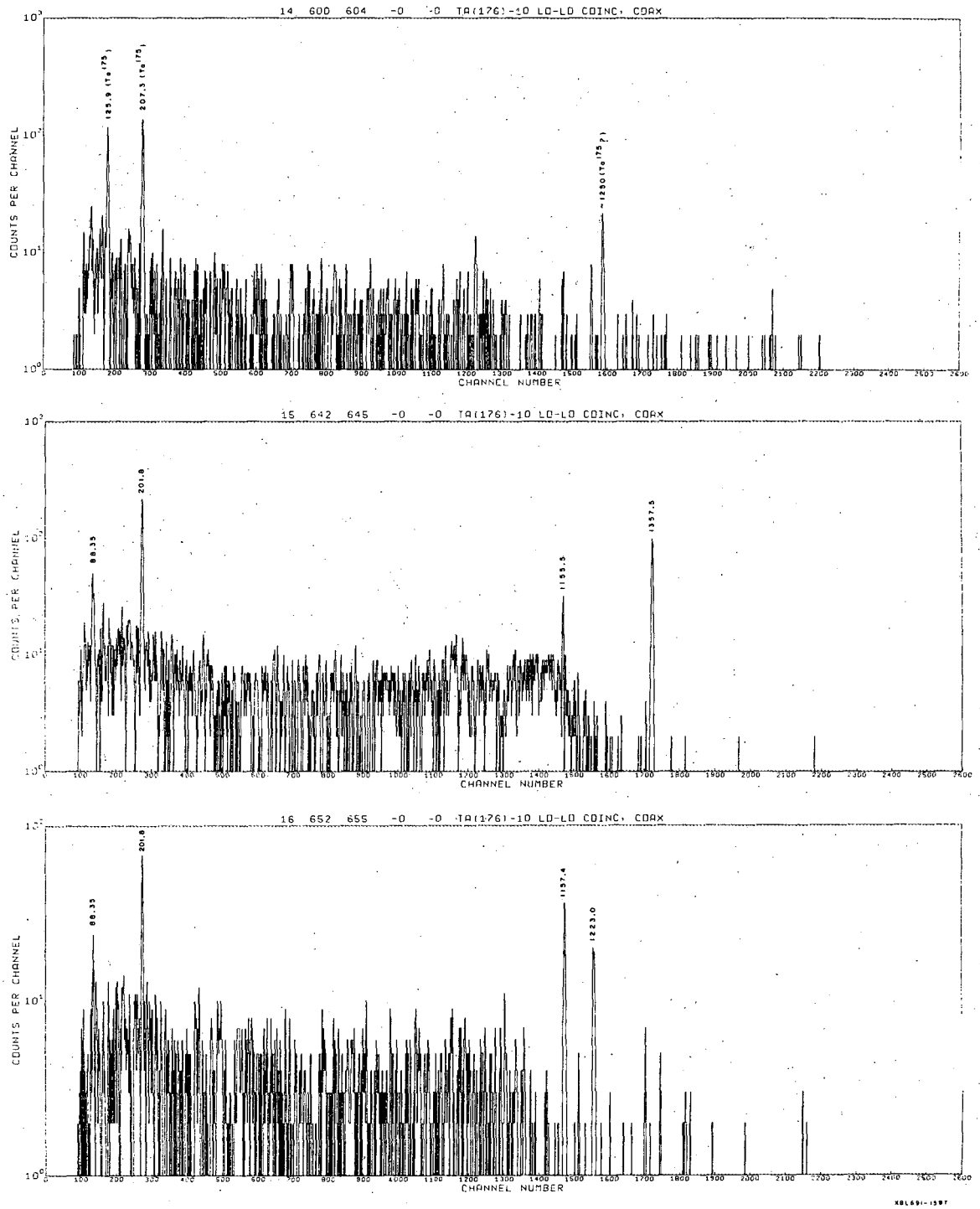

Fig. 55. (continued) The γ-γ coincidence spectra from Ta^{176} decay (90° geometry). Top: 436-keV; Middle: 466-keV; Bottom: 474-keV.

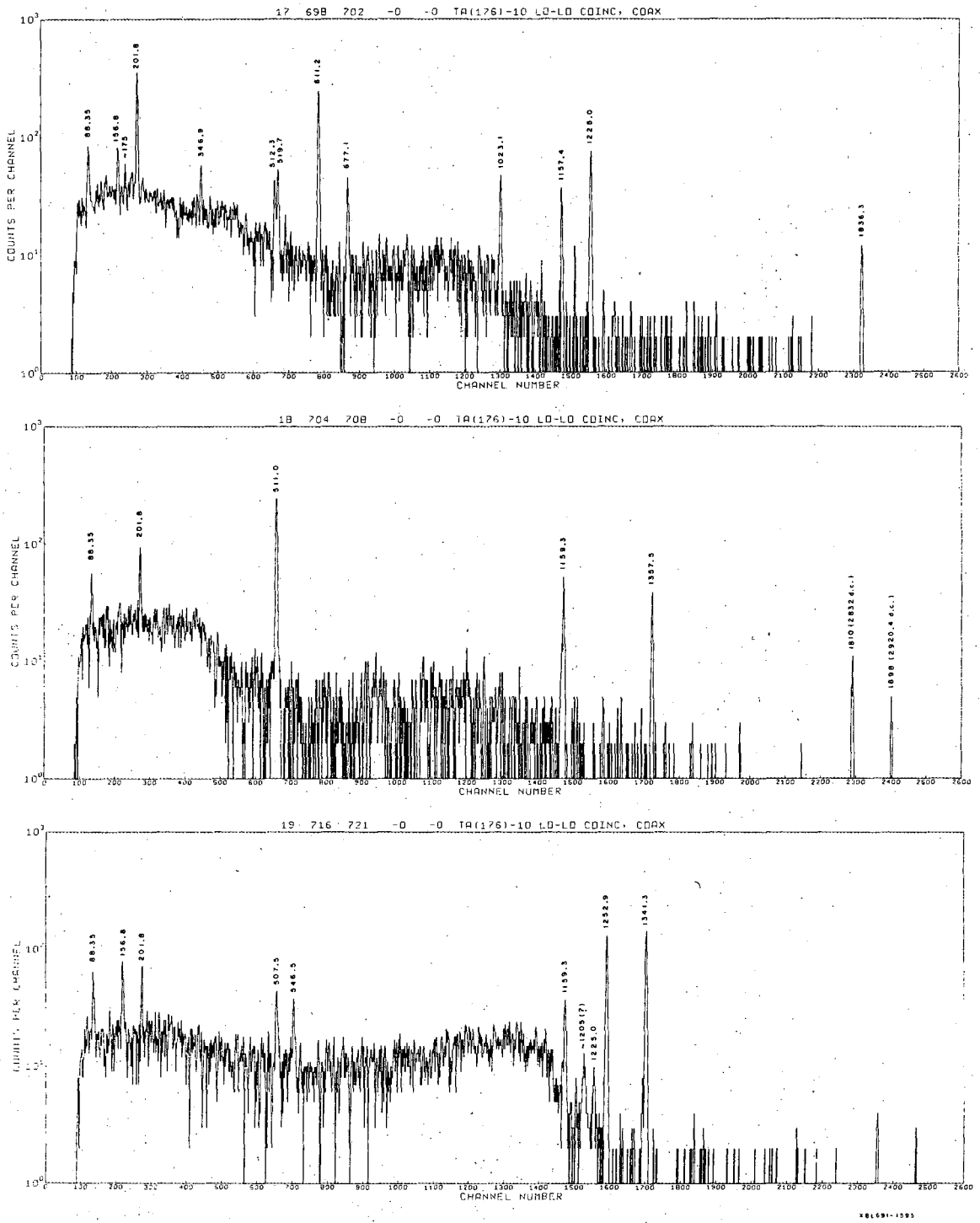

Fig. 55. (continued) The γ-γ coincidence spectra from Ta^{176} decay (90° geometry). Top: 507-keV; Middle: 512-keV; Bottom: 521-keV.

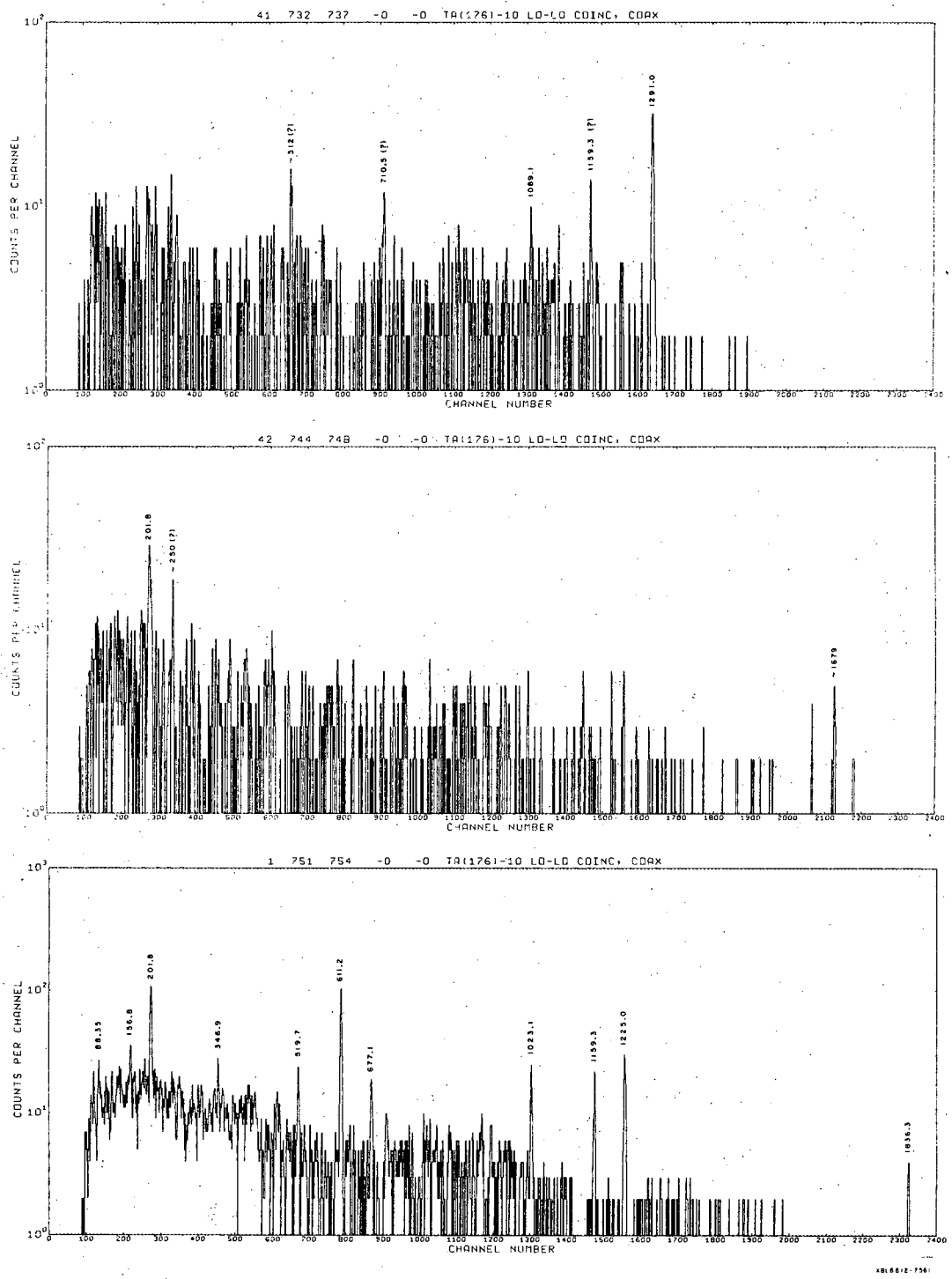

Fig. 55. (continued) The γ-γ coincidence spectra from Ta^{176} decay (90° geometry). Top: 533-keV; Middle: 542-keV; Bottom: 546-keV.

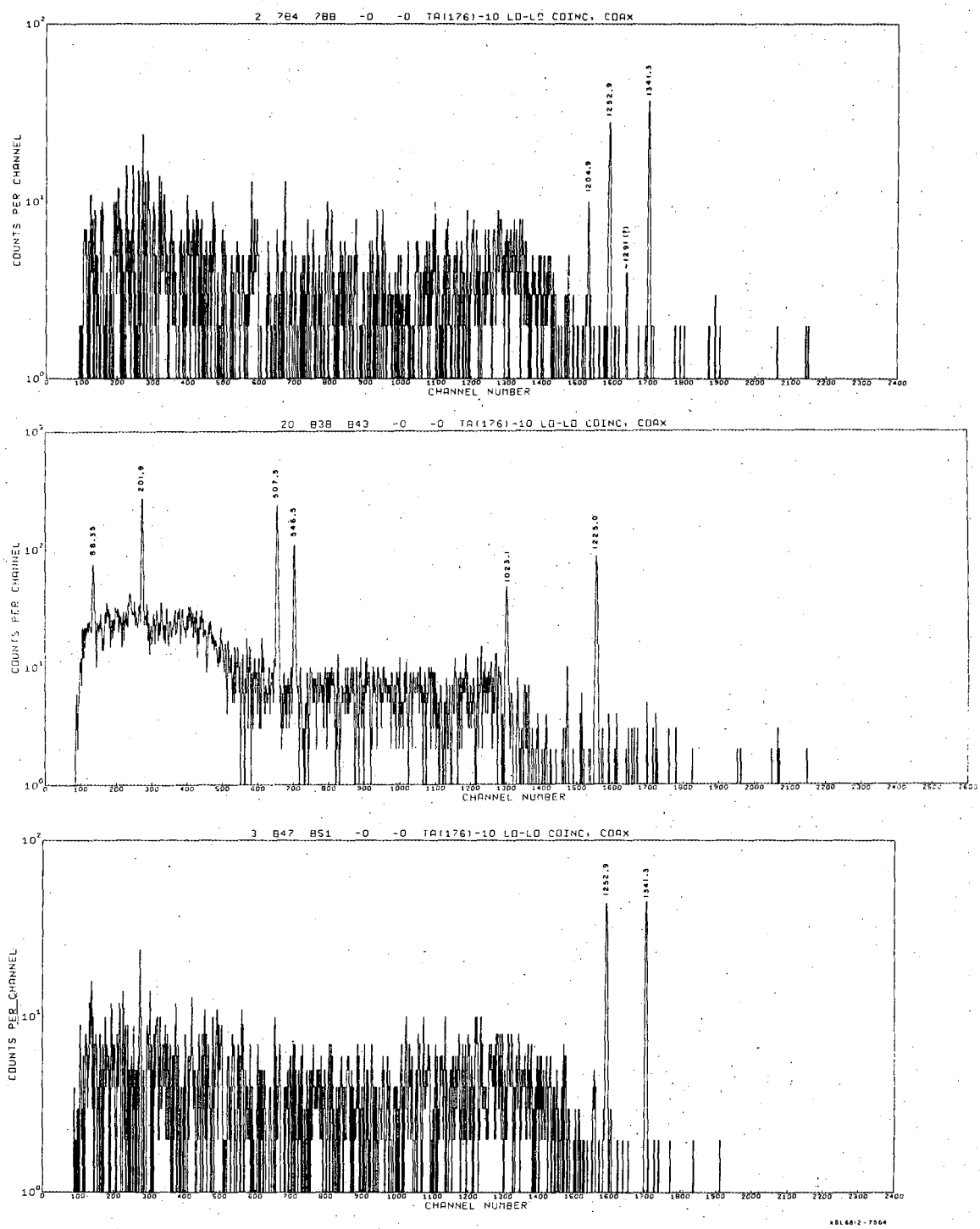

Fig. 55. (continued) The γ-γ coincidence spectra from Ta^{176} decay (90° geometry). Top: 570-keV; Middle: 611-keV; Bottom: 617-keV.

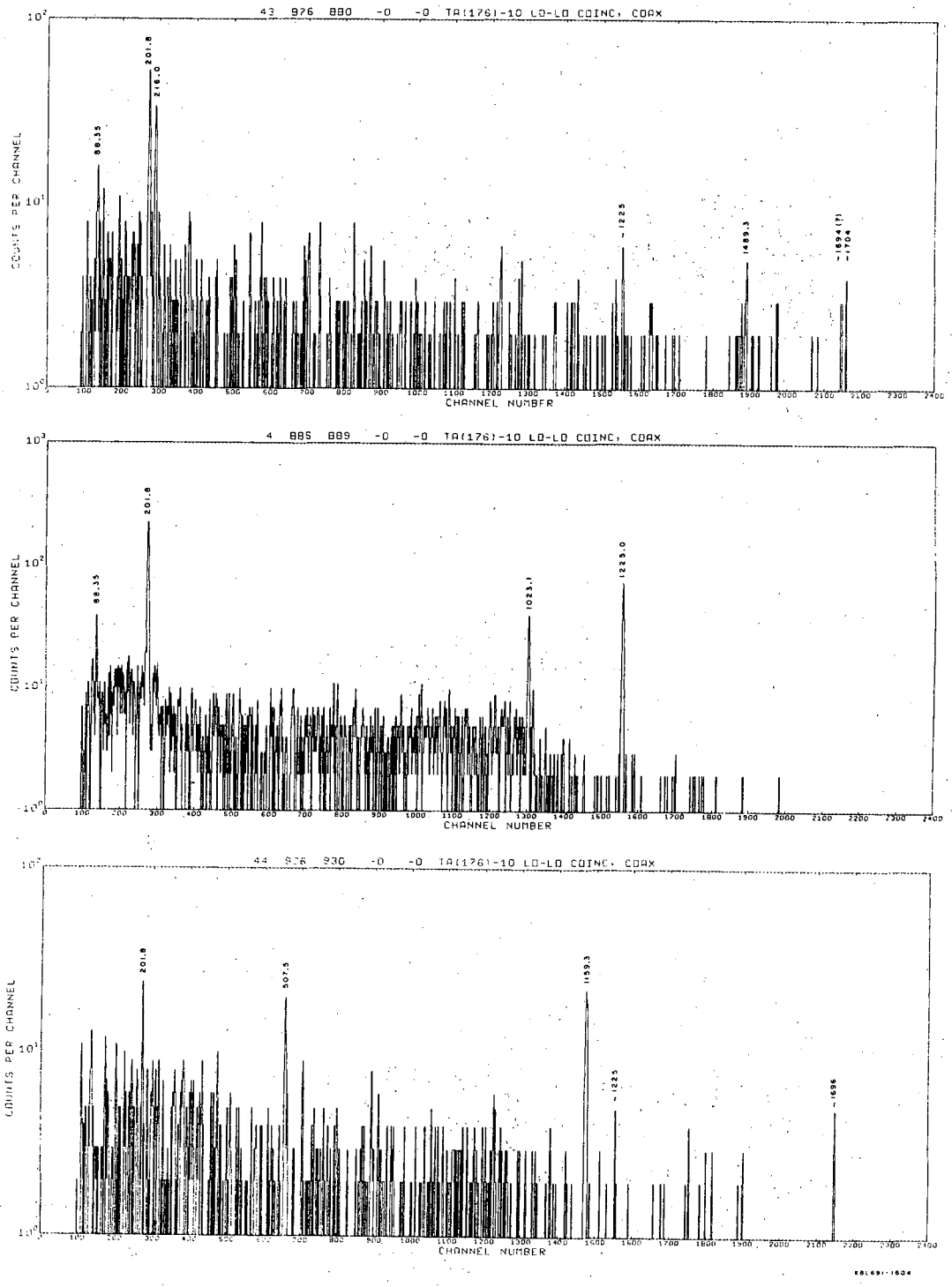

Fig. 55. (continued) The γ-γ coincidence spectra from Ta^{176} decay (90° geometry). Top: 639-keV; Middle: 645-keV; Bottom: 677-keV.

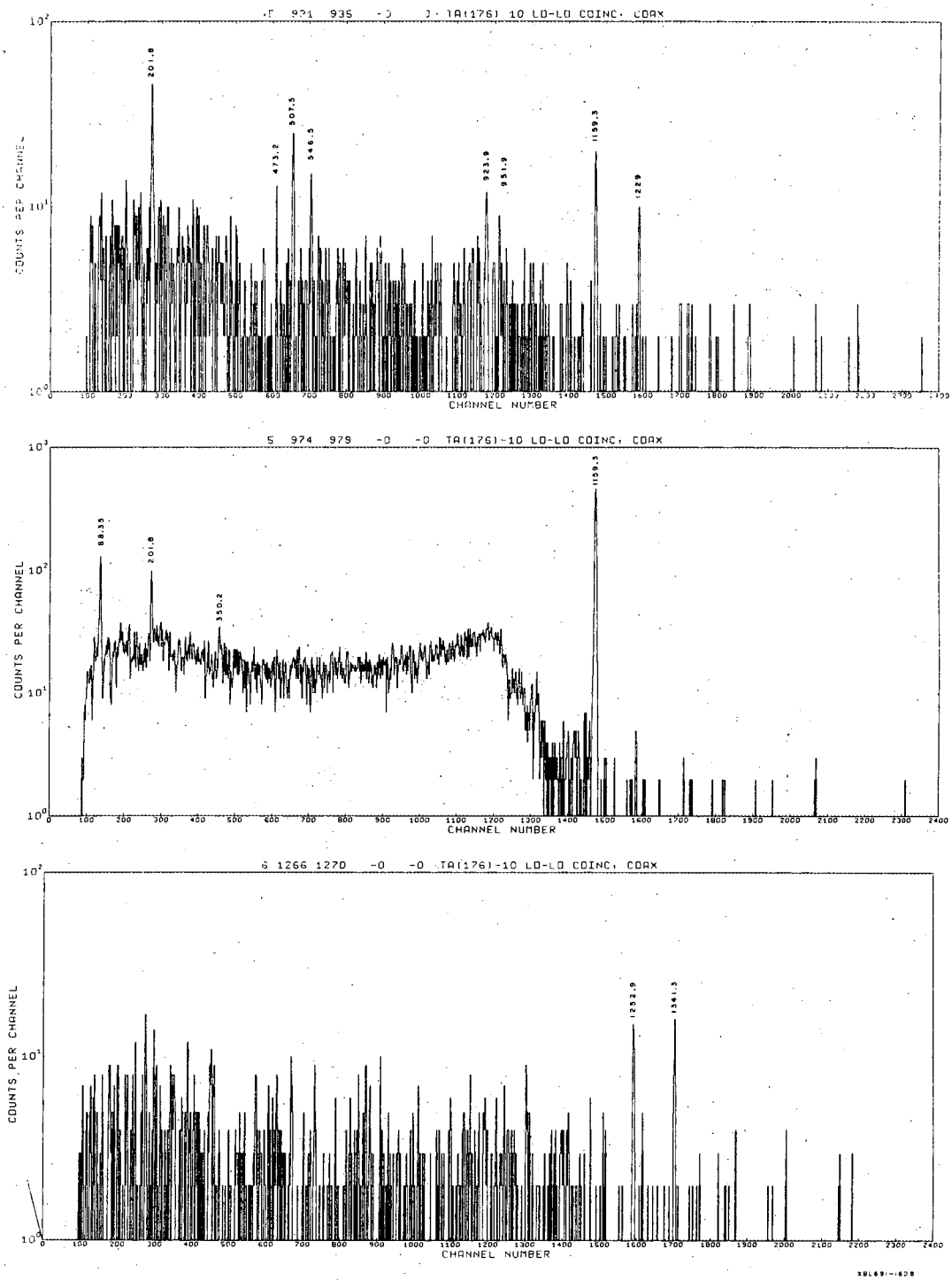

Fig. 55. (continued) The γ-γ coincidence spectra from Ta^{176} decay (90° geometry). Top: 679-keV; Middle: 710-keV; Bottom: 924-keV.

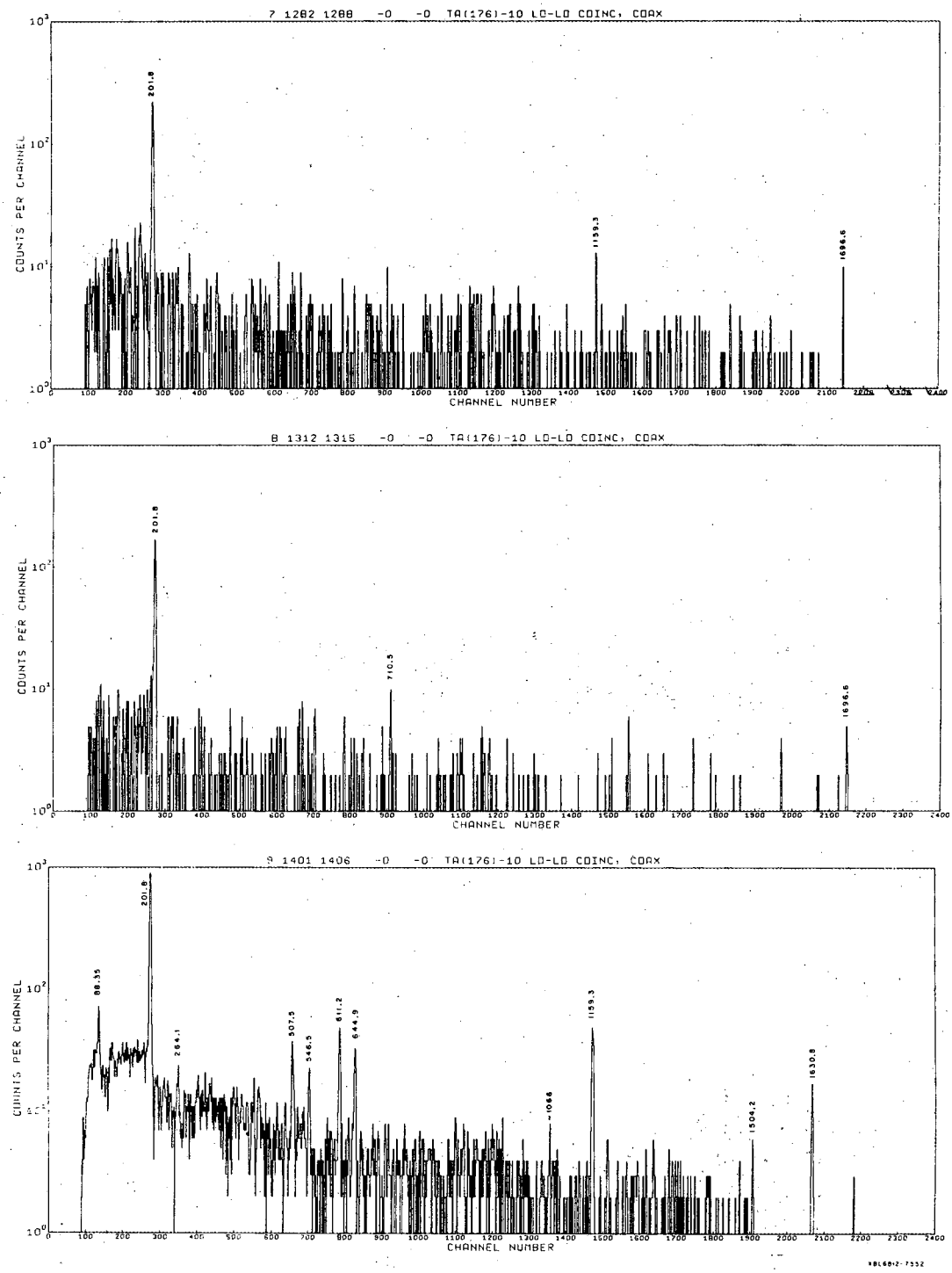

Fig. 55. (continued) The γ-γ coincidence spectra from Ta^{176} decay (90° geometry). Top: 936-keV; Middle: 957-keV; Bottom: 1023-keV.

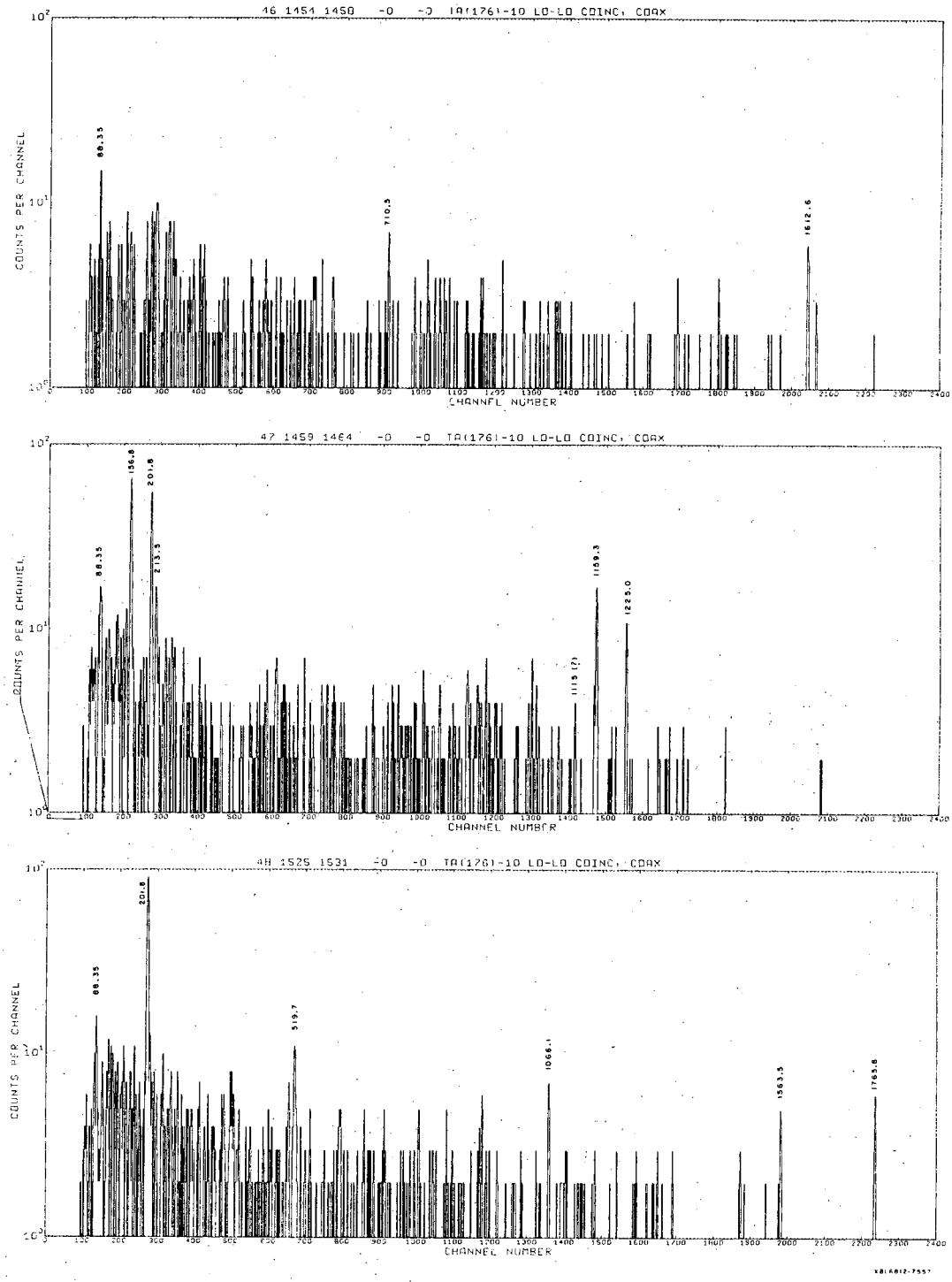

Fig. 55. (continued) The γ-γ coincidence spectra from Ta^{176} decay (90° geometry). Top: 1062-keV; Middle: 1066-keV; Bottom: 1115-keV.

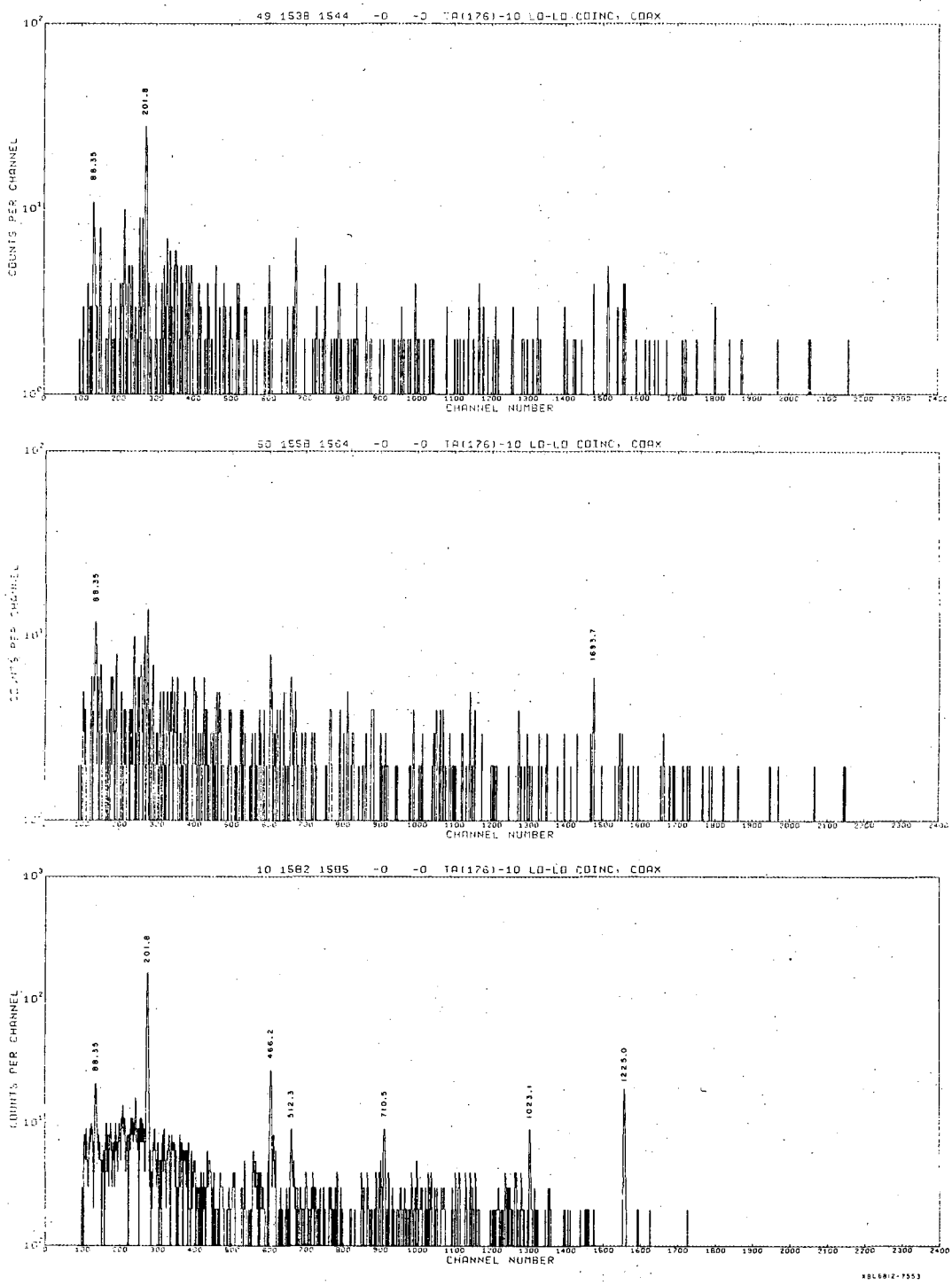

Fig. 55. (continued) The γ-γ coincidence spectra from Ta^{176} decay (90° geometry). Top: 1124-keV; Middle: 1138-keV; Bottom: 1155-keV.

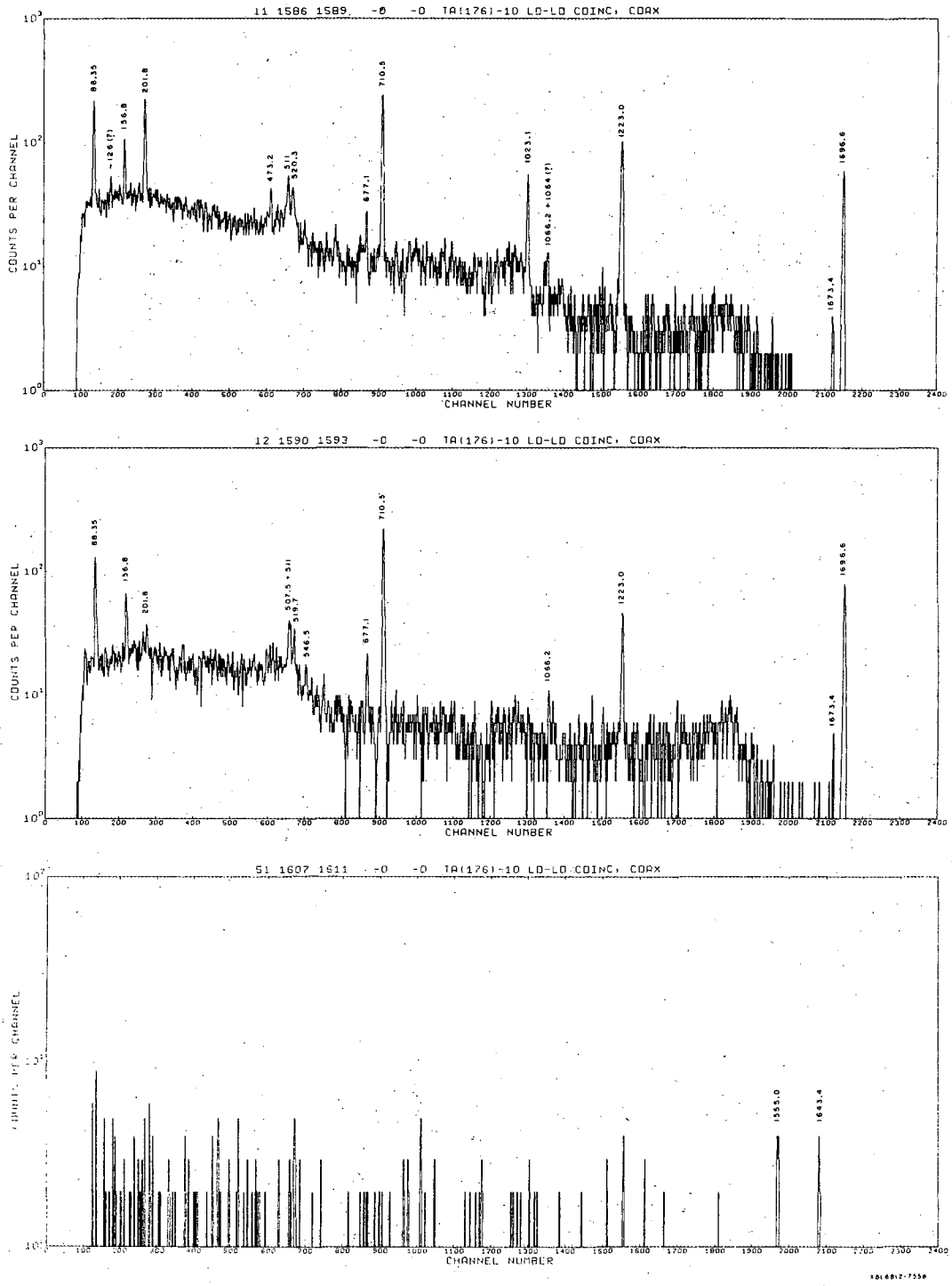

Fig. 55. (continued) The γ-γ coincidence spectra from Ta^{176} decay (90° geometry). Top: 1157 keV; Middle: 1159 keV; Bottom: 1174 keV.

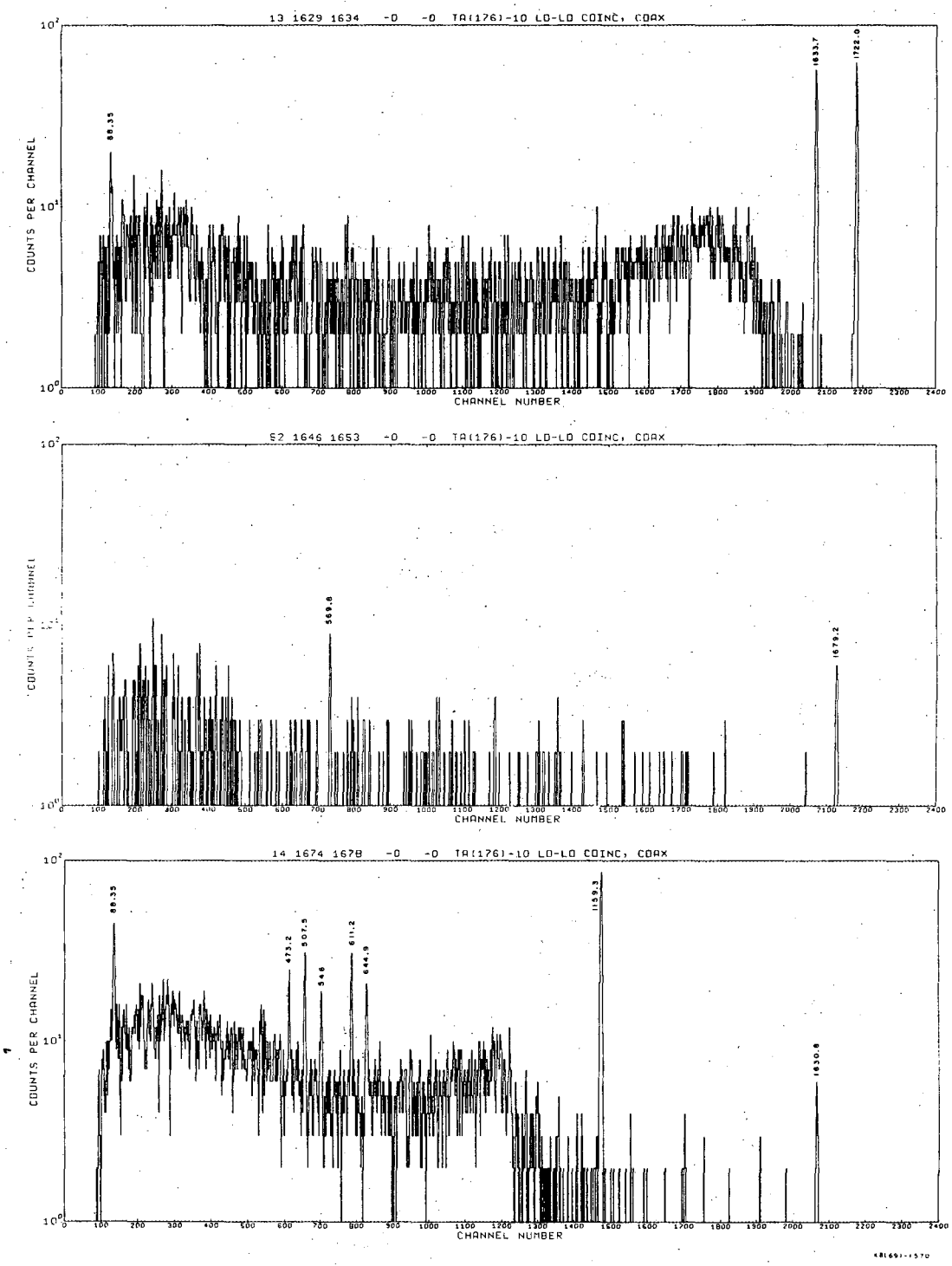

Fig. 55. (continued) The γ-γ coincidence spectra from Ta^{176} decay (90° geometry). Top: 1190-keV: Middle: 1203-keV; Bottom: 1223-keV.

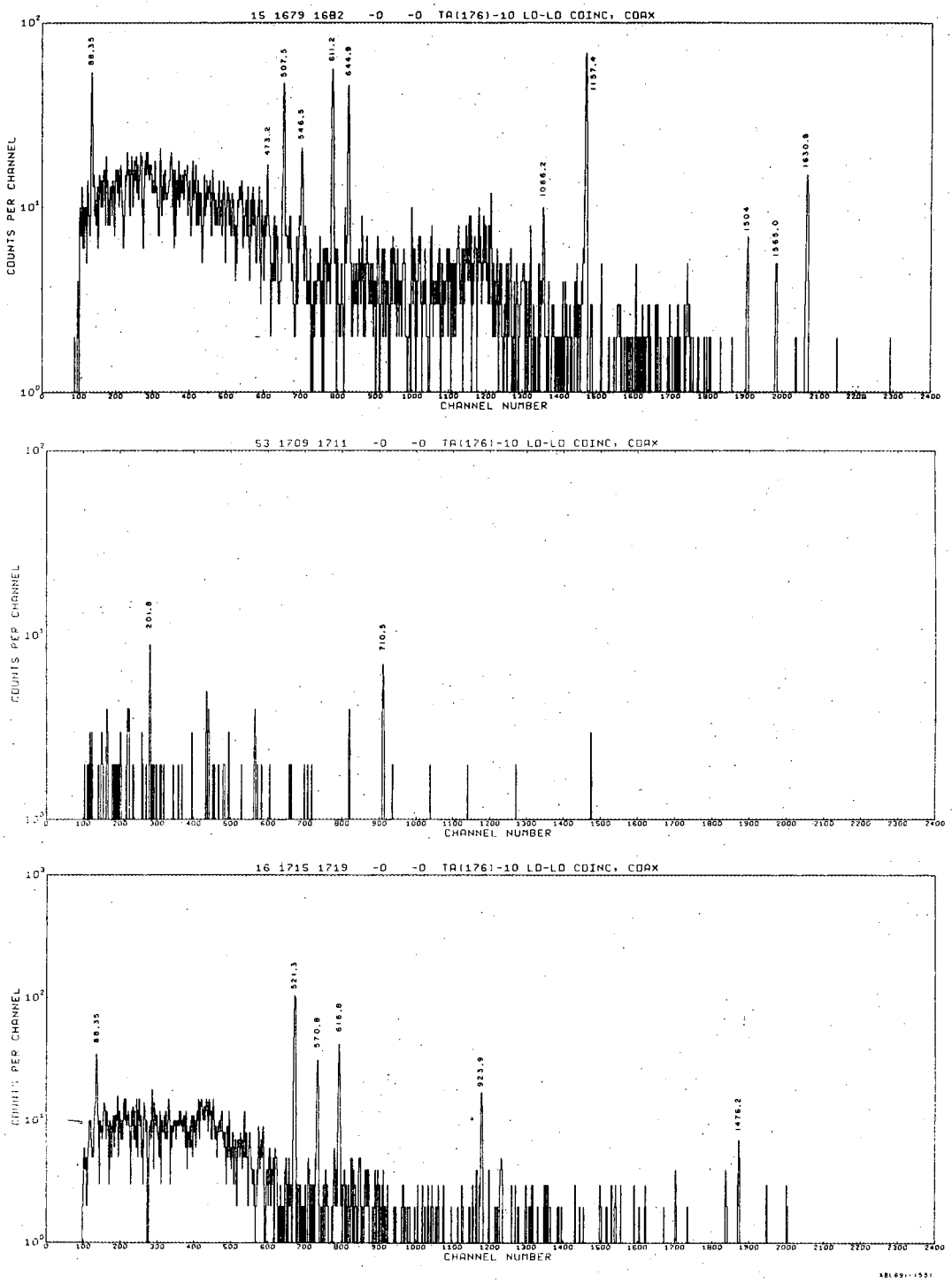

Fig. 55. (continued) The γ-γ coincidence spectra from Ta^{176} decay (90° geometry). Top: 1225-keV; Middle: 1248-keV; Bottom: 1253-keV.

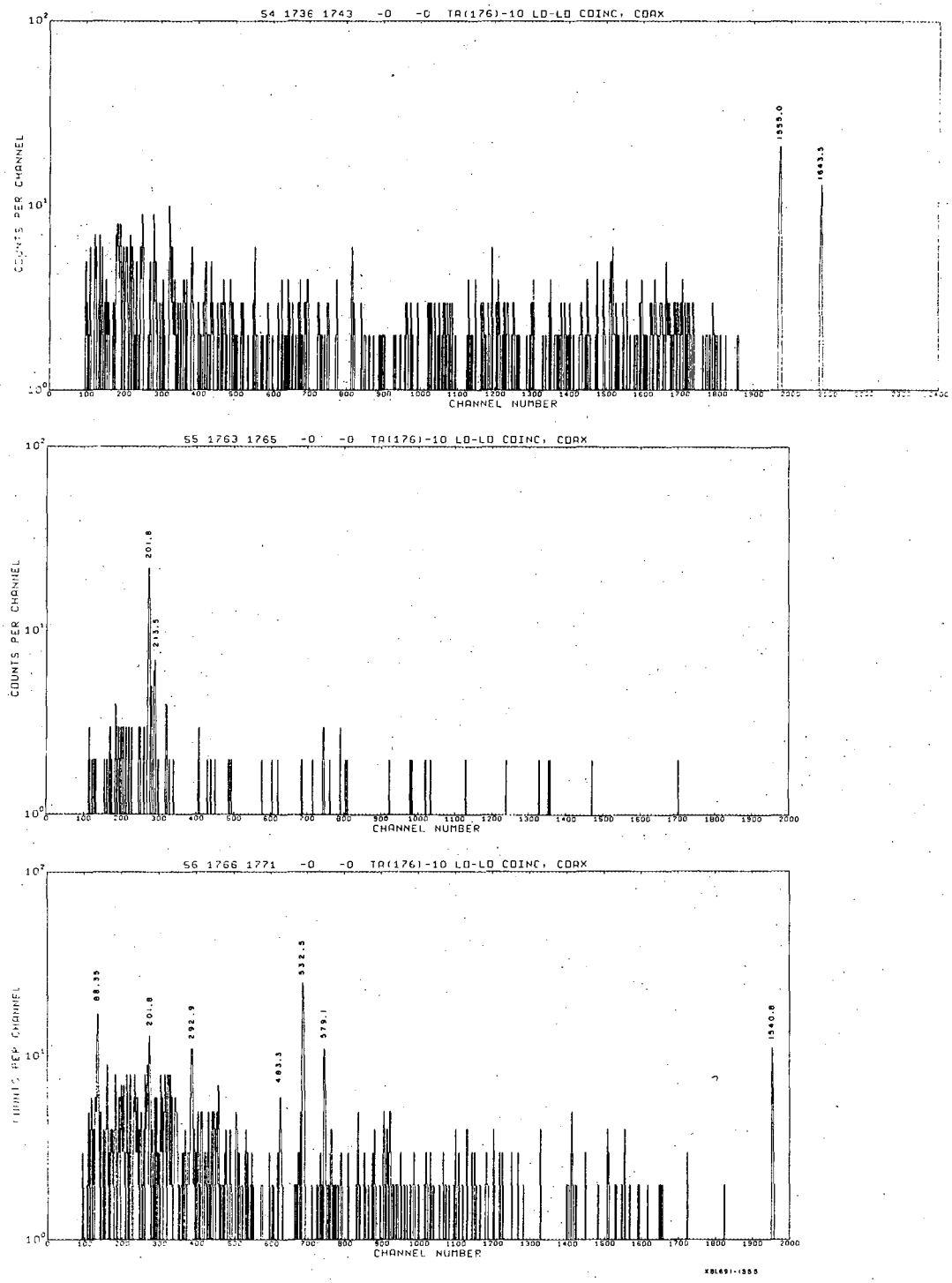

Fig. 55. (continued) The γ-γ coincidence spectra from Ta^{176} decay (90° geometry). Top: 1269-keV; Middle: 1287-keV; Bottom: 1291-keV.

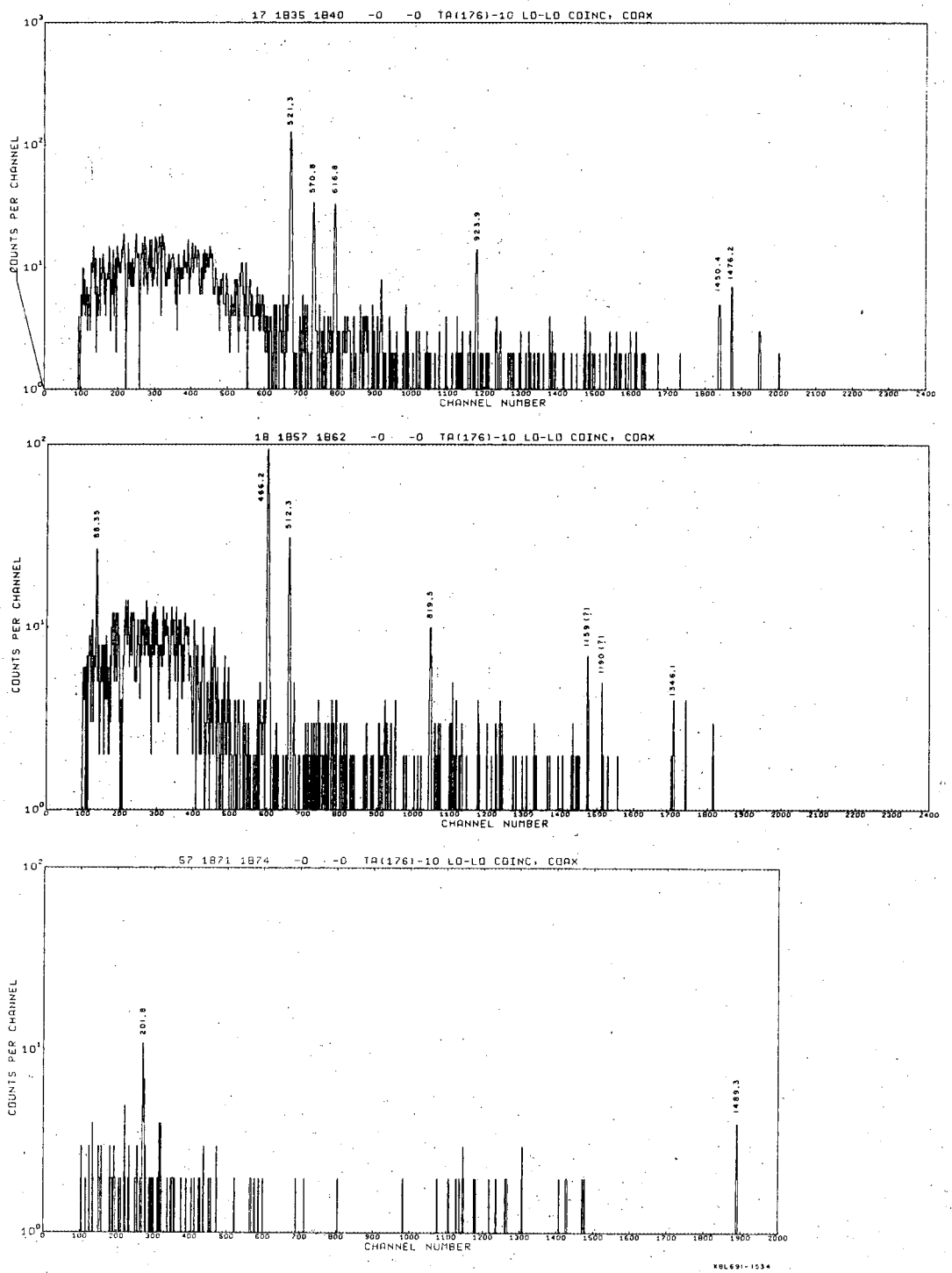

Fig. 55. (continued) The γ-γ coincidence spectra from Ta^{176} decay (90° geometry). Top: 1341-keV; Middle: 1358-keV; Bottom: 1366-keV.

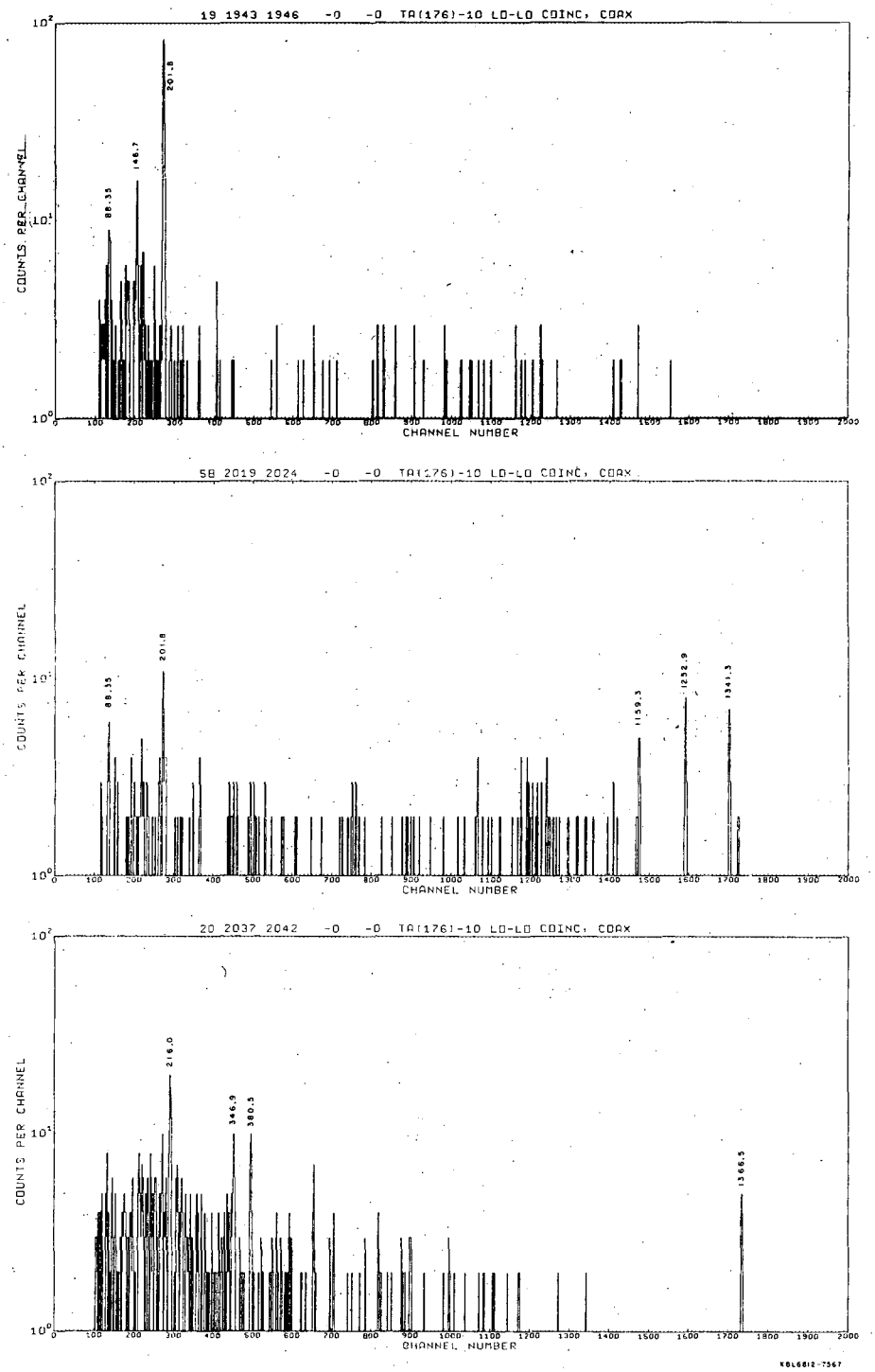

Fig. 55. (continued) The γ-γ coincidence spectra from Ta^{176} decay (90° geometry). Top: 1420-keV; Middle: 1476-keV; Bottom: 1489-keV.

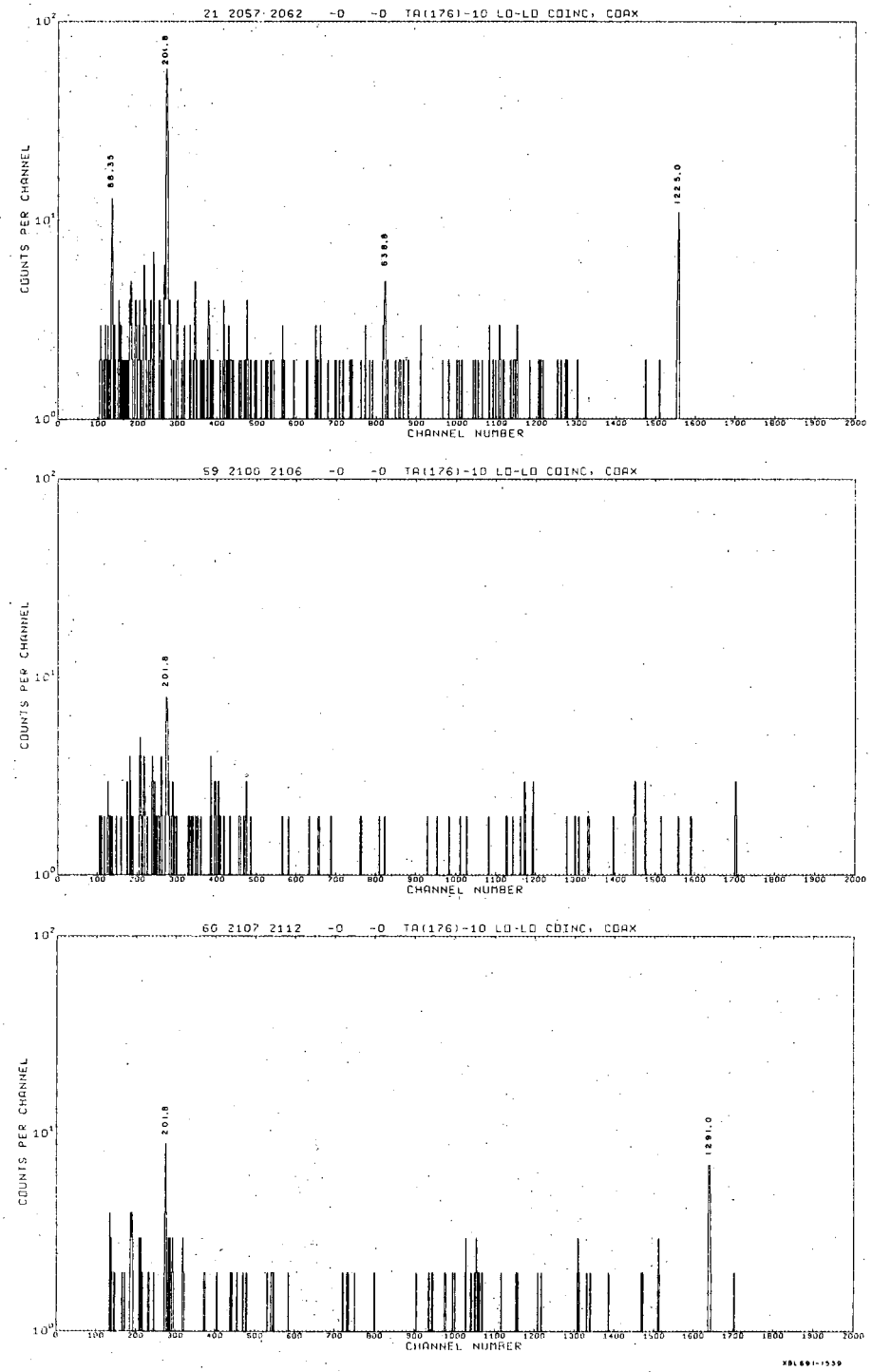

Fig. 55. (continued) The γ-γ coincidence spectra from Ta^{176} decay (90° geometry). Top: 1504-keV; Middle: 1537-keV; Bottom: 1541-keV.

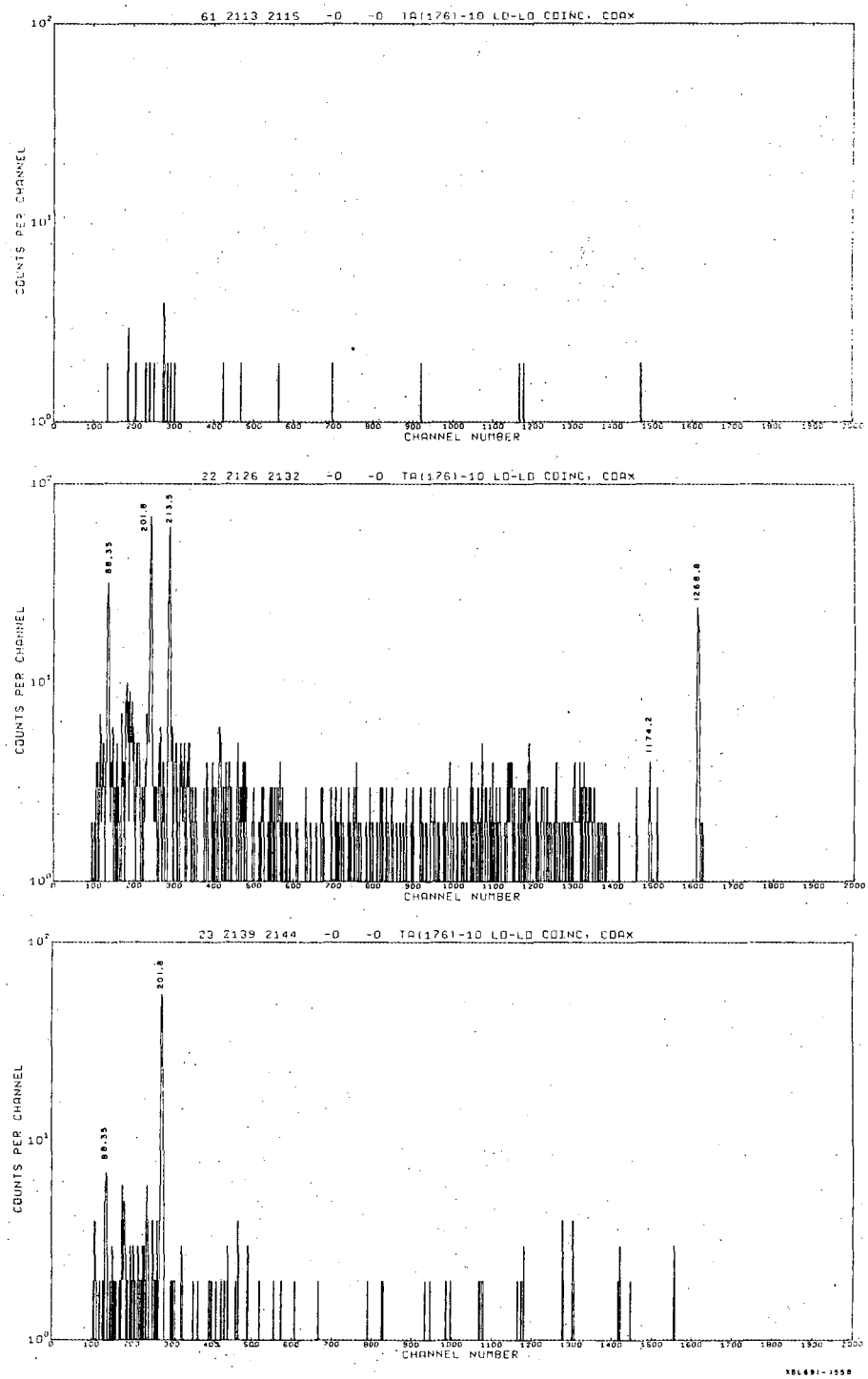

Fig. 55. (continued) The γ-γ coincidence spectra from Ta^{176} decay (90° geometry). Top: 1544-keV; Middle: 1555-keV; Bottom: 1564-keV.

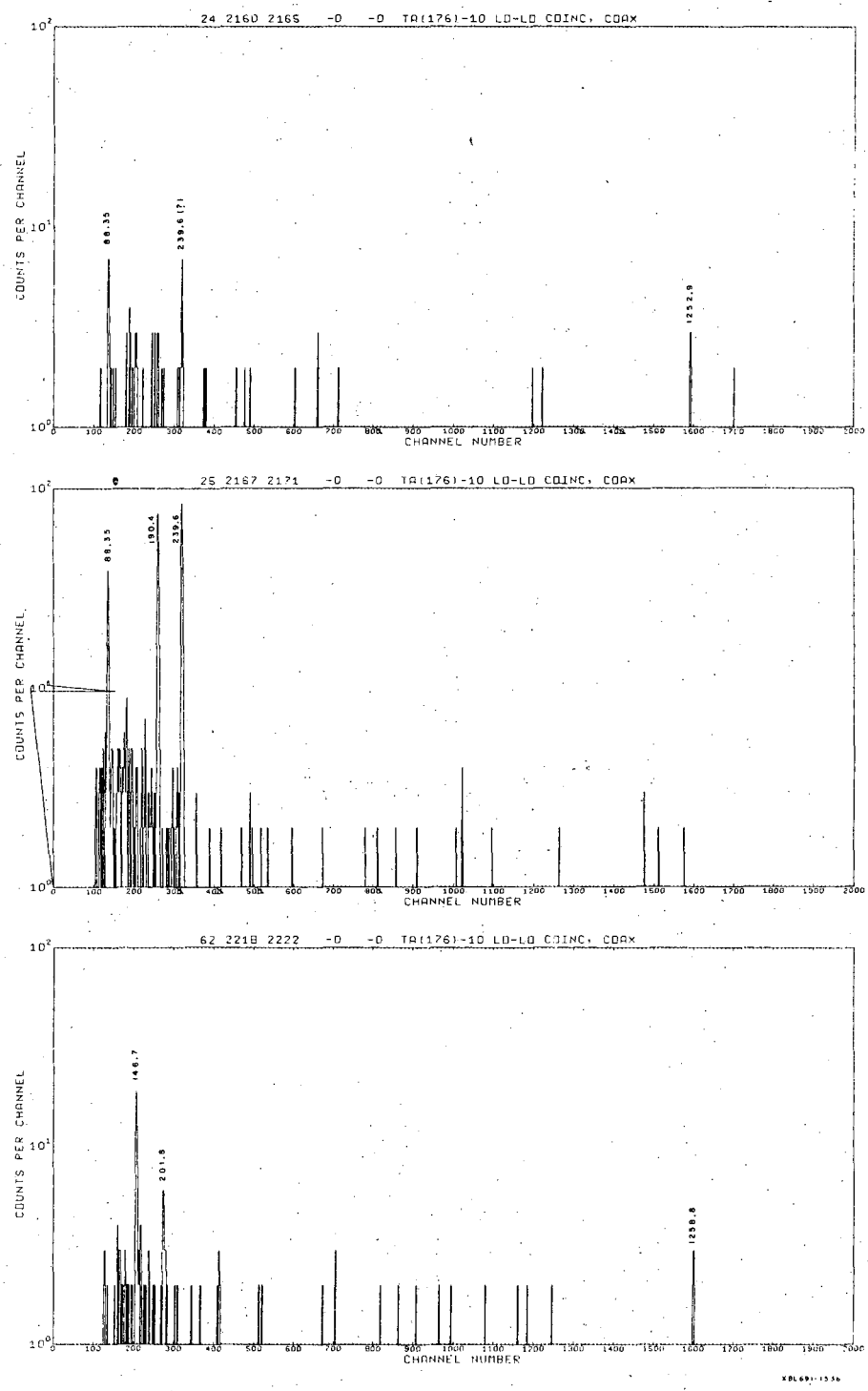

Fig. 55. (continued) The γ-γ coincidence spectra from Ta^{176} decay (90° geometry). Top: 1580-keV; Middle: 1584-keV; Bottom: 1622-keV.

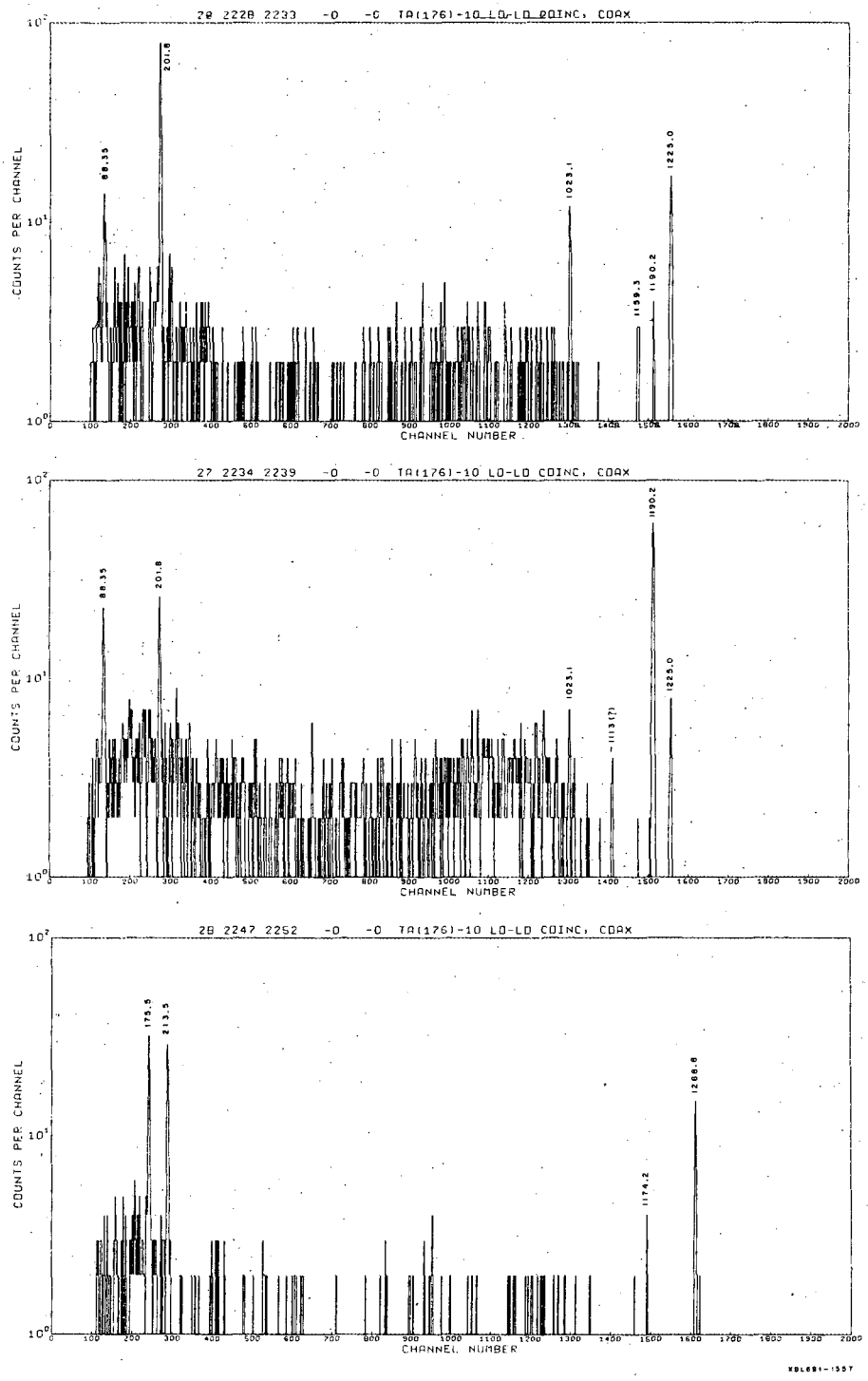

Fig. 55. (continued) The γ-γ coincidence spectra from Ta^{176} decay (90° geometry). Top: 1631-keV; Middle: 1634-keV; Bottom: 1643-keV.

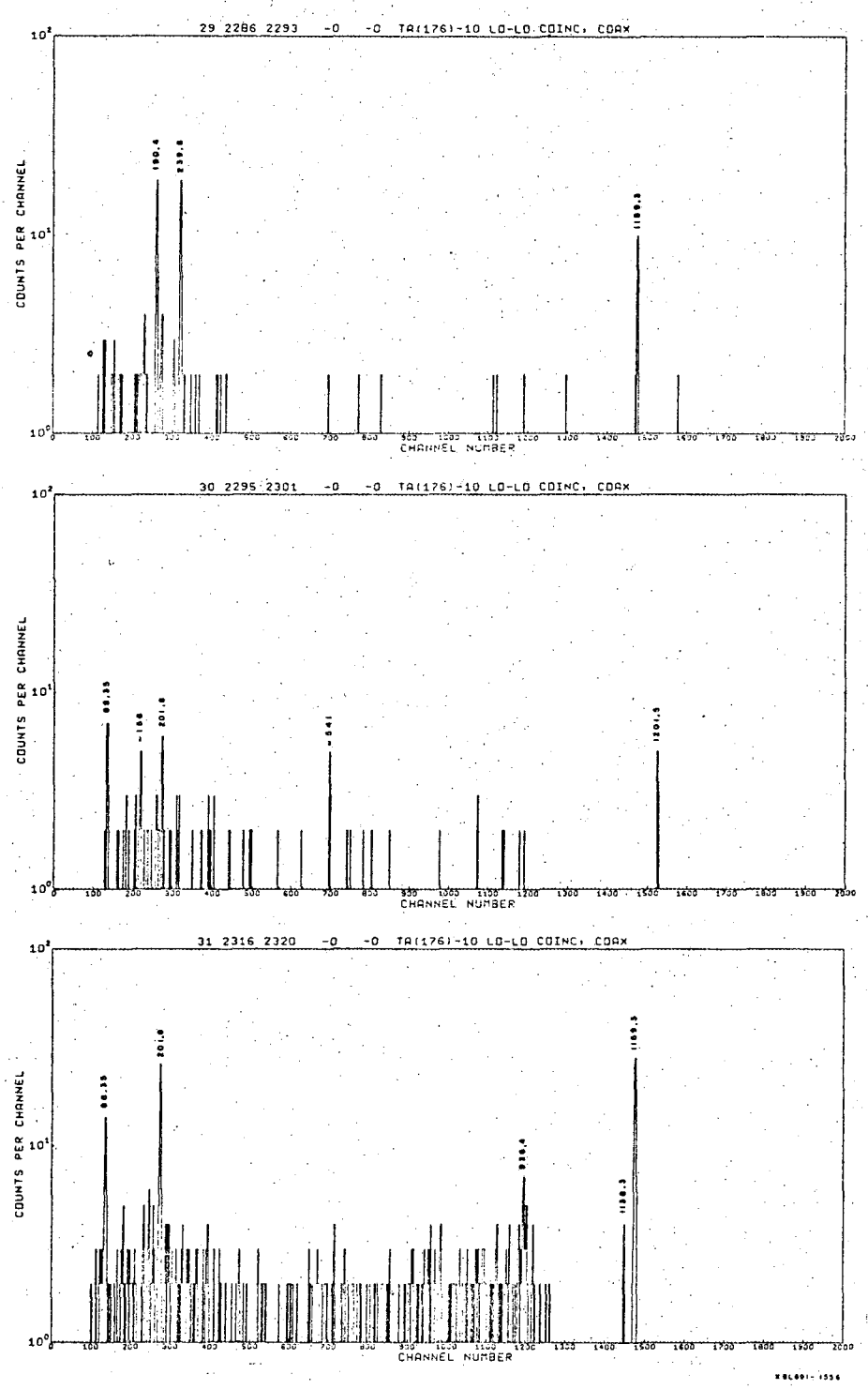

Fig. 55. (continued) The γ-γ coincidence spectra from Ta^{176} decay (90° geometry). Top: 1672-keV; Middle: 1679-keV; Bottom: 1694-keV.

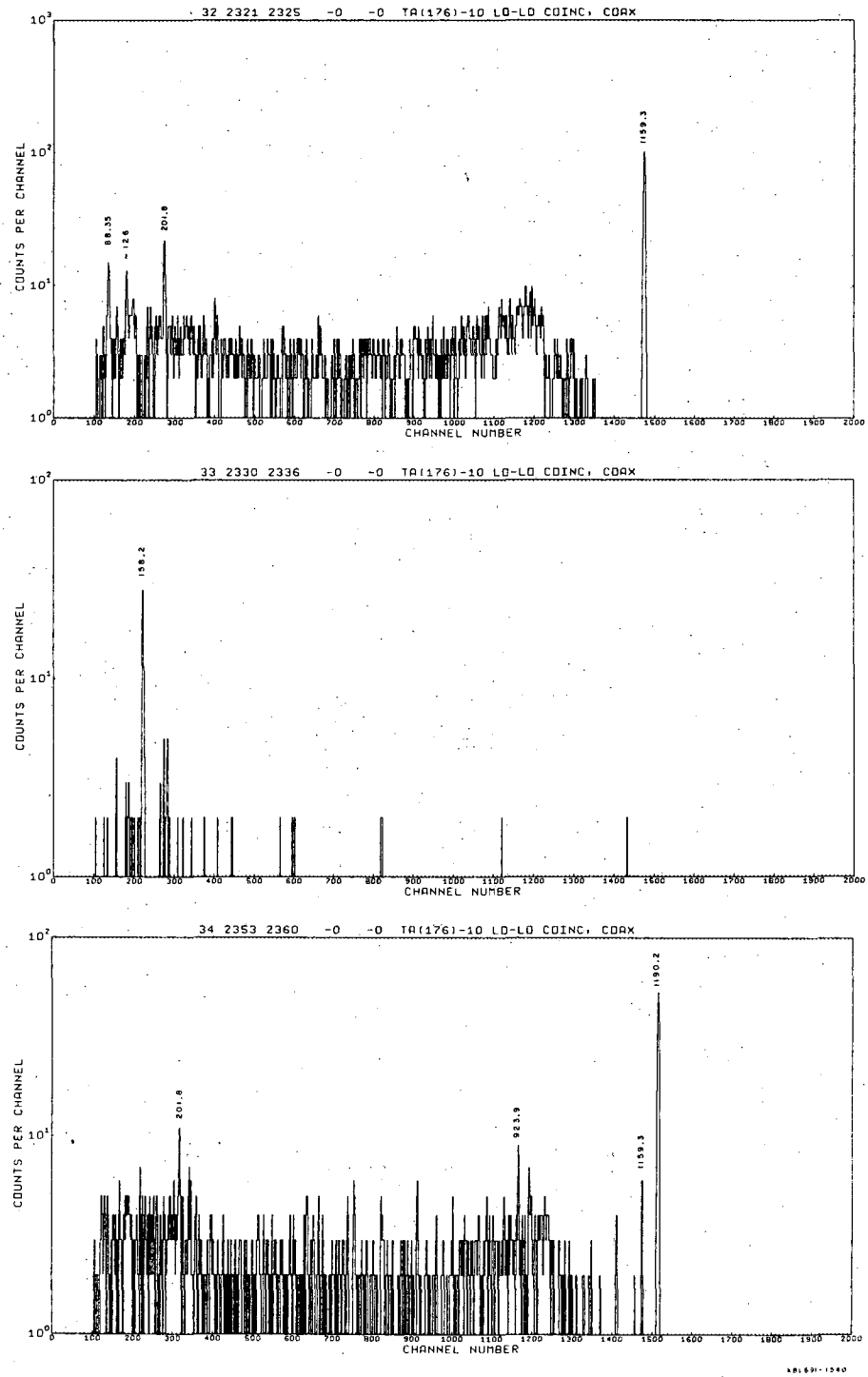

Fig. 55. (continued) The γ-γ coincidence spectra from Ta^{176} decay (90° geometry). Top: 1697-keV; Middle: 1705-keV; Bottom: 1722-keV.

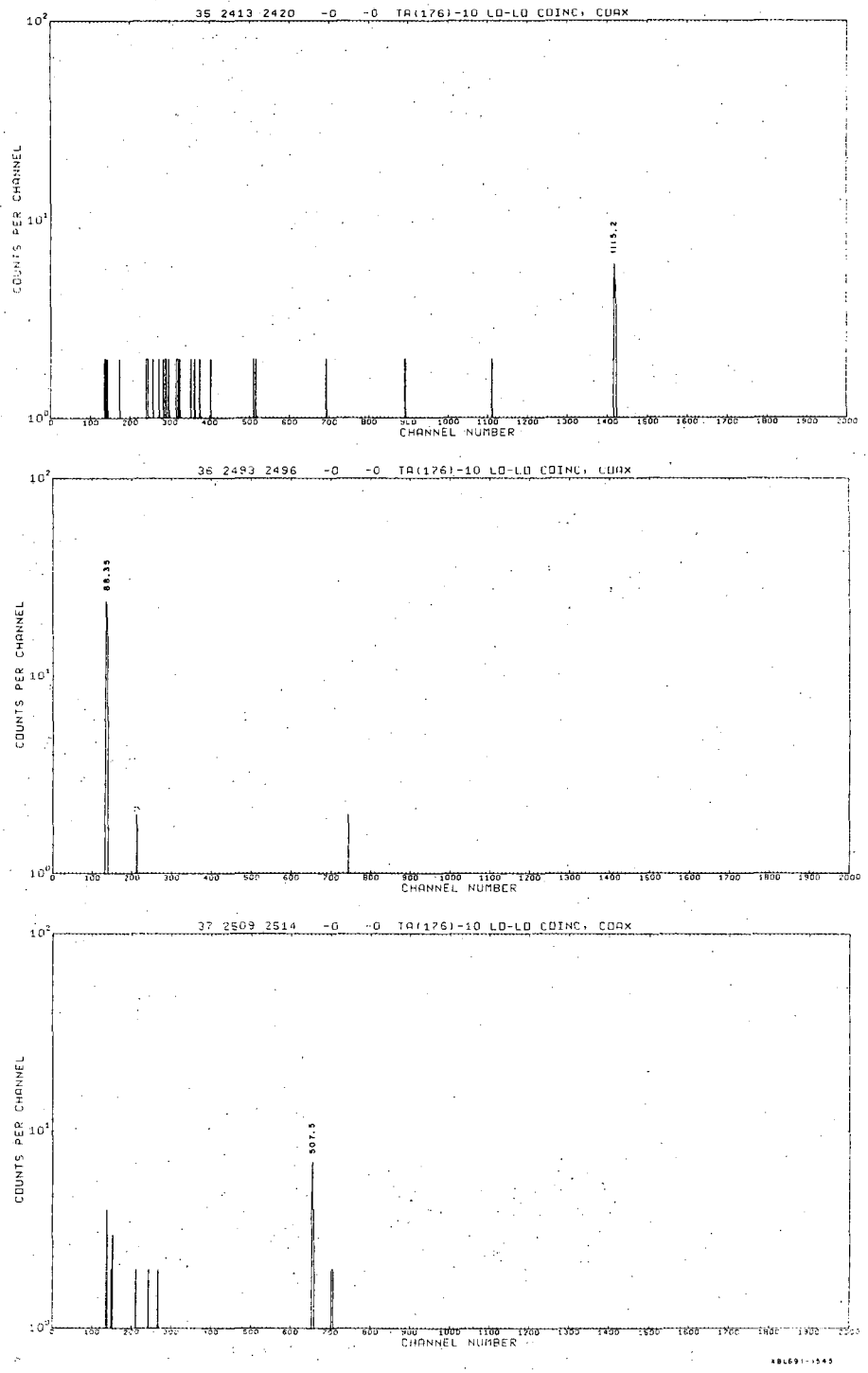

Fig. 55. (continued) The γ-γ coincidence spectra from Ta^{176} decay (90° geometry). Top: 1766-keV; Middle: 1824-keV; Bottom: 1836-keV.

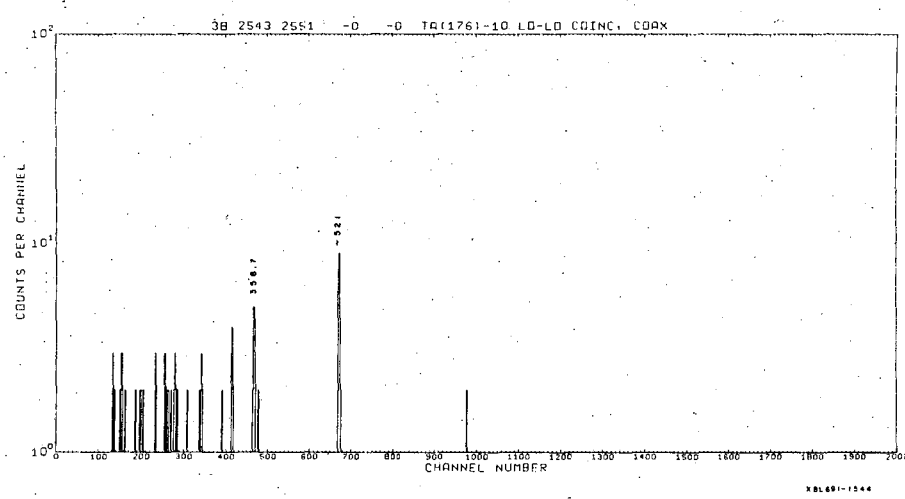

Fig. 55. (concluded) The γ-γ coincidence spectra from Ta^{176} decay (90° geometry). 1863-keV.

Table 21. Peak and background gates for the coincidence spectra, Figs. 55. The channels gated refer to Fig. 52.

Peak Gate Energy (keV)	Channels in Peak Gate	Channels in Bkgd. Gate	Peak Gate Energy (keV)	Channels in Peak Gate	Channels in Bkgd. Gate
88	134-137	141-144	677	926-930	937-941
126	184-187	195-198	679	931-935	937-941
147	212-215	216-219	710	974-979	980-985
156	224-226	221-223	924	1266-1270	1271-1275
158	227-229	221-223	936	1282-1288	1272-1278
175	249-252	241-244	957	1312-1315	1316-1319
190	268-271	273-276	1023	1401-1406	1407-1412
202	283-286	287-290	1062	1454-1458	1465-1469
207	291-294	295-298	1066	1459-1464	1465-1470
213	298-301	295-298	1115	1525-1531	1547-1553
216	302-305	295-298	1124	1538-1544	1547-1553
240	334-337	338-341	1138	1558-1564	1565-1571
264	367-369	375-377	1155	1582-1585	1594-1597
348	479-485	488-494	1157	1586-1589	1594-1597
436	600-604	595-599	1159	1590-1593	1594-1597
466	642-645	646-649	1174	1607-1611	1613-1617
474	652-655	656-659	1190	1629-1634	1635-1640
507	698-702	693-697	1203	1646-1653	1654-1661
512	704-708	709-713	1223	1674-1678	1683-1687
521	716-721	710-715	1225	1679-1682	1683-1686
533	732-737	758-763	1248	1709-1711	1720-1722
542	744-748	758-762	1253	1715-1719	1720-1724
546	751-754	755-758	1269	1736-1743	1745-1752
570	784-788	789-793	1287	1763-1765	1775-1777
611	838-843	832-837	1291	1766-1771	1773-1778
617	847-851	852-856	1341	1835-1840	1828-1833
639	876-880	871-875	1358	1857-1862	1863-1868
645	885-889	891-895	1366	1871-1874	1866-1869

(continued)

Table 21. Continued

Peak Gate Energy (keV)	Channels in peak Gate	Channels in Bkgd. Gate	Peak Gate Energy (keV)	Channels in Peak Gate	Channels in Bkgd. Gate
1420	1943-1946	1948-1951	1631	2228-2233	2240-2245
1476	2019-2024	2027-2032	1634	2234-2239	2240-2245
1489	2037-2042	2031-2036	1643	2247-2252	2253-2258
1504	2057-2062	2065-2070	1672	2286-2293	2303-2310
1537	2100-2106	2090-2096	1679	2295-2301	2303-2309
1541	2107-2112	2118-2123	1694	2316-2320	2326-2330
1544	2113-2115	2118-2120	1697	2321-2325	2326-2330
1555	2126-2132	2119-2125	1705	2330-2336	2338-2344
1564	2139-2144	2145-2150	1722	2353-2360	2361-2368
1580	2160-2165	2172-2177	1766	2413-2420	2402-2409
1584	2167-2171	2172-2176	1824	2493-2496	2498-2501
1622	2218-2222	2256-2260	1836	2509-2514	2516-2521
			1863	2543-2551	2552-2560

APPENDIX D

The Decay of 3.7-hour Lu^{176m} to Levels in Hf^{176}

A 3.7-hour isomer of Lu^{176} has been identified in previous work,[84] and was found to β^--decay essentially 100% to the ground and first excited states of Hf^{176} (cf. Fig. 15). The isomer has been tentatively assigned a spin and parity (1-).

However, scintillation spectroscopy carried out by Rezanka, et al.[148] indicated very weak β^--feeding to a Hf^{176} level proposed to lie at about 1.14 MeV. Weak γ-rays at 1.14 and 1.05 MeV were reported in this early work, and assumed to decay to the ground and first excited states of Hf^{176}.

It thus seemed reasonable to expect that Lu^{176m} decay feeds one or more of the low-lying levels previously deduced from Ta^{176} decay data, so we re-measured the γ-ray spectrum of Lu^{176m} in the region around 1 MeV.

Sources of Lu^{176m} were prepared by irradiating 99.94% samples of $Lu_2^{175}O_3$ with thermal neutrons ($\phi \approx 5 \times 10^{13}$ n/cm^2/sec) for periods of time ranging from 15 minutes to one-half hour. Because of the rapid growth of the Lu^{177} (6.8 day) activity, no chemistry was performed, so that the samples could be counted as soon as possible after the end of irradiation. An appropriate calibrated absorber was employed to attenuate the Hf X-rays and the very strong 88.35-keV γ-ray. (Pb was not used as an absorber because of the proximity of the Pb K_β X-rays to the 88.35-keV γ-ray.)

In Fig. 56 we show the spectrum of Lu^{176m} in the region 900 - 1300 keV taken with a 35 cm^3 Ge(Li) detector. The spectrum clearly indicates feeding to the 1150-, 1227-, 1248-, and 1293-keV levels in Hf^{176}. The weak unlabeled peaks are due to an unidentified longer-lived ($t_{1/2}$ > 5 hours) impurity. In Table 22 we list the relative intensities of the γ-rays observed from the decay of Lu^{176m}. The Lu^{176m} data support the level scheme earlier deduced from Ta^{176} decay data (cf. Fig. 34).

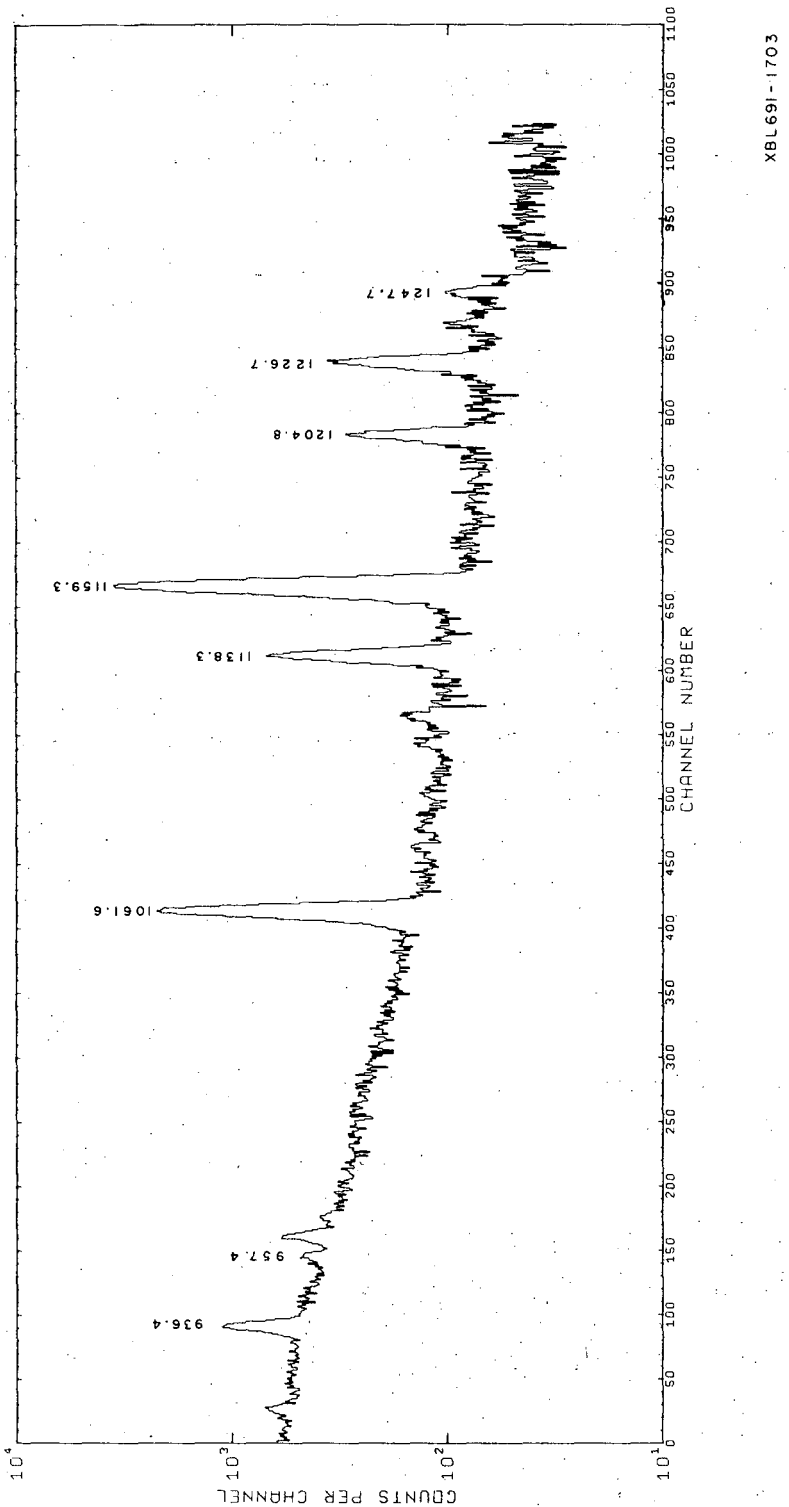

Fig. 56. High energy γ-ray singles spectrum from Lu^{176m} decay.

Table 22. Relative intensity of γ-rays from decay of Lu^{176m} to levels in Hf^{176}.

E_γ (keV)	Relative Intensity	Hf^{176} Level Assignment
88.35	$(1.2 \pm 0.2) \times 10^6$	88.35
936.4	13 ± 2	1226.6
957.4	2.0 ± 0.4	1247.7
1061.6	54 ± 5	1149.9
1138.3	15 ± 2	1226.6
1159.3	100 ± 8	1247.7
1204.8	6.0 ± 1.0	1293.2
1226.7	8.6 ± 1.2	1226.6
1247.7	1.1 ± 0.3	1247.7

REFERENCES

1. V. Weisskopf, Phys. Rev. 83, 1073 (1951).
2. C. F. Perdrisat, Rev. Mod. Phys. 38, 41 (1966).
3. M. G. Mayer, J. H. Jensen, Elementary Theory of Nuclear Shell Structure, New York, (1955).
4. A. Bohr, K. Danske Vidensk. Selsk. Mat. -fys. Medd. 26, No. 14 (1952).
5. A. Bohr and B. R. Mottelson, K. Danske Vidensk. Selsk. Mat. -fys. Medd. 27, No. 16 (2nd edition, 1957).
6. A. K. Kerman, K. Danske Vidensk. Selsk. Mat. -fys. Medd. 30, No. 15 (1956).
7. S. G. Nilsson, K. Danske Vidensk. Selsk. Mat. -fys. Medd. 29, No. 16 (1955).
8. A. J. Rassey, Phys. Rev. 109, 949 (1958).
9. C. Gustafson, I. L. Lamm, B. Nilsson, and S. G. Nilsson, Arkiv für Fysik 36, 613 (1966).
10. E. E. Berlovich, Bull. Acad. Sci. U.S.S.R., Phys. Ser. (trans) 29, 841 (1965).
11. G. Alaga, Nucl. Phys. 4, 625 (1957).
12. D. Strominger and J. O. Rasmussen, Nucl. Phys. 3, 197 (1957).
13. Yu. T. Grin and I. M. Pavlichenkov, Nucl. Phys. 65, 686 (1965).
14. M. N. Vergnes and J. O. Rasmussen, Nucl. Phys. 62, 233 (1965).
15. M. N. Vergnes, Nucl. Phys. 39, 273 (1962).
16. J. W. Bichard, J. W. Mihelich, and B. Harmatz, Phys. Rev. 116, 720 (1959).

17. G. Alaga, K. Alder, A. Bohr, and B. R. Mottelson, K. Danske Vidensk. Selsk. Mat. -fys. Medd. 29, No. 9 (1955).

18. F. M. Bernthal and J. O. Rasmussen, Nucl. Phys. A101, 513 (1967).

19. P. Alexander, F. Boehm and E. Kankeleit, Phys. Rev. 133, B284 (1964).

20. A. J. Haverfield, F. M. Bernthal, and J. M. Hollander, Nucl. Phys. A94, 337 (1967).

21. E. Bodenstedt et al., Zeit. für Phys. 190, 60 (1966).

22. D. R. Nethaway and B. Mendoza, J. Inorg. Nucl. Chem. 29, 865 (1967).

23. E. E. Berlovich, Yu. K. Gusev, V. V. Il'in, and M. K. Nikitin, Journ. Exp. and Theor. Phys. U.S.S.R. (trans) 43, 1625 (1962).

24. H. I. West, Jr., L. G. Mann, and R. J. Nagle, Phys. Rev. 124, 527 (1961).

25. T. C. Clements, privately circulated report, Lawrence Radiation Laboratory (1966).

26. F. A. Rickey, Jr., and R. K. Sheline, Phys. Rev. 170, 1157 (1968).

27. S. G. Nilsson and O. Prior, K. Danske Vidensk. Selsk. Mat. -fys. Medd., 32, No. 16 (1961).

28. M. Y. M. Hassan, Z. Skladanowski, and Z. Szymanski, Nucl. Phys. 78, 593 (1966).

29. C. F. Tsang and W. J. Swiatecki, private communication of results to be submitted to Nucl. Phys.; see also S. G. Nilsson, Lawrence Radiation Laboratory Report UCRL-18355-Rev. (1968).

30. W. D. Myers and W. J. Swiatecki, Nucl. Phys. 81, 1 (1966).

31. C. W. Ma, private communication (1968).

32. B. Elbek, M. C. Olesen, and O. Skilbreid, Nucl. Phys. 40, 294 (1959).

33. A. Bohr and B. R. Mottelson, monograph distributed at LRL (1966), to be published.

34. W. Donner and W. Greiner, Z. Phys. 197, 440 (1966).

35. A. Faessler and A. Plastino, Nucl. Phys. A94, 580 (1967).

36. P. Vogel, Nucl. Phys. A112, 583 (1968).

37. G. Monsonego and R. Piepenbring, Nucl. Phys. 78, 265 (1966).

38. A. Faessler, T. Udagawa and R. K. Sheline, Nucl. Phys. 85, 670 (1966).

39. J. Bardeen, L. N. Cooper, and J. R. Schrieffer, Phys. Rev. 108, 1175 (1957).

40. N. N. Bogolyubov, J. Exp. Theor. Phys. U.S.S.R. 34, 58 and 73 (1958); Nuovo Cimento 7, 794 (1958).

41. S. T. Belyaev, K. Danske Vidensk. Selsk. Mat. -fys. Medd. 31, No. 11 (1959).

42. L. S. Kisslinger and R. A. Sorensen, Rev. Mod. Phys. 35, 853 (1963).

43. Yu. T. Grin, J. Exp. Theor. Phys. (U.S.S.R.) 12, 100 (1960).

44. M. G. Urin, J. Exp. Theor. Phys. (U.S.S.R.) 11, 1331 (1960).

45. V. G. Soloviev, K. Danske Vidensk. Selsk. Mat. -fys. Skr. 1, No. 11 (1961).

46. E. E. Berlovich, W. Meyling, and V. K. Tarasov, Bull. Acad. Sci. U.S.S.R., Phys. Ser. (trans) 29, 849 (1965).

47. O. G. Gadetskii and N. I. Pyatov, Bull. Acad. Sci. U.S.S.R., Phys. Ser. (trans) 29, 833 (1965).

48. H. Ikegami and T. Udagawa, Phys. Rev. 133, B1388 (1964).

49. M. Yamada and Z. Matsumoto, J. Phys. Soc. Japan 16, 1497 (1961).

50. D. R. Bes, K. Danske Vidensk. Selsk. Mat. -fys. Medd. 33, No. 2 (1961).

51. D. R. Bes, Nucl. Phys. 49, 544 (1963).

52. D. R. Bes, P. Federman, E. Magueda, and A. Zuker, Nucl. Phys. 65, 1 (1965).

53. E. R. Marshalek and J. O. Rasmussen, Nucl. Phys. 43, 438 (1963).

54. D. R. Bes and Cho Yi-chung, Nucl. Phys. 86, 581 (1966).

55. R. F. Christy, private communication acknowledged by K. Alder, A. Bohr, T. Huus, B. R. Mottelson, and A. Winther, Rev. Mod. Phys. 28, 432 (1956).

56. F. Asaro, F. S. Stephens, Jr., and I. Perlman, Phys. Rev. 92, 1495 (1953).

57. F. S. Stephens, Jr., F. Asaro and I. Perlman, Phys. Rev. 96, 1568 (1954); 100, 1543 (1955); 107, 1091 (1957).

58. P. O. Lipas and J. P. Davidson, Nucl. Phys. 26, 80 (1961).

59. D. P. Leper, Nucl. Phys. 50, 234 (1964).

60. P. O. Lipas, K. Kurki-Suonio, and E. Peltola, Nucl. Phys. A110, 211 (1968).

61. V. G. Soloviev, Atomic Energy Rev. 3, 117 (1965); JINR preprint P-1973 (1965).

62. V. G. Soloviev and P. Vogel, JINR-E-2561 (1966); see also Soloviev, Vogel, and G. Jungclaussen, Bull. Acad. Sci. U.S.S.R., Phys. Ser. (trans) 31, 515 (1967).

63. L. A. Malov and V. G. Soloviev, Sov. J. Nucl. Phys. (trans) 5, 403 (1967).

64. M. Danos and W. Greiner, Phys. Rev. B134, 284 (1964).

65. H. Arenhövel, M. Danos, and W. Greiner, Phys. Rev. 157, 1109 (1967).

66. V. Strutinski, J. Nucl. Energy 4, 523 (1957).

67. A. Bohr and B. R. Mottelson, Nucl. Phys. 4, 529 (1957); 9, 687 (1958).

68. P. O. Lipas, Nucl. Phys. 40, 629 (1963).

69. R. Piepenbring, thesis, University of Strassbourg (1966); G. Monsonego and R. Piepenbring, Phys. Lett. 21, 180 (1966).

70. A. Faessler, W. Greiner, and R. K. Sheline, TID-20875 (1964).

71. K. Y. Chan and J. G. Valatin, Nucl. Phys. 82, 222 (1966).

72. J. O. Rasmussen and C. W. Ma, Z. Phys. 202, 182 (1967).

73. B. L. Andersen, Nucl. Phys. A112, 443 (1968).

74. S. G. Nilsson, private communication (1967). The wave functions are those used to obtain the results reported in Ref. 9.

75. F. S. Stephens, M. D. Holtz, R. M. Diamond, and J. O. Newton, Nucl. Phys. A115, 129 (1968).

76. R. Bloch, B. Elbek, and P. O. Tjøm, Nucl. Phys. A91, 576 (1967).

77. T. Grutdal, K. Nybø, and T. Thorsteinsen, Nucl. Phys. A110, 385 (1968).

78. P. Tjøm and B. Elbek, Nucl. Phys. A107, 385 (1968).

79. A. J. Haverfield, (Ph.D. Thesis), UCRL-16969, 1966 (unpublished).

80. J. M. Hollander, Nucl. Instr. and Meth. 43, 65 (1966).

81. B. Harmatz, T. H. Handley, and J. W. Mihelich, Phys. Rev. 119, 1345 (1960).

82. H. Verheul, H. M. W. Booy, J. G. R. Okel, and J. Blok, Nucl. Phys. 42, 551 (1963).

83. A. Hashizume and Y. Tendow, J. Phys. Soc. Japan 18, 1107 (1963).

84. C. M. Lederer, J. M. Hollander, and I. Perlman, "Table of Isotopes" (sixth edition), John Wiley and Sons, New York (1967) p. 344.

85. F. F. Felber, Jr., (Thesis), UCRL-3618 (1957).

86. D. C. Camp, UCRL-50156 (1967).

87. F. S. Goulding, D. A. Landis, and R. H. Pehl, submitted to the Gatlinburg Conference on Semi-Conductor Detectors and Associated Circuits, (UCRL-17560, 1967).

88. L. B. Robinson, F. Gin, and F. S. Goulding, Nucl. Instr. and Meth., (to be published), (UCRL-17419, 1968).

89. L. B. Robinson and J. D. Meng, UCRL-17220 (1967), unpublished.

90. L. B. Robinson, private communication.

91. H. T. Easterday, A. J. Haverfield, and J. M. Hollander, Nucl. Instr. and Meth. 32, 333 (1965).

92. T. Yamazaki and J. M. Hollander, private communication.

93. L. B. Robinson, F. Gin, and F. S. Goulding, to be published.

94. L. B. Robinson and J. D. Meng, "MULTID", privately circulated report, (1967).

95. J. M. Jaklevic, F. M. Bernthal, J. O. Radeloff, and D. A. Landis, Nucl. Instr. and Meth. (to be published), (UCRL-18389, 1968).

96. R. Gunnink, R. A. Meyer, J. B. Niday, and R. P. Anderson, Nucl. Instr. and Meth. 65, 26 (1968).

97. J. Routti and S. G. Prussin, UCRL-17672 (1968), to be published.

98. R. S. Hager and E. C. Seltzer, "Internal Conversion Tables", CALT-63-60 (1967).

99. W. I. Fominikh, J. Molnar, N. Nenoff, B. Styczen, and J. Zvolsky, Contributions to the International Symposium on Nuclear Structure, Dubna (1968) p. 46.

100. J. H. Hamilton, A. V. Ramayya, L. C. Whitlock, and A. Meulenberg, Phys. Rev. Lett. 19, 1484 (1967); J. H. Hamilton, A. V. Ramayya, and L. C. Whitlock, Phys. Rev. Lett. 22, 65 (1969).

101. H. L. Nielsen, K. Bonde Nielsen, and N. Rud, Phys. Lett. 27B, 150 (1968).

102. B. R. Mottelson, Proceedings of the International Conference on Nuclear Structure, Tokyo (1967) p. 87.

103. O. Mikoshiba, R. K. Sheline, and T. Udagawa, Nucl. Phys. A101, 202 (1967).

104. N. I. Pyatov, Arkiv für Fysik 36, 667 (1967); K. M. Zheleznova, N. I. Pyatov, and M. I. Chernei, Bull. Acad. Sci. U.S.S.R., Phys. Ser. (trans) 31, 546 (1967).

105. A. A. Kuliev and N. I. Pyatov, Nucl. Phys. A106, 689 (1968).

106. J. Krumlinde, Nucl. Phys. A121, 306 (1968).

107. I. Liu, O. B. Nielsen, P. Salling, and O. Skilbreid, Bull. Acad. Sci. U.S.S.R., Phys. Ser. (trans) 31, 63 (1967).

108. L. L. Riedenger, N. R. Johnson, and J. H. Hamilton, Phys. Rev. Lett. 19, 1243 (1967).

109. G. T. Ewan and G. I. Anderson, Proceedings of the International Conference on Nuclear Structure, Tokyo (1967) p. 667.

110. P. F. Kenealy, E. G. Funk, and J. W. Mihelich, Nucl. Phys. A105, 522 (1967).

111. J. Vrzal, et al., Bull. Acad. Sci. U.S.S.R., Phys. Ser. (trans) 31, 599 (1967).

112. D. C. Camp, private communication of preliminary results.

113. K. Wien, Zeit. für Physik 216, 1 (1968).

114. O. H. Otteson and R. G. Helmer, Phys. Rev. 164, 1485 (1967).

115. E. L. Church and J. Weneser, Phys. Rev. 103, 1035 (1956).

116. J. O. Rasmussen, Nucl. Phys. 19, 85 (1960).

117. K. Alder, A. Bohr, T. Huus, B. R. Mottelson, and A. Winther, Rev. Mod. Phys. 28, 432 (1956).

118. W. H. Brantley, J. H. Hamilton, T. Katoh, and E. F. Zganjer, Nucl. Phys. A118, 677 (1968).

119. E. F. Zganjer, T. M. George, and J. H. Hamilton, Nucl. Phys. A114, 609 (1968).

120. P. G. Hansen, H. L. Nielsen, and K. Wilsky, Bull. Acad. Sci. U.S.S.R., Phys. Ser. (trans) 31, 74 (1967).

121. A. A. Abdurazakov, et al., Contributions to the International Symposium on Nuclear Structure, Dubna (1968) p. 32.

122. N. A. Bonch-Osmolovskaya, E. P. Grigoriev, J. Liptak, and J. Urbanec, Contributions to the International Symposium on Nuclear Structure, Dubna (1968) p. 43.

123. H. L. Nielsen, K. Wilsky, J. Zylics, and G. Sorensen, Nucl. Phys. A93, 385 (1967).

124. A. S. Davydov and V. S. Rostovksy, Nucl. Phys. 60, 529 (1964).

125. E. R. Marshalek, (Ph.D. Thesis) UCRL-10046 (1962).

126. V. G. Soloviev, Nucl. Phys. 69, 1 (1965).

127. I. M. Pavlichenkov, Nucl. Phys. 55, 225 (1964).

128. E. R. Marshalek, Phys. Rev. 158, 993 (1967).

129. A. Bohr, Comptes Rendus du Congres International de Physique Nucleaire, Paris (1964), Vol. I, p. 487.

130. D. R. Bes and R. A. Broglia, Nucl. Phys. 80, 289 (1966).

131. D. G. Burke, et al., Mat. Fys. Medd. Dan. Vid. Selsk., (to be published).

132. B. R. Mottelson and J. G. Valatin, Phys. Rev. Lett. 5, 511 (1960).

133. T. Udagawa, private communication with Riedinger, et al., acknowledged in Ref. 108.

134. S. T. Belyaev, Sov. Journ. Nucl. Phys. (trans) 4, 671 (1966).

135. L. A. Malov, V. G. Soloviev, and U. M. Fainer, Contributions to the International Symposium on Nuclear Structure, Dubna (1968) p. 78.

136. T. Yamazaki and J. M. Hollander, unpublished results (April, 1965).

137. H. Fraunfelder and R. M. Steffen, "α-, β-, and γ-Ray Spectroscopy", (ed. K. Siegbahn), Vol. 2, (1965) p. 997.

138. H. L. Smith and D. C. Hoffman, J. Inorg. Nucl. Chem. 3, 243 (1956).

139. I. Bergström, F. Brown, J. A. Davies, J. S. Geiger, R. L. Graham, and R. Kelly, Nucl. Instr. and Meth. 21, 249 (1963).

140. Neutron Cross Sections, Vol. IIC, BNL 325 (1966).

141. I. E. Dayton and W. G. Pettus, Nucleonics 15, 86 (1967).

142. F. S. Goulding, D. A. Landis, J. Cerny, and R. H. Pehl, IEEE Trans. on Nucl. Sci. NS-13, 514 (1964).

143. R. H. Pehl, F. S. Goulding, D. A. Landis, and M. Lenzlinger, Nucl. Instr. and Meth. 59, 45 (1968).

144. L. B. Robinson, private communication.

145. W. W. Black, Nucl. Instr. and Meth. 53, 249 (1967).

146. J. B. Marion, ORO-2098-58 (1968). See also the 1967 preprint of this report for Ta^{178} energies.

147. R. Gunnink, private communication.

148. I. Řezanka, J. Frána, A. Maštalka, and J. Beneš, Czechoslov. J. Phys. 12, 530 (1962).

LEGAL NOTICE

This report was prepared as an account of Government sponsored work. Neither the United States, nor the Commission, nor any person acting on behalf of the Commission:

A. Makes any warranty or representation, expressed or implied, with respect to the accuracy, completeness, or usefulness of the information contained in this report, or that the use of any information, apparatus, method, or process disclosed in this report may not infringe privately owned rights; or

B. Assumes any liabilities with respect to the use of, or for damages resulting from the use of any information, apparatus, method, or process disclosed in this report.

As used in the above, "person acting on behalf of the Commission" includes any employee or contractor of the Commission, or employee of such contractor, to the extent that such employee or contractor of the Commission, or employee of such contractor prepares, disseminates, or provides access to, any information pursuant to his employment or contract with the Commission, or his employment with such contractor.

TECHNICAL INFORMATION DIVISION
LAWRENCE RADIATION LABORATORY
UNIVERSITY OF CALIFORNIA
BERKELEY, CALIFORNIA 94720